Recent and active tectonics of the central-eastern Betic Cordillera Internal Zone and comparison with the External Zone Front

Manuel Martínez Martos

Ph.D. Thesis 2017

ugr Universidad de Granada
Departamento de Geodinámica

Programa Doctorado
Ciencias de la Tierra

CSIC
Consejo Superior de Investigaciones Científicas

IACT
Instituto Andaluz de Ciencias de la Tierra

Editor: Universidad de Granada. Tesis Doctorales
Autor: Manuel Martínez Martos
ISBN: 978-84-9163-505-5
URI: http://hdl.handle.net/10481/48132

Departamento de Geodinámica

Jesús Galindo Zaldívar, Catedrático de Geodinámica de la Universidad de Granada,

HACE CONSTAR:

Que la presente tesis titulada "Recent and active tectonics of the central-eastern Betic Cordillera Internal Zone and comparison with the External Zone Front" ha sido realizada bajo mi dirección y cumple las condiciones suficientes para que su autor, Manuel Martínez Martos, opte al grado de Doctor en Ciencias Geológicas por la Universidad de Granada.

Granada, febrero de 2017

VºBº del Director

Fdo.: Jesús Galindo Zaldívar

Fdo.: Manuel Martínez Martos

El doctorando Manuel Martínez Martos y el director de la tesis D. Jesús Galindo Zaldívar garantizamos, al firmar esta tesis doctoral, que el trabajo ha sido realizado por el doctorando bajo la dirección del director de tesis y hasta donde nuestro conocimiento alcanza, en la realización del trabajo, se han respetado los derechos de otros autores a ser citados, cuando se han utilizado sus resultados o publicaciones.

Granada, febrero de 2017

Director de la Tesis | Doctorando

Fdo.: Jesús Galindo Zaldívar | Fdo.: Manuel Martínez Martos

Agradecimientos

En estas páginas quiero expresar toda mi gratitud a todas y cada una de las personas que han hecho posible culminar esta etapa. Su apoyo ha sido fundamental en el desarrollo de este trabajo, que es también el suyo en parte.

En primer lugar me gustaría destacar el constante trabajo del director de la Tesis Doctoral Jesús Galindo Zaldívar. El gran apoyo que me ha dado y la confianza que desde un primer momento ha depositado en mí (la mayoría de las veces mayor que la que yo mismo tenía) han sido fundamentales durante todo el desarrollo de este trabajo. Trabajar con él ha sido una gran suerte por lo aprendido tanto de geología y geofísica como de grandes cualidades humanas.

Aunque la Tesis Doctoral va firmada por una sola persona, los trabajos que componen el cuerpo principal de la misma han sido el resultado del esfuerzo y trabajo de muchos compañeros investigadores. Trabajar con ellos ha sido una gran oportunidad. A Francisco Lobo, por su inestimable ayuda en la interpretación de datos de geofísica marina. A Antonio Pedrera y Patricia Ruano que me ayudaron y enseñaron en el comienzo de esta etapa. A Manuel López Chicano, quien siempre me ha animado a andar este camino y se ha interesado por mis avances, siempre con una sonrisa. A Carlos Sanz de Galdeano, por su inestimable ayuda tanto en las conversaciones de índole geológica como etimológica; su sencillez y constante buen humor no enmascaran su gran experiencia. A los compañeros de la Universidad de Jaen y Cádiz: Antonio Gil, Clara de Lacy, Juan Antonio García Armenteros, María Jesús Borque, Antonio Ruiz Armenteros y Alberto Sánchez Alzola por su inestimable colaboración con los datos de geodesia. A Francisco García Tortosa y José Miguel Azañón, por sus aportes al trabajo de la falla de Laujar. A Miguel Ortega Sánchez, por su gran aporte de datos batimétricos. A Ana Ruiz, Sergio Martos, Antonio González y Francisco Javier Roldán García por su ayuda en el trabajo del frente de la Cordillera. A Pedro Alfaro, por su ayuda en los trabajos de CGPS y de la Falla de Padul. A Raquel Calvo-Rayo, por su ayuda en el trabajo de campo en la cuenca de Alhabia.

Al Departamento de Geodinámica, que me acogió y me dio medios para desarrollar mi trabajo. A Ángel Perandrés por poner a mi disposición todos los medios posibles para ayudar en cualquier aspecto. Me gustaría también agradecer a mis compañeros de becaría Ángel, Juampe, Yasmina, Lara, Irene e Idaira, con los que tantos momentos buenos y de desahogo he pasado; especialmente a Fran y Lourdes, compañeros también de trabajo que, además de enseñarme mucho han sabido estar pendientes de mis avances sin hacerse notar. A Pedro al que también debo en parte haber elegido este camino.

No me gustaría olvidarme de los investigadores del GNS Science Te Pu Ao, que tan bien me acogieron durante mi estancia en Nueva Zelanda y con los que tanto

aprendí de geología en una región tan interesante. Agradecer especialmente a Pilar Villamor, quien se encargó de que no me faltase el trabajo y quien me dio una perspectiva diferente de la investigación. A Robert Langridge, por darme la oportunidad de colaborar en un proyecto tan interesante como el Deep Fault Drilling Project – 2. A Will Ries, por estar siempre disponible ante cualquier duda en mi estancia.

Quiero también agradecer a Jean Sanders, que revisó y mejoró el estilo del texto escrito en inglés y a Angela Tate (Angie), quien me ayudó a mejorar notablemente mi nivel de inglés en los primeros años de doctorado.

Llegados a este punto me gustaría también agradecer a mis amigos que, aunque no han tenido una involucración directa en esta Tesis Doctoral, han estado siempre dispuestos a brindarme su apoyo tanto en los buenos como en los malos momentos. A Javi, al que me unen carrera, máster y tesis, y de quien también he aprendido a ser mejor observador, estudiante y persona en general. Al resto de mis amigos Peleteros por su fuente constante de risas y buenos ratos, sin olvidar a Carlos Bernárdez, siempre presente en los pocos ratos de silencio en nuestras reuniones. A mi siamesa Bea, quien sinceramente espero que haya comprado un billete de ida y vuelta. A mis compañeros de promoción, con los que tanto he compartido; especialmente a Mari, que a pesar de no vernos a menudo, siempre se ha esforzado por mantener el contacto.

Especialmente, agradecer su gran apoyo y cariño constantes a mis padres, quienes me han dado sus mejores valores y me han dado todo lo que han tenido a su alcance para poder estar donde estoy hoy, sin ellos este proyecto habría sido literalmente imposible.

A Nani, por ser la mejor compañera que podría haber elegido. A su familia, quienes tan bien me han acogido y a los que tanto cariño tengo ya. Nani me conoció inmerso plenamente en este proyecto, y su cariño y apoyo no sólo han allanado enormemente este camino, sino que han contribuido a hacerme mejor persona. Sin ella esta etapa no habría sido tan bonita ni tan completa.

Este trabajo ha sido posible gracias a una beca de Formación de Profesorado Universitario concedida por el Ministerio de Educación y Ciencia, a los medios materiales del grupo de investigación RNM-148, del Departamento de Geodinámica de la Universidad de Granada, del Instituto Andaluz de Ciencias de la Tierra (CSIC-UGR), y a los proyectos CGL2010-21048, P-09-RNM-5388 y CGL2016-80687-R.

Abstract

The study of the intramontane basins southward Sierra Nevada and the central-eastern Betic Cordillera External Zone Front provides new essential data to understand the western Mediterranean alpine tectonic evolution. This research integrates new acquired geological, geophysical and geodetical data to contribute to the main geodynamic models proposed for the Gibraltar Arc development.

The Betic Cordillera present-day relief begun to develop since the late Serravalian due to the Africa-Eurasia convergence. This setting induced the development of tectonic structures that isolated the intramontane basins as the Alpujarran Corridor, the Tabernas basin or the Gádor-Almería basin. Alhabia basin was formed by the interaction of these three basins and shows a cross-shaped depocentre were a faulted E-W synform is intersected by NW-SE normal faults. The intramontane basins interaction helps to unravel the effects of the Neogene-Quaternary counter-clockwise rotation in the convergence setting between Africa and Eurasia.

Active folds and faults accommodate the present-day deformations. New CGPS data show a present-day regional westward displacement with higher rates in the western sites. In addition, the southern sites undergo a south-westward displacement accommodated by the E-W and NW-SE normal faults south of Sierra Nevada. These faults are contributing to the dismantling of a thickened crust in the frame of the current N-S to NW-SE convergence. In this setting, the large E-W folds of the Internal Zone stopped their activity whilst the new convergence setting favours the developing of NE-SW folds. These structures are responsible of the highest ranges of the Iberian Peninsula in westernmost Sierra Nevada.

Several active faults are located south and west the Sierra Nevada edges. The E-W oriented Laujar Fault Zone is located in the Alpujarran Corridor central part. It shows a N-S relative extension according to recent dip-slip striations and CGPS data. This fault zone evidences the gravitational collapse of Sierra Nevada whilst

the southern region is folded by NW-SE shortening. The Padul normal fault plays an important role in the regional deformation since it accommodates most of the present-day NE-SW extension in the south-western end of Sierra Nevada. According to the fault length and rate, a maximum 6 magnitude earthquake might be expected every 154 years. However, the absence of historical seismic events suggests a creep activity rather than seismic activity for the Padul Fault.

In the Alborán Sea northern coast, buried marine-cut terraces onshore are correlated with marine terraces offshore. Their origin is consequence of sea-level changes rather than tectonic vertical displacements.

The External Zone front developed with NNE-SSW and roughly E-W orientations separated by the Tíscar Fault. Whilst the NNE-SSW oriented front in Sierra de Cazorla is relatively straight, the roughly E-W front in the Jódar area is highly sinuous due to heterogeneous displacement of the fold-and-thrust belt on the main detachment level. At the present-day, tectonic activity in this area is related to an E-W extension accommodated by NW-SE normal faults.

All the data support an active subduction with associated roll-back in the Gibraltar Arc.

Resumen

El estudio de las cuencas intramontañosas del Sur de Sierra Nevada y del frente de la Zona Externa de la Cordillera Bética centro-oriental aporta nuevos datos esenciales para entender la evolución tectónica alpina del Mediterráneo occidental. Este trabajo de investigación integra nuevos datos geológicos, geofísicos y geodésicos para contribuir a los principales modelos geodinámicos propuestos para el desarrollo del Arco de Gibraltar.

El relieve actual de la Cordillera Bética comenzó su desarrollo en el Serravalliense tardío debido a la convergencia entre África y Eurasia. Este contexto indujo el desarrollo de estructuras tectónicas que aislaron las cuencas intramontañosas, tales como el Corredor de la Alpujarra, la cuenca de Tabernas o la cuenca de Gádor-Almería. La cuenca de Alhabia se formó por la interacción de estas tres cuencas intramontañosas y tiene un depocentro en forma de cruz donde un sinforme E-O fallado es intersectado por fallas normales NO-SE. La interacción de cuencas intramontañosas ayuda a aclarar los efectos de la rotación antihoraria de la convergencia entre África y Eurasia.

Las deformaciones actuales están acomodadas por pliegues y fallas activos. Los Nuevos datos de CGPS muestran un desplazamiento regional hacia el Oeste con tasas más altas hacia los vértices más occidentales. Además, los vértices meridionales sufren un desplazamiento hacia el Suroeste que se acomoda por fallas normales E-O y NO-SE al Sur de Sierra Nevada. Estas fallas contribuyen al desmantelamiento de una corteza engrosada en el contexto de la convergencia actual N-S a NO-SE. En este contexto, los grandes pliegues E-O de la Zona Interna pararon su actividad mientras que las nuevas direcciones de convergencia favorecen el desarrollo de pliegues NE-SO. Estas estructuras son responsables de los mayores relieves de la Península Ibérica en la zona occidental de Sierra Nevada.

En los bordes sur y oeste de Sierra Nevada se encuentran varias fallas activas. La zona de falla de Laujar, orientada E-O, se localiza en la zona central del Corredor

de la Alpujarra. Muestra una extensión relativa N-S de acuerdo con estrías en buzamiento recientes y con datos de CGPS. Esta zona de falla evidencia el colapso gravitacional de Sierra Nevada mientras las regiones más al Sur se pliegan por un acortamiento NO-SE. La falla normal de Padul tiene un importante papel en la deformación regional, ya que acomoda la mayor parte de la extensión NE-SO actual en el margen suroccidental de Sierra Nevada. De acuerdo con la longitud y actividad de la falla, sería esperable un terremoto de hasta 6 grados de magnitud cada 154 años. Sin embargo, la ausencia de eventos sísmicos históricos sugiere que la Falla de Padul sufre una deformación por reptación más que sísmica.

En la costa norte del Mar de Alborán, las plataformas de abrasión costeras enterradas se correlacionan con terrazas marinas offshore. Su origen es consecuencia de cambios en el nivel del mar más que de desplazamientos verticales.

El frente externo se formó con orientaciones NNE-SSO y aproximadamente E-O, ambas separadas por la falla de Tíscar. Mientras que el frente NNE-SSO de Sierra de Cazorla es relativamente recto, el frente E-O en el área de Jódar es altamente sinuoso debido al desplazamiento heterogéneo del cinturón de pliegues y cabalgamientos sobre el nivel de despegue principal. En la actualidad, la actividad tectónica en esta zona se relaciona con una extensión E-O acomodada por fallas normales NO-SE.

Todos estos datos apoyan una subducción activa con roll-back asociado en el Arco de Gibraltar.

TABLE OF CONTENTS

PART I

PART II

PART III

Part I

1. Introduction

2. Aims and outline

3. Regional setting

4. Methods

CHAPTER 1

Introduction

The Betic-Rif Cordillera (Fig. 1.1) is a highly arcuated orogenic arc developed since the Cretaceous and constitute the Mediterranean westernmost alpine belt. It surrounds the Alborán Sea and connect the western Mediterranean to the North Atlantic Ocean through the Gibraltar Straight. This orogen is consequence of a continental collision due to the NW-SE Africa-Eurasia plate convergence (Dewey et al., 1989; Rosenbaum et al., 2002). The stable foreland of the Betic Cordillera is the Iberian Massif, which crops out to the NW and were formed in the Variscan orogeny, during the Palaeozoic collision between Laurasia and Gondwana.

The Gibraltar Arc, which comprise the Betic-Rif Cordillera together with the Alborán Sea, has been subject of a complex evolution involving compressional and extensional deformations that, in some places, occurred simultaneously. Due to the high scientific interest of this area, many geological and geophysical studies of international research groups have been focused on the mechanisms responsible for the Gibraltar Arc tectonic evolution. However, the results of these different studies are very controversial and several main models have been proposed for the Gibraltar Arc development: models based on lithospheric delamination of subcontinental lithosphere beneath the Alborán Sea (Houseman et al., 1981; Seber et al., 1996; Calvert et al., 2000, Mancilla et al., 2013) and other models involving a subduction with or without an associated roll-back of the subducted slab (Araña and Vegas, 1974; Torres-Roldán et al., 1986; Wortel and Spakman, 1992; Pedrera et al., 2011; Ruiz-Constán et al., 2011, González-Castillo et al., 2015a).

To discuss the suitability of the proposed regional models, it is essential the analysis of the recent and active tectonic deformations related to the plate motions, crustal structures and seismicity. A key area is the central and eastern

Betic Cordillera Internal Zones, where the highest ranges have been developed in the last 10 Ma (Sanz de Galdeano, 1983; Braga et al., 2003). Moreover, the knowledge of the Cordillera external front evolution during this period is essential to compare the hinterland and foreland behaviour and to discuss the mechanisms involved in the development of the Betic Cordillera alpine belt latest deformational stages.

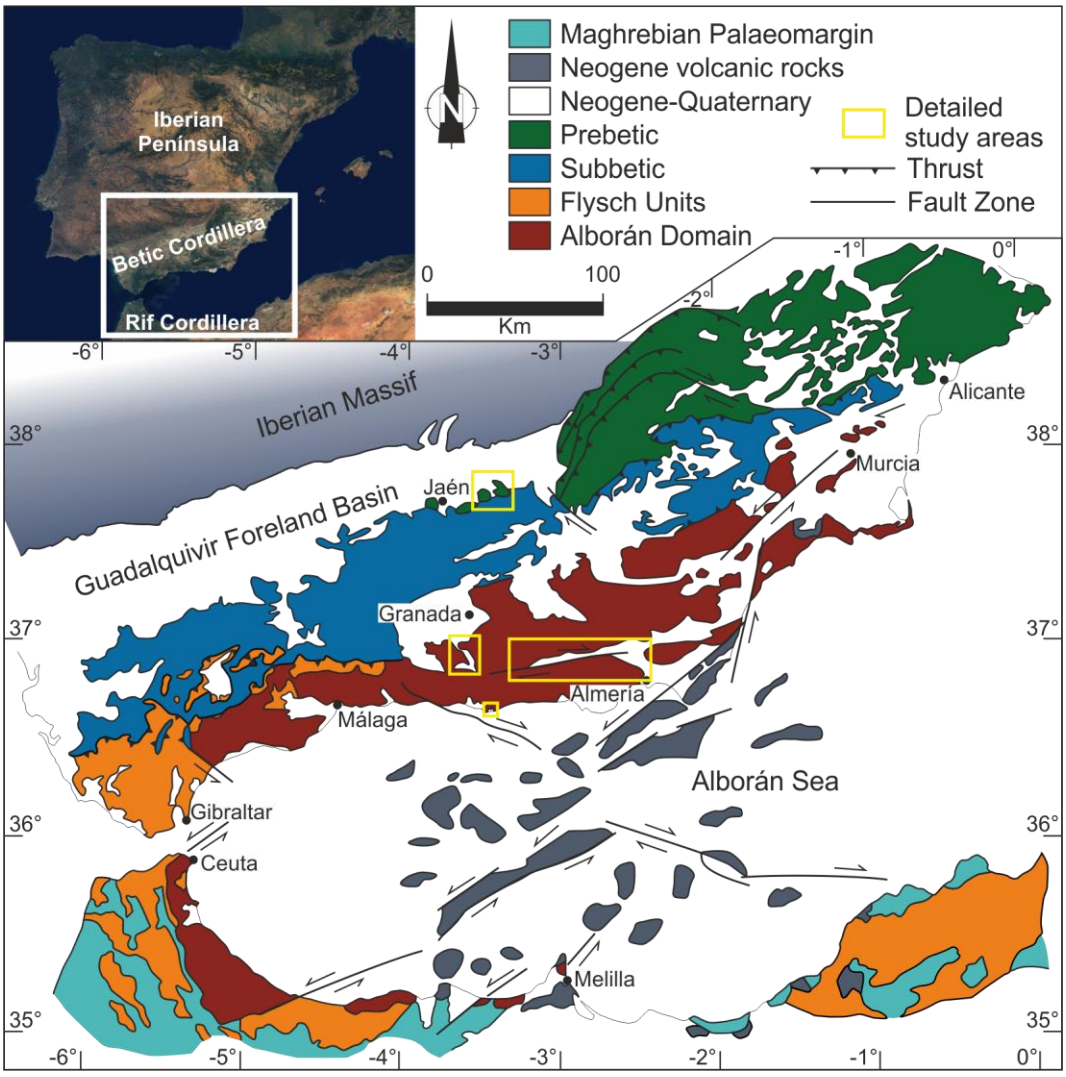

Fig. 1.1 Geographical setting of the Study area and geological sketch of the Gibraltar Arc.

The analysis of Neogene-Quaternary sedimentary basins, is essential to constrain the main tectonic structures development through their relationship with the sedimentary infill. In order to understand the basin evolution it is necessary to

integrate the field geological observations with the geophysical data that provide constraints on the deep geometry. Several recent researches on basin evolution integrating geophysical and geological data have been developed in the eastern (Marín-Lechado et al., 2007; Do Couto et al., 2014; Pedrera et al., 2015) and western (Ruiz-Constán et al., 2010, 2012; González-Castillo et al., 2014, 2015b) Betic Cordillera. The central-eastern sector, South of Sierra Nevada, has been widely studied from a geological viewpoint, although there are little geophysical and geodetical data allowing to unravel the deep structure and the recentmost tectonic activity.

This Ph.D Thesis integrates available and new geological, geophysical and geodetical data in order to unravel the recent and active tectonic evolution of the intramontane basins situated southwards Sierra Nevada and its comparison with the central part of the Betic Cordillera front (Fig. 1.1). Results obtained in these key areas offer a deeper comprehension of the Gibraltar Arc development.

CHAPTER 2

Aims and outline

This Ph.D. Thesis aims to study Late Miocene to present evolution of the central-eastern Betic Cordillera Internal Zone and its comparison with the frontal External Zone part through the analysis of key areas (Fig. 1.1). The region presents an abrupt relief including the Iberian Peninsula highest ranges. To do this, the following objectives were proposed:

a) To constrain the Late Miocene tectonic evolution of the central-eastern Betic Cordillera Internal Zone through the analysis of the Alhabia, Alpujarran Corridor, Gádor-Almería and Tabernas intramontane basins.
b) To unravel the active tectonics in the central-eastern Betic Cordillera Internal Zone with special emphasis on the Sierra Nevada Southern and South-western part.
c) To compare the recent and active evolution of Betic Cordillera Internal Zone with the central part of the External Zone Front.
d) To integrate the general obtained results with the regional geodynamic models previously proposed and to shed light on them in the frame of the Africa-Eurasia convergence.

According with the University of Granada prescriptions, this Ph.D. Thesis is presented as group of publications. The volume is divided in three main parts. Part I is a summary of relevant previous data and the state of the art in the Betic Cordillera knowledge. This part also contains a regional setting and the main geodynamic models proposed for the Gibraltar Arc tectonic evolution. In addition, it includes a chapter explaining the methods used in this contribution. Part II represents the main contribution of this Ph.D. Thesis and comprises four published and two submitted for publication articles providing new geological, geophysical and geodetical data for the central and eastern Betic Cordillera. In

part III, a discussion compare the new obtained data with the previous data. Finally the conclusions of this contribution are presented.

Part II, include results on the Internal Zone followed by those of the External Zone Front. This volume present first the analysis of the Alhabia Neogene to Quaternary basin, located south-eastwards Sierra Nevada whose structures are consequence of the tectonic evolution since the Late Miocene. The following chapters are focused on the active tectonics revealed by the analysis of active faults and GPS motions. First are presented the results of regional studies on the eastern Betic Cordillera, that are later focused on the active Laujar and Padul main faults. Finally, the analysis of marine terraces provides new insights on the recent vertical motions of this tectonic active area. The study of the External Zone Front is focused in the Jódar-Bédmar area, located in the same central-eastern Cordillera transect. In any case, some repetitions in introductory and methodological items can be found as a consequence of presenting each chapter with the same structure in which it appears in the corresponding journal.

In addition to the regional results, some of the structures analysed in this Ph.D. thesis improve the general knowledge on the development of irregular mountain fronts and buried marine terraces, through the detailed analysis of the field examples.

Chapter 5: "Superposition of tectonic structures leading elongated intramontane basin: the Alhabia basin (Internal Zones, Betic Cordillera)". This research aimed to unravel the Alhabia Basin deep structure and the interaction of faults and folds from the Miocene up to Present-day. New acquired gravity data were combined with field geological observations and GPS data. This study enabled to assess the influence of interacting folds and faults in the eastern Betic Cordillera recent evolution.

Chapter 6: "Active shallow extension in central and eastern Betic Cordillera from CGPS data". New continuous GPS (CGPS) data obtained during the Topo-Iberia project are presented in this study. They reveal the location and features of the

main active structures. This chapter attempts to unravel the recent and active tectonic evolution in the central and eastern Betic Cordillera.

Chapter 7: "Latest extension of the Laujar fault in a convergence setting (Sierra Nevada, Betic Cordillera)". The main objective in this research was to constrain the recent tectonic evolution in the Sierra Nevada southern boundary. In this chapter, a tectonic model is proposed in order to explain the existence of an extensional fault zone parallel to the E-W oriented antiform of Sierra Nevada. To do this, different geophysical data (gravity and magnetic data, audio-magnetotelluric data and electrical resistivity tomography) were combined with GPS and geological data and radiocarbon dating.

Chapter 8: "The Padul normal fault activity constrained by GPS data: brittle extension orthogonal to folding in the Central Betic Cordillera". In this research, GPS and geological data are combined to unravel the recent and current behaviour to understand its role in the central Betic Cordillera active deformation.

Chapter 9: "Buried marine-cut terraces and submerged marine-built terraces: The Carchuna-Calahonda coastal area (southeast Iberian Peninsula)". In this chapter new acquired gravity data are combined with previous marine seismic profiles to constrain the morphological evolution of buried and offshore marine terraces in the Alborán Basin northern boundary. This chapter aims to determine the role of tectonics and eustatism during the relief recent evolution.

Chapter 10: "Irregular mountain front development in a fold-and-thrust belt: (Central Betic Cordillera, S Spain)". Finally, it is presented a study showing the recent and active tectonic evolution in the central Betic Cordillera mountain front. In this research, geological field observations where combined with new acquired gravity data and with previous gravity measurements from the Topo-Iberia project. The main aim of this study was to determine the factors influencing the development of irregular mountain fronts whilst they are being formed.

CHAPTER 3

Regional setting

3.1 Geological setting

The Betic Cordillera is located in the south-east of Spain and constitutes the western end of the Mediterranean Sea together with the Rif Cordillera, in Northern Morocco, forming the Gibraltar arc (Fig. 3.1). This arc developed since the late Cretaceous (Dewey et al., 1989; Rosebaum et al., 2002) as a consequence of the N-S to NW-SE Africa-Eurasia plate convergence (Dewey et al., 1989; Srivastava et al., 1990; Muller and Roest, 1992; Mazzolli and Helman, 1994; Rosebaum et al., 2002, Calais et al., 2003) and the westward displacement of the Alborán Domain in the West Mediterranean. The Algero-Balearic Basin oceanic spread coevally in the Oligocene and early Miocene (Dewey et al., 1989; Rosebaum et al., 2002; Rosebaum and Lister, 2004). As a consequence of this tectonic activity, the variscan Iberian Massif were partially subducted under the Betic Cordillera, which constitutes the northern part of the Gibraltar Arc (Morales et al., 1999).

Several tectonic domains have been distinguished in the Betic-Rif Cordilleras (Fallot, 1948; Julivert et al., 1974). The first one is located at the inner arc and made of several alloctonous tectonic units including partially metamorphosed Paleozoic rocks (Internal Zone or Alborán Domain). The second tectonic domain (Flysh units) corresponds to Cretaceous to Miocene deep-water deposits on a probably oceanic basin (Durand-Delga et al., 2000), generally emplaced between the Internal and External zones. The last domain is formed by Mesozoic and Cenozoic sediments deposited on the south Iberian and northern African palaeomargins and mostly deformed as a fold-and-thrust belt forming the outer orogenic arc (External Zone or South Iberian Domain). The Guadalquivir Basin constitute the foreland basin of the Betic Cordillera. The westward displacement of the Betic Cordillera Internal Zone during the Latest Oligocene to Middle

Miocene was the responsible for the thrusting and folding of the Mesozoic-Cenozoic Subbetic Units (Crespo-Blanc and Campos, 2001) together with the Flysch domain (Balanyá and García-Dueñas, 1987; Luján et al., 2003; Platt et al., 2003). This process was coetaneous with an intense extensional episode in the Internal Zone, accommodated by low-angle normal faults.

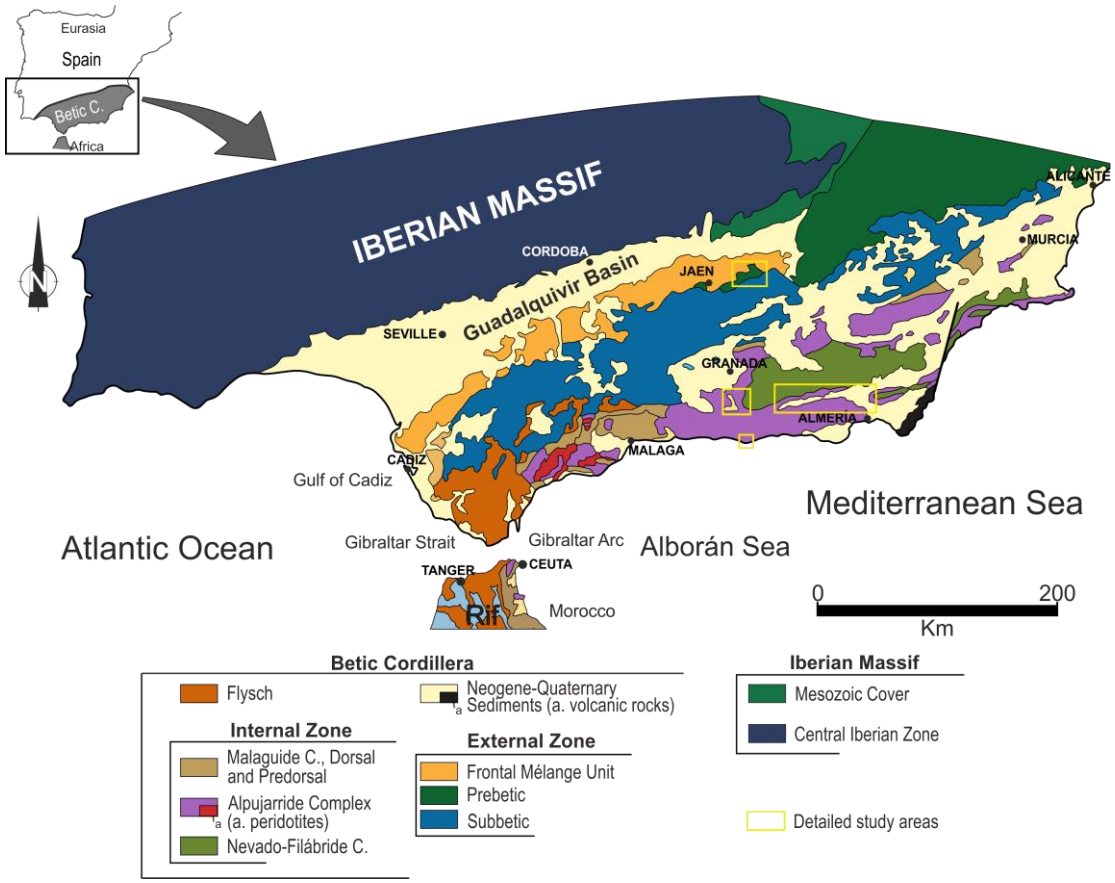

Fig. 3.1 Geological map of the Betic Cordillera.

The study area is mostly located in the central-eastern Betic Cordillera Internal Zone and in the External Zone front (Fig. 3.1). The intramontane basins studied are located in the Internal Zone and developed over metamorphic rocks that crop out in the surrounding ranges. The External Zone study area is south bounding the Guadalquivir Foreland Basin.

The Internal Zone

The Betic Cordillera Internal Zone comprise three main metamorphic complexes, from bottom to top: the Nevado-Filábride (Egeler, 1963), the Alpujárride (Van

Bemmelen, 1927) and the Maláguide (Blumenthal, 1927). The Nevado-Filábride and Alpujárride complexes include Palaeozoic to Mesozoic rocks that have undergone metamorphism. The main high-pressure metamorphic event have been attributed to a crustal-thickening related to thrust-sheet stacking in the Internal Zone. The age attributed to this high-pressure event is very controversial. Some researchers (Monié et al., 1991; Augier et al., 2005a) propose a range of ages between 48 and 17 Ma based in Ar^{39}-Ar^{40} dating. Other ages based on Lu-Hf Nevado-Filabride garnets dating reveal ages between 18 and 14 Ma (Platt et al., 2006). Another age of 15.0 ± 0.6 Myr have also been proposed by means of U-Pb analysis of zircons in Nevado-Filábride ultramafic rocks (López Sánchez-Vizcaíno et al., 2001).

During Early and Middle Miocene, the metamorphic rock uplift determine a ductile to brittle deformation along the low-angle contacts. It is recognizable a low-pressure high-temperature metamorphism with a latter cooling in low-pressure conditions, probably related to the exhumation of deep crustal rocks during the extensional process in the Early Miocene (Zeck et al., 1992; Monié et al., 1994; Balanyá et al., 1997; Platt et al., 2005). The Alpujárride/Maláguide contact underwent a top-to-the-east motion in the Early Miocene (Aldaya et al., 1991; Lonergan and Platt, 1995) whilst a top-to-the-west extension occurred at the Alpujárride/Nevado-Filábride contact in the Middle Miocene (Galindo-Zaldívar et al., 1989; Platt and Vissers, 1989; Martínez-Martínez and Azañón, 1997). The Mecina Fault is the low-angle normal fault that separates these complexes (Aldaya et al., 1984; García-Dueñas et al., 1988; Galindo-Zaldívar et al., 1989; Platt and Vissers, 1989). The Maláguide Complex is formed by Palaeozoic to Middle Miocene rocks. It was affected by variscan deformation, however it does not show alpine metamorphism (Chalouan and Michard, 1990). In addition the Dorsal and Predorsal complexes, formed by Triassic to Early Neogene sedimentary rocks, also belongs to the Internal Zone.

The External Zone and Guadalquivir foreland basin

The External Zone of the Betic Cordillera is composed by Mesozoic and Tertiary sedimentary rocks deposited on the variscan Iberian palaeomargin. These sediments where involved in thin-skin fold-and-thrust belts detached from the variscan basement at the Triassic Keuper facies level. The External Zone in the Betic Cordillera was a passive continental margin and was not affected by metamorphism. It is subdivided in Subbetic, Intermediate Units and Prebetic (García-Hernández et al., 1980).

The Guadalquivir basin, between the External Zone and the Iberian massif, is the Betic Cordillera foreland basin and it is filled by sediments since the Early Miocene, when this basin constituted one of the junctions between the Atlantic Ocean and the Mediterranean Sea (the North Betic Strait) (Sanz de Galdeano and Vera, 1991, 1992; Martín et al., 2009). Moreover, other intramontane basins were developed coetaneous to the Betic Cordillera uplifting. These basins are therefore greatly conditioned by the recent tectonic structures.

Main recent and active tectonic structures

The recent tectonic structures developed since the Tortonian in the Betic Cordillera highly condition the relief morphology. The N-S to NW-SE convergence between the African and Eurasian plates continued during the Late Miocene and Lower Pliocene (Dewey et al., 1989; DeMets et al., 1994; Calais et al., 2003). This process was accompanied by volcanic activity in extensional regions of the Gibraltar Arc (Duggen et al., 2005). In this setting, the mountain ranges coincide with large antiforms, sometimes affected by normal and strike-slip faults (Booth-Rea et al., 2003), whilst the main intramontane basins are located in large synforms (Weijermars et al., 1985; Braga et al., 2003; Galindo-Zaldívar et al., 2003; Martínez-Martínez et al., 2004). Large folds are interacting with normal faults, giving as a result asymmetrical depocentres in the intramontane basins.

The main large folds in the Central-Eastern Betic Cordillera are E-W to NE-SW oriented, like Sierra de Gádor, Sierra Nevada, Sierra de Filabres or Sierra Alhamilla antiforms (Galindo-Zaldívar et al., 2003; Ruano, 2003; Sanz de Galdeano and Alfaro, 2004; Marín-Lechado et al., 2006; Pedrera et al., 2009a,

2009b). They are often separated by faulted synforms that coincide with elongated depressed areas were intramontane basins –such as the Alpujarran Corridor– develop. These main large folds show generally a northwards vergence, especially in Sierra Alhamilla, where Late Tortonian bedding in the northern slopes are vertical and even overturned, whilst in the southern ones the same layers have 20° S dip (Weijermars et al., 1985). Fission-track analysis were carried out in Sierra Nevada and Sierra de Filabres (Johnson et al., 1997) and indicate that the folding age begun during the Tortonian.

NW-SE, NE-SW and E-W oriented fault sets accommodate the Betic Cordillera Internal Zone extension since the Late Miocene (Sanz de Galdeano, 1983; Galindo-Zaldívar et al., 2003). The NW-SE oriented normal faults widely extend from the Granada basin northern part –where their structure have been studied from seismic data and field geological observations (Rodríguez-Fernández and Sanz de Galdeano, 2006)– to the western termination of Sierra Nevada, where the Padul-Nigüelas fault is located (Alfaro et al., 2001). These faults are usually associated to asymmetric basins with Tortonian to Quaternary sedimentary wedges. Block rotation due to the presence of these faults have been reported, and either listric faults or domino-like systems have been invoked to explain it (Galindo-Zaldívar et al., 1996). These faults are considered to be seismic and active, especially in the Granada basin area (Sanz de Galdeano et al., 1995; Galindo-Zaldívar et al., 1999; Alfaro et al., 2001).

In the intramontane basins northwards Sierra Nevada, the most representative fault is the Baza fault, which is N-S to NW-SE oriented and more than 30 km long (Alfaro et al., 2007). This fault deforms the sedimentary infill of the Baza basin probably since Tortonian to Quaternary times (Botella et al., 1986; Martín-Penela, 1988; Azañón et al., 2006).

NW-SE oriented normal faults are also present from the Sierra de Gádor western end and the Campo de Dalías area until the Campo de Níjar, Southwards Sierra Alhamilla (Marín-Lechado et al., 2005) (Fig. 3.2). They condition the straight coastline south-eastwards Almería and the steep relief in the Sierra de Gádor

Western end (Marín-Lechado et al., 2005, 2007, 2010; Pedrera et al., 2007, 2012). Most of these normal faults affect Holocene sediments producing fault scarps, and also the seismicity in Campo de Dalías, which is related to NW-SE epicentres alignment (Marín-Lechado et al., 2005).

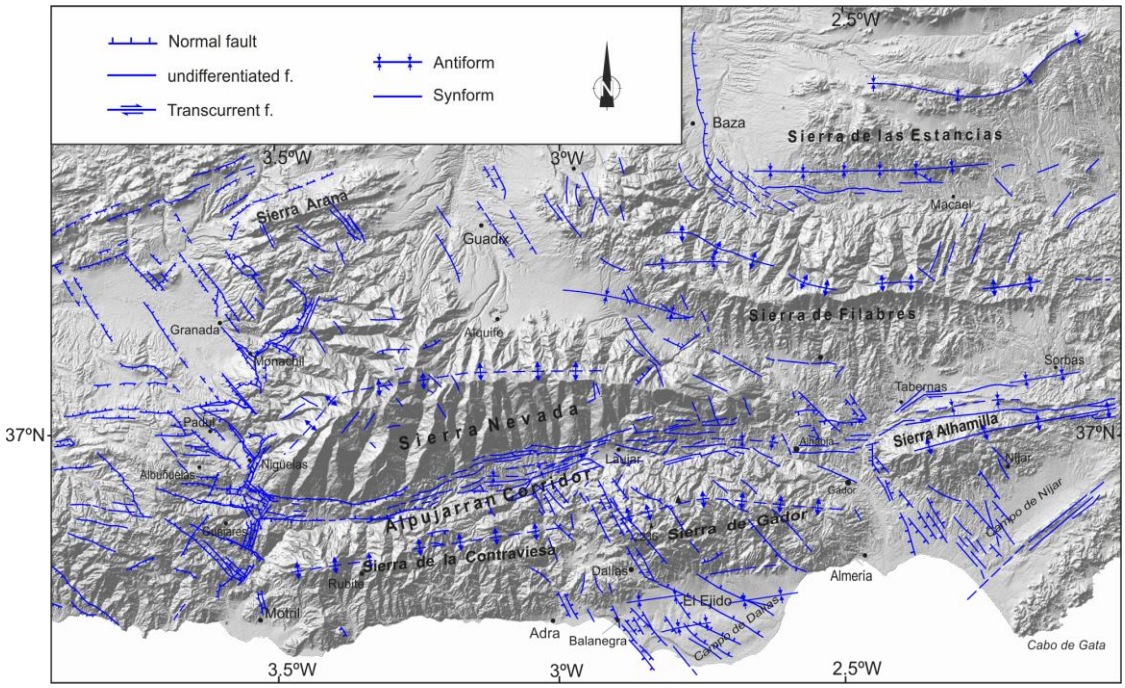

Fig. 3.2 Main tectonic structures of the central-eastern Betic Cordillera Internal Zone.

The E-W and NE-SW faults are scarcer than the NW-SE. However, they are also associated with seismic activity. This is the case of the normal Zafarraya Fault, located in an endorheic basin with sediments from Tortonian up to present-day (Reicherter et al., 2003) and to which the 1884 Andalucía Earthquake has been attributed. E-W faults crop out in less abundance in the Granada basin. However, they tend to be quite present in all the southern part of Sierra Nevada, coinciding with the synformal structure that separates Sierra Nevada from the southern sierras. These faults are related to E-W elongated intramontane basins such as the formed in the Alpujarran Corridor, with a dextral and normal kinematics (Sanz de Galdeano et al., 1985; Sanz de Galdeano, 1996a; Galindo-Zaldívar, 1986; Rodríguez Fernández et al., 1990; Martínez-Díaz, 2000; García et al., 2003; Martínez-Díaz and Hernández-Enrile, 2004; Martínez-Martínez, 2006; Martínez-

Martínez et al., 2006) and in some places interact with the NW-SE faults, as in Alpujarran Corridor eastern part (Sanz de Galdeano et al., 2010).

In addition, large transcurrent sinistral faults are present in the cordillera easternmost part, like the Carboneras and Palomares faults (Sanz de Galdeano, 1983) and in their continuation to the Alborán Sea. Reverse faults cropping out are very scarce in the Betic Cordillera Internal Zone and in the External Zone are restricted to thrusts in the fold-and-thrust belts (Sanz de Galdeano, 1983, 1989; Pedrera et al., 2009a; Giaconia et al., 2012). In the frontal part of the External Zone, recent faults are located in the Bédmar-Jódar area, mainly with NW-SE strikes and recent normal slip (Sanz de Galdeano et al., 2013).

Two main controversial models have been proposed to explain the origin of the recent tectonic structures that determine the present-day relief. It has been proposed that it is consequence of the relative shortening between the African and Eurasian plates in a crustal thickness context during the late Miocene (Galindo-Zaldívar et al., 1993; Galindo-Zaldívar et al., 2003; Sanz de Galdeano and Alfaro, 2004). The normal faulting development in the Internal Zone is due, according to these researchers to an unstable over-thickened crust together with local extension related to folds. The second main model is proposed by authors that suggest that the sedimentary basins developed as a result of an extensional context in which the metamorphic middle to upper crust were thinned and exhumed during the late Miocene (Mora, 1993; Vissers et al., 1995; Augier et al., 2005b; Meijninger, 2006). According to these researchers, the compressive structures are the result of a tectonic inversion since the Late Messinian-Pliocene.

3.2 Previous geophysical and geodetical data

The main geophysical data available in the Betic Cordillera mostly comprise gravity and magnetic data, seismicity, seismic refraction and deep seismic reflection profiles, seismic tomography data, and magnetotelluric soundings. All these geophysical data have provided huge advances unravelling the cordillera deep structure.

3.2.1 Gravity data

The first gravity studies carried in the Betic Cordillera was performed by the IGN, (1976), obtaining the free air and the Bouguer anomaly maps of the whole Iberian Peninsula and the Balearic islands at 1:1,000,000 scale. Moreover, other gravity researches in local areas have increased the knowledge of the geometry of Miocene to present Betic basins (e.g. Marín-Lechado et al., 2006; Pedrera et al., 2006; 2007; Alfaro et al., 2007; Li et al., 2012; Ruiz-Constán et al., 2013; Do Couto et al., 2014).

In addition, gravity models in the Alborán Sea and the Betic Cordillera unravelled the crustal thickness variation in the region (e.g. Hatzfeld, 1976; Suriñach and Udías, 1978; Casas and Carbó, 1990; Galindo-Zaldívar et al., 1998; Torné et al., 2000). The crust thickness distribution shows a decreasing from 38 km thick in the Betic Cordillera Internal Zone to 18-22 km in the Alborán Sea, just 30 km apart (Torné and Banda, 1992).

3.2.2 Magnetic data

The aeromagnetic map of Spain (Ardizone et al., 1989) has a scale of 1:1,000,000 and was carried along 10 km spaced fly lines at 3 km of altitude. This map provides information of regional scale anomalies. The magnetic anomalies in the SE of the Iberian Peninsula are related to the Betic Cordillera structures. In addition, other detailed magnetic studies were carried out in order to better understand the distribution of mineralized bodies along the Betic Internal and External zones (e.g. Pedrera et al., 2009a; Li et al., 2012; Ruiz-Constán et al., 2013; González-Castillo et al., 2014).

3.2.3 Seismicity

Shallow and intermediate seismicity up to 120 km depth in the Gibraltar Arc is widely distributed through an approximately 400-km-wide band (Buforn et al., 1995, 2004; Morales et al., 1997; Bokelmann et al., 2011; Ruiz-Constán et al., 2011). However, deep seismicity is occasional in the central Betic Cordillera (Buforn et al., 1991). Seismic tomography has also been a technique used to study the Betic

Cordillera deep structure at crustal (Dañobeitia et al., 1998; Carbonell et al., 1998) and at mantle depths (Blanco and Spakman, 1993; Morales et al., 1999; Gurria and Mezcua, 2000; Calvert et al., 2000; Spakman and Wortel, 2004; Serrano et al., 2005; Díaz et al., 2010). More recent studies use receiver functions (Mancilla et al., 2013) and anisotropy (Alpert et al., 2013) to unravel the cordillera deep structure, which is characterised by the presence of a subducting slab in an anomalous mantle beneath the Alborán Sea. Lithospheric models integrated seismic and gravity data (Fullea et al., 2007; 2010).

3.2.4 Seismic profiles

Deep seismic and conventional seismic reflection profiles have been carried out in numerous parts of the Betic Cordillera in order to better know the deep crustal structure. The ESCI-BETICAS are deep multichannel seismic reflexion profiles crossing the central Betic Cordillera Internal and External zones. The NW-SE (ESCI-BETICAS-1) extend from the Guadalquivir foreland up to the Baza Basin whilst the NE-SW (ESCI-BETICAS-2) reach up to the coastline. Both combined reach 196 km of length. In addition, the ESCI-ALBORÁN profiles pursued the same objectives than the ESCI-BETICAS, but in the Alborán Basin north-eastern sector. Two profiles were carried out as well, one of them was the continuation of the ESCIBETICAS-1 90 km offshore (ESCI-ALBORÁN-1), and the ESCI-ALBORÁN-2 was WSW-ESE oriented and located in the central sector of the Alborán Basin, covering 400 km long towards the Algero-Balearic Basin. Despite the poor quality of the described deep reflection seismic profiles, they have been used to unravel the Betic Cordillera deep structure and its transition to the Alborán basin (García-Dueñas et al., 1994; Galindo-Zaldívar et al., 1997; Martínez-Martínez et al, 1997; Vegas et al., 1997).

The deep seismic refraction profiles were acquired by the Working Group for Deep Seismic Sounding in the Alborán Sea, 1974-1975 (WGDSSAS-1974-1975, 1978). Inland profiles of this campaign suggest the presence of detachment levels dividing the upper and the lower crust (Banda and Ansorge, 1980; Banda et al., 1993) and an increasing in the crustal thickness toward the east, reaching the

highest thickness beneath Sierra Nevada (Banda et al., 1993). Deep seismic refraction profiles in the Alborán Sea evidence a decrease in the crustal thickness from the Betic Cordillera to the Alborán basin, showing values until ~16 km thick (Hatzfeld. 1976; WGDSSAS-1974-1975, 1978; Suriñach and Vegas, 1993). Results obtained combining these seismic profiles with the high regional heat flow values (Polyak et al., 1996) support the existence of an anomalous mantle under the Alborán Basin (Hatzfeld, 1976).

3.2.5 Magnetotelluric data

Magnetotelluric researches have been carried out underlining the Betic Cordillera anisotropy. In the central and eastern Betic Cordillera, 2D models have been processed from a survey crosscutting from the Iberian Massif to the Internal Zone, showing conductive bodies in the lower crust interpreted as partial melting in the base of a thickened continental crust by several authors (Carbonell et al., 1998; Pous et al., 1999). In the western region, there is remarkable the cross-sections from the Iberian Massif, through the Guadalquivir foreland basin up to the Betic Cordillera, that highlight the mountain belt deep thrusting structure (Ruiz-Constán et al., 2012), and also the study of the deep anisotropy (Ruiz-Constán et al., 2010) that reveal the influence of the Gibraltar Arc in the upper mantle. Other 3D modelling from a different survey in the Internal Zone shows a conductive body beneath Sierra de Filabres (Martí, 2006). Combining these data with other acquired magnetotelluric data in the Almanzora Corridor area, Pedrera et al. (2009) interpreted this conductive body as basic igneous rocks in which the Sierra de Filabres antiform started to nucleate. In addition, other authors have carried 3D magnetotelluric models in the central and eastern Betic Cordillera (Martí et al., 2009; Rosell et al., 2011). In the western part of the Cordillera, 3D MT research support the presence of a very large conductive and deep body probably related to sulfure deposits (González- Castillo et al., 2014)

3.2.6 GPS data

Several GPS researches have been carried out to constrain the active tectonic deformations in the Betic Cordillera due to its proximity to the Africa-Eurasia

plate boundary, which makes this region a tectonically active area. According to plate reconstruction studies, the region undergoes a heterogeneous NW-SE shortening of 4-5 mm/yr (Argus et al., 1989; DeMets et al., 1990; Nocquet et al., 2012). Regional continuous GPS networks evidence the Alborán Domain present tectonic activity showing a WSW to SW displacement of the central-eastern Betic Cordillera with a WNW component in the western part in respect to stable Eurasia (Serpelloni et al., 2007; Vernant et al., 2010; Koulali et al., 2011).

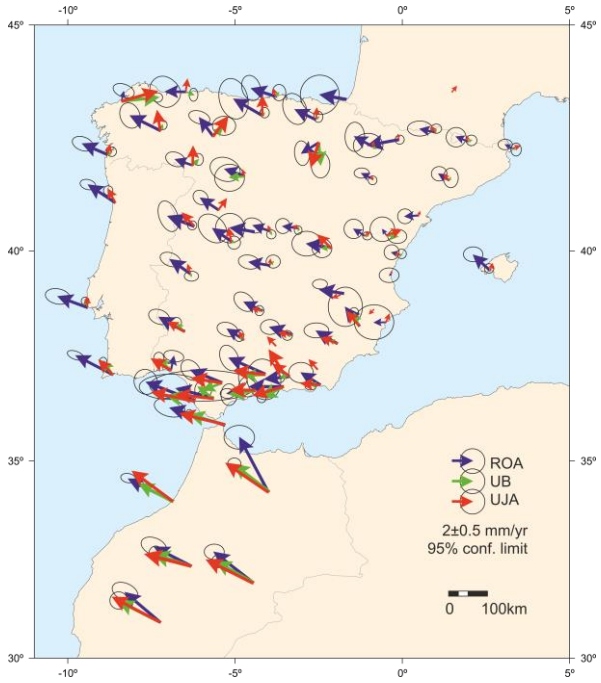

Fig. 3.3 Iberian Peninsula and northern Morocco GPS velocities in respect to stable Eurasia with 95% confidence error ellipses. Modified from Garate et al. (2015).

Data Quality and accuracy have improved in recent times since first studies presented fewer data. Fadil et al. (2006) and Serpelloni et al. (2007) already pointed to a relative westward displacement of the Betic-Rif cordilleras. Nevertheless, more recent studies improved the previous results (Tahayt et al., 2008; Pérez-Peña et al., 2010a; Koulali et al., 2011; González-Castillo et al., 2015a).

In addition, new GPS stations are available since 2008 in the context of the Topo Iberia project, which improve the current GPS data in the Iberian Peninsula. The Real Observatorio de la Armada, the University of Barcelona and the University of Jaén processed these data using different software (Garate et al., 2015) obtaining a roughly westward motion of the Betic Cordillera in respect to the

Iberian Massif with some discrepancies in the areas with low displacement (Fig. 3.3).

3.3 Models of recent tectonic evolution for the Betic and Rif cordilleras

The Gibraltar Arc recent geodynamic evolution is in deep controversy since the 1970s. The gradual advance of geological and geophysical researches contribute to support it (Fig 3.4). The more remarkable features of the Gibraltar Arc are:

a) The Betic-Rif Cordillera is the most arcuated orogen of the Alpine Orogeny.
b) Compressive structures in the External Zone coexist in time with the development of low-angle normal faults during the Early to Middle Miocene.
c) The presence of a thin continental crust in the Alborán basin.
d) The deformation is distributed in a wide area, so it is not possible to define a pure plate boundary.
e) The volcanic activity since the Middle Miocene.
f) Active tectonics in the region present a complex seismic pattern.

The first hypotheses for the Gibraltar arc evolution (Fig. 3.4a) propose that the rigid microplate of Alborán was emplaced westwards between the African and Eurasian plates, which controls its arcuated shape and the fold-and-thrust deformation type in the External Zone (Andrieux et al., 1971; Andrieux and Mattauer, 1973). Tapponier, (1977) attributed the westward motion of the Alborán Plate to a tectonic scape produced by irregularities in plate boundaries. This model was used to explain the existence of dextral strike-slip faults in the Betic Cordillera and sinistral strike-slip faults in the Rif Cordillera (Bourgois, 1978; Sanz de Galdeano, 1983; Leblanc and Olivier, 1984; Dewey et al., 1989), and were explained as transfer faults. Cloetingh and Nieuwland, (1984) and Weijermars et al. (1985) explained the thin crust in the Alborán Sea to be a consequence of an ascensional mantle diapir that leaded to gravitational nappes radial emplacement followed by the cooling beneath the Alborán crust (Fig. 3.4b). This model also explained the Ronda peridotites emplacement (Bonini et al.,

1973; Loomis, 1975). At first, the metamorphic complexes of the Internal Zone were believed to be separated by thrusts (Egeler and Simon, 1969), but later on were reconsidered to be low-angle normal faults (Aldaya et al., 1984; Galindo-Zaldívar, 1986; García-Dueñas and Balanyá, 1986; Galindo-Zaldívar et al., 1989; Platt and Vissers, 1989), so the Alborán Domain back sector had to suffer extensional processes whilst it was being emplaced towards the west during the Miocene (Balanyá and García-Dueñas, 1987; Jabaloy et al., 1992). The latest models try to explain the coexistence of shortening in the External zone and extension in the Internal Zone, accompanied by the exhumation of metamorphic rocks. Even though all of them agree in the existence of the Alborán Domain, the different hypothesis could by assembled into three main groups:

1.- The Alborán subcontinental lithosphere is detached and/or delaminated

This hypothesis suggest that the Africa-Eurasia convergence formed a unstable thick and cold orogenic root that were detached during the Late Oligocene or Early Miocene due to lithospheric delamination (García-Dueñas et al., 1992; Seber et al., 1996; Calvert et al., 2000; Mancilla et al., 2013) (Fig. 3.4c) or mantle convection (Houseman et al., 1981; Platt and Vissers, 1989) (Fig. 3.4d). The lithosphere removal leaded to a crust radial extension that stopped in the Late Miocene, when the Africa-Eurasia convergence became again the main geodynamic process. This delaminated lithosphere model have been supported by the observation of two SE dipping intermediate (60-400 km) and very deep (570-650 km) high velocity bodies by seismic tomography beneath the Alborán Sea (Calvert et al., 2000).

2.- Oceanic lithosphere subducts below the Alborán Basin with or without slab roll-back and/or slab detachment

The subduction polarity have been controversial, leading to different models. Some researchers suggest a northwards dipping subduction (Araña and Vegas, 1974; De Jong, 1991, 1993; Wortel and Spakman, 1992; Zeck et al., 1992). Other studies propose a subducting model with a double oceanic crust subduction (Torres-Roldán et al., 1986; Chalouan and Michard, 2004). Studies based on

seismic tomography suggest the existence of a subduction with associated roll-back dipping eastward to south-eastward (Fig. 3.4e) (Blanco and Spakman, 1993; Morley, 1993; Royden, 1993; Lonergan and White, 1997; Hoernle et al., 1999; Wortel and Spakman, 2000; Gutscher et al., 2002; Gill et al., 2004; Spakman and Wortel, 2004; Thiebot and Gutscher, 2006; Brun and Faccena, 2008; Pedrera et al., 2011; Ruiz-Constán et al., 2011, 2012). GPS based models also support the roll-back both in the Rif (Fadil et al., 2006; Pérouse et al., 2010) and in the Betic cordilleras (González-Castillo et al., 2015a). Other studies have reported a slab ripping and its consequent sinking into the asthenosphere (Buforn et al., 1991; Blanko and Spakman, 1993; Zeck, 1996; Spakman and Wortel, 2004; García-Castellanos and Villaseñor, 2011). In addition, seismic tomography in the southern Iberia lithosphere, intermediate seismicity distribution and stress state, reveal a continental subduction of the Iberian Massif dipping southwards below the Alborán Sea (Serrano et al., 1998; Morales et al., 1999). According to these models, the Alborán Sea is a back-arc basin related to a subduction (Gueguen et al., 1997, 1998; Galindo-Zaldívar et al., 1998; Pedrera et al., 2011; Carminati et al., 2012). Some authors also propose an active subduction in present times (Gutscher et al., 2002; Thiebot and Gutscher, 2006; Pedrera et al., 2011; Ruiz-Constán et al., 2012; González-Castillo et al., 2015b).

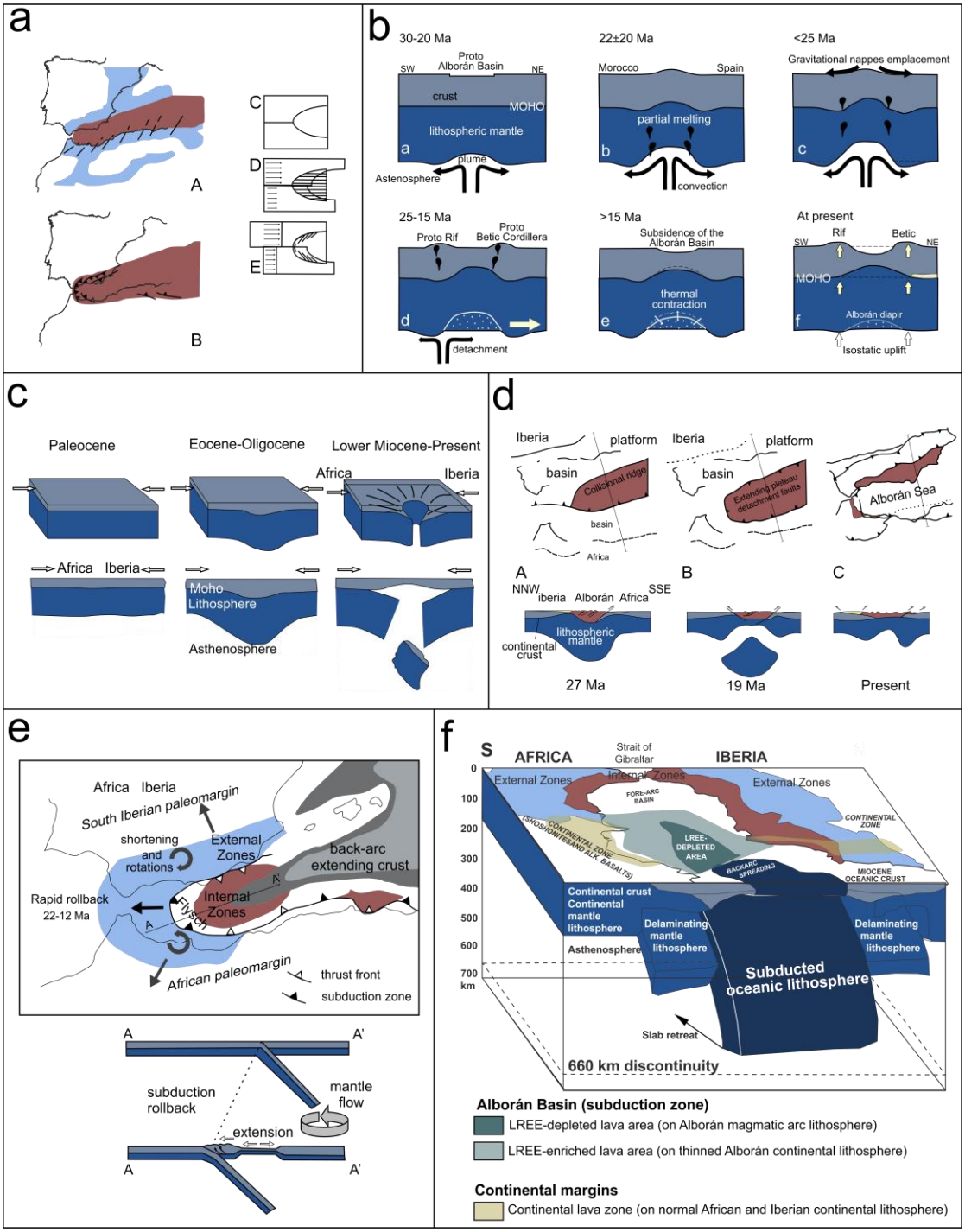

Fig. 3.4 Main proposed models for the Gibraltar Arc recent and active evolution up to date. Modified from González-Castillo (2015). a) Andrieux et al. (1971); b) Weijermars et al. (1985); c) Seber et al. (1996); d) Platt and Vissers (1989); e) Lonergan and White (1997); f) Duggen et al. (2008).

3.- The Alborán subcontinental lithosphere is delaminated whilst oceanic lithosphere subducts beneath it

Duggen et al. (2003, 2005, 2008) proposed this model in order to explain the Neogene magmatism in the region (Fig. 3.4f). Late Miocene delamination in the subcontinental lithosphere below the African and Iberian palaeomargins could have been produced by an eastwards-dipping oceanic slab roll-back beneath the Alborán Sea (Martínez-Martínez et al., 2006). According to this model, the space left by the delaminating asthenosphere were filled by an upwelling of plume-contaminated sub-lithospheric mantle.

The state of the art in the knowledge of the Betic Cordillera geodynamical processes and the controversy existing in the different proposed models, reveals that new geological observations and geophysical data are crucial to clarify the discussion and to improve the proposed models for the Gibraltar Arc tectonic evolution.

CHAPTER 4

Methods

In this Ph.D. Thesis, geological, geophysical and geodetical techniques have been combined to shed light on the central-eastern Betic Cordillera geodynamic evolution by unravelling some aspects of the upper crustal structure in the region. The combination of different techniques helps to avoid results over-interpretation using one single method. The different methods carried in this research are exposed in the chapters that constituting the Part II. In any case, a summary description of the fundaments involving the techniques used in this Ph.D. is provided in this chapter.

4.1 Geological methods

In this contribution, the existent database of geological maps from the Instituto Geológico y Minero de España (IGME) have been always the starting point of every field geology campaign. They allow to identify the large geologic features to study in the region. The main geologic field work carried in these researches have been focused in the analysis of recent and active fault kinematics, determined by the examination of different structural features such as clastic wedges, striations, S-C structures, steps or relay-ramps. In addition, radiocarbon dating of striated calcretes (see chapter 7) or reports of active travertines cut by fractures (see chapter 5) have been criteria taken into account to discern the existence of possible active faults.

4.2 Geophysical methods

4.2.1 Gravity prospecting

Gravity prospecting is a geophysical method based on the measure of gravity acceleration values that are variable by lateral density contrasts. A gravity anomaly is the difference between the gravity value measured in a site and the theoretical gravity value that corresponds to the mentioned location. The gravity

value in a specific place not only varies with the density, but it also depends on time and space factors. Therefore, several corrections have to be applied to the measurements taken on field.

The two time-depending factors affecting the gravity value are the instrumental drift and the tidal effect. The tidal effect is due to the Sun and Moon gravity fields' interaction and, since it is periodical, it is also easy to correct. The remaining instrumental drift is easily corrected by beginning and finishing every measurement cycle in the same base station.

The latitude in which the gravity measurements are taken also affects the obtained valued because of the earth radius variation from the equator to the poles and the differences in the centrifuge acceleration. This factor is corrected applying the Geodetyc Reference System empiric formulae to the g_{obs}. (GRS, 1967):

$$g_l = 978031.849\ (1 + 0.005278895\ sin^2\phi + 0.000023462\ sin^4\phi)\ \text{(mGal)}$$

Where g_l is the theoretical gravity value is at sea level and ϕ is the latitude in degrees.

To consider the elevation difference between the ellipsoid and the measurement point, the Free Air correction (0.3086 mGal/m) is implemented. The Free Air anomaly (FA) is calculated with the equation:

$$FA = g_{obs} - g_l + 0.3086\ h\ \text{(mGal)}$$

where h is the elevation above the sea level.

The Bouguer correction considers the difference of mass in the measurement point due precisely to its elevation difference. Applying both the Free Air and the Bouguer correction, the Bouguer anomaly (BA) is obtained:

$$BA = g_{obs} - g_l + 0.3086\ h - 0.04193\ \rho\ h\ \text{(mGal)}$$

where ρ is the survey area rocks average density in g/cm^3.

Finally, the influence of the topography surrounding the measurement point has to be taken into account. This is achieved applying the Terrain correction (TC), which allows to obtain the Complete Bouguer anomaly (CBA):

$$CBA = g_{obs} - g_l + 0.3086\, h - 0.04193\, \rho\, h + TC \text{ (mGal)}$$

This anomaly only depends on the density variations of the rocks underneath the measurements.

The field gravimeter in all the gravity surveys was a Scintrex CG-5 AutoGrav with accuracy up to 0.001 mGal (Fig. 4.1). This gravimeter performs automatically the tidal correction, stores al the measurements in an internal memory and allows an accurate electronic level to help to avoid levelling mistakes during the acquisition. The gravity stations position were obtained with a differential GPS.

Fig. 4.1 Gravimeter Scintrex CG-5 AutoGrav used to acquire gravity data.

The complete Bouguer anomaly was obtained using Oasis Montaj and all the stations were referred to the absolute gravity station of Granada (National

Geographical Service of Spain, IGN). The terrain correction was calculated using a combination of the methods developed by Kane (1962) and Nagy (1966) up to 160 km of each station and using a 5-m accuracy DEM provided by the IGN.

Bouguer anomaly maps were obtained in each research. Moreover, the regional anomaly maps were obtained by kriging the data acquired in basement. Finally, the residual anomaly maps were derived by the difference between the Bouguer and the regional anomaly maps. The residual anomaly profiles were modelled using the GRAVMAG v1.7 software of the British Geological Survey (Pedley et al., 1993).

4.2.2 Magnetic data

The geomagnetic field can be considered as the field produced by a magnetic dipole. It is produced by the currents originated in the outer core due to the different rotation speeds of the inner core with respect to the mantle and crust. The geomagnetic field intensity varies from 60,000 nT in the poles to 30,000 nT in the equator. Magnetic prospection is based on the study of local magnetic anomalies produced by distortions in the geomagnetic field due to different magnetic properties in the rocks. The remnant and the induced magnetization are related by the Könisberger ratio, which tends to be larger in mineralizated rocks.

The equipment used to acquire total magnetic field measurements was a GSM-8 proton precession magnetometer (Fig. 4.2) with accuracy of 1 nT. Measurements were carried far from anthropic noise sources such as power lines or metallic materials.

The magnetic anomalies were calculated using a standard procedure that included a reduction to the IGRF 2010 (IAGA, 2010). The diurnal magnetic field variation was corrected using the nearest permanent magnetic station (San Fernando, Cádiz) (Real Instituto y Observatorio de la Armada, 2016). GravMag 1.7 (Pedley et al., 1993) was also used to model the magnetic profiles.

Fig. 4.2 Magnetometer GSM-8 used to obtain magnetic data.

4.2.3 Electric Resistivity Tomography

Electric resistivity tomography (ERT) is an induced-electric-current geoelectric prospection method used to detect bodies with different electrical properties. To do so, an electrical current of known intensity (I) is conducted to the ground trough two electrodes (A and B) separated a AB distance. In a symmetric position respect to AB/2 is situated another pair of electrodes (M and N) to measure the potential difference (ΔV). Knowing these parameters and the distance separating the electrodes, it is possible to calculate the resistivity (ρ) in a homogeneous and isotropic medium. However, when this configuration is carried in an anisotropic medium, the obtained resistivity is apparent due to the different bodies through which the current passes. Depending on the AB distance (r), the apparent resistivity will correspond to a different depth.

$$V = \frac{I\rho}{2\pi r}$$

There are several electrode arrangements in ERT and they can be divided into asymmetric and symmetric arrays depending on the M and N electrodes position in respect to the AB/2 situation. The asymmetric arrays provide great ground penetration, but also distorts the bodies' morphology. On the contrary, symmetric arrays provide shallow penetration but lower distortion on the morphology of the registered bodies. In the following researches, the array used

is the gradient array (ABEM, 2006; Loke, 2014) with a 4-channel multiple gradient protocol taking the measurements in two cycles called GRAD4LX8 and GRAD4S8.

The equipment used was a Terrameter SAS 4000 (Fig. 4.3), which has a 1 μV resolution and an accuracy greater than 1% in the entire temperature range. It has also three automatic measurement ranges (±250 mV, ±10 V and ±400V) and four measurement channels, which allows to get larger amounts of data in a small period of time.

Fig. 4.3 Terrameter SAS 4000 used to obtain ERT profiles.

The data were acquired in field in two 400-m-long profiles and with a 5 m electrode spacing. Subsequently, the data were dumped into a computer using SAS4000 Utilities software. The position of each electrode were measured using a differential GPS and introduced manually in the data files in order to take into account the topography during the inversion process. Both profiles were processed using RES2DINV v.3.59 to constrain real resistivity 2D sections from the obtained apparent resistivity sections. With this software a first field data verification is made in order to eliminate bad datum data points that might mask the inversion. The verified data inversion were made using a finite elements

model since it is more suitable in profiles where the topography is taken into account. This software uses the least squares method to calculate the real resistivity from the apparent resistivity pseudosection. Once done that, the software calculates the apparent resistivity to the calculated real resistivity grid and compares the results with the field data. This process is repeated in several iterations until the root mean squares (RMS) error is acceptable (less than 10%). If the RMS error does not reach satisfactory values in a small number of iterations, a second data filtering must be done, this time eliminating data with high error rate in a RMS error statistic. Other key parameters used in the inversion process were:

a) An increasing in depth model with a half-cell electrode spacing in accordance with the great amount of data acquired in each profile.
b) Four nodes in each electrode spacing unit.
c) A smoothed inversion method which provides more realistic morphologies.

To assess data quality the Depth of investigation index (DOI) was calculated, (Oldenburg and Li, 1999). This parameter is calculated cell by cell according to the equation:

$$R_{1,2}(x,z) = \frac{m_1(x,z) - m_2(x,z)}{m_{1r} - m_{2r}}$$

where R is the DOI index, m_{1r} and m_{2r} are two different resistivity models, and $m_1(x,z)$ and $m_2(x,z)$ are the resistivity values for each cell of models 1 and 2, respectively. When the different resistivity models are identical, the DOI index (R) tends to zero, which means the data are reliable. Otherwise, when R tends to one, it means those cells values do not respond to surface data. In order to minimize the damping factor effect the normalized DOI (Robert et al., 2011; Martínez-Moreno et al., 2013) was calculated, following the equation below:

$$R(x,z) = \frac{m_1(x,z) - m_2(x,z)}{R_{max}(m_{1r} - m_{2r})}$$

where R_{max} is the highest value of R obtained in the previous equation. A reasonable cut-off value of R might be 0.1 or 0.2, since from then on the DOI values begin to increase quickly (Oldenburg and Li, 1999). A cut-off value of 0.1 was chosen in this research. In addition, the background resistivity of the reference model in the second inversion was 100 times the background resistivity in the first one, to ensure that the inversion results do not depend on the initial model (Loke, 2014).

4.2.4 Audio-Magnetotellurics

Temporal variations in the natural magnetic field induce an electric field on the upper crust. The primary magnetic field and the electric currents generated are co-dependent and they are related through the impedance tensor (Z_{ij}):

$$Z_{ij} = \frac{E_i}{H_j}$$

where E_i and H_j are the electric and magnetic fields respectively. It is possible to obtain the ground apparent resistivity and the electric and magnetic fields phase.

The electromagnetic fields registered in the surface may come from either natural or induced sources. Examples of natural electromagnetic field sources might be the geomagnetic field, the ionosphere activity or thunderstorms. In audio-magnetotellurics (AMT), only the natural frequencies from 10 Hz to 70 kHz are registered. However, a far transmitter antenna was used to enhance the band from 1 to 5 kHz since the natural signal decreases is such frequencies. The electromagnetic data are registered in the time domain and transformed to the frequency domain using Fourier transformations.

The impedance tensor in AMT is solved through the Maxwell equations in the frequency domain for a medium with the incidence of a plane electromagnetic wave. Cagniard (1953) proved that this relation depends on the range of measured frequencies and on the rocks resistivity and thickness. The wave amplitude dies down according to the medium conductivity and the wave frequency. The skin depth (δ) is the depth in which the fields amplitude is

attenuated a factor e of their value in the Earth surface (Vozoff, 1991) and is given by the equation:

$$\delta \approx 500 \sqrt{\rho T}$$

where ρ is the medium resistivity and T is the wave period.

The depth of investigation (P) is empirically related to the skin depth through the equation:

$$P = \frac{\delta}{\sqrt{2}}$$

which is approximately the 70% of the skin depth.

The method penetration is related to the wave period, so measuring in different frequency bands, information about electric resistivity in different depths is obtained. In AMT the high natural field frequencies are registered, so it can penetrate some hundreds of metres. Additionally, the penetration depth will be larger in the more resistive rocks.

The equipment used was a StrataGem EH4 from Geometrics (Fig. 4.4) with which several AMT soundings were acquired. In each sounding two electric field components (E_x and E_y) were registered in the time domain simultaneously to two magnetic field components (H_x and H_y). Being x and y the N-S and the E-W directions respectively. The spacing between electrodes was 50 m in the higher frequencies and 100 m in the lower band register.

In the data processing the amplitude of the electric and magnetic temporal series are transformed to the frequency domain. The relation between the horizontal electromagnetic components is known:

$$E_x = Z_{xx}H_x + Z_{xy}H_y$$

$$E_y = Z_{yx}H_x + Z_{yy}H_y$$

From the impedance tensor values the apparent resistivity (ρ_a) and the phase (φ) values are obtained for each period (Vozoff, 1972):

$$\rho_{a_{xy}}(T) = \frac{T}{(2\pi\mu)\left[Z_{xy}(T)\right]^2}$$

$$\varphi_{xy}(T) = arctan\left\{\frac{Im\left[Z_{xy}(T)\right]}{Re\left[Z_{xy}(T)\right]}\right\}$$

where μ is the magnetic permeability of free space and $Im\left[Z_{xy}(T)\right]$ and $Re\left[Z_{xy}(T)\right]$ are the xy imaginary and real components of the impedance tensor for a period T respectively. These equations are defined equally for the tree others components of the impedance tensor: Z_{xx}, Z_{yx} and Z_{yy}. Stratagem directly provides the resistivity and phase curves in each station for each diagonal and anti-diagonal impedance tensor components. Since the data acquisition is done in two orthogonal directions, this method is sensitive to dimensionality and a proper analysis needs to be done. The obtained curves dimensionality was analysed by means of Bahr decomposition (Bahr, 1988, 1991), showing a 1D and 2D behaviour. The obtained data were integrated in a 2D profile were the topography (Parker and Booker, 1996) was taken into account. The data were processed using WinGlink software and with an error flor of 5% for the phases and the apparent resistivity.

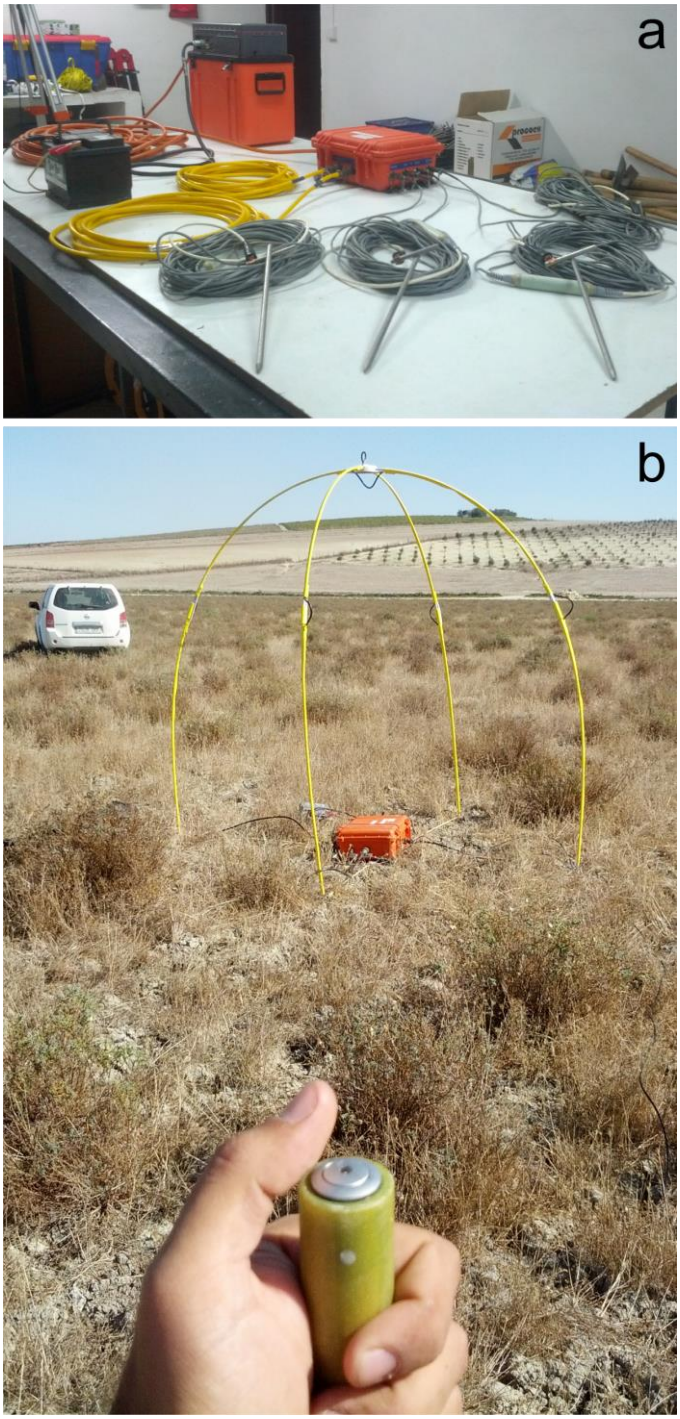

Fig. 4.4 StrataGem EH4 used to obtain AMT data. a) Main record components. b) Far antenna transmitter.

4.3 Other geophysical and geodetical methods

Some others geophysical techniques were also used offshore close to the Alborán Sea northern coast, in the Carchuna-Calahonda sector, namely, multibeam bathymetry, backscatter and seismic data. While geophysical data are used to unravel the underlying rocks geometry, GPS data show the relative tectonic displacement.

Multibeam bathymetry and back scatter data

Multibeam imagery was collected in the Carchuna-Calahonda sector with a 300 kHz Simrad EM3000D multibeam echo sounder (MBES) and with an Elac Seabeam 1185 echo sounder. The data positioning was determined using a DGPS navigation. The obtained data were processed to obtain a 5×5 m resolution grid with Neptune™ software. Backscatter data was also processed with Neptune™ software and obtained from echo sounder data

Seismic data

The seismic data were collected using a 3.5-kHz sub-bottom profiler and a 1000-4500 J Sparker source with a recording length of 1 s and a shooting rate of 1-2 s.

Geodetical methods

Two kind of GPS researches were developed. To unravel the current velocity field in the central-eastern Betic Cordillera it has been undetaken a continuous GPS (CGPS) study with observations from 1st March, 2008 up to 31th December, 2013 in a sub-network of 11 sites belonging to the Topo-Iberia research project (http://www.igme.es/TopoIberia/default.html), the Euroref Permanent Network (http://www.epncb.oma.be) and the Andalusian Permanent Network (http://www.ideandalucia.es/portal/web/portal-posicionamiento/rap).

A non-permanent local GPS network of 8 sites with 72 hours of continuous observations in different field campaigns (March 1999, May 2000, July and September 2011, and November 2012) was used to study the Padul Fault. More details of the geodetic data acquisition and processing are explained in the methods section of each study and is omitted in this section to avoid unnecessary repetitions.

Part II

5. **Superposition of tectonic structures leading elongated intramontane basin: the Alhabia basin (Internal Zones, Betic Cordillera)**
6. **Active shallow extension in central and eastern Betic Cordillera from CGPS data**
7. **Latest extension of the Laujar fault in a convergence setting (Sierra Nevada, Betic Cordillera)**
8. **The Padul normal fault activity constrained by GPS data: brittle extension orthogonal to folding in the Central Betic Cordillera**
9. **Buried marine-cut terraces and submerged marine-built terraces: The Carchuna-Calahonda coastal area (southeast Iberian Peninsula)**
10. **Irregular mountain front development in a fold-and-thrust belt: (Central Betic Cordillera, S Spain)**

CHAPTER 5

Superposition of tectonic structures leading elongated intramontane basin: the Alhabia basin (Internal Zones, Betic Cordillera)

Int J Earth Sci (Geol Rundsch)
DOI 10.1007/s00531-016-1442-9

ORIGINAL PAPER

Superposition of tectonic structures leading elongated intramontane basin: the Alhabia basin (Internal Zones, Betic Cordillera)

Manuel Martínez-Martos[1,2] · Jesús Galindo-Zaldivar[1,2] · Francisco José Martínez-Moreno[3] · Raquel Calvo-Rayo[1] · Carlos Sanz de Galdeano[2]

Received: 20 September 2016 / Accepted: 22 December 2016

[1] Departamento de Geodinámica, Universidad de Granada, 18071-Granada, Spain

[2] Instituto Andaluz de Ciencias de la Tierra, CSIC-Universidad de Granada, Avenida de las Palmeras, nº 4, 18100-Armilla, Spain

[3] IDL-Universidade de Lisboa, Faculdade de Ciências, Campo Grande, Ed. C8, Lisboa, Portugal

ABSTRACT

The relief of the Betic Cordillera was formed since the late Serravallian inducing the development of intramontane basins. The Alhabia basin, situated in the central part of the Internal Zones, is located at the intersection of the Alpujarran Corridor, the Tabernas basin, both trending E-W, and the NW-SE oriented Gádor-Almería basin. The geometry of the basin has been constrained by new gravity data. The basin is limited to the North by the Sierra de Filabres and Sierra Nevada antiforms that started to develop in Serravallian times under N-S shortening and to the south by Sierra Alhamilla and Sierra de Gádor antiforms. Plate convergence in the region rotated counter-clockwise in Tortonian times favouring the formation of E-W dextral faults. In this setting, NE-SW extension, orthogonal to the shortening direction, was accommodated by normal faults on the SW edge of Sierra Alhamilla. The Alhabia basin shows a cross-shaped depocentre in the zone of synform and faults intersection. This field example serves to constrain recent counter-clockwise stress rotation during the latest stages of Neogene-Quaternary basin evolution in the Betic Cordillera Internal Zones, and underlines the importance of studying the basins´ deep structure and its relation with the tectonic structures interactions.

Keywords: Basin geometry; gravity prospecting; superimposed sedimentary basins; recent tectonic evolution.

5.1 Introduction

Orogenic intramontane basins record regional tectonic evolution and deformation patterns over time. They are filled by sediments either in synformal structures perpendicular to compression (Burg and Podladchikov 1999; Guest et al. 2007), in grabens orthogonal to extension (Carmignani et al. 2004) or in pull-apart basins related to wrench regimes (Jacobs and Thomas 2004). Due to the interaction and overlapping of such tectonic features, intramontane basins may cross-cut one another, leading to superimposed basins. Such basin interaction has been described in collisional orogens such as the Anatolian Fault Zone (Gürer et al. 2001; Yilmaz and Gelisli 2003; Tari et al. 2014) or the Balkan Peninsula (Zagorčev 1992). Superimposed basins in collisional contexts are usually consequence of an advanced orogenic stage and/or a complex deformational history.

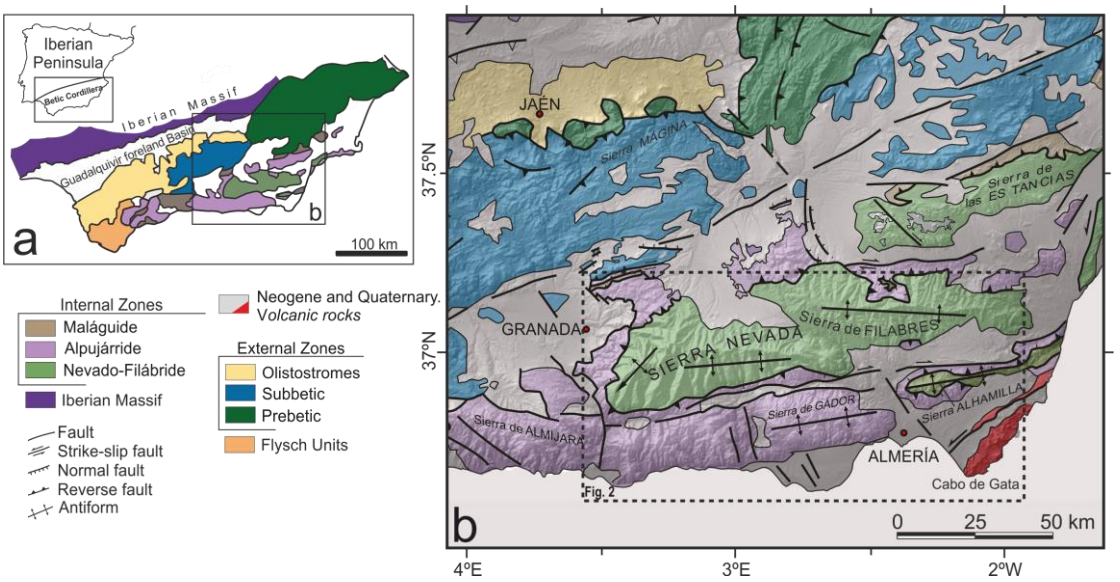

Fig. 5.1 Geological setting of the central and eastern Betic Cordillera. a) Geological sketch of the Betic Cordillera. b) Geological map with main geological structures.

In the Betic Cordillera of southern Spain (Fig. 5.1), intramontane basins developed due to relief uplift since the late Tortonian (Braga et al. 2003; Sanz de Galdeano and Alfaro 2004; Pedrera et al., 2007). Elongated basins are often close

to the highest reliefs of the Internal Zones. The interaction between faults and folds in the Betic Cordillera gave rise to the formation of superimposed intramontane basins (Galindo-Zaldivar et al. 2003). In the Central-Eastern Betic Cordillera, three intramontane elongated basins intersect: the Alpujarran Corridor, the Tabernas basin and the Gádor-Almería basin. In this study, we denominate the intersection of these intramontane basins as the Alhabia basin (Fig. 5.2).

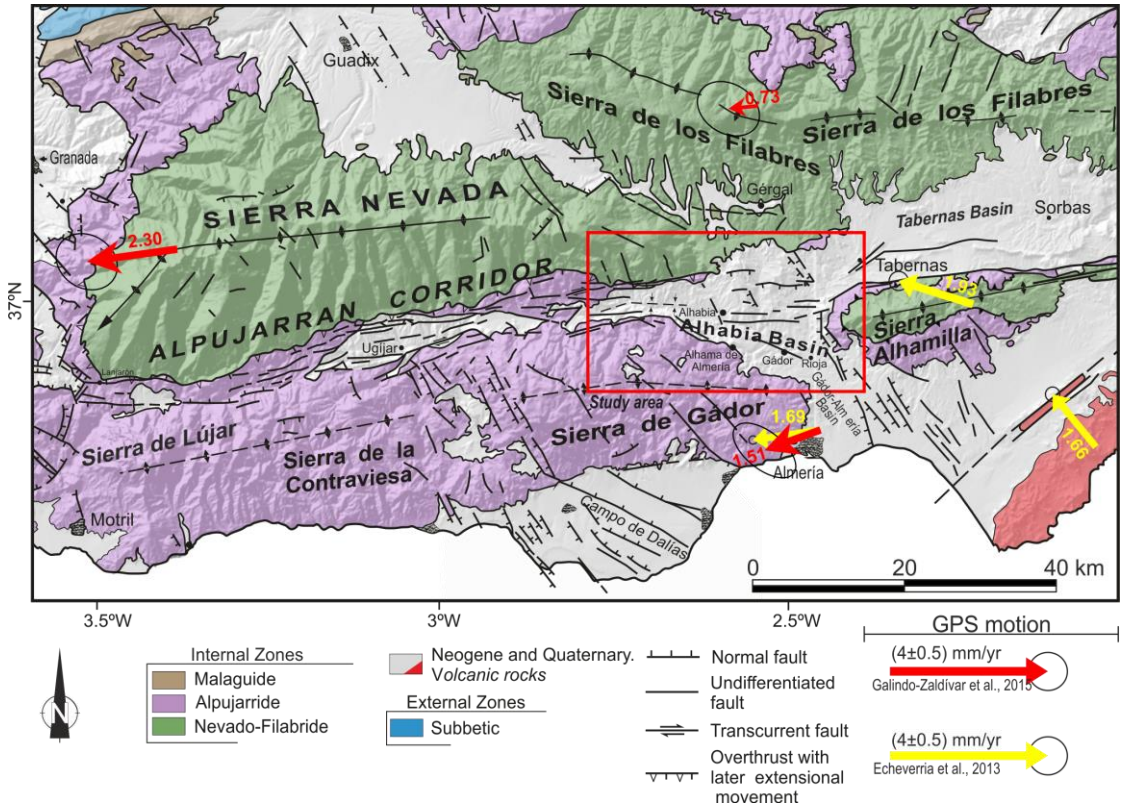

Fig. 5.2 Geological map of the Alhabia Basin including CGPS (red) and GPS (yellow) arrows with their 95% confidence ellipses, respectively from Galindo-Zaldivar et al. (2015) and Echeverría et al. (2013).

The Alpujarran Corridor is a mainly dextral-faulted synformal structure that separates the Sierra Nevada and the Sierra de Gádor antiforms (Sanz de Galdeano et al. 1985; Galindo-Zaldivar 1986; Sanz de Galdeano 1996; Rodríguez-Fernández et al. 1990; Martínez-Díaz 2000; García et al. 2003; Martínez-Díaz and Hernández-Enrile 2004; Martínez-Martínez 2006; Martínez-Martínez et al. 2006). The Tabernas basin is likewise a synformal structure, in this case separating the

Sierra de Filabres and Sierra Alhamilla antiforms, yet it is south-bounded by a southward-dipping dextral reverse fault zone (Sanz de Galdeano 1989; Giaconia et al. 2012). This basin has also been widely studied to better understand the cordillera evolution and the exhumation of metamorphic bedrock in the area (Weijermars et al. 1985; Do Couto et al. 2014). The Gádor-Almería basin, in turn, separates the Sierra de Gádor and Sierra Alhamilla antiforms, and is formed by NW-SE normal faults (Marín-Lechado et al. 2005; Pedrera et al. 2006). GPS research provides evidence that the region is affected by a westward displacement with regard to the stable Iberian Massif (Fig. 5.2) (Echeverria et al. 2013; Galindo-Zaldivar et al. 2015).

Although these basins have been previously studied from tectonic and stratigraphic points of view, applications of geophysical prospection to determine their structure are scarce. Gravity research has been undertaken in the central Alpujarran Corridor (Ruiz-Constán et al. 2013), in the eastern Tabernas basin (Li et al. 2012; Do Couto et al. 2014) and in the Gádor-Almería basin (Pedrera et al. 2006), but to date it does not cover the intersection of these three elongated basins.

The aim of this paper is to stablish the geometry of the Alhabia basin and discuss its tectonic evolution. To constrain the variation in thickness of the sedimentary infill, we carried out gravity measurements along several profiles and performed 2D forward models. These new geophysical data enable us to evaluate the influence of recent and active faults and folds on the latest tectonic evolution of the Betic Cordillera. This field example illustrates the importance of elongated intramontane basins to elucidate the cordilleras regional evolution.

5.2 Geological setting

The Betic Cordillera is located in the westernmost part of the Mediterranean Alpine Orogen (Fig. 5.1). Its origin lies in the Africa-Eurasia plate convergence, thereby constituting an example of continental collision (Ruiz-Constán et al. 2012). Two main controversial models have been proposed to explain this orogen formation: models based on subduction with associated roll-back detachment of

the subducting slab (Ruiz-Constán et al. 2011; González-Castillo et al. 2015) and models based on lithospheric delamination of subcontinental lithosphere beneath the Alboran Sea (Calvert et al. 2000; Mancilla et al. 2013). The Betic Cordillera is divided into the Internal and External Zones and the Flysch Units. The Internal Zone comprises three main metamorphic complexes of Palaeozoic and Mesozoic rocks —from bottom to top, the Nevado-Filábride, Alpujárride and Maláguide complexes— in addition to the Pre-dorsal and Dorsal complexes (Azañón et al. 2010).

During lower Serravallian, in a first stage of relief development along the South Iberian Margin, the Mediterranean Sea and the Atlantic Ocean were connected by the North-Betic Strait —located at the former Guadalquivir basin (Sanz de Galdeano and Vera 1991, 1992)— and the North-Betic basin (Soria 1988). From the late Miocene to the Quaternary, most of the intramontane basins became isolated by the continuous deformation related to Africa-Eurasia convergence (Vera 2000).

The large relief of Sierra Nevada, Sierra de Filabres, Sierra de Gádor and Sierra Alhamilla were uplifted by E-W to NE-SW antiforms during the Miocene, and E-W dextral faults developed (Sanz de Galdeano 1996), creating synformal depressed areas such as the Alpujarran Corridor and the Tabernas basin (Weijermars et al. 1985; Sanz de Galdeano and Alfaro 2004; Pedrera et al. 2012). In addition, E-W normal faults with a dextral component affected Neogene-Quaternary sediments along the eastern Alpujarran Corridor (Sanz de Galdeano et al. 2010). Moreover, E-W reverse-dextral faults deform the southern border of the Tabernas basin (Sanz de Galdeano 1989; Giaconia et al. 2012). NW-SE normal faults in the study area are located between Sierra de Gádor and Sierra Alhamilla, contributing to the formation of the Gádor-Almería basin and merging it with the Alpujarran Corridor and the Tabernas basin (Pedrera et al., 2006; Marin-Lechado et al. 2005).

Unconformable sediments fill the intramontane basins developed in between these sierras (Fig. 5.2). In the Alhabia basin, the lowest sediments correspond to

Burdigalian to Serravallian patches (Kleverlaan 1987, 1989). Atop these sediments, late Tortonian calcareous sandstones and marly calcarenites were unconformably deposited (Ruegg 1964), followed by Messinian reefs in the southwesternmost part. The upper Messinian deposits include evaporites, covered by Pliocene continental conglomerates, sands and silts (Martin and Braga 1994). During the latest Pliocene and the early Pleistocene, the study area was emerged and deposits developed only in rivers and ravines.

5.3 Methods

Gravity prospecting was carried out to estimate the Alhabia basin geometry. The measurement site positions were determined by means of differential GPS. In addition, direct field observations (Fig. 5.3) helped to link the outcropping tectonic structures to the deep basin geometry.

Gravity prospecting makes it possible to determine the geometry of bodies with contrast of density. Sedimentary infill of the Alhabia basin has lower density than the metamorphic basement. A total of 475 new gravity measurements were obtained, mainly along N-S and NE-SW profiles, roughly orthogonal to the main tectonic features and basin boundaries and along the most accessible paths. Some additional stations between the profiles were considered to improve the gravity anomaly maps (Fig. 5.4). The gravimeter used was a Scintex Autograv CG-5, which has 1 μGal of accuracy. The obtained measurements were referred to the absolute gravity station of Granada (National Geographical Service of Spain, IGN, www.ign.es). Free Air, Bouguer and Terrain corrections were calculated for each gravity site using a standard terrain density of 2.67 g/cm3 (Martínez-Moreno et al. 2016). The Terrain correction was derived combining the methods developed by Kane (1962) and Nagy (1966) up to 160 km around each gravity site, using the 5 m accuracy DEM provided by the IGN (www.ign.es). After applying corrections, the Bouguer anomaly map of the study area was obtained (Fig. 5.4a). The regional anomaly map (Fig. 5.4b) was obtained by kriging the gravity data located in the bedrock (Martínez-Moreno et al. 2015). The residual

anomaly map was derived from the difference between the Bouguer and the regional anomaly maps (Fig. 5.4c).

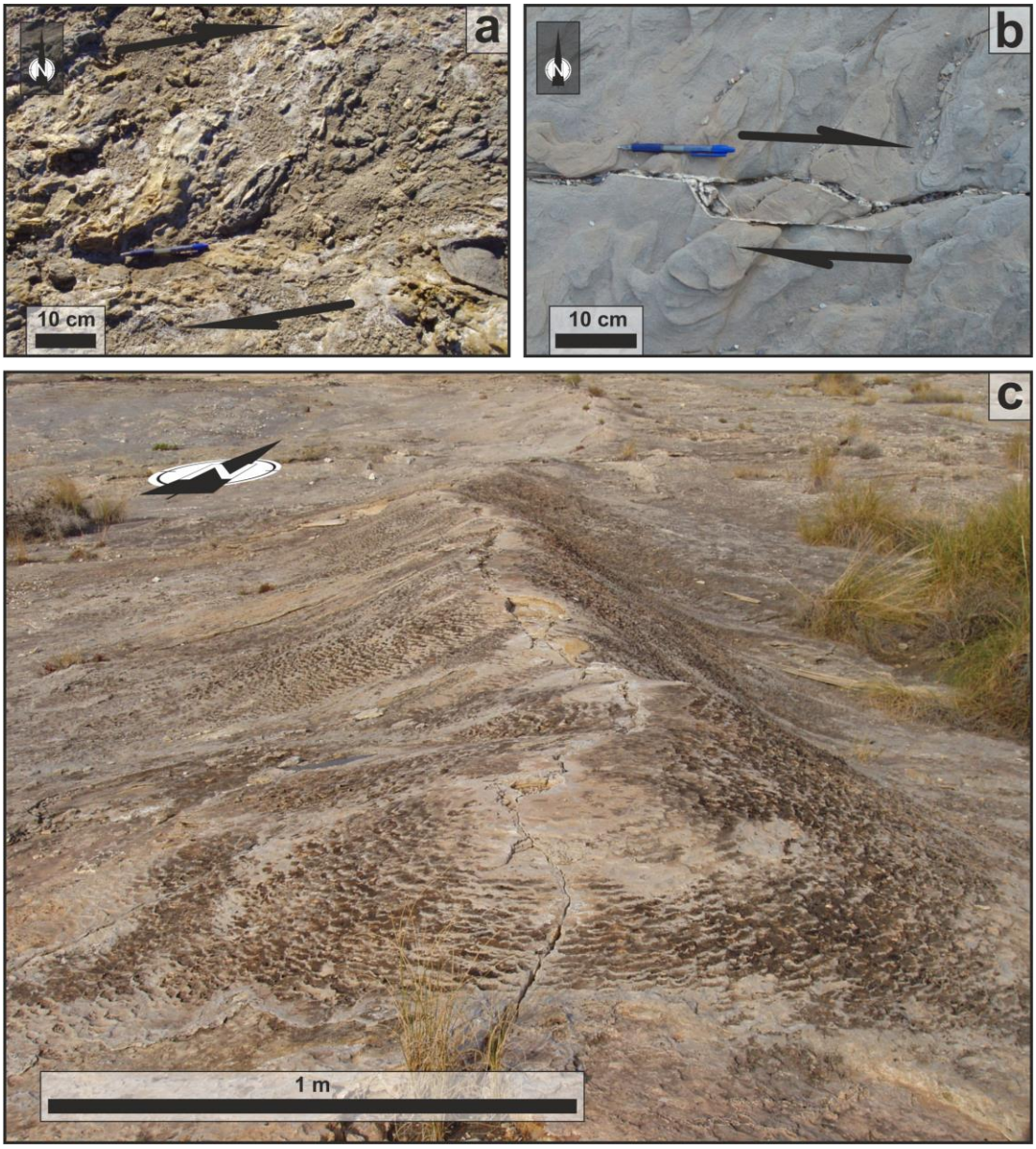

Fig. 5.3. Field examples of tectonic structures. a) S-C and b) dextral off-set seen in plain view on Miocene sediments. c) Example of present-day travertines related to a NW-SE trending fracture in the northeast part of the Alhabia Basin.

2D forward models were obtained using GravMag v.1.7 software (Pedley et al. 1993). The densities used to model were 2.25 g/cm3 for the sedimentary infill and 2.67 g/cm3 for the bedrock, in view of previous studies in the area (Marín-Lechado et al. 2007; Pedrera et al. 2009; Li et al. 2012; Ruiz-Constán et al. 2013; Do

Couto et al. 2014), and according to standard values (Telford et al. 1990). In addition, we present alternative gravity models to assess the uncertainty in the sedimentary infill thickness determination, considering the maximum and minimum possible density values (from 2.00 to 2.40 g/cm3). In any case, an average 2.25 g/cm3 density for the sedimentary infill has been estimated to provide the most suitable results. The standard deviation (SD) and RMS error have been calculated for each gravity model with the proposed sedimentary infill density at 2.25 g/cm3 (Fig. 5.5).

5.4 Structure of the Alhabia basin

5.4.1 Field observations on main faults

E-W and NW-SE faults are superposed in the Alhabia basin, although they have different ages (Sanz de Galdeano et al. 2010). E-W faults are common in the northern part of the study area, affecting the Alpujarran Corridor and Tabernas basin sediments. These faults present mainly dextral and locally normal slip, evidenced by striae together with S-C fabric and stretch marks affecting the Miocene and Pliocene sediments (Fig. 5.3a and b). Quaternary sediments are clearly affected by recent faults in the Alpujarran Corridor´s central part (García-Tortosa and Sanz de Galdeano 2007). The NW-SE normal faults, however, present mainly dip slip. They are located in western part of the Tabernas basin and in the Gádor-Almería basin, deforming the sediments between Sierra de Gádor and Sierra Alhamilla (Marín-Lechado et al. 2005). These faults activity probably started during Tortonian time, affecting up to Quaternary sediments and allowing the development of travertines up to present times (Fig. 5.3c).

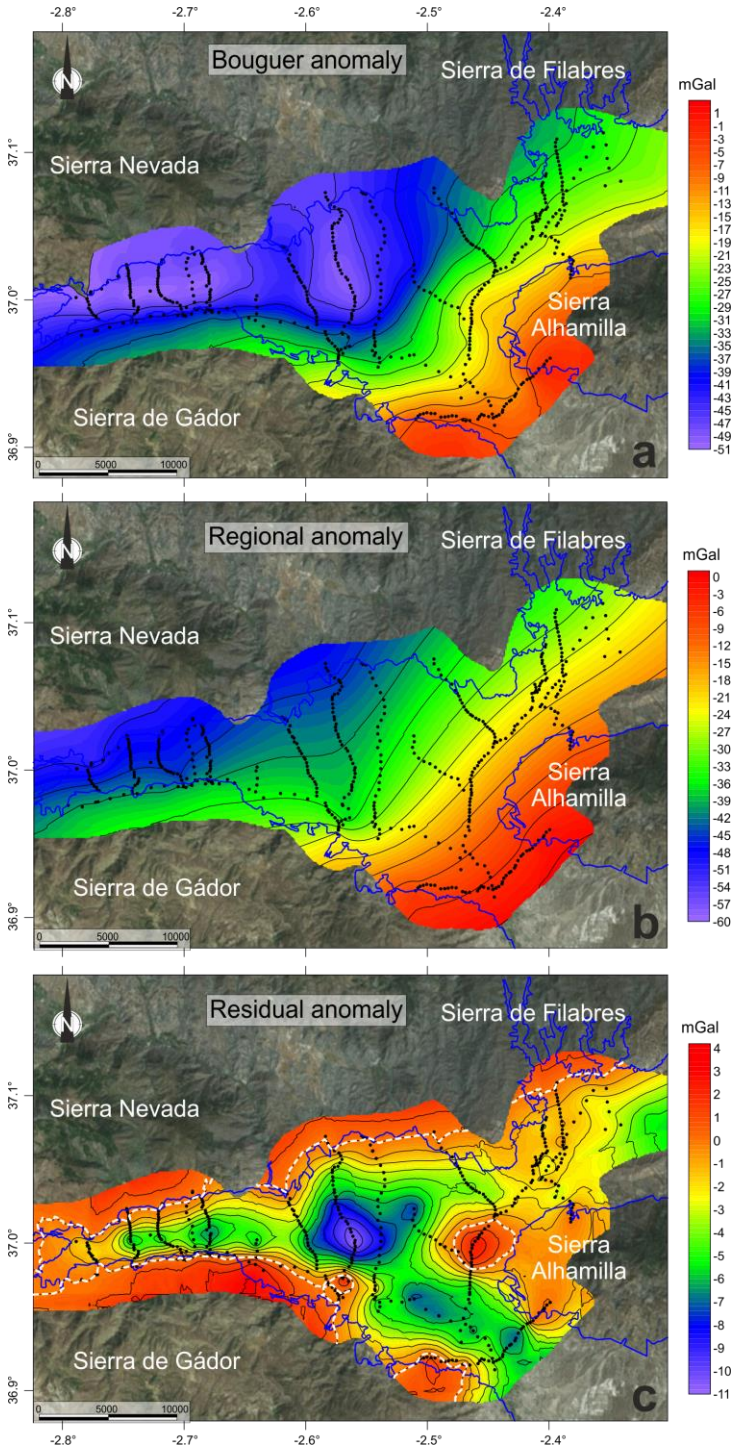

Fig. 5.4 Gravity anomaly maps. Black dots show the location of gravity measurements and blue line indicates the basin's boundaries. a) Bouguer anomaly map and its separation into b) regional anomaly map, and c) residual anomaly map. White-dashed line shows the residual anomaly 0 value.

5.4.2 Basin infill geometry from gravity research

The values of the Alhabia basin Bouguer anomaly map (Fig. 5.4a) are between -51 and -2 mGal in agreement with regional Bouguer maps (e.g. IGN, 1976; Ayala et al. 2016). Still, this map does not provide much information about the sedimentary infill because of the masking effect of the intense regional anomaly

(Fig. 5.4b) related to southeastward crustal thinning from the Betic Cordillera towards the Alboran Sea (Torné and Banda 1992). The residual anomaly (Fig. 5.4c) values are between -10.6 and 2.3 mGal, and the 0 mGal line roughly coincides with the basin limits. It presents a cross-shaped minimum within the Alhabia basin, where the elongated basins merge together. Each branch of this cross-shaped minimum point to relative elongated minima, related to the Tabernas basin (eastward), the Gádor-Almería basin (southward), and the Alpujarran Corridor (westward). The northern branch, however, points to Sierra de Filabres and is poorly developed. The anomaly westward Tabernas basin and between Sierra Nevada and Sierra de Filabres is very minor, supporting a thinner sedimentary cover.

Three residual gravity anomaly profiles were modelled to highlight the structure of the gravity minima related to the western and southern depocentre branches (Fig. 5.5). The N-S profiles (P1 and P2 in Fig. 5.5a) transect the Alpujarran Corridor´s westernmost part, from Sierra Nevada to Sierra de Gádor, whereas the NE-SW profile (P3 in Fig. 5.5a) cross-cuts the Gádor-Almería basin from Sierra de Gádor to Sierra Alhamilla. Profile 1 is asymmetric, with a gradual residual anomaly decreasing southward from Sierra Nevada, reaching a minimum value of -7 mGal, yet showing an abrupt increase towards the Sierra de Gádor. Profile 2 is located the eastern Alhabia basin and presents a pronounced minimum of -10.6 mGal displaced southwards. A noteworthy characteristic of this profile is the presence of a local maximum of 2 mGal in the southern part of the sedimentary infill. Profile 3 is also asymmetric, presenting its minimum value displaced towards the NE. There is a gradual decrease in value of -7.5 mGal from Sierra de Gádor eastwards, with an abrupt increase at the Sierra Alhamilla boundary.

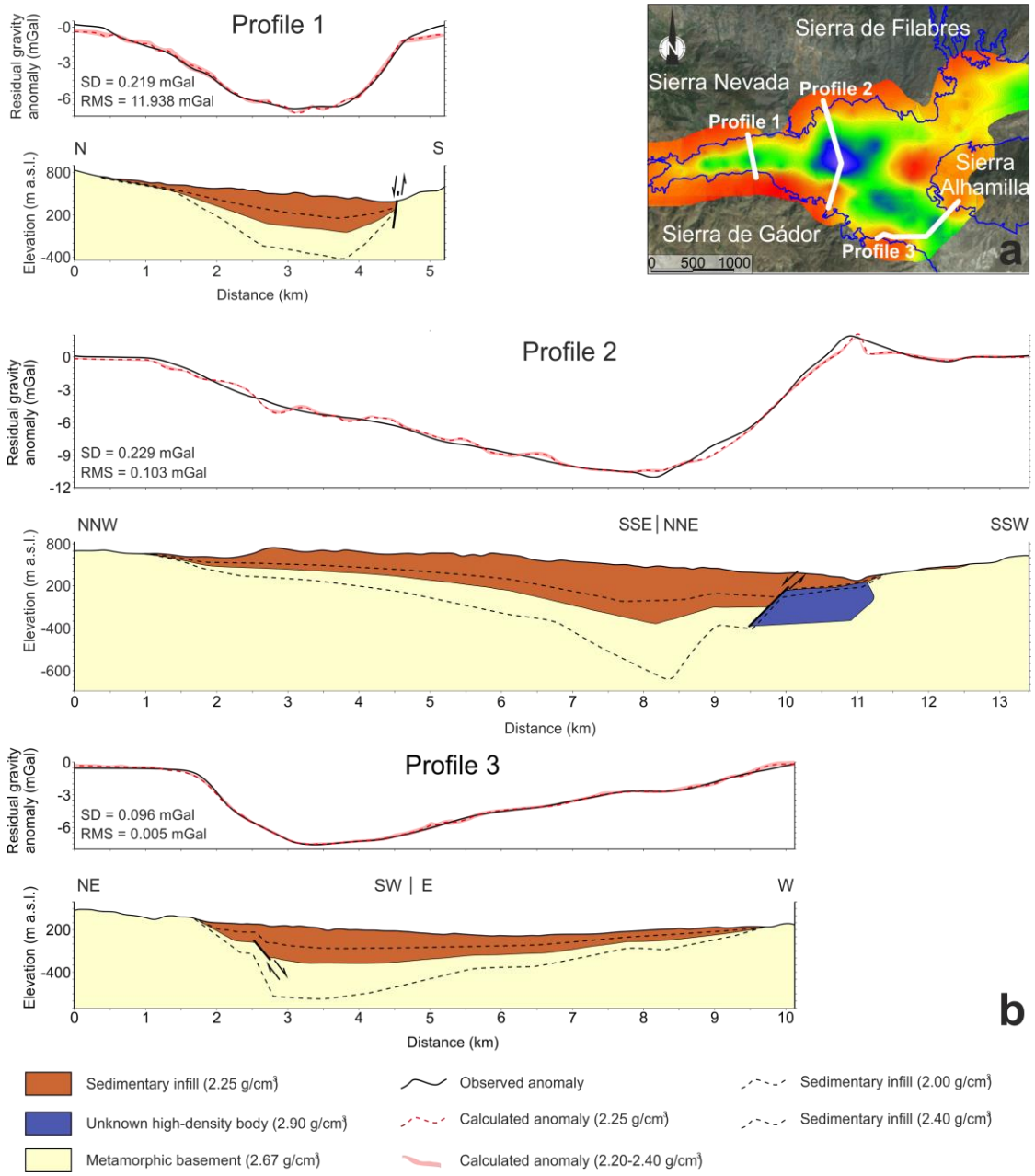

Fig. 5.5 Gravity survey modelling in the study area. a) Location of residual anomaly profiles and b) their observed/calculated residual anomaly fitting (top) with their related models (bottom).

Gravity models for profiles 1, 2 and 3 (Fig. 5.5) reveal the sedimentary infill geometry (2.25 g/cm3) on top of the metamorphic basement (2.67 g/cm3). The positive residual anomaly maximum at ~11 km length in profile 2 suggests the presence of a high density body (2.9 g/cm3) in the southern part of the metamorphic basement.

5.5 Discussion

The Alhabia basin illustrates the interaction and evolution of tectonic structures in complex collisional orogens, with the development of cross-cutting elongated basins. Intramontane basins are the shallow expression of crustal deformation in collisional contexts. The Betic Cordillera Internal Zones was deformed by several tectonic structures favouring the development of elongated basins. In the Alhabia basin, the E-W Alpujarran Corridor —in continuity to Tabernas basin— is connected to the NW-SE Gádor-Almería basin (Fig. 5.2). The Alpujarran Corridor formed as a faulted synformal structure between Sierra Nevada and Sierra de Gádor antiforms due to the N-S to NW-SE Africa-Eurasia convergence (Sanz de Galdeano et al. 1985; Galindo-Zaldivar 1986; Sanz de Galdeano 1996; Martínez-Díaz and Hernández-Henrile 2004; Martínez-Martínez 2006). Faults developed afterwards, with normal and dextral components, due to extension orthogonal to the NW-SE compression that was probably related to the relief uplift (García-Tortosa and Sanz de Galdeano 2007).

The Tabernas basin appears to have a similar initial evolution, in connection with the Alpujarran Corridor (Do Couto et al. 2014; Li et al. 2012). However, it features the remarkable presence of a dextral-reverse fault zone at its southern boundary and the absence of active N-S extension recorded in the Alpujarran Corridor. The Gádor-Almería basin, situated between Sierra de Gádor and Sierra Alhamilla, is bounded by highly active NW-SE normal faults with related seismicity; they propagate northwestward and cross-cut the former E-W Alpujarran Corridor and the Tabernas basin (Sanz de Galdeano et al. 2010). Main fractures facilitate deep circulation and the presence of travertine deposits in the Alhabia basin (Sanz de Galdeano et al. 2008) (Fig. 5.3c).

The new gravity data reveal the deep Alhabia basin infill geometry. It is noteworthy the cross-shape structure of the depocentre that extends towards the Alpujarran Corridor and the Gádor-Almería basin. Two branches have scarce sedimentary infill: the eastern Tabernas basin and the northern branch towards Sierra de Los Filabres. Three geological models based on gravity data highlight

these basins main characteristics. The model in profile 1 (Fig. 5.5) reveals that the sedimentary infill accumulated in a synformal structure with a southward-displaced hinge zone, reaching a maximum sedimentary thickness of 450 m. In addition, an E-W normal highly dipping fault is located at the southern boundary of the basin. The model for profile 2 also reveals the thickest sedimentary infill of a synformal structure, reaching 800 m. The high density body (2.9 g/cm3) in the metamorphic bedrock related to the positive residual anomaly maximum at 11 km length may be related to mineralizations. This model also supports the presence of faults cross-cutting the southern part of the basin and causing the bedrock to crop out abruptly. Model 3 shows sedimentary infill gradually increasing in thickness toward the NE until reaching 500 m at 7 km from the beginning. Then, around Sierra Alhamilla a high-angle normal fault separates the sedimentary infill from the metamorphic basement (Fig. 5.2).

The gravity models reveal the asymmetry of the synform in the Alpujarran Corridor, with a depocentre located close to the south boundary. This asymmetry is consistent with the northward vergence observed in Sierra Nevada and Sierra Alhamilla folds (Jabaloy et al. 1993; Marín-Lechado et al. 2007; Pedrera et al. 2009). The presence of high-angle faults is also remarkable both in the southern part of the Alpujarran Corridor, with E-W orientations, and in the Gádor-Almería basin, NW-SE oriented. Together with the asymmetric synformal structures, these faults interacted and contributed to superimposed basin formation and to the uplift of the surrounding reliefs.

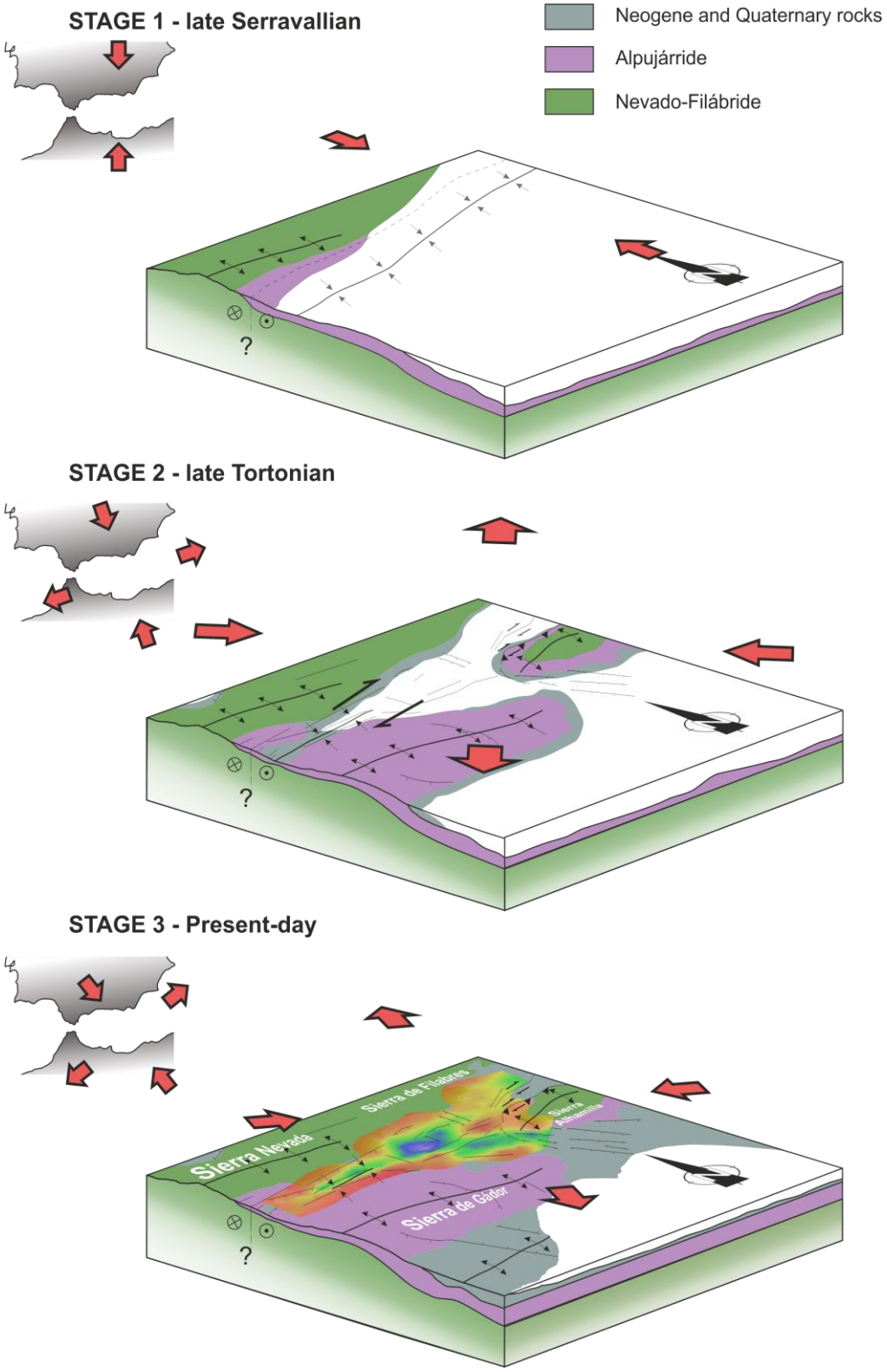

Fig. 5.6 Tectonic evolution in the Alhabia basin related to the Africa-Eurasia convergence changes over time. a) Geodynamic setting in the Alhabia Basin in late Serravallian, b) late Tortonian, and c) present day stages. The gravity residual anomaly map is superposed in the present day sketch.

Active surface deformation is revealed by continuous GPS (Galindo-Zaldivar et al. 2015) and non-permanent GPS networks (Echeverría et al. 2013) (Fig. 5.2). They suggest differential displacements of the metamorphic blocks that surround the intramontane basins. Sierra de Filabres remains steady with respect to the Iberian Massif. Western Sierra Nevada moves westwards, with no major recent structures separating it from Sierra de Filabres. This motion has been interpreted as a widespread E-W stretching of the metamorphic basement due to the presence of N-S to NW-SE extensional joints (Galindo-Zaldivar et al. 2015), although it may also be favoured by the activity of the northwestward-propagating faults of the Gádor-Almería basin. Sierra de Gádor moves west-southwestward, according to the Alpujarran Corridor faults dextral and extensional character, evidencing the end of the synform development. Sierra Alhamilla moves towards the northwest, accommodating this displacement with reverse and dextral faults at its northern boundary, perhaps in conjunction with the latest stages of folding. Normal faults at the western edge determine the opening of the Gádor-Almería basin (Fig. 5.6).

Although basin superposition is a common phenomenon in collision orogens, most studied examples correspond to superimposed grabens as in the Balkan Peninsula (Zagorčev 1992) or the Anatolian Fault Zone (Gürer et al. 2001; Yilmaz and Gelisli 2003; Tari et al. 2014). However, in the Betic collision orogen, the elongated basin development is a consequence of the interaction between synform and faults. Metamorphic rocks crop out along antiforms that are separated by faulted synformal structures which, due to the relatively thinner crust, represent the weakest and most easily deformable areas to be faulted.

5.6 Conclusions

The Alhabia basin is a remarkable example of interacting elongated intramontane basins in a collisional orogen formed along main crustal weakness zones. According to new gravity data, field tectonic observations, and GPS motions, the recent deformations related to the E-W Alpujarran Corridor and the Tabernas

basin intersection, together with the NW-SE oriented Gádor-Almería basin, produced a cross-shaped depocentre. In the context of Africa-Eurasia convergence, N-S compression formed large asymmetric folds verging northwards during late Serravallian-early Tortonian (Martín-Algarra et al. 2009). Counter-clockwise rotation of stresses to NW-SE compression, also including orthogonal extension, determines the propagation of new folds (Sierra de Gádor and Sierra Alhamilla), as well as the development of dextral strike-slip faults and NW-SE trending normal faults since late Miocene times. Faulted synform developed E-W elongated sedimentary basins whose depocentres are located in the central or southern part. This setting favoured the E-W dextral and reverse fault formation in the weak crustal zone. At this stage, Sierra Alhamilla and Sierra de Gádor antiforms, were separated by a synformal faulted structure. In this framework, Sierra de Filabres would be attached to the stable Iberian Massif, whereas Sierra Nevada moves westward, Sierra de Gádor southwestward, and Sierra Alhamilla northwestward. These displacements agree with recent fault activity affecting the elongated basins that intersect in the Alhabia basin, the activity of the Gádor-Almería basin normal faults being most remarkable. The Alhabia intramontane basin illustrates the tectonic structure interaction during late orogenic processes in a collisional mountain belt.

Acknowledgements

We acknowledge the comments of Dr. Fernando Bohoyo and Dr. Antonio Pedrera that highly improved this research. This study was funded by the CGL2016-80687-R and the RNM148 research group of the Junta de Andalucía.

CHAPTER 6

Active shallow extension in central and eastern Betic Cordillera from CGPS data

Tectonophysics 663 (2015) 290–301

Contents lists available at ScienceDirect

Tectonophysics

journal homepage: www.elsevier.com/locate/tecto

Active shallow extension in central and eastern Betic Cordillera from CGPS data

J. Galindo-Zaldivar [a,b,*], A.J. Gil [c,d], C. Sanz de Galdeano [b], M.C. Lacy [c,d], J.A. García-Armenteros [c,d], P. Ruano [a,b], A.M. Ruiz [c,d], M. Martínez-Martos [b], P. Alfaro [e]

[a] Dpto. de Geodinámica, Universidad de Granada. 18071 Granada, Spain.

[b] Instituto Andaluz de Ciencias de la Tierra (CSIC-UGR), 18071 Granada, Spain.

[c] Dpto. Ing. Cartográfica, Geodesia y Fotogrametría, Universidad de Jaén. Campus de las Lagunillas, 23071 Jaén, Spain.

[d] Centro de Estudios Avanzados en Ciencias de la Tierra (CEACTierra), Universidad de Jaén, Campus de las Lagunillas, 23071 Jaén, Spain.

[e] Dpto. Ciencias de la Tierra, Universidad de Alicante, San Vicente del Raspeig, Alicante, Spain.

ABSTRACT

The Betic Cordillera is an Alpine belt formed in the western Mediterranean by the westward displacement of the Alboran Domain in between the Eurasian and African convergent plates. New CGPS data from the central and eastern Betic Cordillera and its foreland —obtained mainly from the Topo-Iberia project— allowed us to precisely determine the rate of tectonic deformation. Most of the displacements of the central and eastern Betics are westward, with a variable southwestward component, in relation to the Eurasian stable plate. While in the Iberian foreland the displacements are extremely low, some deformation related to low compressional deformation occurs in the easternmost foreland basin and eastern Betic Cordillera. The displacement increases substantially southwards and westwards in relation to present-day extensional deformation. Major active discontinuities correspond to the NW-SE normal fault zones, which dip westwards; they are located in Almeria-Tabernas; Balanegra, and western Sierra de Gador; whereas the Padul fault zone located west of Sierra Nevada extends northwards to the Granada Basin. NW-SE extensional faults are also observed to the north, in the Baza Basin. Moreover, the activity of dextral faults along the Sorbas-Tabernas-Alpujarras-Guajares band, generally considered as a transfer fault zone, is evidenced by the displacement data. These results come to demonstrate the low activity or inactivity of the large northern E-W oriented folds of the central and eastern Internal Zone, such as the Sierra de Los Filabres antiform. They also point to the possible residual activity of the northern part of the NE-SW Sierra Nevada antiform, where the maximum relief of the Cordillera is found. Altogether, our data support a heterogeneous present-day westward extension that affects the upper crust of the Betic Cordillera and increases towards the thinned continental crust of the Alboran Sea and towards the west, is compatible with roll-back subduction along the Gibraltar Arc.

Keywords: Continuous GPS; Active deformation; Extensional tectonics; faults and folds; SE Iberian Peninsula.

HIGHLIGHTS

- Displacements to the W and SW occur in the Betics with respect stable Eurasia.

- Deformations are mainly concentrated along NW-SE oriented normal fault zones.

- E-W dextral faults and, locally, NE-SW folds continue to be active.

- Large E-W folds of the northern Internal Zone are scarcely active or inactive.

- Extension is related to Gibraltar Arc subduction roll-back.

6.1 Introduction

Geodetic techniques provide the most accurate means of quantifying the deformation of the Earth´s surface. GPS networks serve to characterize the tectonic activity of vast areas (Dixon, 1991; Hager, 1991). The use of continuous GPS measurement during long periods in stable sites highly reduces the error when determining displacement.

The Betic Cordillera along with the Rif constitute the Gibraltar Arc. It surrounds the Alboran Sea and represents the main Alpine belt in the westernmost Mediterranean. The development of this arcuate orogen is due to interaction of the Eurasian and African plates, which undergo an oblique dextral convergence of 4.5 mm/yr (Argus et al., 1989; DeMets et al., 1990, 1994), and the westward motion in between of the Alboran domain (Alboran plate of Andrieux et al., 1971). In arcuate orogens the trend of convergence and extension help determine behavior, but the trend may also be largely oblique to crustal buldges (Fernández-Ibáñez and Soto, 2008). Processes of subduction (Blanco and Spakman, 1993; Royden, 1993; Zeck, 1996; Lonergan and White, 1997; Gutscher et al., 2002; Spakman and Wortel, 2004; Pedrera et al., 2011; Ruiz-Constán et al., 2011) and delamination (Platt and Vissers, 1989; García-Dueñas et al., 1992; Docherty and Banda, 1995; Seber et al., 1996; Calvert et al., 2000; Fadil et al., 2006; Mancilla et al., 2013) have been invoked for the development of this orogenic belt. After Alpine crustal thickening and up to middle Miocene times, the region has undergone both extensional tectonics in the Internal Zone (Galindo-Zaldívar et al., 1989; García-Dueñas et al., 1992; Jabaloy et al., 1992) and dextral transcurrence in relation to the External Zone (Sanz de Galdeano, 1990). Late Miocene sediments sealed the Internal-External zone boundary, and the region has undergone recent uplift (Braga et al., 2003).

Previous GPS studies in the area are largely focused on delimiting the sharp geometry of the plate boundary (Fernandes et al., 2007; Vernant et al., 2010; Koulali et al., 2011) and have poor regional coverage. The region is affected by a band of seismicity and active deformation that is over 300 km wide, meaning that

the plate boundary corresponds to a broad deformation zone (Buforn et al., 2004). The Topo-Iberia project provided for an improved observation network, including intermediate sites in key sectors (Garate et al., 2014). Still, CGPS studies focused on the Cordillera (Pérez-Peña et al., 2010a; Koulali et al., 2011; Garate et al., 2015) lack a detailed description of the relationships with main active tectonic structures. González-Castillo et al. (2015) analyze the relationships of the CGPS displacements and the active tectonics of the western Betic Cordillera and its foreland.

The aim of this contribution is to present new CGPS data observed during the Topo-Iberia project and integrated with other available sites, in order to better constrain the active motions of the central-eastern Betic Cordillera in relation to the foreland. Our data highlight the location of the main active tectonic structures —mainly faults— which are presented in detail. Finally, on the basis of all the data, an enhanced regional model is proposed for the cordillera development.

6.2 Geological setting

The Betic Cordillera (Fig. 6.1) belongs to the Alpine belt of the westernmost Mediterranean. The Betic and Rif cordilleras are connected through the Gibraltar Arc, and they surround the Alboran Sea. The Betic Cordillera comprises (García-Dueñas and Balanyá, 1986) the Internal (Alboran Domain) and External (South Iberian Domain) zones, the Flysch units, and Neogene-Quaternary basins (Sanz de Galdeano, 1990). The Internal Zone contains three main overprinted metamorphic complexes with Paleozoic and Mesozoic rocks —from bottom to top, the Nevado-Filábride, the Alpujárride and the Maláguide complexes— in addition to the Dorsal and Predorsal complexes. The Flysch units correspond mainly to siliciclastic sediments of Oligocene to Miocene age separating the Alboran and South Iberian domains. The External Zone (South Iberian Domain) constitutes a fold-and-thrust belt that deformed carbonate sedimentary sequences of Mesozoic to Cenozoic age, locally including Mesozoic volcanic rocks. Wide olistostromic deposits in its frontal area are known as the Trias de

Antequera or frontal mélange (Perconig, 1960-62; Peyre, 1974; Pérez-López and Sanz de Galdeano, 1994; Roldán-García, 1994).

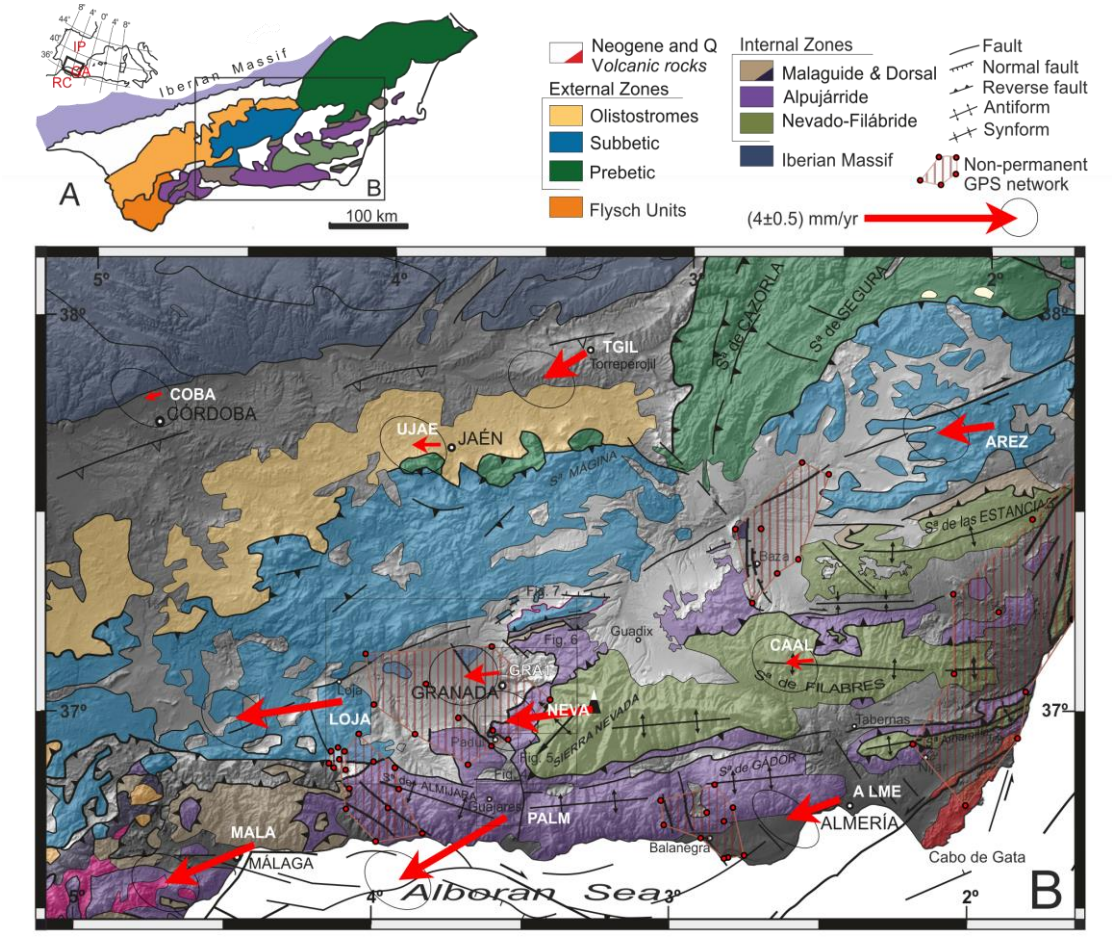

Fig. 6.1 Geological setting of the Eastern Betic Cordillera and GPS sites. A. Location of the Betic Cordillera. IP, Iberian Peninsula. GA, Gibraltar Arc. RC, Rif Cordillera.B. Geological sketch of the study area including main tectonic structures, non-permanent GPS networks and CGPS data with residual velocity field with respect to the Eurasia fixed reference frame and 95% confidence ellipses. Locations of Fig. 4, 5, 6 and 7 are indicated.

The main deformation in the Betic Cordillera stems from the Cretaceous and implies large dextral displacements in between the External and Internal zones (Sanz de Galdeano, 1990). Their contact is covered by sedimentary rocks since the Late Miocene. After the initial compressive stages, possibly reaching up to early Miocene, the Internal Zone was affected by intense NE-SW extensional tectonics.

These deformations produced crustal thinning, the exhumation of the metamorphic complexes, and the development of low-angle normal faults with top-to-the-SW displacement (Galindo-Zaldívar et al., 1989; Jabaloy et al., 1992; Galindo-Zaldívar et al., 2003).

The buildup of the present day relief occurs mainly since the Tortonian which is the result of the geodynamic setting: a horizontal N-S to NNW-SSE compression with perpendicular extension (Braga et al., 2003, Sanz de Galdeano and Alfaro, 2004). It is a consequence of the activity of E-W oriented dextral and normal faults, conjugate NW-SE dextral, and NE-SW sinistral and normal faults (Sanz de Galdeano, 1990) together with large E-W and NE-SW folds (Galindo- Zaldívar et al., 2003). There is a widespread development of Neogene-Quaternary intramontane basins (Granada and Guadix-Baza basins, among others). At the front of the Cordillera lies the Guadalquivir foreland basin, while the Alboran Sea, in between the Betic and Rif Cordillera, remains the largest Neogene and Quaternary basin developed on a thin continental crust. The foreland of the Cordillera is formed by the Variscan Iberian Massif that extends below the Betic Cordillera, as demonstrated by deep seismic reflection profiles and the continuity of magnetic anomalies (Galindo-Zaldívar et al., 1997).

Seismicity in the region is widespread, associated with the Eurasian- African plate boundary convergence (Buforn et al., 2004, Morales et al., 1997). Although most is shallow, there is also intermediate seismicity (up to 150 km depth) in the western Alboran Sea (Morales et al., 1999) and deep seismicity (650 km depth) south of Granada. Given the heterogeneous distribution of seismicity in the Betic Cordillera, it is not always possible to correlate it with the outcropping faults (Galindo-Zaldívar et al., 1999).

The deep structure of the central and eastern Betic Cordillera was derived from geophysical research. ESCIBETICAS deep seismic reflection profiles supported by gravity and magnetic data suggest the presence of a main crustal detachment that superposes the Betic Cordillera above the Iberian Massif (Galindo-Zaldívar et al., 1997; Ruano et al., 2004). The Moho is roughly flat below the Cordillera and

shows a moderate crustal thickening with respect to the Iberian Massif. A sharp crustal thinning towards the Alboran Sea is supported by gravity modelling (Casas and Carbó, 1990; Torné and Banda 1992). Seismic refraction and wide angle profiles (Banda et al., 1993), together with seismological research, support the presence of a major crustal discontinuity located west of Sierra Nevada and crossing towards the Granada Basin (Andeweg and Cloethingh, 2001; Mancilla et al., 2013). However, interpretations vary, some researchers proposing a sharp decrease towards the east in crustal thickness (Banda et al., 1993), others a sinistral fault zone (Andeweg and Cloethingh, 2001) or a tear fault related to slab delamination (Mancilla et al., 2013).

6.3 Previous geodetic studies

Regional GPS networks have been used to estimate the geodynamics of the Eurasian-African plate boundary (see Nocquet, 2012 and references therein). Plate model reconstruction is based on a NW-SE convergence of about 4.5 mm/yr between the Eurasian and African plates for the westernmost Mediterranean Sea (De Mets et al., 1990, 1994). In any case, the development of the Gibraltar Arc has largely modified the regional displacement patterns signalled by detailed GPS research.

Previous CGPS research (Fadil et al., 2006; Serpelloni et al., 2007; Vernant et al., 2010; Koulali et al., 2011) aimed to differentiate the main undeformed blocks separating the Eurasian and African plates. The westward motion of the Betic-Rif Cordillera was reported by Serpelloni et al. (2007) and further supported by the more detailed data of Perez-Peña et al. (2010a), who tried to relate the displacement to active tectonic zones. Vernant et al. (2010) and Mancilla et al. (2013) present scarce data for the Betics, indicating W and WSW displacements in the central and eastern regions. The most recent extensive compilation by Koulali et al. (2011) considers data between 1999 and 2009. Meanwhile, the latest results from the Topo-Iberia sites (2008-2013) (Garate et al., 2014) show that the most intense deformation of the Iberian Peninsula occurs in the central and eastern Betic Cordillera (Figs. 6.1 and 6.2). These new data provide for a more

precise appraisal of the direction and the motion rates put forth by Koulali et al. (2011), largely decreasing the error ellipses and adding new intermediate observation points.

Moreover, survey-mode local GPS networks were installed in the region to study the activity of key structures (Fig. 6.1). The CuaTeNeo network covers the south and central part of the Eastern Betic Shear Zone (Colomina et al., 1988; Echeverria et al., 2013). The Bajo Segura network is located by the NE end of the EBSZ (Sánchez-Alzola et al., 2014) and the Granada basin network was implemented in 1998 (Gil et al., 2002). Other GPS local networks control several active faults of the study area: the Padul fault (Ruiz et al., 2002; Gil et al., 2002), Zafarraya fault (Galindo-Zaldívar et al., 2003), Balanegra Fault (Marín-Lechado et al., 2010), or the Baza fault. By compiling these data, future research will manage to complete the picture of local tectonic displacements in the Cordillera, beyond the slow displacement rate established thus far.

6.4 GPS sites, data processing and velocity field estimation

This study presents the current GPS velocity field in the eastern Betic Cordillera derived from continuous GPS observations carried out from 1st March, 2008, up to 31th December, 2013. Analysis of the velocity field was based on a sub-network of 11 sites belonging to different Institutions. Stations AREZ, LOJA, NEVA, PALM, and TGIL pertain to the Topo-Iberia research project (http://www.igme.es/TopoIberia/default.html); ALME, COBA and MALA are stations of the Euref Permanent Network (http://www.epncb.oma.be) and in this case we have continuous GPS observations from 2004, 2005 and 2006 respectively; finally CAAL, GRA1 and UJAE are part of the Andalusian Permanent Network (http://www.ideandalucia.es/portal/web/portal-posicionamiento/rap). It is very important to underline that the locations of the Topo-Iberia sites are in open fields, not on buildings, and founded on bedrock, implying great stability of the concrete pillars and a high quality of observations.

The data analysis was performed using the Bernese Processing Engine (BPE) of Bernese 5.0 software, after checking the quality of data by means of TEQC

software developed by UNAVCO (Estey and Meertens, 1999). The options used to process GPS data are indicated in Garate et al. (2015). At the end of this step, one daily solution in a loosely constrained reference frame was estimated. The output file is composed of the coordinates of the stations along with their covariance matrix in SINEX format. Loosely constrained solutions can be combined regardless of the datum definition of each contributing solution. The solution reference frame is defined stochastically by the input data; although it is basically unknown, there is no need to estimate or to apply relative rigid transformations (rotation-translation-scale) for reference frames, which naturally leads to a combined solution not distorted by any constraint or transformation. Our daily loosely constrained cluster solutions were then merged into global daily loosely constrained solutions of the whole network, applying a classical least squares approach where the mathematical model is defined by the time propagation operator (Bianco et al., 2003). After that, the daily combined network solutions can be minimally constrained and transformed into the IGb_08 frame, estimating translations and scale parameters. In this particular case the realization EPN_A_IGb08 was used. The rigid plate motion is statistically inferred using a simple $\chi 2$ test-statistics to select the coherent subset of sites defining a stable plate. Beginning from some central European sites, in this case GRASS, GRAZ, SJDV and ZIMM, a total of 13 sites result assigned to the reference frame. These stations are: AJAC, BOR1, BUCU, CAGL, EBRE, GRAS, GRAZ, LAMP, MATE, NOT1, SFER, SJDV and ZIMM. Then, the velocity field was estimated from the IGb_08 time series of daily coordinates with the complete covariance matrix using ad hoc software (NEVE) that manages the stochastic model (Devoti et al., 2008, 2011). The time series of the 11 stations under study are included in Fig. 6.3. Velocities were estimated simultaneously, together with annual signals and sporadic offsets at epochs of instrumental changes. Velocity errors were derived through direct propagation of the daily covariance matrix and the formal errors of the GPS rates were scaled using the approach developed in Williams (2003). The IGb_08 solutions were transformed into the Eurasian Reference Frame using a pole estimated by NEVE with 13 stations. Specifically,

the absolute Eurasia pole and rotation rate are: 53.604º N, 100.465º W and 0.26097 ± 0.037 deg/Myr.

6.5 Displacements from new CGPS data

All the sites located in the eastern Betic Cordillera move towards the WSW at different rates with respect to stable Eurasia (Figs. 6.1 and 6.2; Table 6.1). There are great differences in rates, and limited yet relevant variability in terms of directions, determining areas of very high displacement gradients.

The most stable CGPS sites of the region are located in the Guadalquivir foreland basin. They show a very low westward displacement with respect to Eurasia (Table 6.1 and Fig. 6.1, COBA, 0.47 mm/yr; UJAE, 0.73 mm/yr), supporting the notion that this part of the region is in transition to the stable Iberian Massif. However, site TGIL, located in the easternmost Guadalquivir basin, shows a higher SW displacement of 1.32 mm/yr. In the northeastern region, AREZ (in the eastern Betic Cordillera external zones) has a WSW displacement of 1.51 mm/yr.

The CGPS stations CAAL and GRA1 respectively located in the Internal Zones of the Betic Cordillera and near the boundary with the External Zones, show very low westward motion; the very moderate SW components of 0.73 mm/yr and 0.95 mm/yr, respectively, are very similar to the relatively stable COBA and UJAEN sites of the Guadalquivir foreland basin.

Towards the south and west, the displacements are higher. In ALME (1.51 mm/yr), displacement is not only larger but it also has a moderate SW component with respect to CAAL. NEVA station (2.30 mm/yr) shows a displacement roughly parallel to the nearby GRA1 and the farthest CAAL stations, but with a higher westward component.

To the west and southwest, the highest rates are reached with WSW displacements in LOJA (2.84 mm/yr), MALA (2.53 mm/yr) and PALM (3.25 mm/yr), while the southwestward component increases towards the coastline.

6.6 Main recent and active tectonic structures related to CGPS displacements

The central and eastern Betic Cordillera are affected by folds and faults from Late Miocene to Present (Galindo-Zaldívar et al., 2006; Pedrera et al., 2011) (Figs. 6.1 and 6.2). In the Internal Zones, several kilometer-size late folds —generally open antiforms and synforms, with general E-W elongation— determine the present-day reliefs. An antiformal structure is located parallel to the coastline (Sierras de Lujar, Contraviesa, and Gádor), extending eastward toward the Sierra Alhamilla. There is geological evidence of recent folding, since the Late Tortonian or Messinian, in the Sierra Alhamilla antiform (Weijermars et al., 1985) or the Sierra de Gádor (Marín-Lechado et al., 2005), affecting up to the recent sediments of the Campo de Dalías (Marín-Lechado et al., 2005). To the north, a synform located along the Guajares-Alpujarras-Tabernas-Sorbas Basin is also affected by dextral faults (Sanz de Galdeano, 1996a; Martínez-Díaz and Hernández-Enrile, 2004; Martínez-Martinez et al., 2006).

Further to the north, the antiform of Sierra Nevada is in relay with the Sierra de Los Filabres antiform (Figs.1 and 2). The elevation of the Sierra Nevada antiform increases from the east, where it is characterized by E-W orientation, towards the west, where the maximum topographic height is reached and the fold axis turns to the NE-SW. However, the present-day activity of the large antiforms located northwards is only indirectly inferred from geomorphic data, e.g. Sierra Nevada (Perez-Peña et al., 2010b) or Sierra de Las Estancias (Pedrera et al., 2009). A roughly synformal structure separates Sierra Nevada and Sierra de Los Filabres, and there are no other main faults in between these two sierras. Only a widespread set of open tensional joints, generally NW-SE to N-S oriented, affect this area (Galindo-Zaldívar and González-Lodeiro, 1990).

The most relevant active and recent faults in the central Betic Cordillera overall are the NW-SE normal faults dipping generally toward the SW. From E to W, the southern part of the Cordillera contains the Almeria-Tabernas, Balanegra-western Sierra de Gador, and the Padul fault zones, the latter extending towards the Granada Basin. In addition, the Baza Fault is located to the north.

A significant NW-SE normal Almeria-Tabernas fault zone separates Sierra Alhamilla and Sierra de Gádor (Marín-Lechado et al., 2005) and extends northwards towards a tip point in southern Sierra de Los Filabres with related seismicity (Sanz de Galdeano et al., 2010). A roughly similar NW-SE oriented fault set likewise separates Sierra de la Contraviesa and Sierra de Gádor (Fig. 6.2) extending to the southeast as far as Campo de Dalias (Marín-Lechado et al., 2005). The activity of this fault is confirmed by high precision levelling data obtained in the Balanegra Fault Zone (Galindo-Zaldívar et al., 2013).

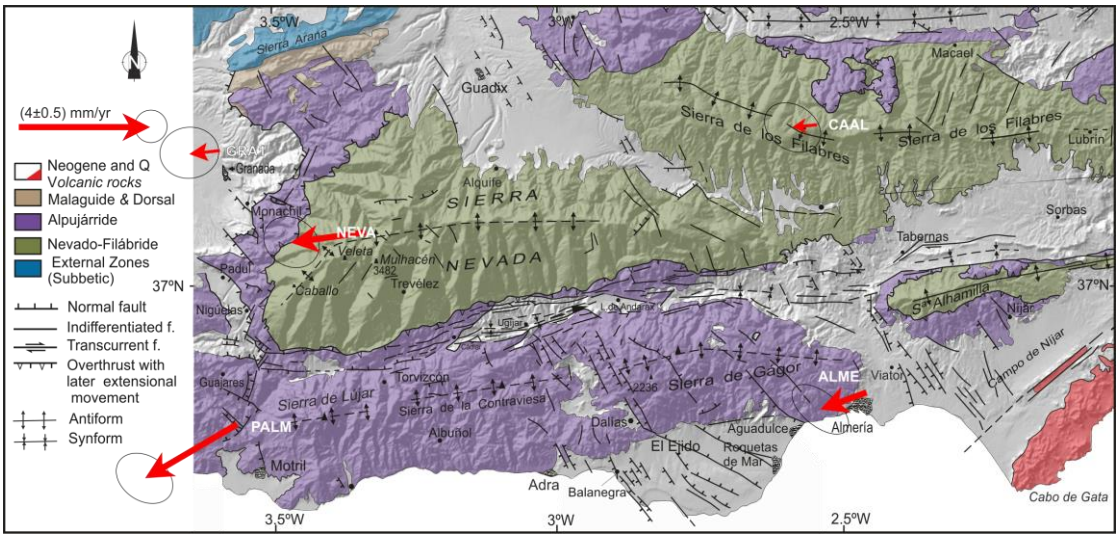

Fig. 6.2 Detailed geological sketch of the southeastern Betic Cordillera. Main tectonic structures are indicated. CGPS data with residual velocity field with respect to the Eurasia fixed reference frame and 95% confidence ellipses.

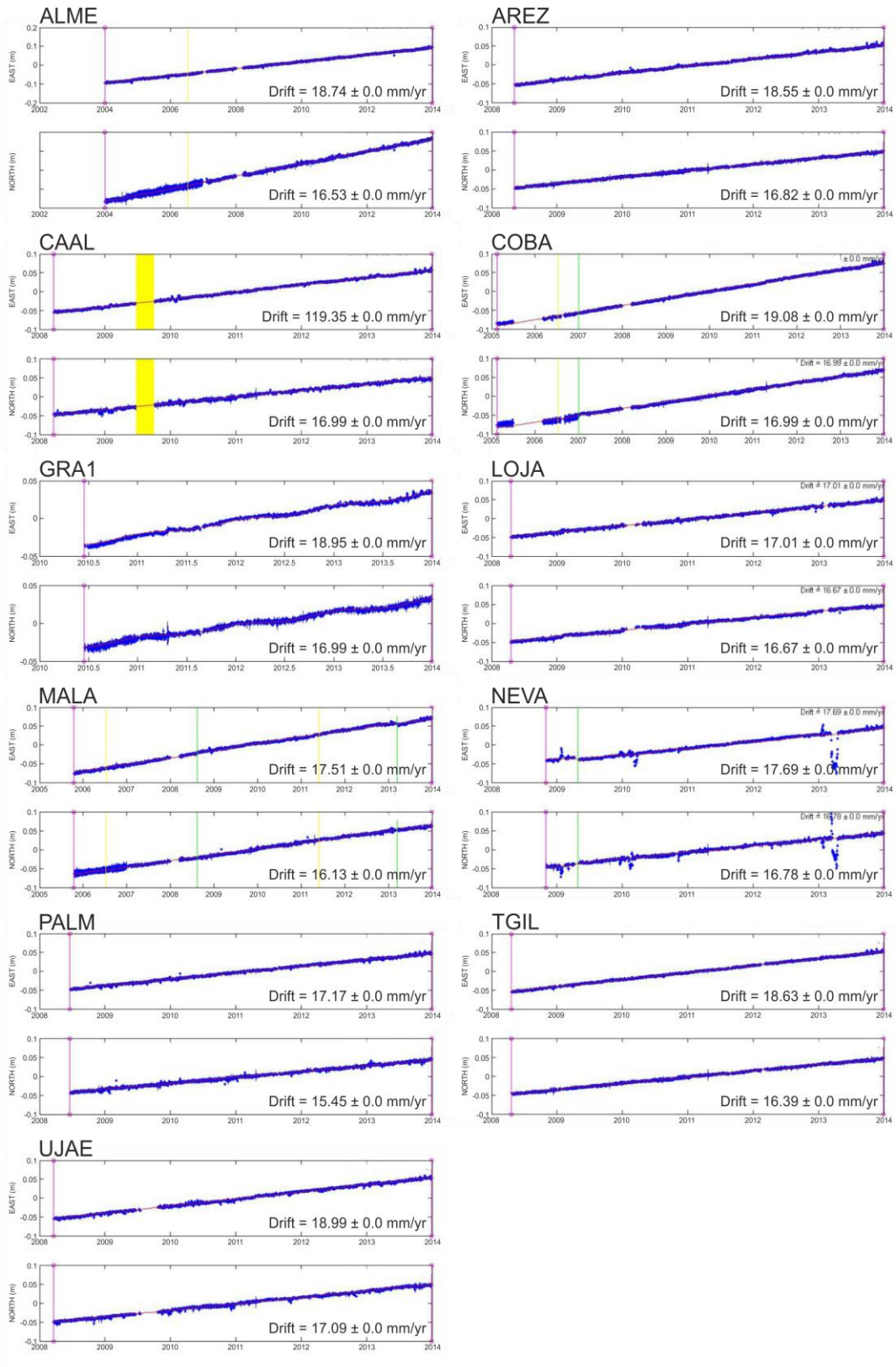

Fig. 6.3. Position time series of the network stations (North and East components in meters). Yellow lines are considered outliers according to the software applied. Absolute velocities are included in Table 6.1.

The above normal fault zones are bounded towards the north by the dextral faults located along the Alpujarras corridor (South of Sierra Nevada); they extend through the Tabernas basin along the northern boundary of Sierra Alhamilla (Fig. 6.2) (Sanz de Galdeano, 1990; Sanz de Galdeano et al., 2010) with roughly E-W orientation. This fault zone has been interpreted as a transfer extensional zone (Martinez-Martinez et al., 2006; Martinez-Diaz and Hernández-Enrile, 2004). To the west, towards the Los Guajares, the dextral zone becomes transtensive as well, in a conspicuous fault zone with minor faults of different orientations where fault surfaces are locally very well exposed (Fig. 6.4).

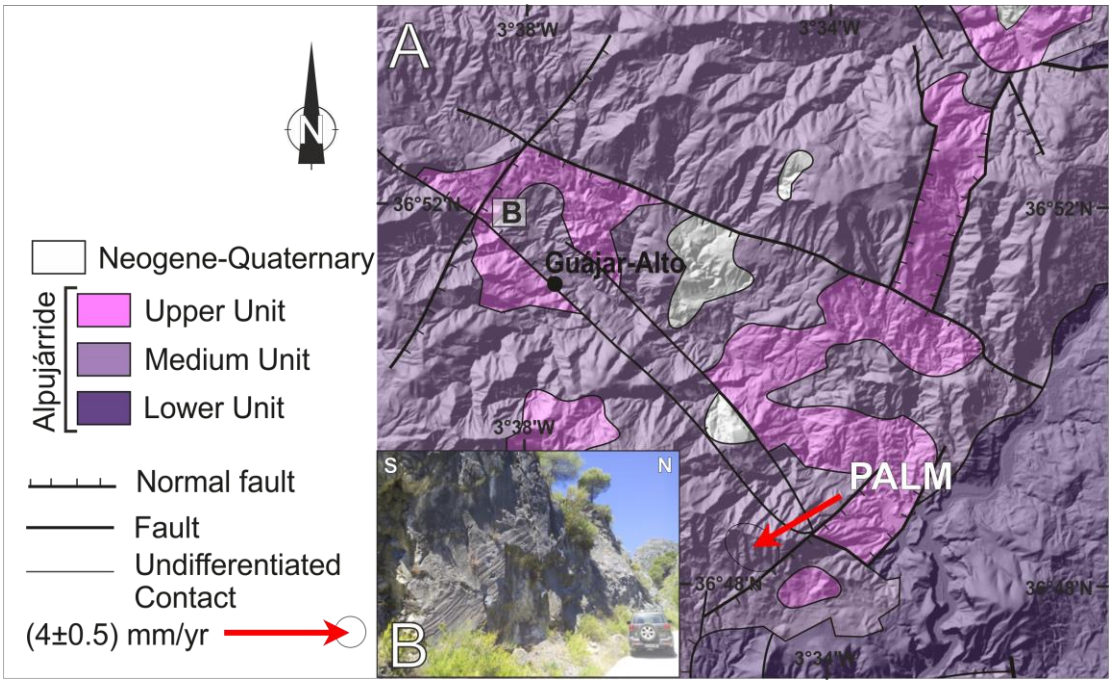

Fig. 6.4 Main tectonic structures in Los Guajares area including PALM CGPS site. A. Tectonic map of Los Guajares. CGPS data with residual velocity field with respect to the Eurasia fixed reference frame and 95% confidence ellipses. B. Field example of a normal-dextral fault. Location in part A.

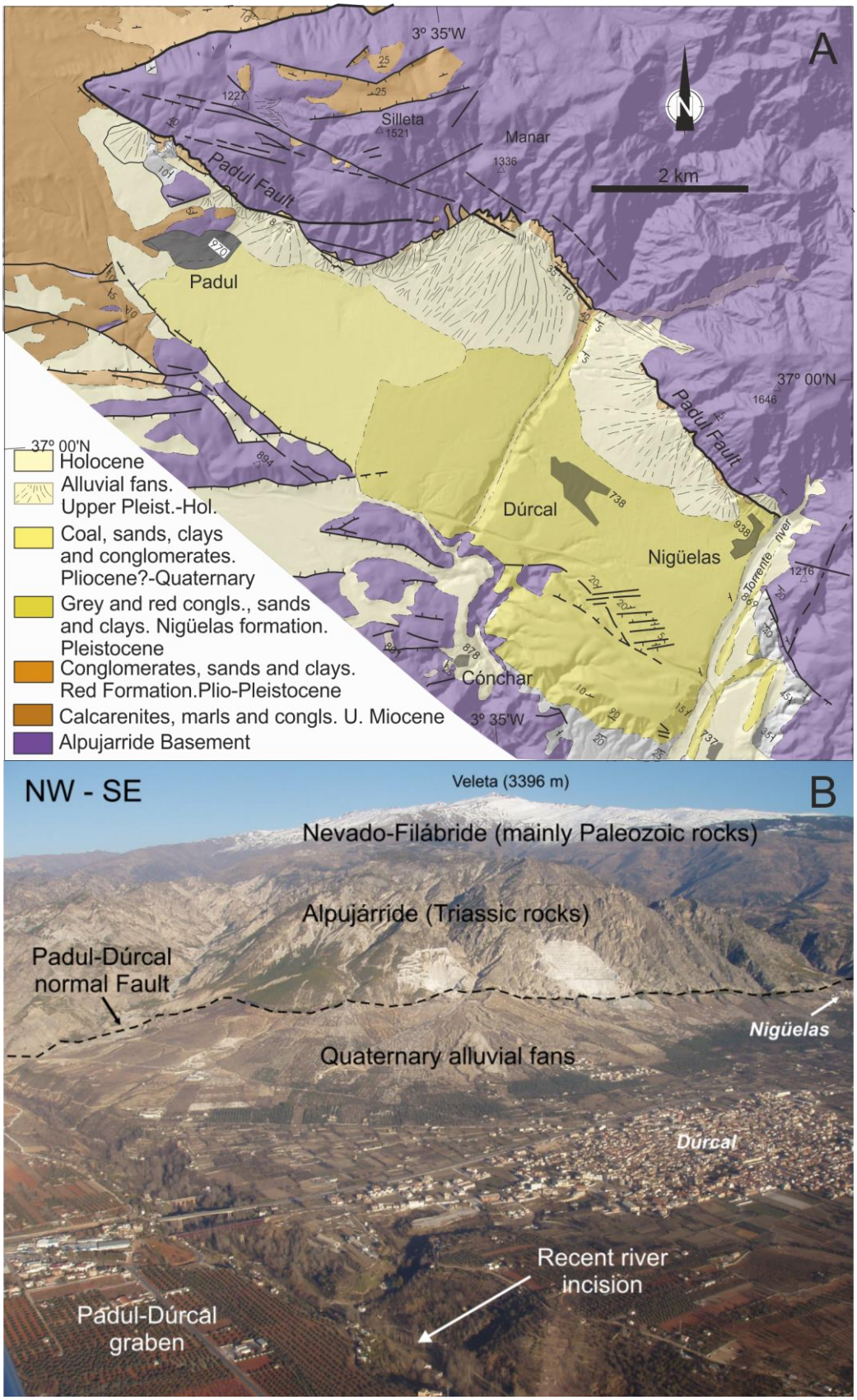

Fig. 6.5. Main tectonic structures in Padul Fault Zone. A. Tectonic map of Padul Fault. B. Oblique view of the Padul-Durcal fault zone.

The most important NW-SE fault of the central Betic Cordillera is the Padul Fault (Alfaro et al., 2001), located by the southwestern border of Sierra Nevada (Fig. 6.5). This southwestward-dipping normal fault has over 1.5 km of vertical slip since the Tortonian (Sanz de Galdeano, 1996b). The Padul fault zone comprises two segments, Padul and Nigüelas, featuring huge alluvial fans and a graben in the hanging wall (Fig. 6.5); it extends towards the Granada Basin and towards the western border of Sierra de Lujar (Figs. 6.1 and 6.2). Geomorphic and geological evidence including clastic wedges and recent scarps support its present-day activity (Alfaro et al., 2001) and elevation of the relief.

The northwestern part of Sierra Nevada corresponds to an eroded fold limb of the late antiformal structure with a regional NE-SW axis, leaving the Nevado-Filábride and Alpujarride metamorphic complexes exposed (Fig. 6.6). Although the main active faults are normal and NW-SE oriented, roughly orthogonal to the fold axis, a very recent or active NE-SW oriented normal dextral fault with associated fault scarp is also recognized in the Monachil area (Fig. 6.6).

Granada´s intramontane depression is an extensional basin (Figs. 6.1, 6.2 and 6.7) mainly controlled by NW-SE normal faults tilting blocks toward the NE on its eastern side, and an E-W, ENE-WSE to NE-SW set of strike slip and normal faults that generally develop half graben structures with sediment tilting towards to the NNW along its N and S boundaries (Ruano et al., 2004; Rodriguez-Fernandez and Sanz de Galdeano, 2006). In addition, NNE-SSW faults affected the eastern boundary of the basin. The activity of the faults is supported by paleoseismic research (Reicherter et al., 1999, 2003) as well as geological and seismological data (Morales et al., 1997). Sierra Elvira represents a horst in the NE part of the Depression. It exposed rocks of the External Zones surrounded by Neogene-Quaternary sediments, its formation due to the interaction of the NW-SE and the NE-SW orthogonal normal faults.

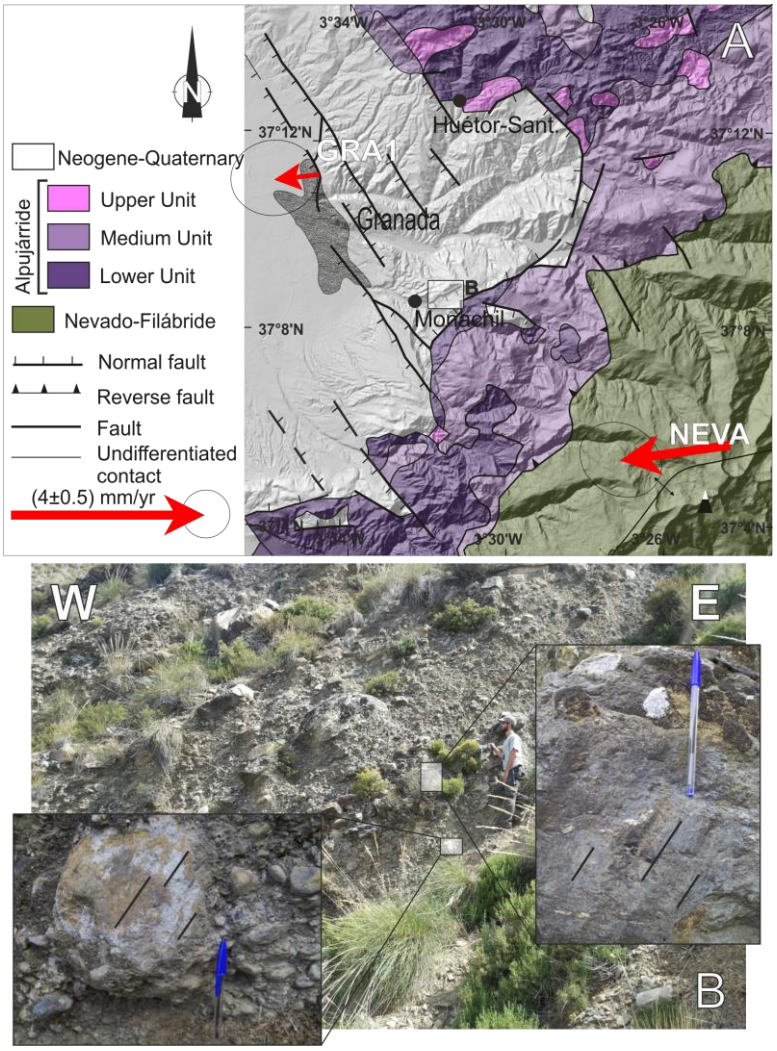

Fig. 6.6 Main tectonic structures in NE Granada Basin area including NEVA and GRA1 CGPS sites. A. Tectonic map of NE Granada Basin. CGPS data with residual velocity field with respect to the Eurasia fixed reference frame and 95% confidence ellipses. B. Field example of a normal-dextral fault. Location in part A.

In the External Zones, to the north, deformation mainly occurred before Late Miocene. Nevertheless, the Cazorla fold-and-thrust belt, with W to WNW vergence, may have affected up to Late Miocene rocks (Guezou et al., 1991; Frizon de Lamotte et al., 1995). The Baza Fault (Alfaro et al., 2008) (Fig. 6.1) moreover indicates recent NE-SW extensional deformation nearby the boundary between the External and Internal zones within the central Betic Cordillera.

6.7 Discussion

6.7.1 GPS and active tectonics

New CGPS data (Garate et al., 2014) make it possible to more precisely appraise previous tectonic displacements in the central and eastern Betic Cordillera, avoiding the large determination errors of past studies (Koulali et al., 2011).

Although in both datasets used here the displacement of reference sites is towards the W or SW, the new CGPS data include sites installed during the Topo-Iberia project so as to constrain the present-day tectonic activity. Moreover, survey-mode local GPS networks have been installed to study local structures in Betic Cordillera (Fig. 6.1) but they do not provide up to date enough accuracy for the aim of this regional research. We prefer to base our geological interpretations on the most accurate regional CGPS data available and not on local networks that may increase the error and the uncertainties of this regional study. Whereas most previous research focuses on the determination of the plate boundaries (Fernandes et al., 2007; Vernant et al., 2010; Koulali et al., 2011), we will discuss the main results in the framework of active tectonic structures.

	Coordinates		Residual velocities (mm/yr)			
Site	Lat. (°N)	Long. (°E)	VE	σE	VN	σN
ALME	36.8525	-2.4594	-1.42	±0.35	-0.52	±0.31
AREZ	37.8354	-1.9405	-1.50	±0.35	-0.21	±0.31
CAAL	37.2211	-2.5476	-0.73	±0.35	-0.07	±0.31
COBA	37.9156	-4.7211	-0.45	±0.35	-0.14	±0.31
GRA1	37.1899	-3.5964	-0.94	±0.36	-0.11	±0.33
LOJA	37.1073	-4.1064	-2.81	±0.35	-0.44	±0.31
MALA	36.7261	-4.3935	-2.33	±0.35	-0.99	±0.31
NEVA	37.0626	-3.3856	-2.28	±0.35	-0.32	±0.31
PALM	36.8090	-3.5623	-2.81	±0.35	-1.65	±0.31
TGIL	38.0342	-3.3026	-1.13	±0.35	-0.69	±0.31
UJAE	37.7878	-3.7817	-0.73	±0.35	0.00	±0.31

Table 6.1 CGPS-derived residual velocities with respect to Eurasia fixed.

Considering a stable Eurasia, the lowest residual velocities are found in the sites COBA and UJAE, located in the Guadalquivir foreland basin, supporting that in this region the basement is roughly attached to Iberia and to the Eurasian plate. In any case, site TGIL (Fig. 6.1, Table 6.1) may be considered as an anomalous emplacement in the relatively stable Guadalquivir foreland basin, because this sector is affected by active deformation and seismicity (Pedrera et al., 2013; Morales et al., 2014) resulting from propagation to the foreland of the eastern Betic Cordillera deformations (Pedrera et al., 2013).

The westward displacement of the AREZ station, located in the External Zones of the Eastern Betics, is also indicative of Alpine deformation that has not ended in this region; indeed, westward displacement may continue at low rates. The increasing displacement from AREZ and TGIL, as compared to the stations located westwards (COBA, UJAE), suggests that shortening still occurs in this sector of the Cordillera, similar to the displacement taking place during the development of the fold-and-thrust system of the Cazorla Arc (Fig. 6.1). In several previous works, most of the velocities in this part of the Cordillera are oriented N-S to NNW-SSE (Echeverria et al., 2013) showing a clear active compressional regime that is confirmed during the Quaternary by paleoseismological studies that evidence strike-slip movements with transpressional component in the major NE-SW to E-W faults that form the Eastern Betics Shear Zone (Silva et al., 1993; Masana et al., 2004).

The fact that the behavior of stations GRA1 and CAAL is similar to that of stations UJAE and COBA would support that the structures of the External Zones in the central Betic Cordillera are mainly inactive or have extremely low activity. This finding agrees with the absence of seismicity and geological observations on recent faults in the northern sector of the Betic Cordillera, even though recent sediments appear to be locally deformed (Ruano et al., 2004). The similar displacement of CAAL, located in the Internal Zones at the top of the E-W oriented Sierra de Los Filabres antiform, further supports that this fold at present has low activity or is inactive.

The higher rates of westward motion of the NEVA, having a trend similar to that of CAAL and GRA1 (Figs. 6.1 and 6.2), together with the absence of relevant brittle deformations in between these sites, can only be explained by tectonic activity of low intensity in northwestern Sierra Nevada. The development of the NE-SW oriented western Sierra Nevada antiform, related to the highest present-day reliefs, could produce NW displacement and the presence of NW-SE to N-S tensional joints, which are widespread throughout Sierra Nevada and Sierra de

Los Filabres (Galindo-Zaldívar and González-Lodeiro, 1990), evidencing a W to SW displacement. This final NE-SW extensional deformation also led to the development of NW-SE oriented active normal faults in the Granada Basin (Fig. 6.7). The sum of both deformations produces the moderate westward displacement of the NEVA site. In turn, the normal-dextral NE-SW oriented active fault in the Monachil area (Fig. 6.6) may be a secondary structure formed by extension along the outer limb of the western Sierra Nevada NE-SW oriented antiform, also supporting the activity of this main fold in its northern sector.

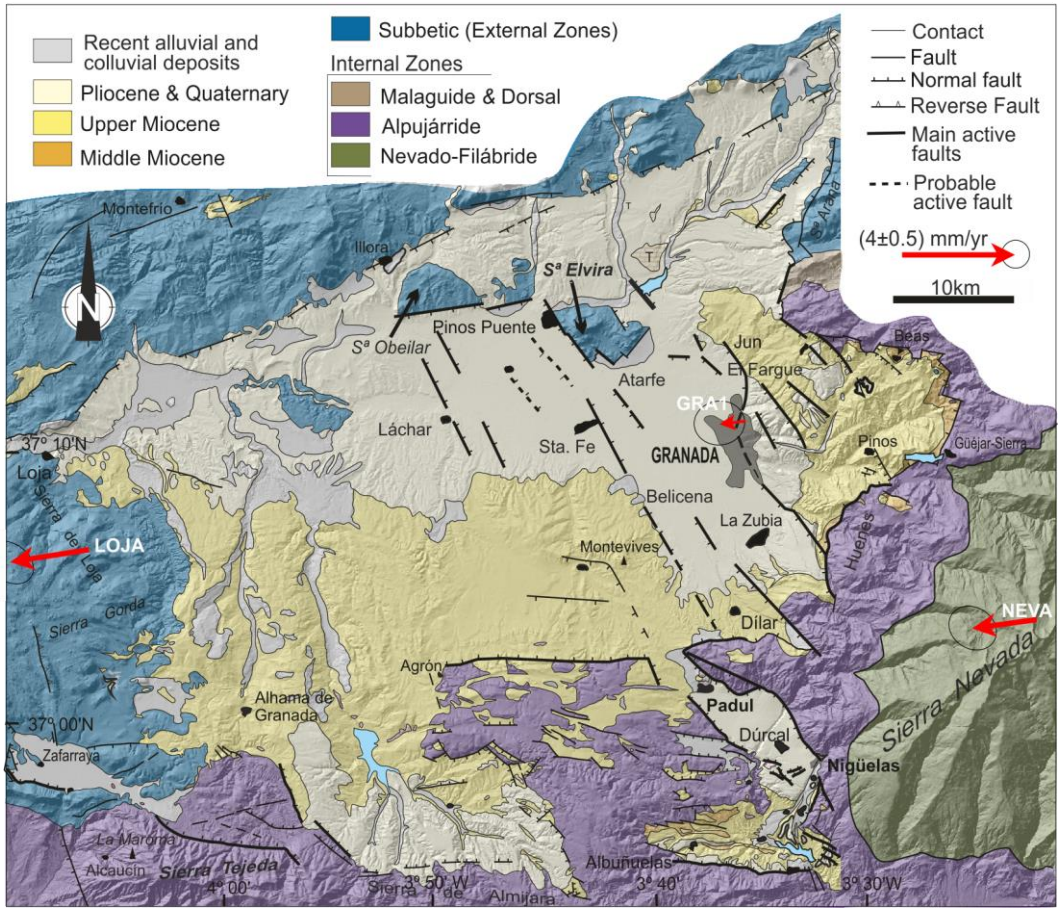

Fig. 6.7 Tectonic sketch of the Granada Basin. In bold, main active faults. CGPS data with residual velocity field with respect to the Eurasia fixed reference frame and 95% confidence ellipses.

The largest displacements are observed towards the south and the west of the study region. The highest westward displacement of ALME with respect to CAAL and the rotation of the displacement towards the WSW may be a

consequence of the activity of the NW-SW oriented normal fault zone that separates Sierra Alhamilla and Sierra de Gador, and extends towards the Campo de Nijar (Marín-Lechado et al., 2005; Sanz de Galdeano et al., 2010).

The highest WSW displacement rates (up to 3.25 mm/yr) are reached at PALM, a site located southwest of Sierra Nevada; the higher rates than ALME are probably a result of the NW-SE oriented normal fault zone west of Sierra de Gádor extending towards the Campo de Dalias (Marín-Lechado et al., 2005) along the active Balanegra Fault zone (Galindo-Zaldívar et al., 2013).This fault zone even deforms the present-day coastline of the Alboran Sea.

These displacements would be transferred through the dextral and transtensional faults located South of Sierra Nevada towards the Padul fault Zone (Martinez-Martinez et al., 2006; Martinez-Diaz and Hernandez-Enrile 2004), and finally, towards the Granada Basin and to the Alboran Sea, thereby determining the different displacements of GRA1 and LOJA. Dextral and transtensive deformation of the Alpujarras Corridor is likewise transferred towards the Guajares, producing a greater southward displacement component from LOJA towards MALA and PALM.

The present-day rate of PALM with respect to NEVA points to a relative displacement towards the SSW of 1.43 mm/yr. The trend is roughly orthogonal to the Padul fault. If we consider fault surfaces dipping 60º, typical of normal faults (Anderson, 1951), the vertical slip rate is of 2.47 mm/yr. However, if the fault dip is 30º, as is characteristic of the Niguelas Fault (Alfaro et al., 2001), then the vertical rate would amount to 0.83 mm/yr more close to geological relative uplift rates (Sanz de Galdeano et al., 2012).

The large folds that produced the main E-W oriented relief are scarcely active or inactive in the northern region, although they may be active near the Alboran Sea (Marín-Lechado et al., 2005). Only the NE-SW oriented antiform affecting northwest Sierra Nevada exhibits low activity, developing the present-day high reliefs of the Cordillera.

6.7.2 Geodynamic setting

During the Early Miocene there is a transition from compressional to extensional deformations. The main westward-southwestward Middle Miocene extension that determined the exhumation of metamorphic rocks of the Internal Zones continues to be active since the Late Miocene, in the central Betic Cordillera affecting an anisotropic crust (Fig. 6.8). Although the entire region continued to shorten by the slow motion of Africa to the NNW-NW (Iribarren et al., 2007), the new GPS data show the increased westward displacement from the eastern Betic Cordillera to the west and south that supports the active extension related to the tectonic processes that occurred in the westernmost Betic Cordillera. In this setting, the most suitable tectonic model would be present-day extension related to a back-arc, probably involving roll-back associated with a subducting slab along the Gibraltar Arc (Gutscher et al., 2002; Duggen et al., 2005; Ruiz-Constán et al., 2011; Pedrera et al., 2011; Gonzalez-Castillo et al., 2015).

This extension affected the continental crust heterogeneously —thin in the Alboran Sea and thick in the Betic Cordillera, where a main middle crustal detachment level separates the Betic Cordillera from the Iberian crust basement (Galindo-Zaldívar et al., 1997; Ruano et al., 2004) (Fig. 6.8). In this setting, the westward motion mainly affected the southern thinned continental areas of the Alboran Sea and the neighboring region, with the thick Betic Cordillera developing the extensional Almeria-Tabernas, Balanegra-Sierra de Gador, and southern Padul fault zones. Meanwhile, the dextral and transtensional Sorbas-Tabernas-Alpujarras-Guajares fault zone accommodate the increase to the South of the westward displacements. This fault zone was interpreted as a fault bounding a crustal block that escape westward due to space constrictions, coherent with a compressional regime with N-S shortening (Martinez-Diaz and Hernandez-Enrile, 2004). The Esci-Béticas II deep seismic reflection profile (Galindo-Zaldívar et al., 1997) does not evidence that the lower crust below the Alpujarras is affected by a vertical fault zone, suggesting that this fault zone only reach shallow crustal levels and probably acted as a transfer fault above a crustal

detachment. West of Sierra Nevada, deformation extended northward through the Padul Fault Zone, producing the conspicuous extensional Granada Basin at shallow crustal levels, featuring NE-SW and NW-SE normal faults as well as E-W normal and dextral faults. These faults develop asymmetrical sub-basins tilted towards the NE or to the N (Ruano et al., 2004; Rodríguez-Fernández and Sanz de Galdeano, 2006). Although previous authors (Banda et al., 1993; Andeweg and Cloetingh, 2001 and Mancilla et al., 2013) propose a major crustal and upper mantle discontinuity zone west of Sierra Nevada, the absence of any related Bouguer gravity anomaly displaying E-W differences in the crustal structure of the area (Casas and Carbó, 1990; Torné and Banda, 1992) suggests that this extension only affects the upper crust. In fact, it is probably accommodated in the detachment level that separates the Betic Cordillera from the underlying Iberian Massif (Ruano et al., 2004).

In this setting, compressional structures continue to occur in the central part (northwestern Sierra Nevada antiform) and in the eastern Betic Cordillera. The local tectonic processes in the Betic Cordillera may overlap the effect of the regional NW-SE oblique convergence of the Eurasian and African plates.

The main results of this contribution, focused in the central Betic Cordillera, are in agreement with those obtained in western Betic Cordillera (González-Castillo et al., 2015), also supporting the presence of a subduction with roll-back. The integration of these studies with the recent researches of eastern Betic Cordillera (Echeverria et al., 2013) provides a new and detailed framework of whole the Betic Cordillera that relate the velocity field with the main active tectonic structures.

6.8 Conclusions

New CGPS data from the central and eastern Betic Cordillera provide a precise regional displacement pattern with heterogeneous W and WSW residual displacement of the studied sites with respect to the Eurasia reference frame. These present-day displacements display diverse behavior, suggesting that the current geologically homogeneous domains do not fit with the classical subdivision between External and Internal zones of the Betic Cordillera. Displacement is oblique to the expected NW-SE Eurasian-African plate convergence. Overall, it is related to the dismantling of a thickened crust during extension at shallow crustal levels.

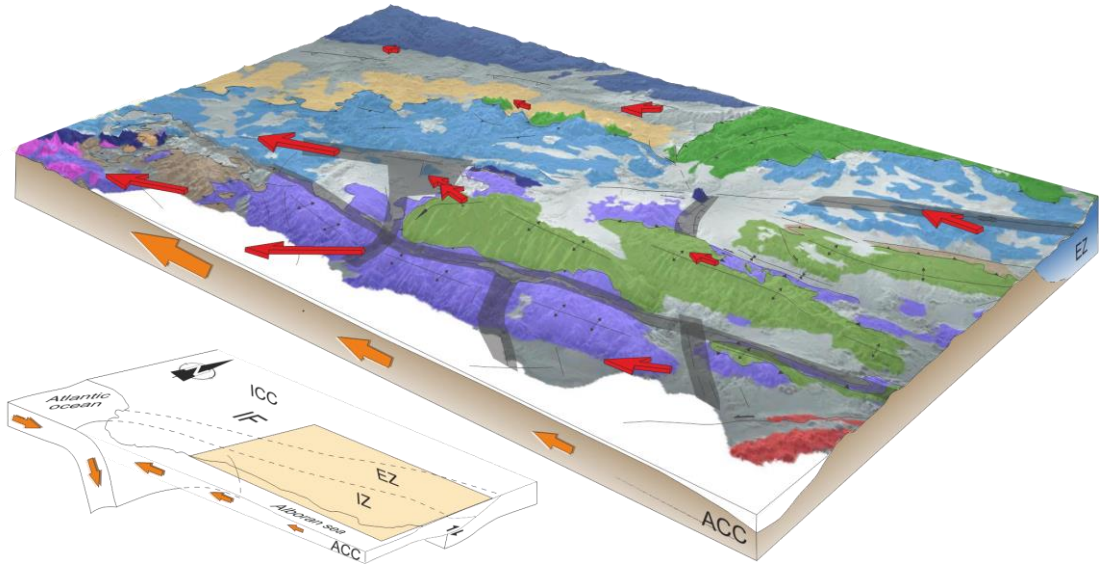

Fig. 6.8 Tectonic model of southeastern Betic Cordillera including CGPS sites and position of main active fault zones (in grey) accommodating E-W to ENE-WSW extension. The westward increasing of displacements is compatible with subduction rollback. ACC, Alboran Continental crust; EZ, External Zones; IC, Internal Zones; ICC, Iberian continental crust; IF, Iberian Massif foreland. Legend in Fig. 6.1.

The most stable area corresponds to the sites located to the northwest, in the Guadalquivir foreland basin. The eastern External Zones move slowly

westwards (about 0.75mm/yr) with respect to the stable foreland, supporting that moderate compressional tectonics continue to be active at present in the eastern Betic Cordillera. Deformation reaches the eastern region of the Guadalquivir foreland basin in TGIL site, currently undergoing moderate seismicity.

The absence of relative displacement between the stable Guadalquivir Basin, the Sierra de Los Filabres and the NE Granada Basin support that most of the External Zone structures in the central sector of the Cordillera and the E-W oriented folds located to the N have very low activity or are inactive. The relative displacement of NEVA site in Sierra Nevada supports the residual activity of the northwestern Sierra Nevada antiform, where the highest reliefs are located, combined with orthogonal extensional brittle structures.

The increase of the westward and southward displacement from the relatively stable Sierra de Los Filabres (CAAL) towards Almeria (ALME) and PALM, Malaga (MALA) and Loja (LOJA), would support the present-day activity of the NW-SE oriented fault set, including the fault zones separating Sierra de Filabres and Sierra de Gádor (Balanegra fault zone and West Sierra de Gador) and the Padul fault zone and Granada basin fault area. In addition, to the north, the Baza fault apparently continues to be active.

These faults signal a relatively undeformed core in Sierra Nevada surrounded by the dextral and transtensional transfer faults located from N Sierra Alhamilla, crossing the Tabernas Basin and continuing along the Alpujarras corridor towards the Guajares.

The fact that extension developed oblique to the present-day Alboran Sea borders, and to the main geological division of the Betic Cordilllera, fits better in developmental models entailing back-arc extension with related roll-back along the Gibraltar Arc. Such extension would mainly affect the weakest or thinnest crustal sections located nearby the Betic Cordillera-Alboran Sea boundary, and then extend northwards at upper crustal levels separating Sierra Nevada from the westward regions along the Padul Fault zone and Granada Basin faults.

Acknowledgements

We acknowledge the comments of Prof. M. Fernández, Prof. L. Jolivet and two anonymous reviewers, which have improved the quality of the contribution. This research was funded by the Spanish Government through projects AYA2010-15501, CGL2010-21048, P09-RNM-5388 and CSD2006-0041 (European Regional Development Fund-ERDF) and the RNM148 and RNM282 research groups of the Junta de Andalucía. We thank all those persons involved in maintenance of the Topo-Iberia GPS network.

CHAPTER 7

Latest extension of the Laujar fault in a convergence setting (Sierra Nevada, Betic Cordillera)

Journal of Geodynamics 104 (2017) 15–26

Contents lists available at ScienceDirect

Journal of Geodynamics

journal homepage: http://www.elsevier.com/locate/jog

Latest extension of the Laujar fault in a convergence setting (Sierra Nevada, Betic Cordillera)

Manuel Martínez-Martos[a,b,*], Jesus Galindo-Zaldívar[a,b], Carlos Sanz de Galdeano[b], Francisco Juan García-Tortosa[c], Francisco José Martínez-Moreno[d], Patricia Ruano[a,b], Lourdes González-Castillo[a], José Miguel Azañón[a,b]

[a] Dpto. De Geodinámica, Universidad de Granada. 18071 Granada, Spain.

[b] Instituto Andaluz de Ciencias de la Tierra, CSIC-Universidad de Granada, Avenida de las Palmeras, nº 4, 18100 Armilla, Spain.

[c] Departamento de Geología, Facultad de Ciencias, Universidad de Jaén, Campus Las Lagunillas, 23071 Jaén, Spain.

[d] Instituto Dom Luiz, Universidade de Lisboa, Faculdade de Ciencias, Campo Grande, Ed. C8, Lisboa, Portugal.

ABSTRACT

The present-day relief of the Betic Cordillera formed since the Late Miocene through the regional N-S to NW-SE Africa-Eurasia convergence that developed large folds. The Laujar Fault Zone is a south-dipping E-W oriented structure located at the northern boundary of the Alpujarran Corridor Neogene intramontane basin, which separates Sierra Nevada and Sierra de Gador antiforms, in the Internal Zones of the Betic Cordillera. The fault zone acted in a first stage as a dextral strike-slip fault. Currently it moves as a normal fault evidenced by striated calcretes, also in agreement with regional continuous GPS (CGPS) data that support the hypothesis of an active N-S extension in the fault area.

In order to analyse the deep geometry of the Laujar Fault Zone, we combined several geophysical techniques (gravity, magnetic, electric resistivity tomography and audio-magnetotelluric data) with field geological observations. Fault surfaces seem to join at a southward-dipping shallow detachment level, including faults covered by the sedimentary infill. The fault zone was developed in a previously weakened area by wrench faults parallel to the Alpujarran Corridor. The recent normal activity of this fault zone may be a consequence of a change in the Africa-Eurasia convergence orientation, which implies a decrease in the N-S compression component. This structure along the southern limb of Sierra Nevada antiform evidences the gravitational collapse of previously thickened crust in a regional compressional context simultaneous to metamorphic core uplift.

Keywords: Active tectonics; Neogene-Quaternary basin; geophysical prospecting; metamorphic core uplift.

HIGHLIGHTS

- Metamorphic core uplift by folding and faulting in Betic Cordillera Internal Zones.

- Active extensional deformation parallel to compression in continental collision

- Normal fault reactivation of previously weakened strike-slip fault zones.

7.1 Introduction

Normal faulting related to extension parallel to regional convergence has been reported in collision orogens such as the Himalayas (Zhang et al., 2000) or the Alps (Sue et al., 2007). These structures contribute to metamorphic complex exhumation in the internal zones of orogenic belts (Platt, 1986; Dewey, 1988), widely reported by P-T-t studies (e.g. Jolivet et al., 1996; Hermann et al., 2001). Low-angle normal faults have been invoked to explain metamorphic core uplifting in several extensional settings such as the Basin and Range (e.g. Coney and Harms, 1984; Reynolds and Spencer, 1985; Wernicke et al., 1987), or the continental Crete and the Aegean Sea (e.g. Jolivet et al., 1996; Ring et al., 2001; Hinsbergen and Meulenkamp, 2006). In compressional settings, the development of large antiforms as a consequence of continental collision has also been proposed as an exhumation mechanism of deep continental rocks (e.g. Cello and Nur, 1988).

In the Betic Cordillera (Fig. 7.1), fission-track analysis (Vazquez et al., 2011) and geomorphological studies support a continuous very recent activity for Sierra Nevada uplift (Pérez-Peña et al., 2010) that may go on today at a rate of 0.43-0.75 mm/yr (García-Tortosa and Sanz de Galdeano, 2007). Proposed exhumation mechanisms include core complex related to E-W to NE-SW extension (Martinez-Martinez et al., 2004; Augier et al., 2005; Jabaloy-Sanchez et al., 2015). Antiformal development with N-S to NW-SE compression and orthogonal extension forming horst and graben structures has also been proposed (Galindo-Zaldivar et al., 2003; Sanz de Galdeano and Alfaro, 2004; Rodriguez-Fernandez and Sanz de Galdeano, 2006). Folds remain active south of the study area, affecting up to the recentmost sediments (Marin-Lechado et al., 2007; Pedrera et al., 2015).

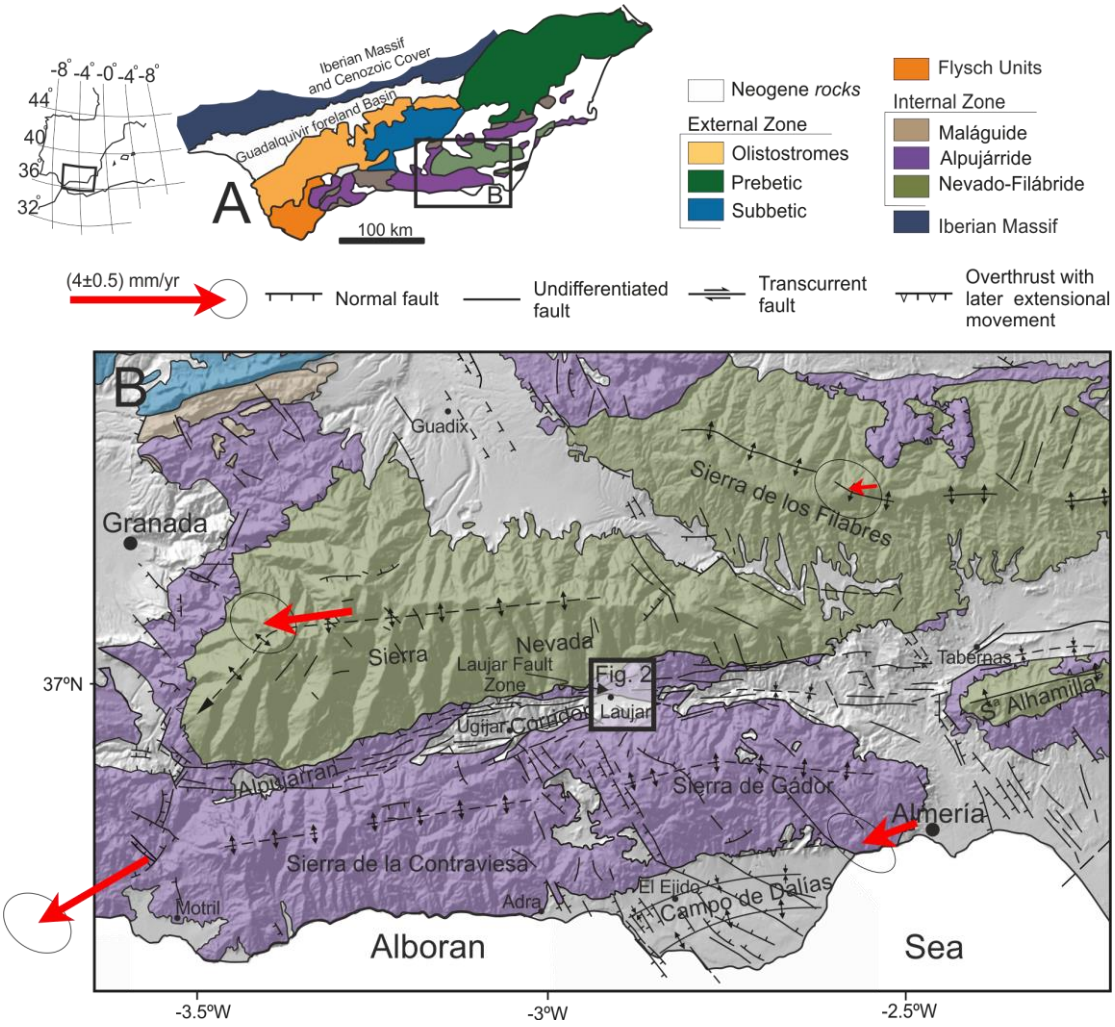

Fig. 7.1 Geological setting of the Alpujarran Corridor and its surrounding mountain ridges. A) Synthetic geological sketch of the study area in the Betic Cordillera. B) Geological map and main tectonic structures, including some CGPS arrows and their 95% confidence ellipses from Galindo-Zaldivar et al. (2015).

The central-eastern sector of the Betic Cordillera (Fig. 7.1) holds great interest in terms of the interaction of relief-dominating large-radius recent folds with low and high-angle normal faults in the upper crust. The Laujar Fault Zone (Fig. 7.2) is formed by strike-slip and normal faults with an E-W strike located at the northern boundary of the Alpujarran Corridor, a faulted synformal structure constituted by the southern part of the Sierra Nevada antiform and the northern part of the Sierra the Gador and Sierra de la Contraviesa (Fig. 7.1). Seismic activity

related to the fault zone has a maximum expected magnitude (Mw) of 6.4 ±0.37 and a recurrence period of 3243 yr. (http://info.igme.es/qafi, García-Tortosa and Sanz de Galdeano, 2007), based on Stirling et al. (2002) and Wesnousky (1986) methods. Yet there are no subsurface studies describing this fault zone and its relationship with the geometry of the related intramontane basin deposits located at its hanging wall. The stress deduced from the Laujar Fault Zone –with related N-S extension– and the large recent folds –supporting N-S compression– would appear to be contradictory. However, in both cases they facilitate the metamorphic core uplift.

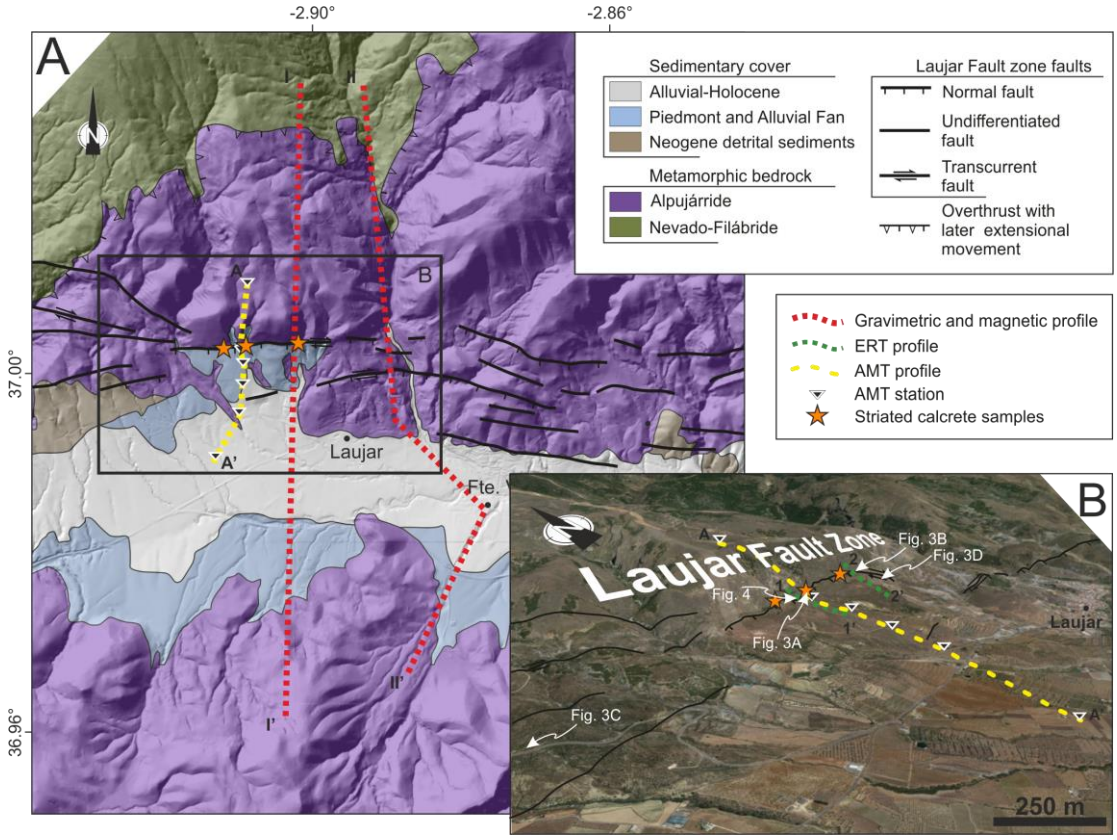

Fig. 7.2 Detailed geology and geophysical survey of the Laujar Fault Zone. A) Main tectonic structures in the study area and location of gravity, magnetic and audio-magnetotelluric profiles. Location of radiocarbon dating samples is also shown. B) Laujar Fault Zone oblique aerial view where the main fault planes, calcrete collection samples and AMT and ERT profiles locations are indicated.

The aim of this research is to characterize the E-W oriented Laujar Fault Zone's recent normal behaviour developed on a regionally N-S to NW-SE compressive stress regime, in order to better understand the late orogenic extensional tectonics. We present a detailed characterization of the structure, combining field geological observations and near-surface geophysical data, including electrical resistivity tomography (ERT), audio-magnetotellurics (AMT), gravity and magnetic prospecting. New dating was performed on striated calcretes belonging to the Laujar Fault to better characterize its recentmost activity.

7.2 Geological setting

The study area is located within the Betic Internal Zone (Figs. 7.1 and 7.2), formed mainly by three tectonically superimposed complexes: from bottom to top, Nevado-Filábride, Alpujárride and Maláguide (Azañón et al., 2002). Sierra Nevada, situated north of the Laujar Fault, is an E-W antiformal structure. The Nevado-Filábride Complex occupies the nucleus of this sierra, while the Alpujárride complex surrounds it and crops out in its southern slopes, the Alpujarran Corridor, and continues to the Alboran Sea (Fig. 7.1). These tectonic complexes are formed by Paleozoic to Triassic rocks including gneisses, schists and quartzites (also phyllites in the Alpujarride) and marbles.

The Alpujarran Corridor development began in the Middle Miocene with remarkable tectonic deformation and uplifting since the Late Miocene (Sanz de Galdeano et al., 1985). Unconformably upon the Alpujárride Complex lie detrital marine sediments that were deposited from the Serravallian (Middle Miocene) and evolve into lacustrine facies at the end of the Tortonian-Messinian (Late Miocene) (Sanz de Galdeano, 1996). Their deformation was controlled by E-W strike-slip dextral faults with transpressional and transtensional structures parallel to fold trends (Sanz de Galdeano et al., 1985; Sanz de Galdeano, 1996; Galindo-Zaldívar, 1986; Rodríguez-Fernández et al., 1990; Martínez-Díaz, 2000; García et al., 2003; Martínez-Díaz and Hernández-Enrile, 2004; Martínez-Martínez, 2006; Martínez-Martínez et al., 2006). However, the faults became normal during their latest period of activity. The Laujar Fault Zone affects Plio-

Quaternary colluvial and alluvial fan continental sediments. This active extensional regime is supported by new GPS data from the central Betic Cordillera (Galindo-Zaldivar et al., 2015).

7.3 Methods

Several geophysical techniques (gravity, magnetic, electric resistivity tomography and audio-magnetotelluric) were carried out in combination with field observations and radiocarbon dating to characterize the Laujar Fault Zone. All measurement points were positioned with Differential GPS.

7.3.1 Gravity prospecting

Gravity prospecting provides the depth distribution of different density bodies and allows one to determine the geometry of material distribution underground. Therefore, through this method the geometry of the sedimentary infill in the study area was obtained. A total of 137 new gravity measurements were acquired mainly along N-S oriented profiles, with some sparse additional measurements, to derive gravity anomaly maps. We used a Scintex Autograv CG-5 gravity meter with 0.001 mGal accuracy. All measurements were referred to the Granada absolute gravity station (National Geographical Service of Spain, IGN, www.ign.es). We processed the data and calculated Free Air, Bouguer and Terrain corrections with a standard density of 2.67 g/cm3. Terrain correction was calculated based on a combination of Nagy (1966) and Kane (1962) methods, with DTM of 5 m pixel accuracy and up to a distance of 160 km from the measurement stations. Afterwards, the Bouguer anomaly map was determined. The regional anomaly was calculated by kriging the gravity measurements located in the bedrock according with the methodology described by Martínez Moreno et al. (2015) and the residual anomaly was obtained from the difference between the Bouguer and the regional anomalies.

2D profile forward models were calculated with GravMag 1.7 software (Pedley et al., 1993). The densities used were 2.67 g/cm3 for the basement and 2.25 g/cm3 for the sedimentary infill, according to previous studies in the surrounding areas

(Ruiz-Constán et al., 2013) and the average values of the dominant lithologies (Telford et al., 1990).

7.3.2 Magnetic data

The total intensity of the magnetic field was measured at 71 stations in the same position as the gravity sites without anthropic noise. Measurements were taken using a GSM 8 proton precession magnetometer with a maximum accuracy of 1 nT. Magnetic anomalies were determined after correction of diurnal variation using the nearest San Fernando (Cadiz, Spain) permanent magnetic station (http://www.intermagnet.org/data-donnee/dataplot-eng.php?type=hdz). In addition, data were reduced to the IGRF 2010 using a standard procedure (IAGA, 2010).

We also used GravMag 1.7 (Pedley et al., 1993) to model the magnetic data simultaneous to gravity data in 2D profiles. A magnetic susceptibility of 0.03 SI was considered for not outcropping anomalous bodies located at the top of Nevado-Filabride complex, according to previous studies in the region (Li et al., 2012).

7.3.3 Electrical resistivity tomography

Two 400 m-long ERT profiles were acquired. Both of them crossed the main Laujar fault scarp with 500 m of split, approximately (Fig. 7.2B).

We used an ABEM Terrameter SAS 4000 with four-channel multiple electrode array. Considering the accuracy and depth penetration target, electrodes were deployed at 5 m, reaching a penetration depth up to 65 m in this study. The profiles were acquired with GRAD4LX8 and GRAD4S8 gradient electrode array protocols (ABEM, 2006; Dahlin and Zhou, 2006).

The profile inversion calculation was carried out using a standard least-squares model constrain inversion method with Res2Dinv software (v 3.59, Geotomo Inc.). The software attempts to minimise, in an iterating process, the square of the difference between measured and calculated apparent resistivity values.

7.3.4 Audio-magnetotelluric data

Six AMT sites were used to carry out a profile perpendicular to the Laujar Fault Zone (Fig. 7.2). The equipment used was a Stratagem EH4 in a 10 Hz to 100 kHz frequency range, which made it possible to obtain information from surface to several hundred meters depth. The natural magnetic field signal shows a decrease between 800 Hz and 70 kHz. To enhance this poor range of frequencies, we used a far transmitter antenna placed to ensure that a plane wave field was received.

We analysed the geoelectric dimensionality by means of Bahr decomposition (Bahr, 1988; 1991). The obtained curves present a general 1D structure up to 100 Hz and a 2D behaviour from 100 Hz to 10 Hz. The strike obtained was N80-100°E. We also checked the consistency of resistivity and phase estimated at each station (Parker and Booker, 1996). All data were integrated in a 2D inversion profile (Parker and Booker, 1996) using WinGlink software. An error floor of 5% was selected for the apparent resistivities and the phases.

7.3.5 Radiocarbon dating

Radiocarbon is the most important chronometer for the late Pleistocene and Holocene. Stable carbon isotope ratios (δ13C) are widely used, coupled with 14C dating, to document ages in natural samples where C3 and C4 plant communities coexist or may have coexisted (Boutton, 1996). Three collected samples of striated calcrete located in the fault surface (Fig. 7.3A) were analysed in the University of Granada Radiocarbon Laboratory. 14C dating was performed by means of the liquid scintillation method (Balesdent and Guillet, 1982). Sample LA-3 is out of range to calibrate to calendar years, although samples LA-1 and LA-2 were calibrated using Calib 4.2 (Stuiver and Reimer, 1993; Stuiver et al., 1998).

7.4. The Laujar Fault Zone structure

7.4.1 Main field tectonic features of the Laujar Fault Zone

The WNW-ESE oriented Laujar Fault Zone (Figs. 7.1 and 7.2) is formed by several almost parallel surfaces dipping between 65° and 88° southwards, with well-preserved escarpments 1 to 2.5 m high (Fig. 7.3B). The fault is well exposed for about 8 km east of Laujar village, although it continues several tens of kilometres westwards (Fig. 7.1), affected by the erosion of the drainage system. Striae analysis evidences a former dextral strike-slip followed by a normal regime (García-Tortosa and Sanz de Galdeano, 2007). In addition, a distribution of penetrative tensional joints parallel to the fault scarps can be seen in the Plio-Quaternary alluvial fan sediments (Fig. 7.3C).

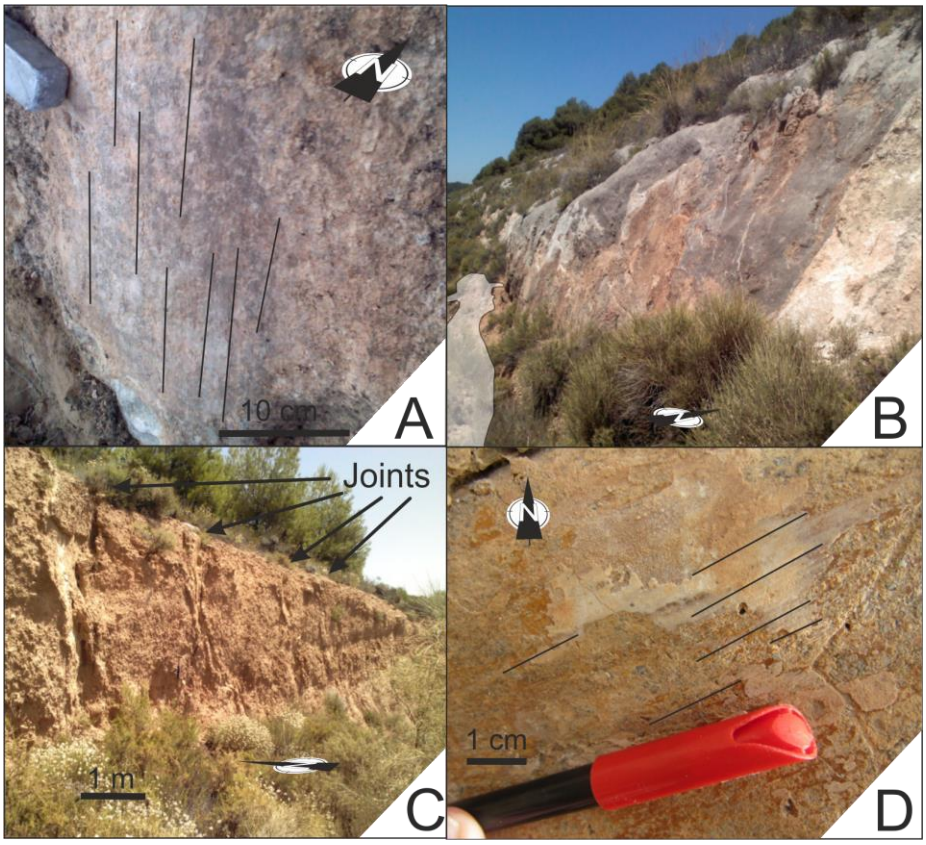

Fig. 7.3 Brittle deformation in the Laujar Fault zone. A) Striated calcrete in the main fault plane. B) Main Laujar fault scarp. C) Penetrative joints in Plio-Quaternary detrital sediments. D) Sub-horizontal striations in the main fault plane without calcretes.

In some zones of the main Laujar fault, patches of dip-slip striated calcretes (Fig. 7.3A) can be found on the fault plane. We collected striated calcrete samples in order determine their radiocarbon ages (Fig. 7.2); the ages, previously corrected from δ13C, were as follows:

Sample LA-1: 14560 ± 220 yr. BP

Sample LA-2: 18080 ± 120 yr. BP

Sample LA-3: 26448 ± 510 yr. BP

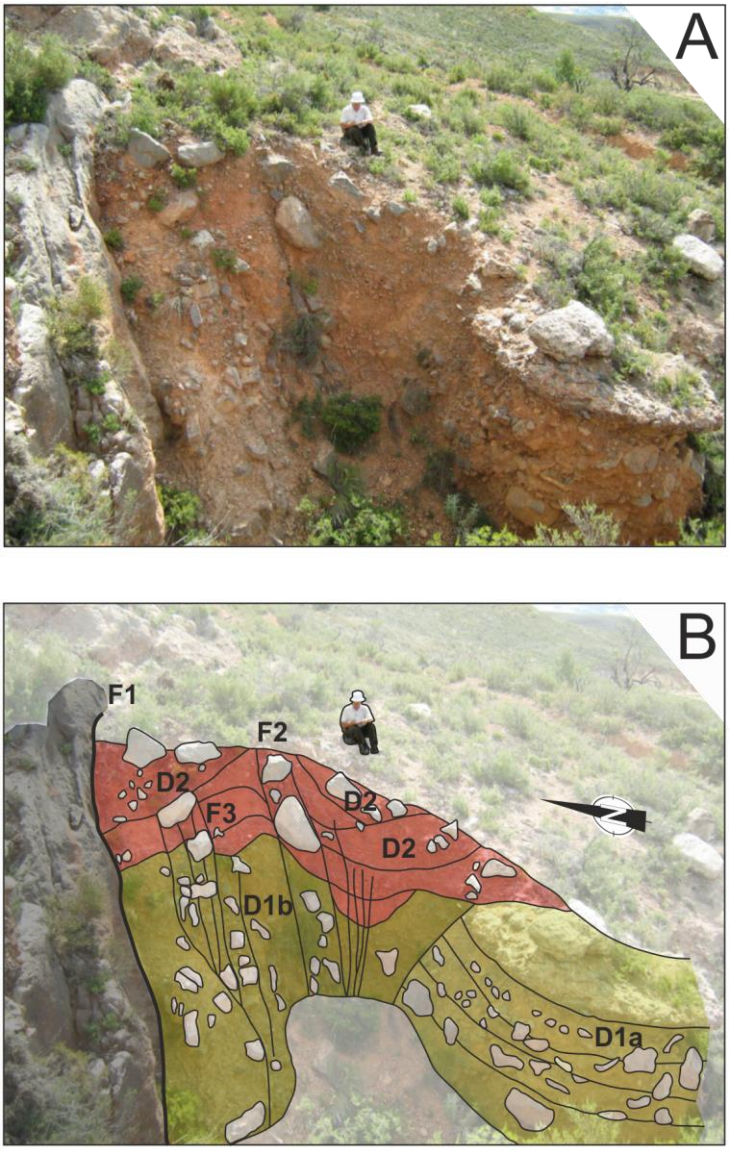

Fig. 7.4 Fault plane and its relation to Neogene and Quaternary sediments. A) Main Fault plane and hanging-wall Neogene and Quaternary sediments crosscut by river incision. B) Sedimentary interpretation showing different fault surfaces in the Plio-Quaternary sediments with associated clastic wedges.

In areas of river incision, it is possible to establish realtionships between the reddish uncemented colluvial deposits and the Laujar Fault Zone (Fig. 7.4). Three

different deposits can be differentiated from bottom to top. Firstly, D1, formed by the alluvial and colluvial sediments, are characterized by bedding with marked vertical grain-size contrast (D1a, Fig. 7.3B) and become highly deformed (D1b, Fig. 7.4B) by the main fault (F1) and secundary faults (F2 and F3). Above them lies D2 (Fig. 7.4B), a fractured and folded colluvial level at the front of the main fault scarp formed by heteromertic angular cobbles embedded in a sandy-clayey matrix.

7.4.2 Gravity and magnetic data and models

The Bouguer anomaly map (Fig. 7.5A) shows a range of values between -63 and -43 mGal, but it does not provide much information about the sedimentary infill geometry due to the high influence of the regional anomaly (Fig. 7.5B), which increases towards the SE due to the southwards crustal thinning. The residual anomaly map (Fig. 7.5C) presents E-W elongated minima matching the sedimentary deposits of the Alpujarran Corridor in a range between 0 and -2.1 mGal. N-S oriented profiles show an abrupt anomaly drop at approximately 1 to 1.5 km south of the main Laujar fault scarp (Fig. 7.6). The anomaly values increase smoothly in the southern basin border, reaching 0 mGal again close to the metamorphic basement outcrops.

Gravity models for profiles I-I' and II-II' (Fig. 7.6) present a similar basin structure, formed by a thin low density sedimentary body (2.25 g/cm^3) on a metamorphic basement (2.67 g/cm^3). In both models, a 40° to 70° S dipping fall in the sediment-metamorphic bedrock contact produce a sharp increase of 60 to 75 m in the basin sedimentary thickness, indicating the presence of a second sealed normal fault. The basin depocentre is located southward in model II-II', at 6 km in length, and has an estimated 150 to 160 m maximum sedimentary infill thickness.

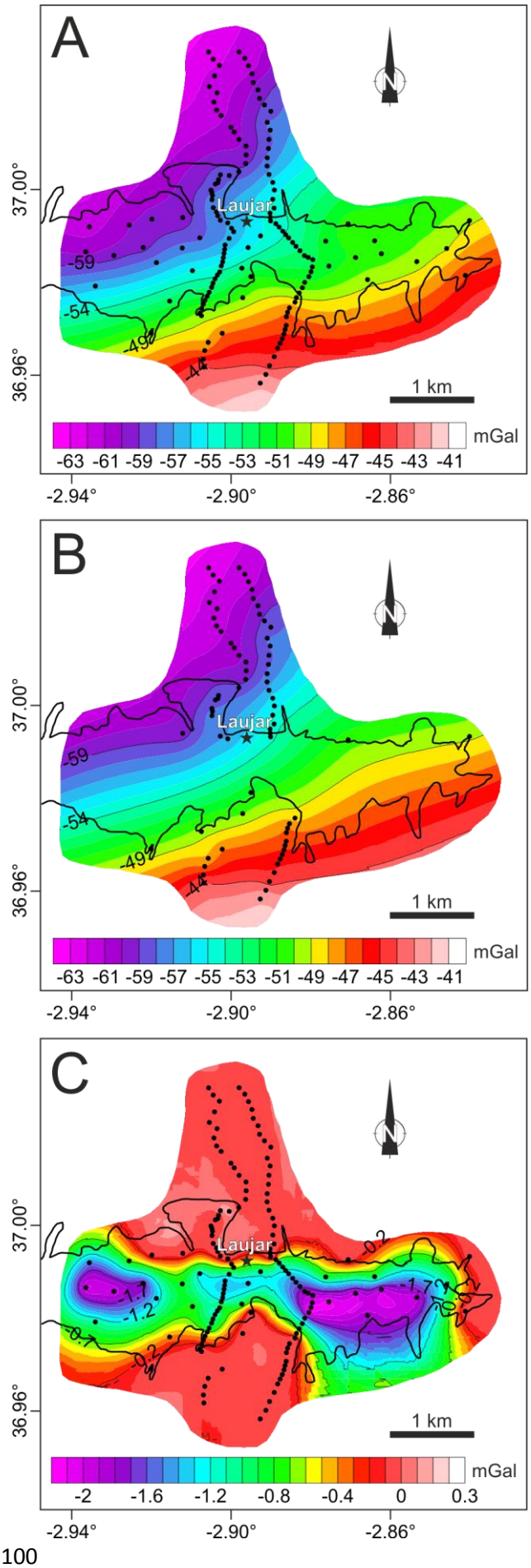

Fig. 7.5 Gravity anomaly maps and gravity station positions. A) Bouguer anomaly map and its decomposition in B) Regional anomaly map and C) Residual anomaly. Black line represents the Neogene and Quaternary sediments boundary.

Magnetic data in this area present anthropic noise in the southern part of the profiles due to the proximity of an urban area and several power lines. Both profiles show magnetic dipoles in the northern part, with the maximum southwards and the minimum northwards (Fig. 7.6). The dipole anomaly is in a range between -37 and 29 nT in profile I-I' and between -60 and 60 nT in profile II-II'. Both dipoles have been modelled with structures with a value of 0.03 SI magnetic susceptibility related to Fe-mineralisations associated to the Alpujárride – Nevado-Filábride contact. However, we did not observe any magnetic anomalies related to the Laujar fault.

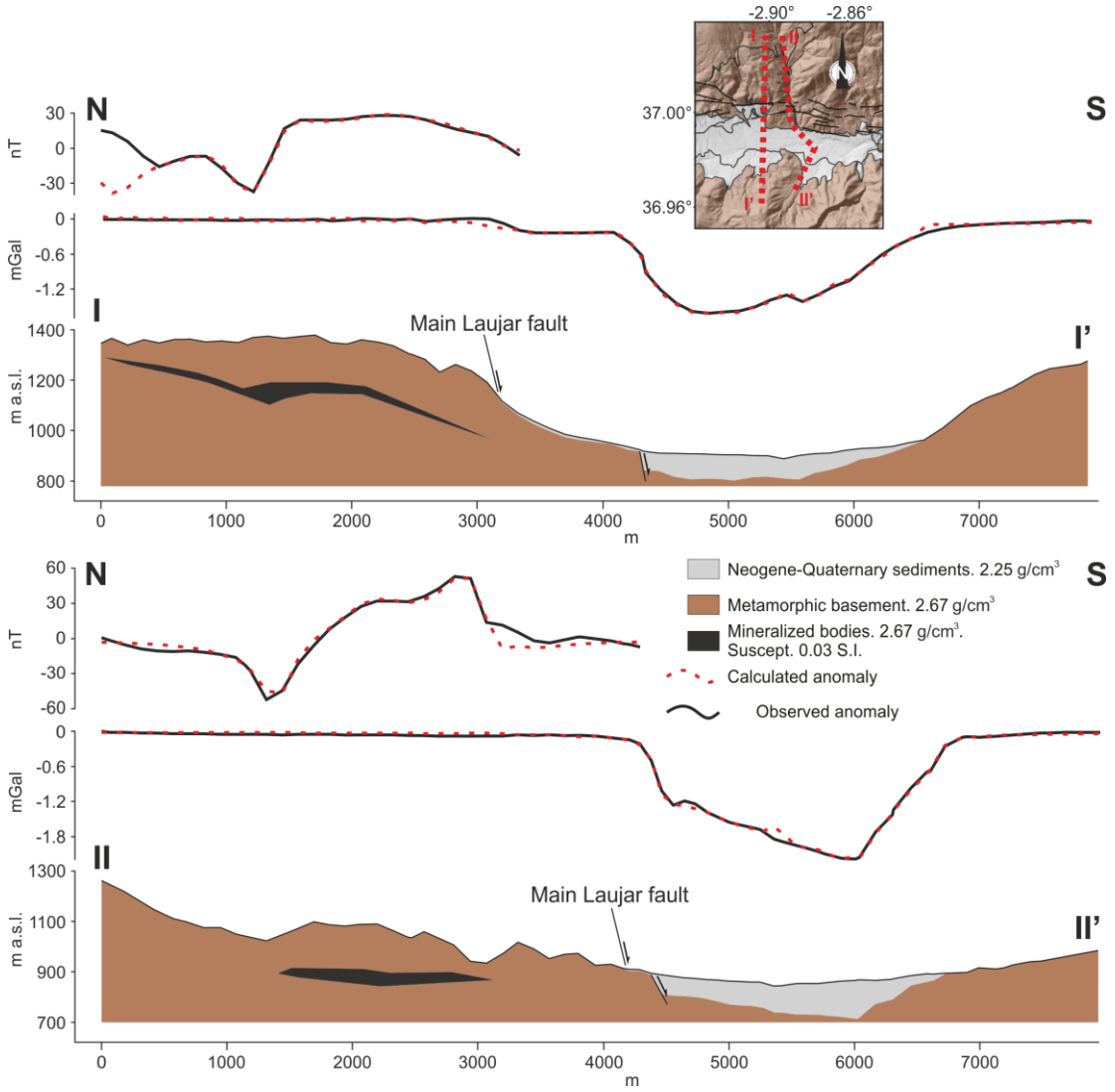

Fig. 7.6 Gravity and magnetic residual anomaly profiles (top) and gravity-magnetic associated models (bottom). Vertical exaggeration is twice the vertical scale.

7.4.3 Electrical resistivity tomography

ERT profiles present resistivities ranging from 45 to 98400 Ω·m and show a high resistivity contrast at the main Laujar fault position (Fig. 7.7). High resistivity values are found in the northern part of both profiles, corresponding with the Alpujárride marbles. Medium to low resistivity values are found in the hanging wall of the main fault. Medium resistivity values (880 to 1600 Ω·m) correspond to conglomerates and breccias of the Neogene and Quaternary alluvial fan, varying in thickness from 5 to 30 m towards the south. These sediments lie atop the Alpujárride phyllites (low resistivity values, from 45 to 880 Ω·m) in the hanging wall. Further distinguished in both profiles are intermediate resistivity values embedded in low resistivity ones (at 100-150 m length in profile 1-1′ and 100-125 m length in profile 2-2′) that present straight limits parallel to the main outcropping fault plane. This structure suggests that its lateral southward limit represents a secondary sealed normal fault plane parallel to the outcropping one.

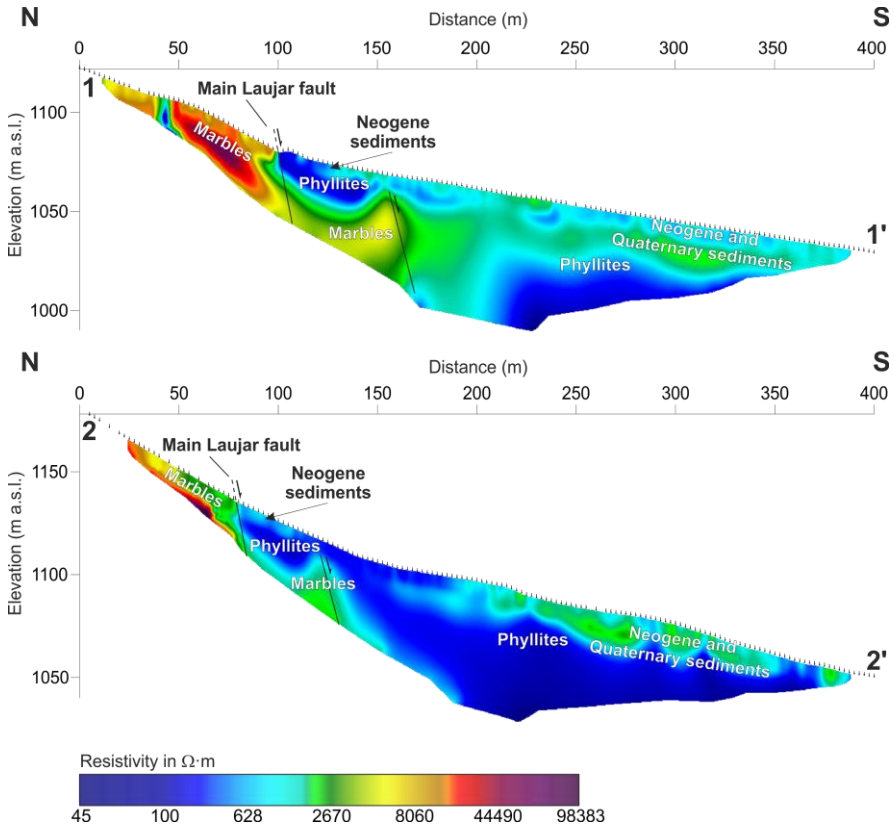

Fig. 7.7 ERT profiles with interpreted lithologies and different fault planes marked.

7.4.4 Audio-magnetotelluric data and 2D inversion

Several bodies with diferent resistivity values can be identified in the profile. The northern part of the profile (Fig. 7.8) shows a low resistivity body (~70 ohm·m) corresponding with a shallow outcrop of Alpujárride phyllites. Resistivity rapidly increases (~670 Ω·m at 400-800 m length) towards the south, where the Alpujárride marbles crop out. The main Laujar Fault scarp appears at 900 m as a marked resistivity contrast, where the fault crosscuts the Alpujárride phyllites, orienting them with a north-dipping basal boundary. At 1500 m length intermediate resistivity values (~200 Ω·m) are linked to the detrital sediments, showing that the sedimentary infill thickness increases abruptly at this point due to the presence of a sealed second normal fault. Also observed is a very low resistivity body in depth (~50 Ω·m), most likely corresponding to Nevado-Filábride metapelites based on the geological information.

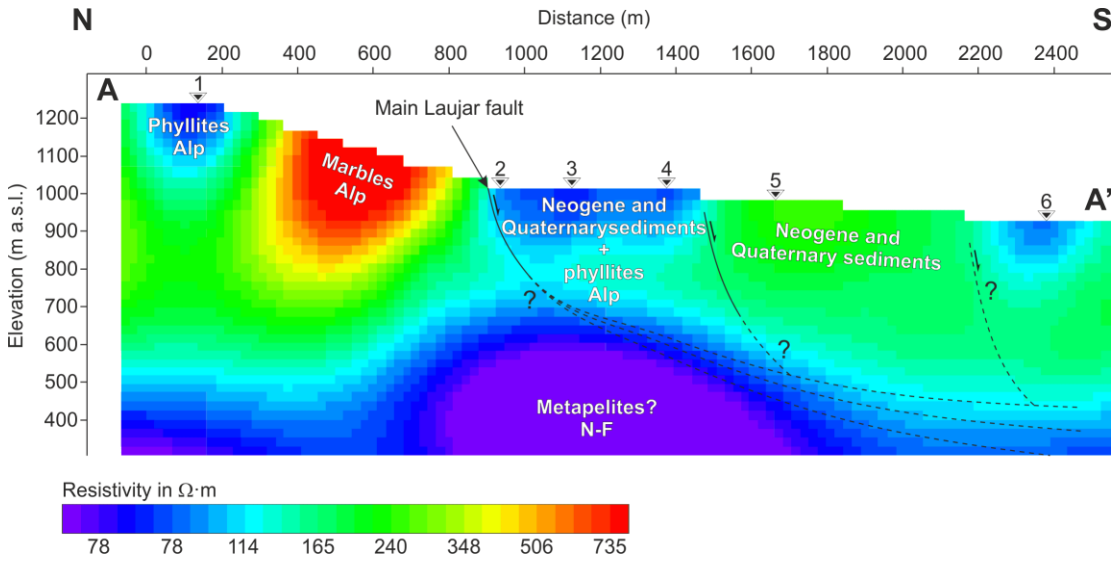

Fig. 7.8 AMT profile with interpreted lithologies and several fault planes marked. Location in Figure 2. Alp (Alpujarride) and N-F (Nevado-Filábride) indicate the metamorphic complex corresponding to each lithology.

7.5 Discussion

Study of the Laujar Fault Zone provides the chance to analyse the development of extensional structures in compressional settings. The fault zone is located along the Alpujarran Corridor, an E-W aligned synformal structure affected by parallel faults (Figs. 7.1 and 7.2). This region of the central-eastern Betic Cordillera has been studied by several researchers that recognize the presence of strike-slip, reverse and normal faults, but under different tectonic models. Sanz de Galdeano et al. (1985) and Sanz de Galdeano (1996) described the Alpujarran Corridor as the surface expression of a flower structure between two blocks with different westward tectonic transport rates. Galindo-Zaldivar (1986) proposes alternate reverse and normal components of strike-slip in the Ugíjar area as the result of fault plane curvature related to a main extensional fault. Martinez-Diaz and Hernandez-Enrile (2004) support west-southwest escape tectonics southwards of Sierra Nevada due to the Africa – Europe compression related to vertical crustal-scale faults. Martinez-Martinez et al. (2006) suggest that a N-S compression with a subsequent E-W extension make the Nevado-Filábride crop out as a metamorphic core-complex. In the latter model, the Alpujárride units are transported westwards by normal faults, perpendicular to the Alpujarran Corridor, that converge in the Alpujárride – Nevado-Filábride detachment, as earlier proposed by Jabaloy et al. (1992). Still, none of these models explains the existence of normal recent faults affecting Plio-Quaternary sediments in the Laujar Zone.

CGPS results determine that the Central Betics undergo westward tectonic transport in respect to the Iberian Massif foreland as a result of rollback subduction in the Gibraltar Arc (Galindo-Zaldivar et al., 2015; González-Castillo et al., 2015). The stations located at Sierra de los Filabres and Almería have westward CGPS displacement (Fig. 7.1), but Almería, located at the southeastern edge of Sierra de Gádor, includes additional southward and westward components. Sierra Nevada station shows a higher westward component than Sierra de Los Filabres toward the west, without additional southward

displacement. Moreover, the station located nearby Motril, at the western termination of the Alpujarran Corridor presents a higher W-SW displacement. This high rate have been attributed to NNW-SSE normal faults located in western Sierra Nevada and between Sierra de la Contraviesa and Sierra de Gádor (Fig. 7.1), which displace the Alpujárride units toward the WSW simultaneous to the NW-SE to N-S shortening related to E-W to NE-SW folds well exposed in Campo de Dalías area (Marín-Lechado et al., 2005; 2010; Galindo-Zaldivar et al., 2015; Pedrera et al., 2015). In any case, the geological field observations in the study area support a N-S extension for the latest stage of the Laujar Fault Zone, since only vertical striations affect the recent calcretes in the fault plane (Fig. 7.3). These results suggest that the Sierras de Gádor and La Contraviesa are currently moving towards the south-southwest with respect to Sierra Nevada and Sierra de los Filabres. Such a setting is moreover compatible with the activity of E-W normal faults like the Laujar Fault Zone along the Alpujarran Corridor separating the two sierras.

Local studies in the Laujar Fault Zone suggest that seismicity has a maximum expected magnitude (Mw) of 6.4 ±0.37 and a recurrence period of 3243 yrs (http://info.igme.es/qafi). However, these observations are supported taking into account simple fault models. Results provided by combining different geophysical techniques in this area suggest that faults converge in a relatively shallow detachement (Fig. 7.9). Several sealed fault planes have been detected at different depths as can be identified in ERT, gravity and AMT profiles, some of them having 30 to 65 m of vertical slip. In addition, AMT results suggest that several listric faults converge in a southwards-dipping detachment and make the Alpujárride formations dip against the fault surfaces (Fig. 7.8). These observations could highly modify the palaeosismological parameters previously mentioned, pointing to the presence of a complex fault zone with lower related seismic hazard.

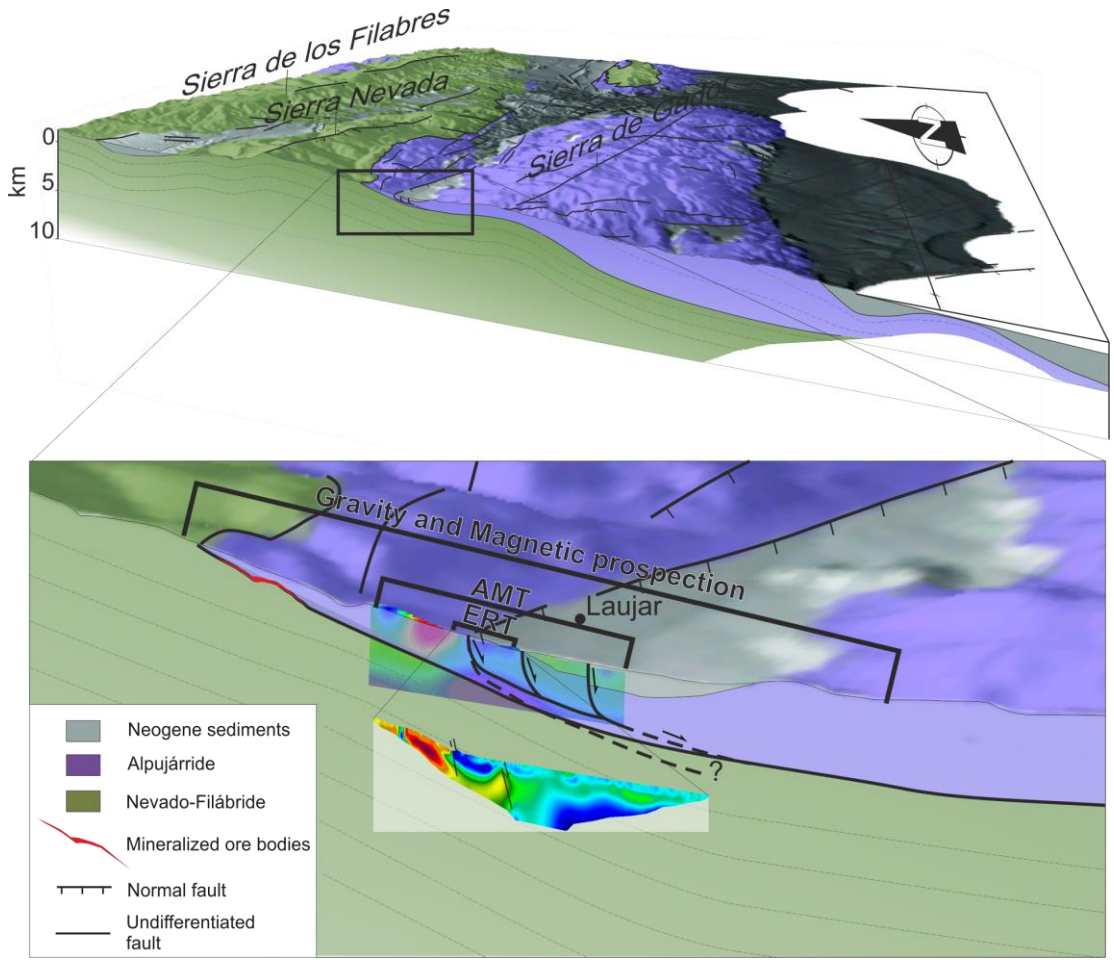

Fig. 7.9 Integrated interpretation of geophysical data applied in the Laujar Fault Zone.

Recent fault activity is supported by the continuous exposure of the outcropping fault plane and the clastic wedges of Quaternary sediments on the hanging wall of the main outcropping fault plane (Fig. 7.4). Although radiocarbon dating has some limitations due to the incorporation of 14C from surrounding rocks, organic matter or atmospheric CO2, it has been widely applied to calcretes to evidence recent fault activity (e.g. Talma and Netterberg, 1983; Yijian et al., 1988; Amundson et al., 1994; Geyh and Eitel, 1998; Deuth et al., 2001; Potts et al., 2009). Striated calcrete ages suggest that the Laujar Fault Zone has been active at least until the last 14560 yrs BP and may be considered as a main active normal fault of the southern limb of eastern Sierra Nevada. In addition, these new geophysical data suggest that the deformation progresses northwards in the fault zone, since

the southern faults are progressively covered by higher thicknesses of sedimentary infill towards the south.

Geological observations on recent E-W normal faults and joints in addition to CGPS results confirm the existence of a relative N-S extension in the study area that displaces the regions south of Sierra Nevada further southwards. Such local N-S extension contrasts with the regional present-day convergence between Africa and Eurasia (Dewey et al., 1989; DeMets et al., 1994; Rosenbaum et al., 2002; Sanz de Galdeano and Alfaro, 2004). However, plate tectonic models compared with GPS data reveal an anticlockwise rotation in the convergence trend 3.2 Myrs ago in the western Mediterranean (Calais et al., 2003), which result in a decrease in the N-S convergence component. Possibly due to the mentioned decrease, crustal thickening in Sierra Nevada, north of the Alpujarran Corridor is no longer stable, and this area acts as a deformation backstop that may show signs of collapse since the N-S compression rate can no longer hold it (Platt, 1986). In this setting, we propose that the N-S extension evidenced by the Laujar Fault Zone is a direct consequence of an extensional collapse in the southern part of Sierra Nevada that is also related to the south-westwards displacement of Sierra de Gádor and Sierra de la Contraviesa. Simultaneously, NW-SE compression remains active to the south of the study area with a thinner crustal continental crust, easily deformable by the present day regional plate convergence, as can be evidenced by the folded Neogene sediments in coastal regions of the Alboran Sea (Marin-Lechado et al., 2007; Pedrera et al., 2015) (Fig. 7.10). The N-S extension accordingly contributes to the latest stages of the Sierra Nevada metamorphic antiformal core uplift with respect to the southern domains.

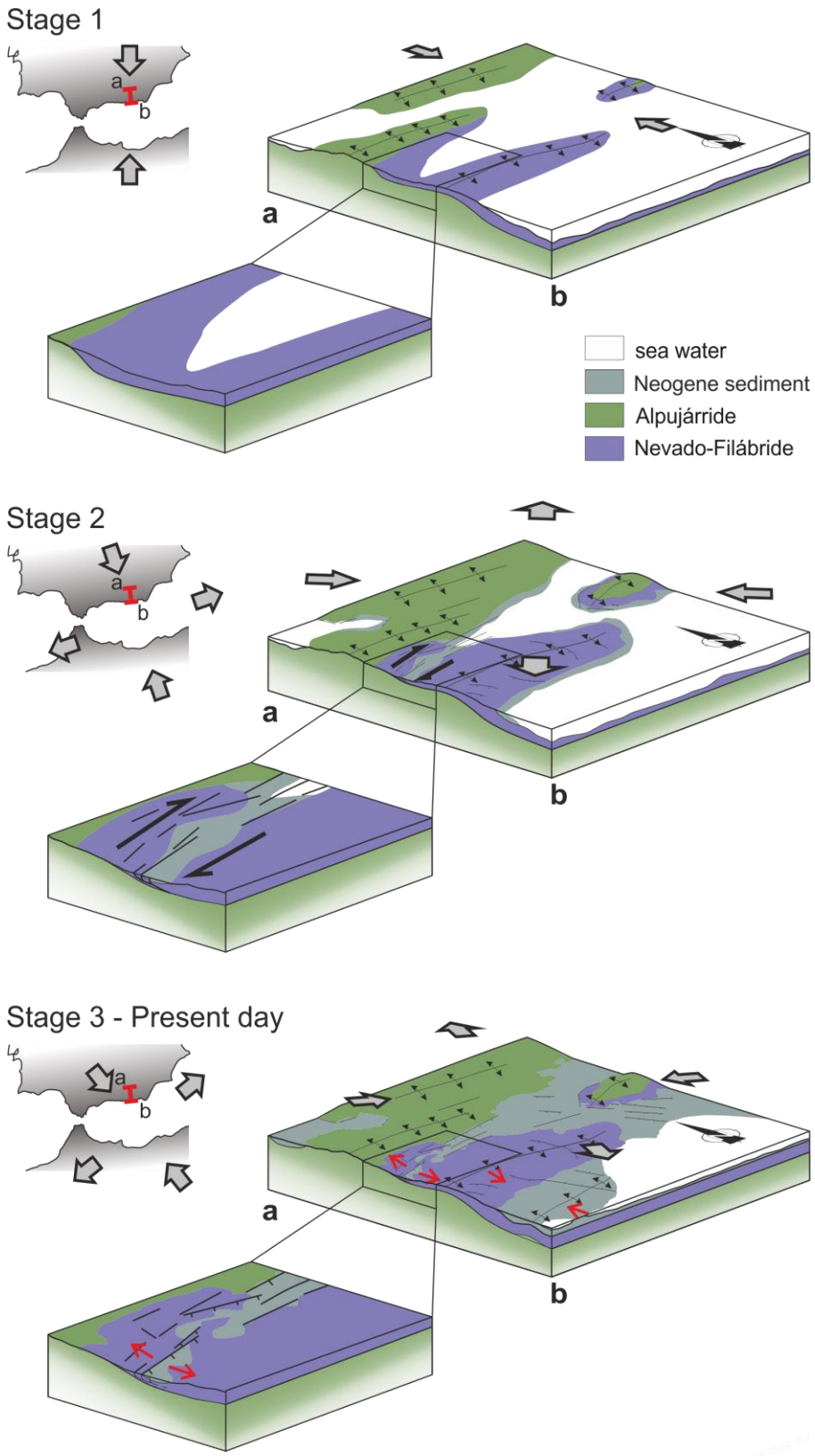

Fig. 7.10 Geodynamic evolution of the study area in the context of the Cordillera and the Africa-Eurasia convergence changes.

7.6 Conclusions

Laujar Fault Zone is an E-W oriented southward-dipping active normal fault parallel to the recent compressional large folds, both contributing to the Sierra Nevada metamorphic core exhumation. Outcropping fault scarps, Quaternary colluvial wedges and striated calcrete ages, in addition to regional CGPS data, support the recent normal fault activity developed on a previous dextral strike-slip fault zone. Shallow geophysical data including ERT, AMT, gravity and magnetic researches suggest the presence of sealed normal faults below the Alpujarran Corridor sediments and fault activity propagation northwards, towards the southern edge of Sierra Nevada antiform. Faults probably join a southward-dipping low-angle normal fault segment. The apparent contradiction of active extension parallel to regional compression may be a consequence of the extensional collapse of the crustal thickened areas such as the Sierra Nevada antiform in a tectonic scenario of decreasing N-S compression, due to recent rotation of the plate convergence trend, coetaneous with the continuity of shortening in other southward regions of the plate boundary.

Acknowledgements

We acknowledge the comments of Prof. Marcello Schiattarella and an anonymous reviewer that have improved the quality of the study. This research was funded by the Spanish Government through projects CGL2016-80687-R and the RNM148 research group of the Junta de Andalucía.

CHAPTER 8

The Padul normal fault activity constrained by GPS data: brittle extension orthogonal to folding in the Central Betic Cordillera

Antonio J. Gil[a,b], Jesús Galindo-Zaldivar[c,d], Carlos Sanz de Galdeano[d], Mª Jesús Borque[a,b], Alberto Sánchez-Alzola[e], Manuel Martinez-Martos[c,d], Pedro Alfaro[f]

Submitted to:
Tectonophysics, 2017
(Under second review from February 2, 2017)

[a] Dpto. Ingeniería Cartográfica, Geodésica y Fotogrametría, Universidad de Jaén, 23071 Jaén, Spain.

[b] Centro de Estudios Avanzados en Ciencias de la Tierra (CEACTierra), Universidad de Jaén. 23071 Jaén, Spain.

[c] Dpto. Geodinámica, Universidad de Granada, 18071Granada, Spain.

[d] IACT, CSIC-Universidad de Granada, 18071 Granada.

[e] Dpto. Estadística e Investigación Operativa, Universidad de Cádiz. 11405 Cádiz, Spain.

[f] Dpto. Ciencias de la Tierra y Medio Ambiente, Universidad de Alicante, Alicante, Spain.

ABSTRACT

The Padul Fault is located in the Central Betic Cordillera, formed in the framework of the NW-SE Eurasian-African plate convergence. In the Internal Zone, large E-W to NE-SW folds of western Sierra Nevada accommodated the greatest NW-SE shortening and uplift of the cordillera. However, GPS networks reveal a present-day dominant E-W to NE-SW extensional setting at surface. The Padul Fault is the most relevant and best exposed active normal fault that accommodates most of the NE-SW extension of the Central Betics. This WSW-wards dipping fault, formed by several segments of up to 7 km maximum length, favored the uplift of the Sierra Nevada footwall away from the Padul graben hanging wall. A non-permanent GPS network installed in 1999 constrains an average horizontal extensional rate of 0.5 mm/yr in N66ºE direction. The fault length suggests that a (maximum) 6 magnitude earthquake may be expected, but the absence of instrumental or historical seismic events would indicate that fault activity occurs at least partially by creep. Striae on fault surfaces evidence normal-sinistral kinematics, suggesting that the Padul Fault may have been a main transfer fault of the westernmost end of the Sierra Nevada antiform. Nevertheless, GPS results evidence: (1) shortening in the Sierra Nevada antiform is in its latest stages, and (2) the present-day fault shows normal with minor oblique dextral displacements. The recent change in Padul fault kinematics will be related to the present-day dominance of the ENE-WSW regional extension versus ~NNW-SSE shortening that produced the uplift and northwestwards displacement of Sierra Nevada antiform. This region illustrates the importance of heterogeneous brittle extensional tectonics in the latest uplift stages of compressional orogens, as well as the interaction of folding during the development of faults at shallow crustal levels.

Keywords: Betic Cordillera; Padul Fault; Active Tectonics; GPS; extensional deformation.

8.1 Introduction

The development of normal faults at shallow crustal levels accompanies shortening during the latest stages of cordillera uplift (Hodges et al., 1998; Galindo-Zaldívar et al., 2003; McDermott et al., 2015). The Eurasian-African plate convergence has a NW-SE trend in the westernmost Mediterranean (Nocquet, 2012), where the Betic-Rif Cordillera is located. In the Central Betic Cordillera, present-day deformation is split into E-W to NE-SW folding accommodating ~NNW-SSE shortening, and normal faulting accommodating ~ENE-WSW extension (Galindo-Zaldívar, 2003, 2015; Ruano et al., 2004).

The most important fault sets in the Betic Cordillera (Fig. 8.1), developed from the late Miocene onward, show NNE-SSW (mainly affecting the eastern part of the cordillera) and NW-SE orientations (Sanz de Galdeano, 1983). These faults interact with large folds promoting the formation of the intramontane Neogene basins. Normal faults contributed together with the development of large antiforms to the uplift of the Sierra Nevada and the relative subsidence of the Granada Basin (Figs. 8.1 and 8.2). The total throw, considering multiple faults, is of the order of 5000 m. These faults formed under NNW-SSE compression (from NW-SE to NNE-SSW) combined with orthogonal extension, displacing upper Neogene to Quaternary sediments. Therefore, several of them remain active and producing seismicity (Sanz de Galdeano et al., 2003; Sanz de Galdeano et al., 2012). Sierra Nevada constitutes a large antiformal structure (Fig. 8.1) formed since the late Serravallian, with a roughly E-W orientation that westwards becomes NE-SW at the southwestern antiformal end (Pedrera et al., 2012).

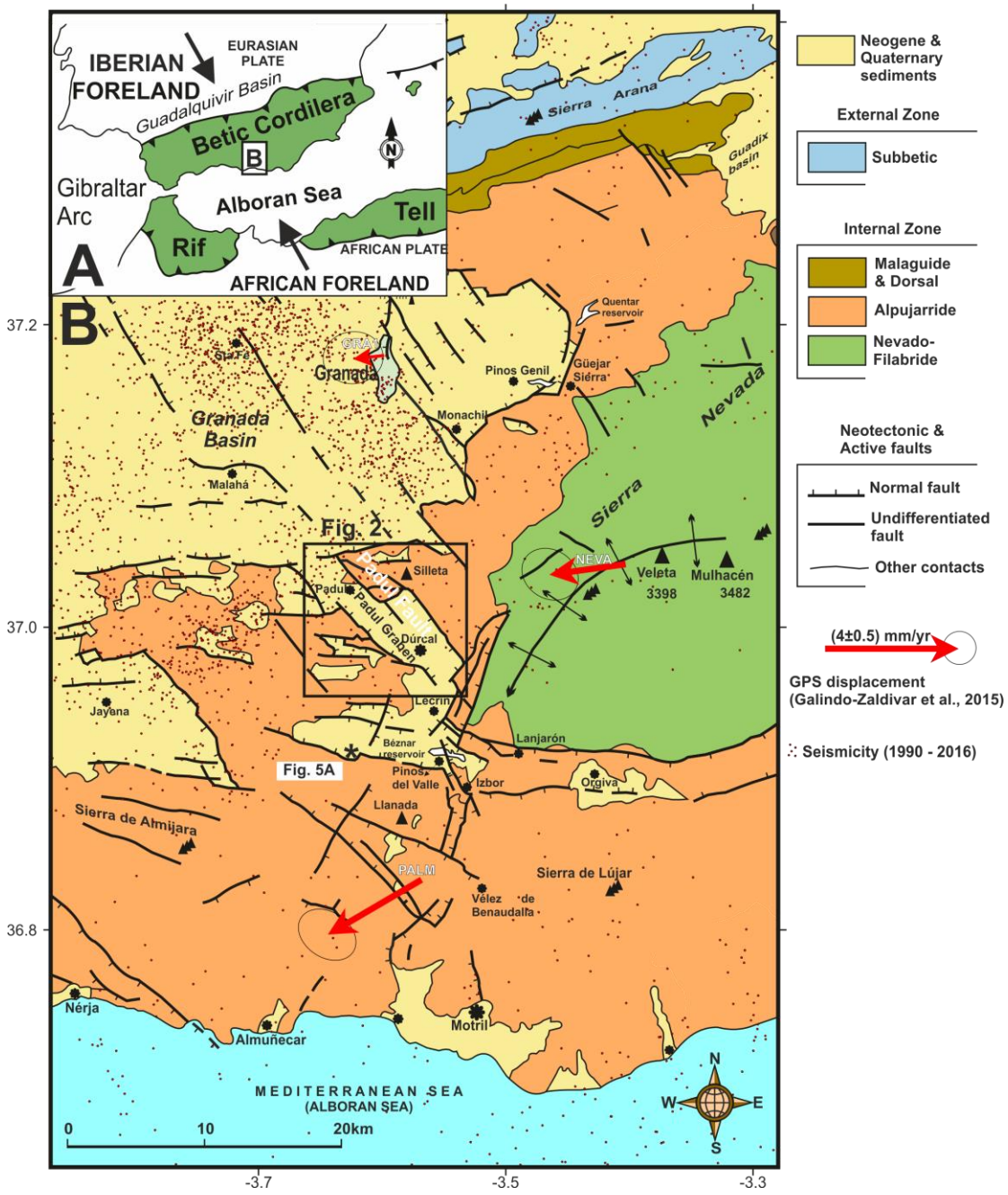

Fig.8.1 Regional geological setting of the Padul Fault. A. Betic Cordillera and Rif placed in between Iberian and African forelands. B. Geological map of the central part of the Betic Cordillera. Epicenters (depth <30 km; 1990 to 2016) from IGN database (www.ign.es).

The development of folds, the elastic behavior of faults, and the rheological heterogeneities in deformation zones can disturb local stresses, as revealed by the earthquake focal mechanisms of the Central Betics and paleostress analysis

(Galindo-Zaldívar et al., 1999). Local GPS networks improve the determination of present-day fault kinematics and rates obtained from geological observations, contributing to better understand the variability and behavior of active faults. GPS processing methods such as Precise Point Positioning (PPP) (Zumberge et al., 1997) stand as valuable tools for investigating geodynamical processes at the millimetric level (Larson et al., 2004; Smith et al., 2004, Kouba 2005; Hreinsdóttir et al., 2006).

The aim of this research is to analyze the present-day and the recent behavior of the Padul Fault from geological and GPS data (period 1999-2012) in order to determine its relevance in the framework of regional deformation and the development of the Sierra Nevada antiform. This research provides new data on the present-day tectonic activity of the Padul Fault, the best exposed fault of the Central Betics, and contributes to discussion of its seismic behavior. Its activity is analyzed in the context of fault and fold interaction accommodating roughly simultaneous extensional and compressional deformation.

8.2 Geological setting

The Betic Cordillera, together with the Rif (Fig. 8.1), belongs to the Alpine belt of the Western Mediterranean, forming the Gibraltar Arc in the Eurasian and African plate boundary. The Alboran Sea is the main Neogene basin located in the central part of the orogen. The Internal Zone is formed by several superposed metamorphic complexes, the main ones (from bottom to top) being the Nevado-Filábride, the Alpujárride and the Malaguide. Flysch Units crop out discontinuously along the contact between the Internal and the External Zones. Sierra Nevada (Fig. 8.1) belongs to the Internal Zone and is formed by Nevado-Filabride and Alpujarride complexes, composed of graphite-bearing schist, quartz- feldspar rich schist and marbles of Paleozoic to Triassic ages that have undergone HP/LT alpine metamorphism (Monié et al., 1991). These complexes are separated by the low-angle normal Mecina fault, active during the Early to Middle Miocene (Galindo-Zaldívar et al., 1989; Jabaloy et al., 1992). The Late Miocene to present-day NW-SE to N-S shortening in the Betic Cordillera has been

accommodated by large E-W to NE-SW folds and several strike-slip and normal fault sets (Sanz de Galdeano, 1983; Galindo-Zaldívar et al., 2003) producing the main reliefs and also the development of intramontane sedimentary basins (Braga et al., 2003; Sanz de Galdeano and Alfaro, 2004). Sierra Nevada constitute the largest and highest antiformal structure of the Betic Cordillera. The main fault sets have NW-SE, NE-SW and E-W orientations and were active since the Miocene (Sanz de Galdeano, 1993). N-S compression and orthogonal extension paleostress fields was related to NW-SE dextral and NE-SW sinistral faults. Anticlockwise rotation of compression to NW-SE produced the development of E-W dextral faults and the reactivation of NW-SE faults that became normal (Sanz de Galdeano, 1993).

Seismicity in the region is irregularly distributed and belongs to the broad active deformation band, more than 300 km wide, which separates Eurasian and Africa in the westernmost Mediterranean (Udías and Buforn, 1991; Galindo-Zaldivar et al., 1993). The seismic activity in the 1990-2016 period obtained from I.G.N. database (www.ign.es) reveals a high concentration of epicenters in the Neogene-Quaternary Granada Basin, located west of Sierra Nevada (Fig. 8.1), mainly related to NW-SE active normal faults (Sanz de Galedano et al., 2003; 2012). However, seismicity decreases southeastward, in Sierra Nevada, Sierra de Lujar and Sierra de la Almijara and also in the Padul graben, with scarce widespread activity (Fig. 8.1).

A regional GPS network was deployed by the Topo-Iberia project (Garate et al., 2015). The available data support the present-day W and WSW displacements of the Internal Zones of the Central Betic Cordillera with respect to the relatively stable Iberian foreland (Galindo-Zaldívar et al., 2015). This displacement field evidences an E-W to ENE-WSW extensional deformation in the westernmost part of Sierra Nevada, in addition to a locally very moderate NW-SE shortening along the westernmost part of the Sierra Nevada antiform.

8.3 The Padul Fault

The Padul Fault (Figs. 8.1, 8.2, 8.3 and 8.4), located in the Internal Zone of the Betic Cordillera, is the most remarkable normal fault of this region from a geomorphic point of view. This active fault separates the highest reliefs of Sierra Nevada (footwall) from the Granada basin that in this sector is represented by the Padul graben (Sanz de Galdeano and Alfaro, 2004), developing a spectacular mountain front (Figs. 8.3A and 8.3B) sculpted in Alpujarride marbles (Lhénaff, 1965; Calvache et al., 1997). This NW-SE fault is formed by a northern segment of 5.25 km and a southern segment of 7 km connected by a 1.5 km relay fault (Figs. 8.1 and 8.2). The throw of the fault is substantial —over 800 m in its central part— (Santanach et al., 1980).

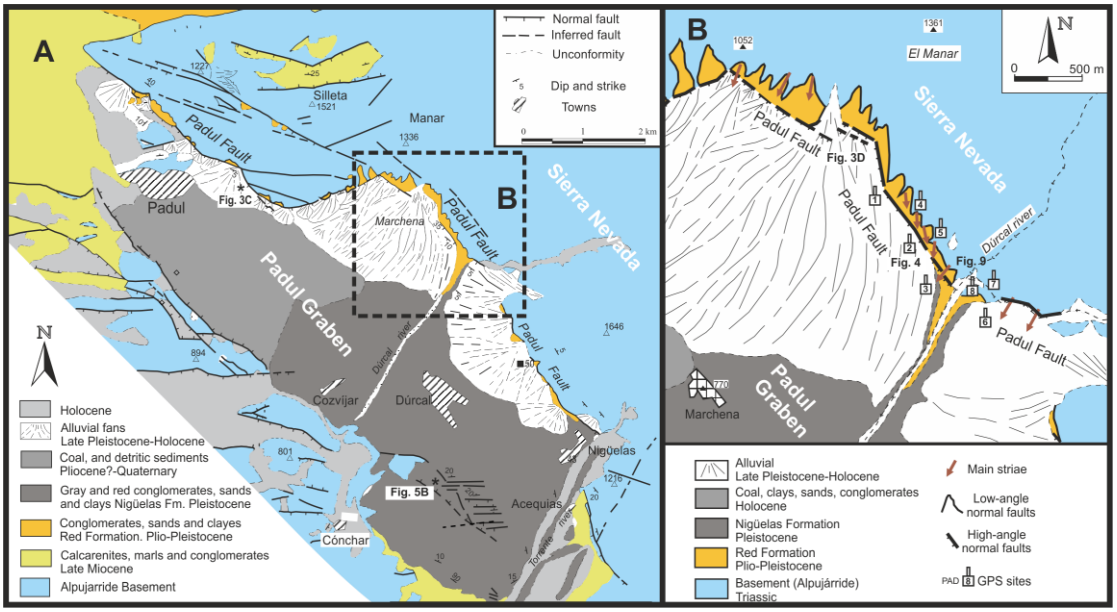

Fig. 8.2 The Padul Fault. Detailed geological maps of the fault (A), including position of GPS network and straie in its central part (B). Location is marked in Fig. 8.1.

The fault surfaces have a variable dip to the SW, ranging from 60-65º to less than 20º. Its displacements are predominantly normal, although in many places there is a slight to moderate left lateral component (Fig. 8.3C). In the hanging wall

block, the Padul graben formed since the end of the Miocene, and it is filled by Late Tortonian calcarenites and Messinian marls. During the Pliocene and the Quaternary, the basin was filled by mainly alluvial fans and peat deposits, which merge laterally with lacustrine deposits towards the center of the basin (Domingo-García et al., 1983; Delgado et al., 2002). The most recent alluvial deposits, dating from Late Pliocene to Pleistocene in age, can be grouped into various units (Fig. 8.2). At the base there is a Plio-Pleistocene unit called the Red Formation, made up of reddish-brown clays, sands and alluvial conglomerates. Overlying these rocks are conglomerates with grey and reddish boulders deposited by the Torrente River (Nigüelas Formation). At the top of the sequence, the alluvial fans of the Late Pleistocene-Holocene are found, developed along the north-eastern edge of the basin.

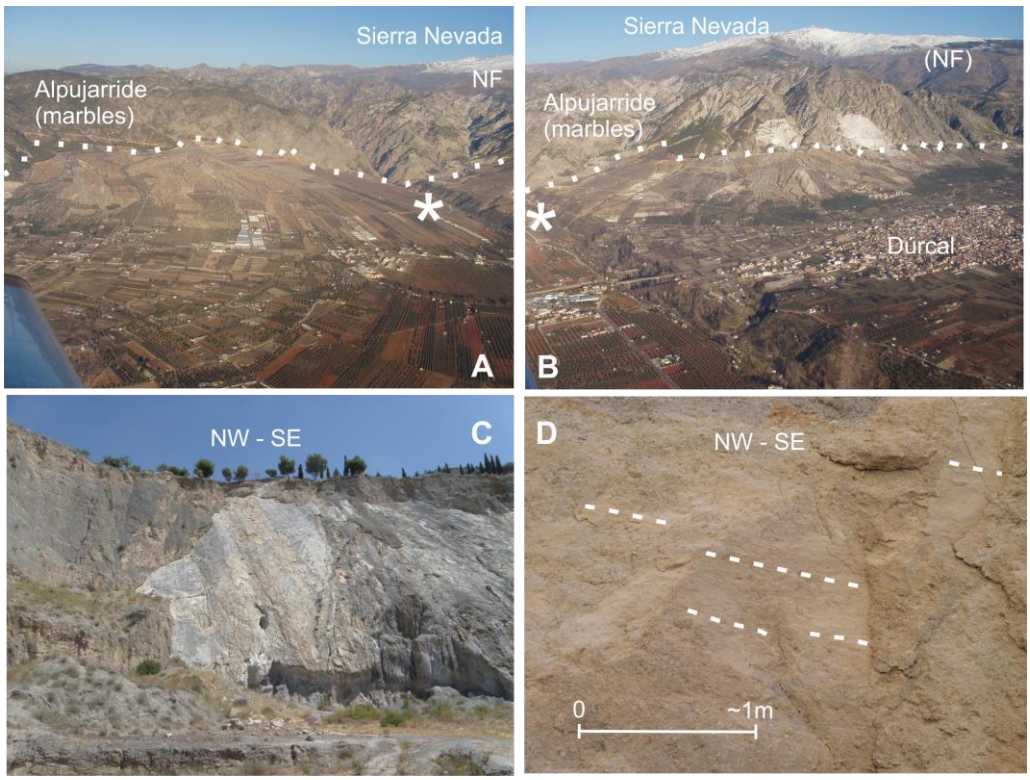

Fig. 8.3 Field structures of the Padul Fault. Aerial view (A and B). Main fault surface separating Alpujarride Triassic marbles and Plio-Quaternary alluvial fan deposits with normal sinistral striae (C) in a segment indicated in Fig. 8.2A. Recent dextral striae in alluvial fan deposits (D) in a segment indicated in Fig. 8.2B.

The fault has a continuous scarp developed in the contact with the footwall basement, and well preserved small scarps (1-2 m high) in recent sediments, in some cases showing a complex geometry locally including dextral striae (Fig. 8.3D). In the sector where the GPS-network is installed, the complex geometry of the Padul fault zone has produced a wide variety of dips in the Plio-Quaternary alluvial deposits (Fig. 8.4). The older Plio-Pleistocene alluvial sediments from the Red Formation lie directly over low-angle fault planes, showing a back-tilting of 5º-45º towards the NE (Fig. 8.4). These alluvial sediments cover the triangular facets of the mountain front (Fig. 8.4). Contrariwise, the Late Pleistocene and Holocene alluvial unconsolidated sediments dip basinwards. Even though the Padul Fault shows evidence of paleoseismic activity (Alfaro et al., 2001), there is no significant related seismicity in the historical and instrumental record.

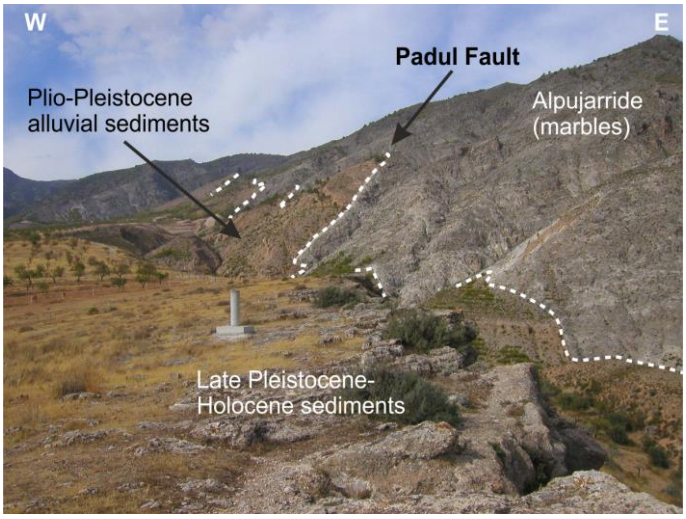

Fig. 8.4 Field view of the Padul Fault in the segment of GPS network. Location in Fig. 8.2B.

Southwest of Sierra Nevada, a set of roughly E-W oriented normal faults offers evidence of recent activity (Figs. 8.1, 8.2 and 8.5): fresh fault scarps and/or recent sediments are deposited on the hanging wall accommodating a roughly N-S regional extension.

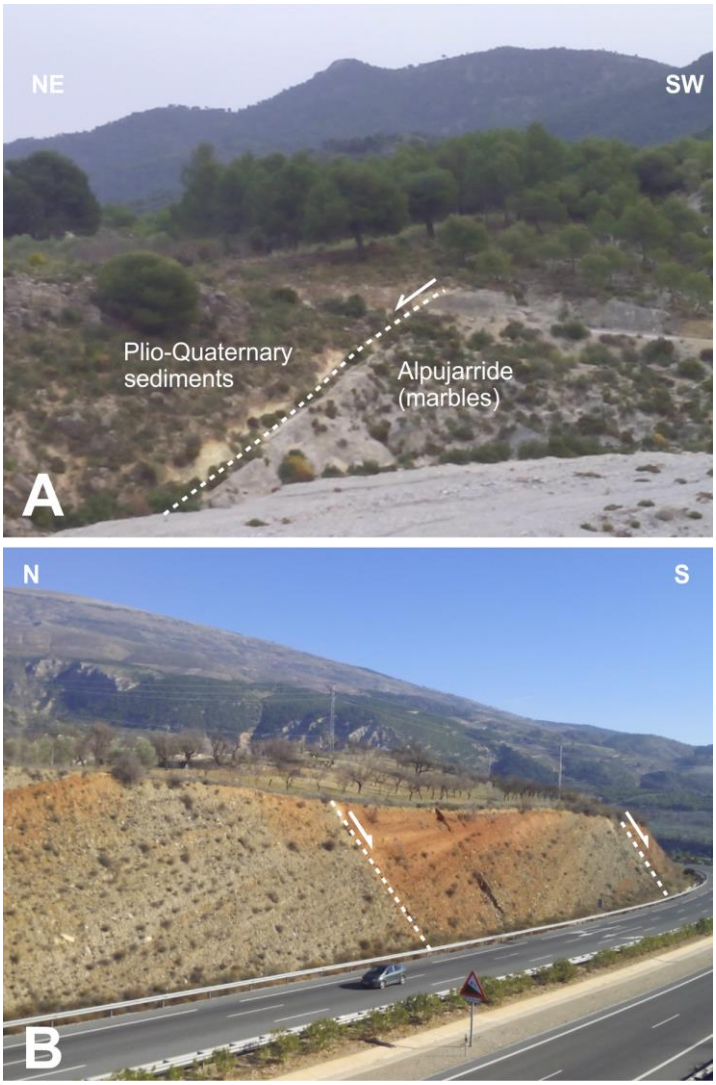

Fig. 8.5 E-W recent and active faults SW of Sierra Nevada. Faults affecting Plio-Quaternary conglomerates at the base of the sedimentary infill (A) and small half grabens in Plio-Quaternary sediments (B). Locations in Figs. 8.1B and 8.2A respectively.

8.4 GPS observations and data processing

In 1999, an eight-site network was established over the Padul Fault (Fig. 8.2B) (Ruiz et al., 2003). The location of each individual site was selected to provide good coverage of the main geological structure in both fault blocks. They were installed on exposed rocks using a self-centering mounting device that guarantees the reinstallation of the antenna exactly at the same horizontal position in each campaign. Thus far five GPS field campaigns were carried out —in March 1999, May 2000, July and September 2011, and finally November 2012— reoccupying the sites for a minimum period of five hours during three days in the older campaigns (1999 and 2000) and 72 hours of continuous observation in the more recent ones (2011 and 2012).

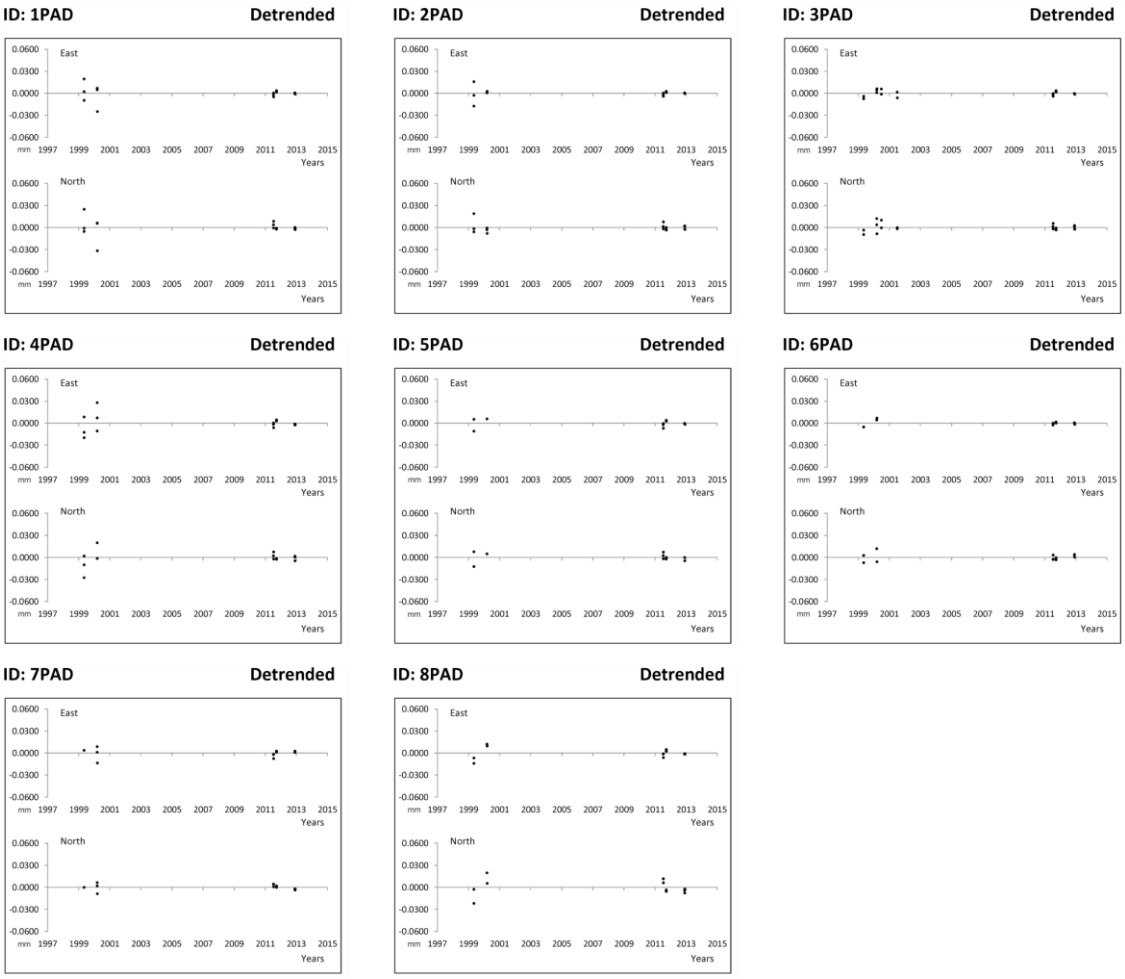

Fig. 8.6 Detrended station position time series. The 3PAD time series has an additional observation campaign in July 2001 from the Granada Basin monitoring network observed in that year (Gil et al., 2002).

In our work the 6.2 version of GIPSY-OASIS software (Gregorius, 1996) was used together with the Precise Point Positioning (PPP) method and the zero-ambiguity resolution strategy described in Bertiger et al. (2010). An identical standard procedure was applied for all campaigns as shown in Sánchez-Alzola et al. (2014): JPL final ephemeris and Pole products were used from a JPL server in a homogenous IGS08 reference frame. The FES2004 ocean tide loading model (Lyard et al., 2006) was also applied. Additionally, the hydrostatic and wet components of the zenith tropospheric delay were included, a 10° cut-off angle was set up, and a calibration file was used to correct the Antenna Phase Center.

8.5 Padul Fault active displacements from GPS data

8.5.1 GPS station position time series

The best trend line was fitted to the time series of positions for each station using linear regression. Figure 8.6 shows the GPS position time series for Padul Fault sites in the IGS08 frame. The 3PAD time series has an additional observation campaign in July 2001 because this site belongs to the Granada Basin monitoring network observed in that year (Gil et al., 2002). Older campaigns have more dispersion due to the poorer quality of the support files; accuracy is better in the campaigns where the JPL products feature modern data analysis.

	Coordinates		Absolute velocities (mm/yr)			
Site	Lat. (°N)	Long. (°E)	VE	σE	VN	σN
1PAD	39.017657	-3.567929	17.1	±0.4	16.3	±0.5
2PAD	37.014799	-3.565582	16.9	±0.3	16.2	±0.3
3PAD	37.012640	-3.564447	17.2	±0.2	16.4	±0.2
4PAD	37.016539	-3.565072	17.8	±0.5	16.8	±0.5
5PAD	37.015511	-3.564049	17.4	±0.3	16.4	±0.3
6PAD	37.009529	-3.560453	17.1	±0.2	16.2	±0.3
7PAD	37.011713	-3.558993	17.5	±0.3	16.4	±0.2
8PAD	37.011390	-3.560405	18.0	±0.3	16.5	±0.5

Table 8.1 Site coordinates and GPS-derived horizontal velocities at the Padul Fault monitoring network in IGS08 reference frame. VE, VN: Absolute velocities in East and North components.

Table 8.1 shows the absolute velocities in the horizontal components with respect to the best-fit trend line, instead of the associated formal uncertainties derived from the processing software. Associated errors are computed considering the

standard deviation of the slope component. Absolute velocity values are consistent with the theoretical tectonic velocity in the area and velocity deviations have magnitudes between 3.0-9.0 mm/yr, similar to those of other studies with GPS episodic campaigns (Perez-Peña et al., 2010a; Rayan et al., 2010). Given the small number of solutions, we did not eliminate any observation unless we had objective reasons such as an incorrect installation or unreliable solution.

8.5.2 GPS-derived velocity field and strain rates

Figure 7 shows the absolute velocity field of the Padul Fault network, derived using solutions from the five campaigns between 1999 and 2012. The large time interval, spanning about 13 years, seems suitable to reduce slope error in episodic campaigns and allowed us to compute reliable estimations of velocity for our sites. Position time series longer than 7.5-8 years long allow for reliable deformation rates in horizontal motion with episodic GPS campaigns (Sanli et al., 2012; Gianniou and Stavropoulou, 2016). The standard error ellipses are based on the formal error derived from the linear trend estimation and deviations. We did not consider the existence of any change in site position during the campaign (the effects of secular motions are negligible). The dispersion is attributed to white noise due to the errors in acquired observations. Figure 8 shows the residual velocity field computed with respect to the average velocity of 4PAD, 5PAD, 7PAD and 8PAD sites. This model is based on the theoretical fault line between these points situated in the footwall, and 1PAD, 2PAD, 3PAD and 6PAD sites located in the hanging wall. Angles and magnitudes of the vectors in the downthrown hanging wall sites are consistent with the fault activity and shows a southwestwards relative displacement with respect to the footwall block. A rate of roughly 0.5 mm/yr of extension in N66^{o}E was determined for the region.

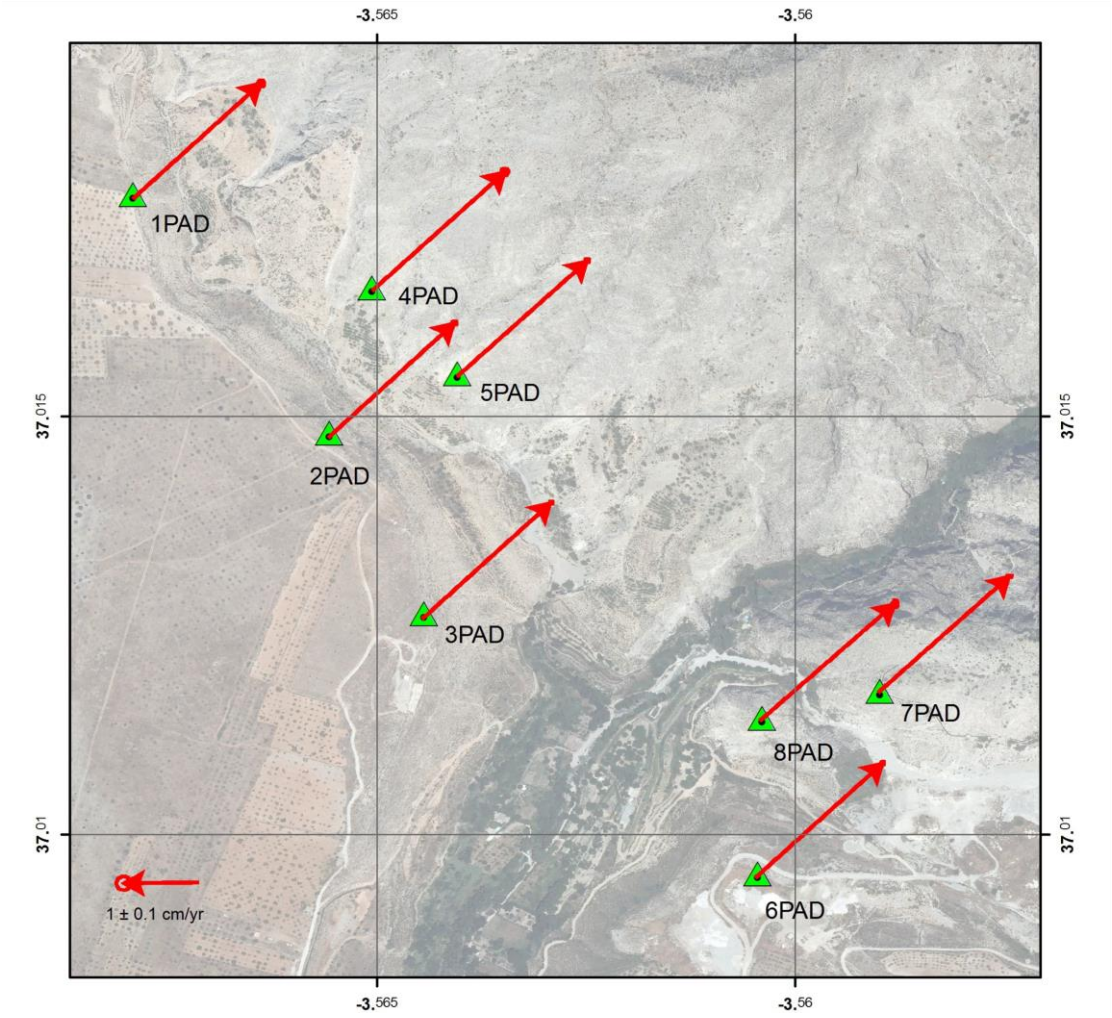

Fig. 8.7 GPS-derived absolute horizontal velocity field in IGS08 frame and standard error ellipses.

In addition, we calculated 2D strain tensors and dilatation and extension values with the maximum shear strains. GRID_STRAIN software (Teza et al., 2008) was used. Figure 8 presents a map with the principal axes of the 2D strain rate. The extension pattern prevails in the fault, and the strain angle shows the main direction of horizontal component of fault slip. The Padul Fault may be considered at present as an active normal fault with moderate oblique dextral kinematics.

8.6 Discussion

The present-day activity of the Padul Fault in the two sectors best constrained by the GPS network (Figs. 8.2, 8.7 and 8.8; Table 8.1) has an approximate horizontal rate of 0.5 mm/yr (0.44 to 0.55 mm/yr; 0.4 to 0.5 mm/yr of E-W component and 0.2 mm/yr of N-S component) horizontal extension in a N66ºE trend. Considering that the average fault dip is 55º, the average displacement on the fault surface should be of 0.78 mm/yr. These geodetic results, obtained for the first time in the Padul Fault, are slightly higher than those (0.16 to 0.35 mm/yr) deduced from stratigraphic markers (Sanz de Galdeano et al., 2012).

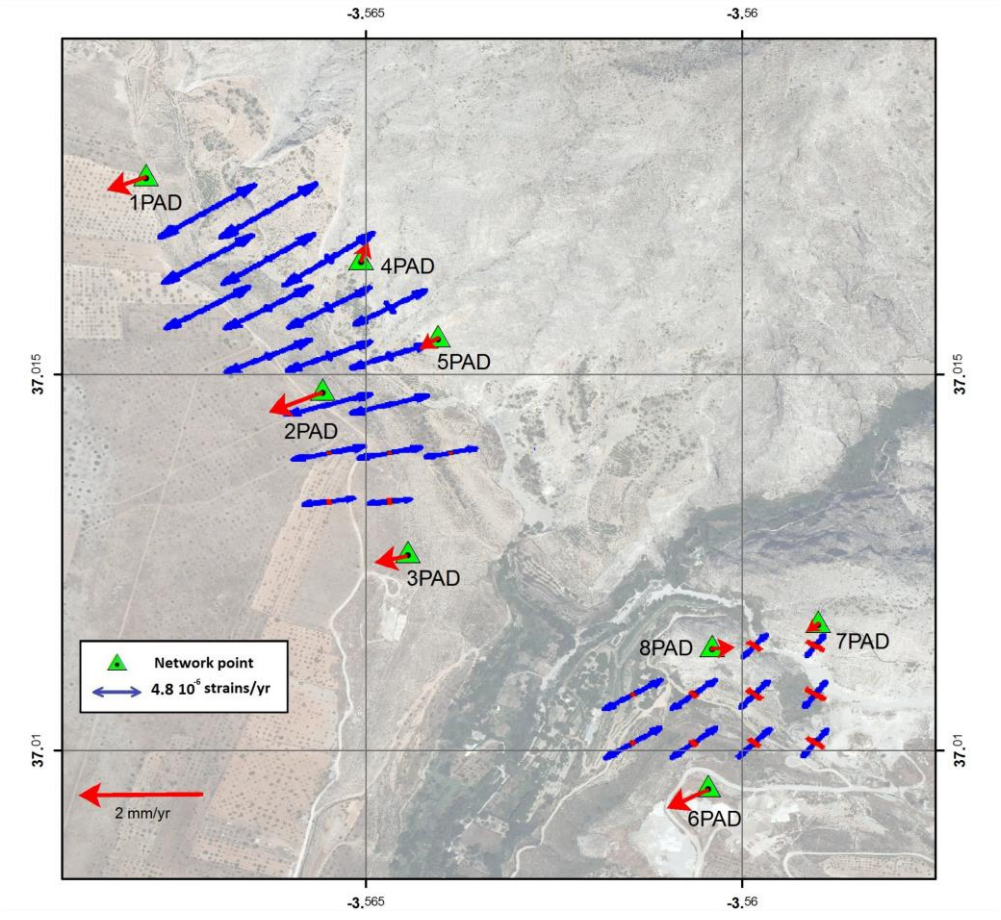

Fig. 8.8 GPS-derived horizontal velocity field with respect to average velocity of 4PAD, 5PAD, 7PAD and 8PAD sites. Map of the principal axes of the 2D strain rate tensor in units of 10-6 strain/yr. Blue and red strains respectively show extension and contraction.

Taking into account that the largest fault segment is about 7 km in length, a hypothetical earthquake of M=6 might be produced by this segment with a total slip of 0.12 m, according to the Wells and Coppersmith (1994) relationships. With the measured GPS rates, this slip is accumulated every 154 years. However, the historical and instrumental seismic records (www.ign.es) do not provide any evidence of large earthquakes in this sector, at least in the last 500 yrs. Despite geological evidence of seismic events in the area (Alfaro et al., 2001), these results suggest that this major fault may have a mixed behavior, including seismic and aseismic deformation.

The activity of the Padul Fault evidenced by the local GPS network (Figs. 8.2, 8.7 and 8.8) may be considered in the framework of the regional deformation (Fig. 8.1) established by the Topo-Iberia network (Galindo-Zaldívar et al., 2015; Gárate et al., 2015). The relative displacement of the PALM site, located in the Alpujarride Complex southwestward of the fault, with respect to the NEVA site, located in the Sierra Nevada footwall, indicated a 1.43 mm/yr horizontal extension in N22^{o}E orientation with a 0.53 mm/yr eastward component and 1.33 mm/yr southward component. These data suggest that the Padul Fault accommodated most of the ENE-WSW regional extension southwestward of Sierra Nevada.

According to the regional GPS network (NEVA and PALM GPS sites), the deduced N-S regional extension (1.13 mm/yr) is only partially justified by the Padul Fault, and would entail the activity of other brittle structures. This N-S extension is related to a set of roughly E-W normal faults, of smaller sizes than the Padul Fault and with widespread deformation in the entire region, such as those observed in several localities southwest of Sierra Nevada (Figs. 8.1, 8.2 and 8.5).

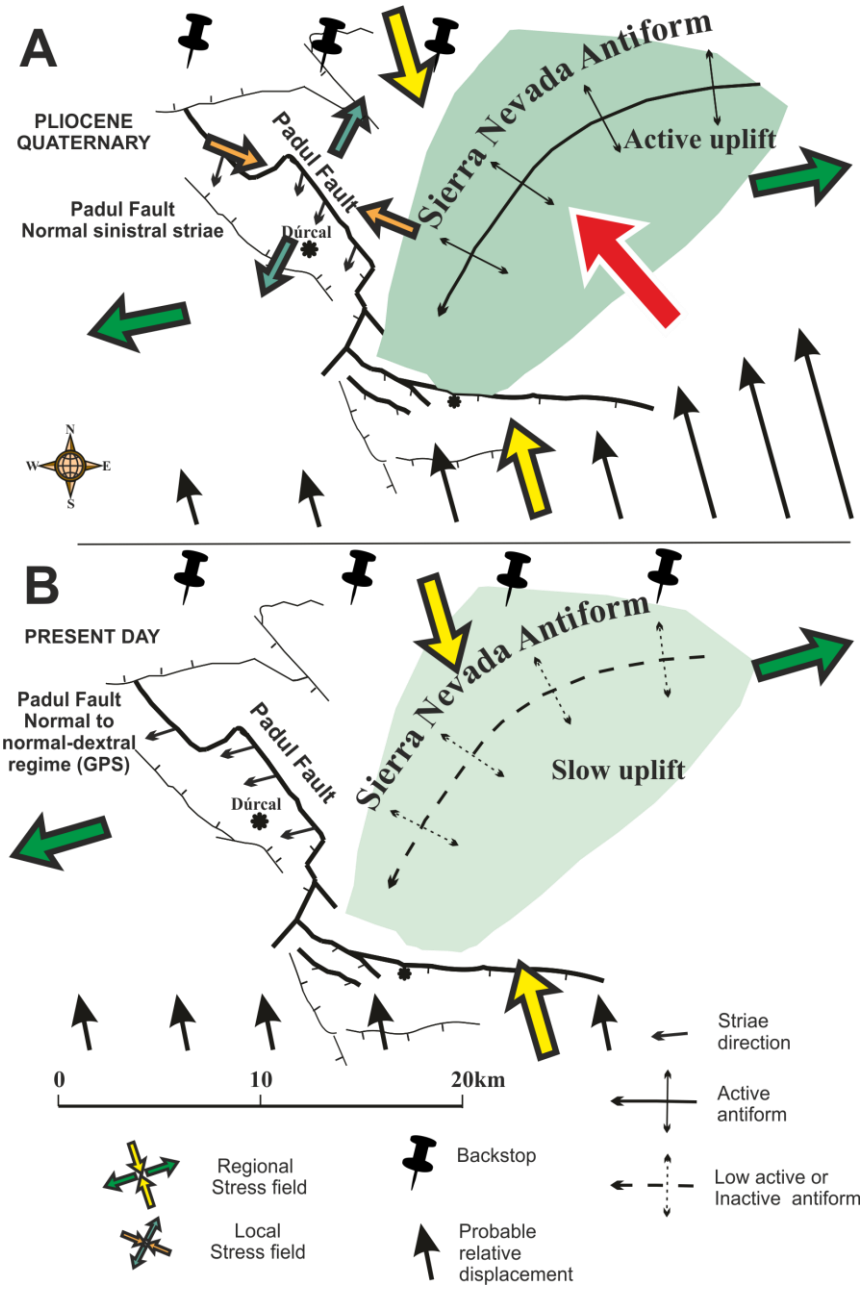

Fig. 8.9 The Padul Fault kinematics influenced by the Sierra Nevada Antiform. A, Active uplift of Sierra Nevada in the frame of the regional NW-SE compression and Padul Fault accommodating the NE-SW orthogonal extension. Northwestwards displacement of the Sierra produced a rotation of the regional stress field and the local stress field in the Padul Fault determined a normal sinistral kinematics, in agreement with most of the observed striae. B, The recent decreasing of northwestwards transport of the Sierra, evidenced by GPS data, determined a present-day normal to normal dextral kinematics according to the regional stress field.

Simultaneous compression and orthogonal extension generally determine the presence of strike-slip faulting (Anderson, 1951). However, while compression produces folding, extension should be accommodated in the same regional deformation field by the development of normal faults. This setting is favored in regions with rheological layered crusts, where large crustal detachment levels may develop, as in the Betic Cordillera (Galindo-Zaldívar et al., 1997, 2003). Although the interaction of folds and faults has been accurately studied in fold-and-thrust belts (Chapple, 1978; Davis et al., 1983), there are no well-constrained examples of major normal faults driven by the interaction of nearby fold development. This process occurs in the complex tectonic scenario of the Granada Basin area, one of the regions of the Betic Cordillera with most intense seismic activity (Morales et al., 1997; Sanz de Galdeano et al., 2003). The NW-SE Eurasian-African plate tectonic convergence (Nocquet, 2012) is resolved in the central part of the Internal Zones of the Betic Cordillera by a regional NNW-SSE shortening that favors the uplift of the Cordillera during the development of the Sierra Nevada antiform, and orthogonal NE-SW extension accommodated by the WSW-dipping normal Padul fault zone (Fig. 8.9).

The comparison of geologic and geodetic data reveals a slightly different behavior of the Padul Fault during the Plio-Quaternary and at Present (Fig. 8.9). The striae in the well-exposed fault surfaces separating Alpujarride marbles in the footwall and Plio-Quaternary alluvial fans in the hanging wall reveal a normal sinistral component of movement (Figs. 8.2 and 8.3C). These kinematics may be a consequence of the activity of the Padul Fault as a transfer fault that accommodated higher shortening rates in the northeastern block (deformed by the large antiform of Sierra Nevada) than in the southwestern block (Fig. 8.9), producing a local deviated stress field.

Nevertheless, GPS data (Fig. 8.8) determine a present purely normal, or even slightly normal-dextral slip. Although Perez-Peña et al. (2010b) evoke an active elevation of Sierra Nevada, the present-day decrease in uplift rates supported by

regional GPS data (Galindo-Zaldívar et al., 2015) may influence the change in kinematics of the Paul fault —formerly transtensional sinistral, but now mainly pure-normal or slightly normal dextral (Fig. 8.9), which is in agreement with present regional stresses (e.g., Pedrera et al., 2011). The recent change in kinematics due to the interaction of folds and faults evidences the variability of the local stress fields both in space and time, and the occurrence of poorly congruent earthquake focal mechanisms (Galindo-Zaldívar et al., 1999).

8.7 Conclusions

The Padul Fault, located southwest of Sierra Nevada is one of the main active faults of the south Iberian Peninsula and accommodates most of the ENE-WSW extension in this sector of the Central Betic Cordillera. This NW-SE oriented southwestwards dipping normal fault separates Alpujarride marbles of the footwall from the Padul Graben Plio-Quaternary alluvial fan sediments in the hanging wall. GPS data determines an extensional horizontal rate of 0.5 mm/yr in a N66^{o}E trend, slightly higher than those deduced previously from stratigraphic markers. Padul Fault probably has a significant part of aseismic deformation, without remarkable seismic activity in the last 500 yr, although more data covering a broad time period are necessary in order to quantify the percentages of aseismic and seismic deformation of this active fault.

Strain partitioning occurs in the central Betics; while compression is accommodated by folding, extension produced the simultaneous activity of NW-SE and E-W extensional faults (Fig. 8.9). The decrease activity of the Sierra Nevada antiform probably influenced changes in fault kinematics from normal sinistral to purely normal or slightly normal dextral. In this setting, the Padul Fault can be considered as a transfer fault accommodating the deformation at the southwestern end of the Sierra Nevada antiform. The Padul Fault and Sierra Nevada antiform constitute an excellent example of the interaction between faults and folds that determines relief uplift in the latest stages of shortening of the Betic Cordillera.

Acknowledgements

We acknowledge the comments of Dr. A. Pedrera and an anonymous reviewer which have improved the quality of this paper. This research was funded by UJA 2016/00086/001 project, CGL2016-80687-R project and RNM148 and RNM282 research groups of Junta de Andalucía. We also thank J. Sanz de Galdeano for A and B photographs of Figure 3. Some figures were generated using GMT (Wessel and Smith, 2013).

CHAPTER 9

Buried marine-cut terraces and submerged marine-built terraces: The Carchuna-Calahonda coastal area (southeast Iberian Peninsula)

Geomorphology 264 (2016) 29–40

Contents lists available at ScienceDirect

Geomorphology

journal homepage: www.elsevier.com/locate/geomorph

Buried marine-cut terraces and submerged marine-built terraces: The Carchuna-Calahonda coastal area (southeast Iberian Peninsula)

Manuel Martinez-Martos [a,b,*], Jesus Galindo-Zaldivar [a,b], Francisco José Lobo [b], Antonio Pedrera [c], Patricia Ruano [a,b], Manuel Lopez-Chicano [a], Miguel Ortega-Sánchez [d]

[a] Departamento de Geodinámica, Universidad de Granada, 18071-Granada, Spain.

[b] Instituto Andaluz de Ciencias de la Tierra, CSIC-Universidad de Granada, Avenida de las Palmeras, nº 4, 18100-Armilla, Spain.

[c] Instituto Geológico y Minero de España, Urbanización Alcázar del Genil, 4-Edificio Zulema, Bajo, 18006 Granada, Spain.

[d] Instituto Interuniversitario de Investigación del Sistema Tierra en Andalucía, Avenida del Mediterráneo S/N, 18006 Granada, Spain.

ABSTRACT

The Carchuna-Calahonda coastal area is located between the onshore Betic Cordillera and the Alboran Sea. Its onshore sector is formed by detrital sediments that cover a metamorphic basement mostly composed of marbles, contiguous to an offshore shelf setting. New onshore gravity data allow us to characterize the location of flat marine-cut terraces carved into the metamorphic bedrock, which are covered by detrital sediments. In addition, multibeam bathymetry data, 3.5 kHz and sparker reflection seismic profiles, reveal offshore flat features linked to marine terraces that are related with the onshore buried marine-cut terraces. Gravity data are newly used to detect marine-cut terraces covered by sediments, enhancing the integration of onshore and offshore data. The marine terraces are distinguished based on the relative sea-level trend (regressive versus transgressive) and on the dominant sedimentary regime (erosional versus depositional). These data help constrain the ages of the marine terraces younger than 150 ka, using available Late Quaternary sea-level curves. Although previous geodetic research suggests a rapid sinking of the Carchuna-Calahonda coast, the heights of the marine-cut terraces and depositional terraces are mainly driven by sea-level changes, not tectonics.

Keywords: Gravity prospection; Marine terraces; Sea-level change; Bathymetry.

HIGHLIGHTS

- Marine terraces record recent sea-level changes in the westernmost Mediterranean.
- Gravity prospecting reveals main onshore buried marine-cut terraces.
- Gravity and seismic data establish onshore-offshore marine terraces relations.
- Study of marine terraces evidence a tectonically stable coast.

9.1 Introduction

Marine terraces are flat to gently inclined surfaces of marine origin bounded by a distinctive break in slope. In temperate regions, most terraces are related to erosion processes, forming marine-cut terraces or shore platforms along rocky coasts (Pirazzoli, 2005). Erosional processes linked to marine terrace formation are usually driven by waves, and secondarily by coastal currents (Passaro et al., 2011). The accumulation of materials derived from shore erosion also may form depositional features known as marine-built terraces (Pirazzoli, 2005). These coastal geomorphological features are reliable sea-level indicators, recording periods of stationary sea-levels (Bradley and Griggs, 1976; Passaro et al., 2011). The position of marine terraces is controlled by eustatism and/or tectonics. Thus, they may emerge on uplifted coasts, where sets of terraces are genetically linked to past interglacial highstands of sea level (Masselink and Hughes, 2003; Pirazzoli, 2005). Emerged marine terraces are essentially used to constrain tectonic uplift rates (Merritts and Bull, 1989; Zazo et al., 1999; Rostami et al., 2000; Pirazzoli et al., 2004; Choi et al., 2008), or as markers of active tectonic tilting (Kelsey, 1990; Muhs et al., 1990; Berryman, 1993).

Additional sets of features can be found submerged on continental shelves, where submarine terraces have been linked to periods of decreased rates of sea-level rise during the postglacial transgression (e.g., Collina-Girard, 1999, 2002). However, some recent interpretations point to more complex geomorphological responses to fluctuating sea-levels; e.g. seafloor scarps have been interpreted as paleo shelf edges related to regressive sea-levels previous to the Last Glacial Maximum (Goff et al., 2013; Reis et al., 2013). Such submarine features may therefore result from multiple transient sea-levels, and their correct interpretation is critical for constraining the past evolution of shallow continental margins.

In coastal areas, marine-cut terraces may be buried by the fast accumulation of sediments, especially when they are below sea-level (Alvarez-Marrón et al.,

2008). The usually high density contrast between sediments and basement makes gravity research a reliable geophysical technique to constrain the thickness of the sedimentary infill and to highlight the presence of buried marine terraces. This non-invasive technique makes it possible to study large areas in a relatively short time because it is less dependent than other geophysical methods on the location of measurement sites. As far as we know, however, gravity data have not been applied to buried marine terraces.

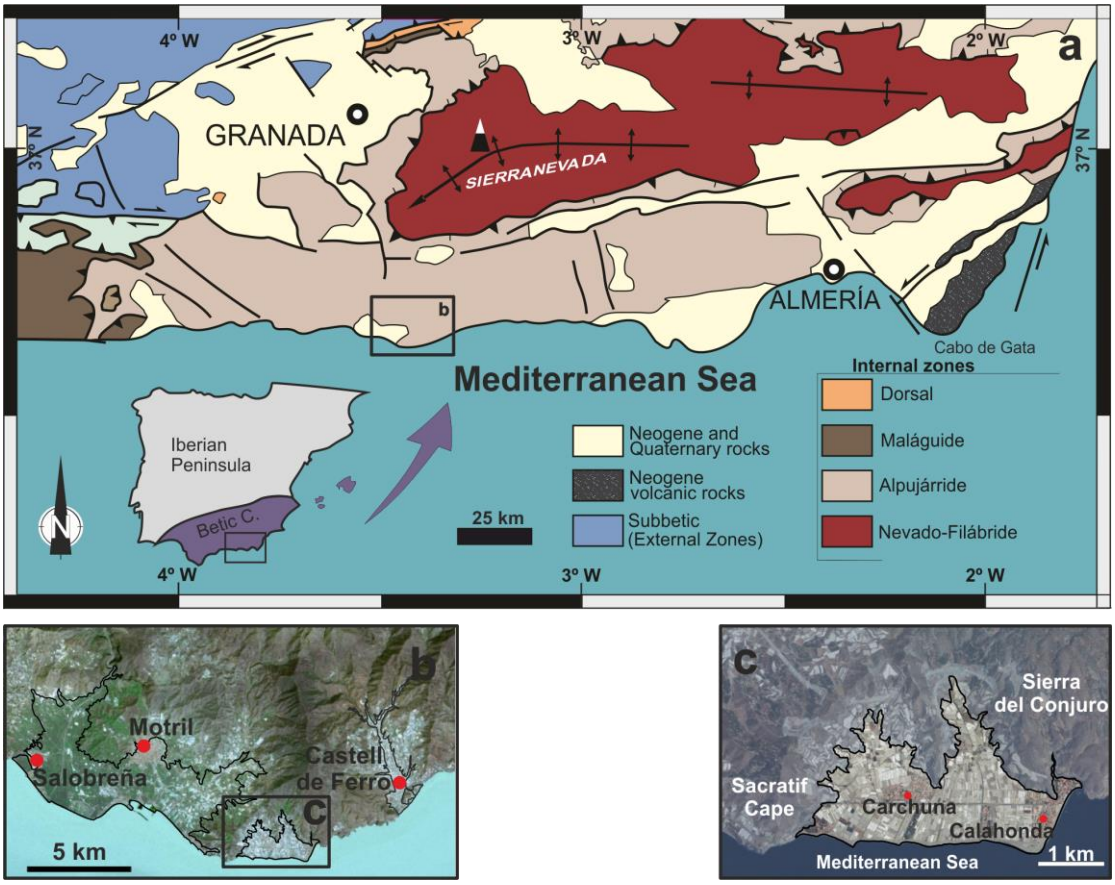

Fig. 9.1 Settings of the Carchuna-Calahonda area. (a) Regional geological setting. (b and c) Main geographical features.

In the Mediterranean region, sets of submerged marine terraces and related features of (mostly) erosional origin have been described at water depths up to 120 m, where they are generally interpreted as the record of postglacial sea-level stillstands (Ulzega et al., 1986; Mart and Belknap, 1991; Lagares, 2008; Passaro et al., 2011). In some cases these features are related with older sea-level highstands

(Rovere et al., 2011). In certain Mediterranean settings, the record of transgressive still stands is represented by depositional terraces, bounded seaward by abrupt increases of slope gradients (Chiocci and Orlando, 1996). In the Alboran Sea, emerged terraces have been reported along the cordillera coasts of both the Betic (Lario et al., 1993; Zazo et al., 1999; Sanz de Galdeano, 2006) and the Rif (Poujol et al., 2014). This region allows us to study the different effects of uplifted, subsident and stable sectors (Groupe de Recherche Néotectonique, 1977; El Kadiri et al., 2010). Multiple submerged terraces have also been described on the Alboran Shelf east of the Strait of Gibraltar (Hernández-Molina et al., 1996).

The aim of this research is to reconstruct the morphology of both buried and submerged marine terraces developed in the Carchuna-Calahonda area in a coastal to shallow-marine sector off the Betic Cordillera, northern Alboran Sea, in order to integrate their genesis into a wider context of recent tectonics and sea-level changes. We acquired new onshore gravity data and combined it with an updated interpretation of available multibeam bathymetry and seismic reflection data.

9.2 Geological setting of the study area

9.2.1 Emerged coastal plain

The coastal fringe of southern Iberia is tectonically active, with areas undergoing uplift and subsidence (Giménez et al., 2000). The coastline is generally steep and mountainous, interrupted by valley mouths with small deltas (Bird, 2010).

The Carchuna-Calahonda coastal area, located at the boundary between the onshore Betic Cordillera and the Alboran Sea, is filled with detrital sediments and includes a flat emerged region of 4.5 km2. The coastal plain lies on a metamorphic basement that crops out to the north and northeast (Sierra del Conjuro) as well as to the west (Sacratif Cape) (Fig. 9.1). The metamorphic basement belongs to the Alpujárride Complex of the Internal Zones of the Betic Cordillera. It is made up of Paleozoic schists, Permo-Triassic phyllites and Triassic marbles (Aldaya et al., 1979; Aldaya, 1981).

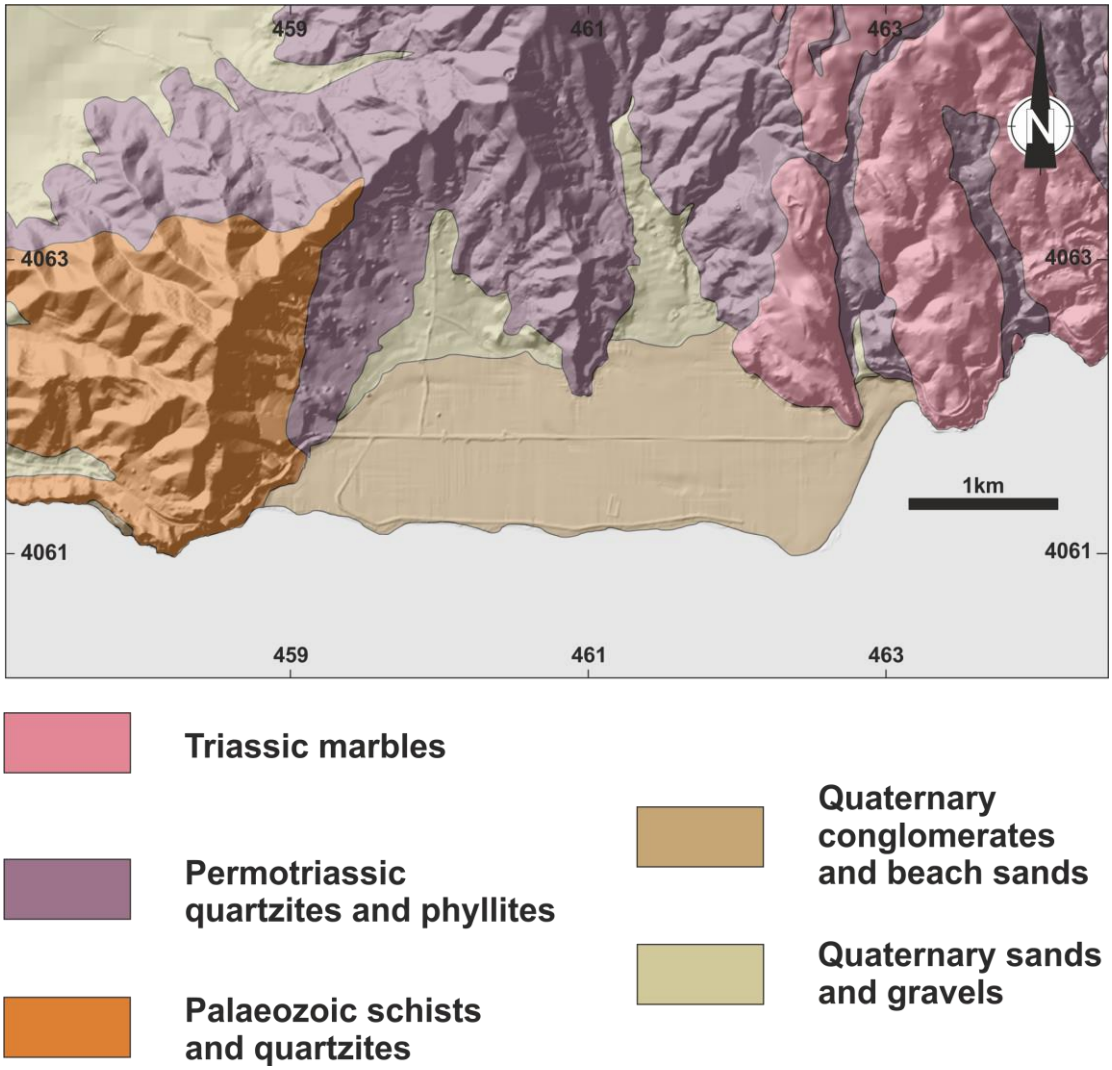

Fig. 9.2 Geology of the Carchuna-Calahonda area on shaded relief. UTM coordinates are in km.

The sedimentary infill of the coastal plain is composed of two main lithologies: conglomerates and gravels in the northern part and the bottom of the ravines, and sands and gravels in the southern half of the coastal plain. The conglomerates were formed in Upper Pleistocene to Middle Holocene alluvial fans, whereas the sands and gravels are Holocene sediments deposited by coastal drift (Lario et al., 1999; Fernández-Salas et al., 2009) (Fig. 9.2). A coastal spit system prograding during the Holocene stabilization is the main morpho-sedimentary feature. The progradation onset is not well constrained; yet morphological studies and scarce age data indicate that the major progradation of the coastal spit took place over

a period of at least 2,400 years (Lario et al., 1999), and probably no more than 5,000 years.

In the Motril aquifer, near the Carchuna-Calahonda area, hydrogeological research involving geophysical studies (Duque et al., 2008) determined the geometry of the sedimentary infill and the presence of flat buried surfaces. Detailed geodetic research giving high-precision leveling profiles (Gimenez et al., 2000) suggests the irregular fast sinking of this tectonically active area related to seismic events.

9.2.2 Adjacent shelf

The coastal segment is affected by wave trains makedly oblique to the main E–W coastal trend, coming from different directions (W, WSW, SW, ESE, and E; Ortega-Sánchez et al., 2014). On the shelf, storm flows change according to the wind pattern. Westward depth-averaged flows may attain mean velocities of 0.15 m s−1, whereas eastward flows reach velocities up to 0.1 m s−1 (Bárcenas et al., 2011).

An infralittoral prograding wedge (IPW; a sandy sediment body deposited beyond the shoreface) has been identified off the Carchuna coastal plain. The sediment wedge, known as the Carchuna IPW (Ortega-Sánchez et al., 2014), shows a break in slope at 20 m depth, though the sedimentary body extends to 60 m depth. The IPW is bounded laterally by the Carchuna Canyon, whose head is located at a short distance from the coastline (Fig. 9.3). The Carchuna IPW exhibits a high backscatter indicative of a coarse-grained composition. The internal structure shows the prevalence of prograding configurations, and erosion associated with the canyon head (Ortega-Sánchez et al., 2014). The IPW appears to be composed of minor units arranged in an offlap pattern, which would be consistent with the organization of the coastal spit system, suggesting the existence of a genetic link (Fernández-Salas et al., 2009).

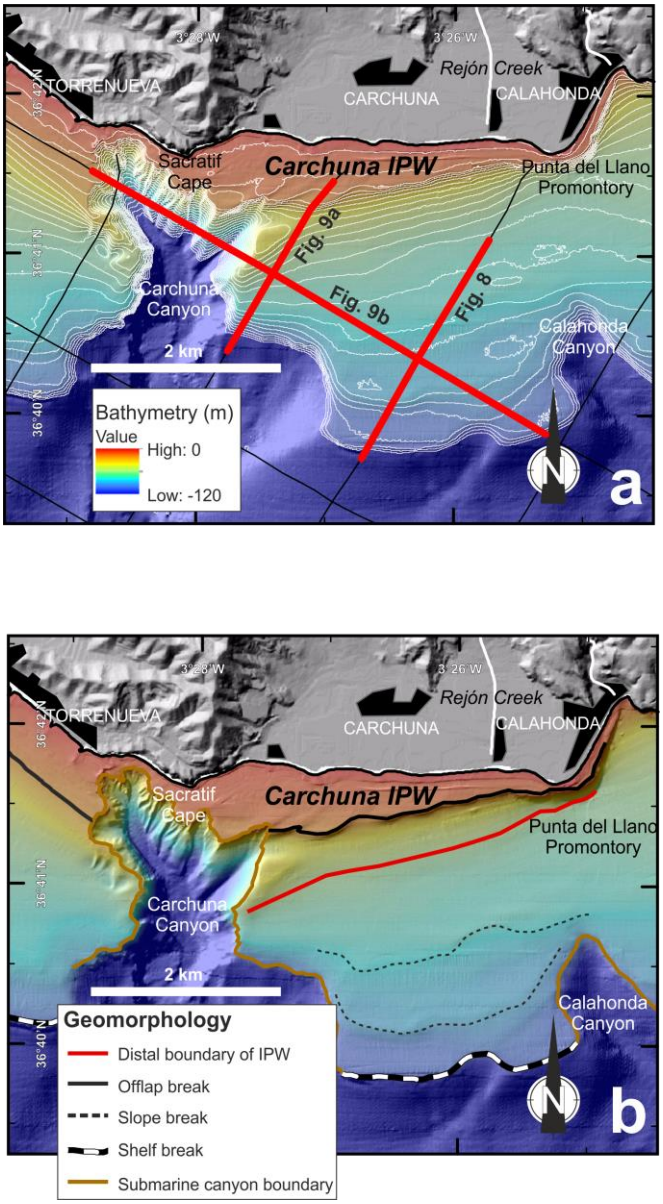

Fig. 9.3 Detailed topography and bathymetry of the study area. a) 2 km spaced grid where seismic profiles were acquired. b) Principal geomorphic features observable in the bathymetry data.

The presence of the canyon promotes coastal erosion during extreme events; the available sediment is then advected laterally by the coastal drift and the prograding wedge is formed. The IPW morphology subsequently modifies wave patterns in the area, and by extension the coastal morphology (Ortega-Sánchez et al., 2014).

Off the Carchuna IPW, seafloor backscatter shows relatively low values, except around the −100 m isobath, where backscatter values are again high (Ortega-Sánchez et al., 2014). In general, sediment size in the area is mainly sand, with minor amounts of gravels (Bárcenas et al., 2011). The area is a shelf sector east of

the Carchuna Canyon dominated by hydrodynamic processes (Bárcenas et al., 2011).

9.3 Methods

The methodology used allows us to determine the depth of the marine terraces. Depths of onshore marine-cut terraces were determined by modeling of gravity anomaly data, while offshore marine terrace depths were established by seismic profile interpretation.

9.3.1 Onshore

The topography of the region is well constrained by the digital terrain model (DTM) of the IGN (www.ign.es). The DTM has a horizontal resolution of 5 × 5 m and vertical accuracy of 1 m.

Geometry of the Carchuna-Calahonda sedimentary infill was determined by means of new gravity data. The gravimeter used was a Scintex Autograv CG-5 with 0.001 mGal accuracy. The station location was measured with a GPS Garmin Oregon 450 having an accuracy of 1 m. Altitude was obtained with a barometric altimeter with 1 m of accuracy and corrected with a barograph ADC Silva with an accuracy of 1 m. Relative measurements were calibrated in view of the Granada reference station, with data from the Instituto Geográfico Nacional.

We carried out a survey of 130 measurements, mostly organized along four profiles, oriented parallel and orthogonal to the coastline. This gives an approximate density of 26 stations per km2. Although the gravity survey was designed to obtain four accurate Bouguer anomaly profiles, some additional intermediate measurements were carried out in order to determine gravity anomaly maps in the study area which allow us to relate the different anomalies. The Bouguer anomaly was calculated considering a reference density of 2.67 g cm−3 and included topographic correction.

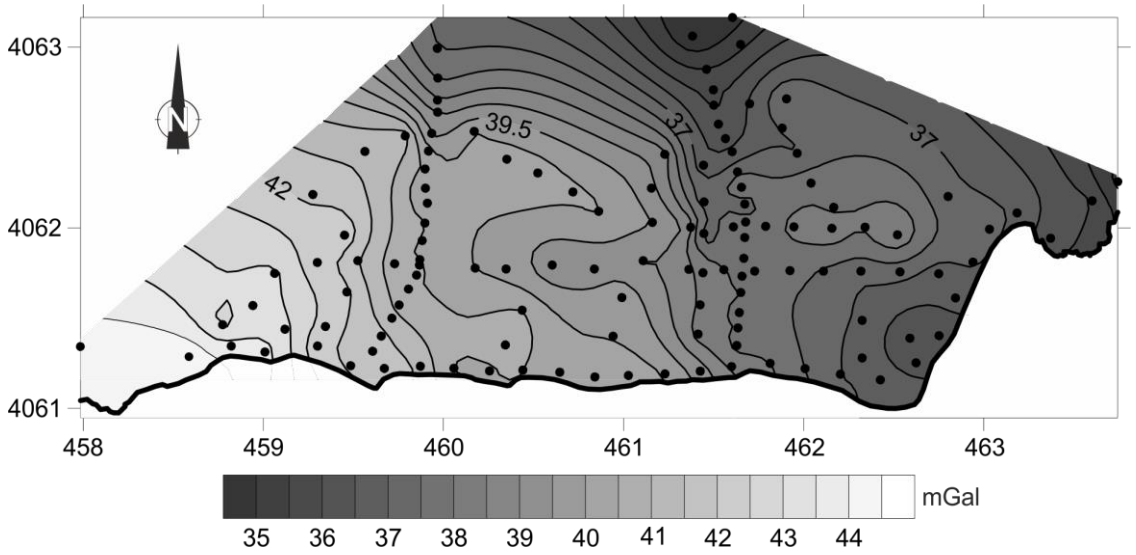

Fig. 9.4 Bouguer anomaly map of the Carchuna-Calahonda area. Black dots represent all gravity stations. UTM coordinates are in km.

The Bouguer anomaly map (Fig. 9.4) was determined from the interpolation between measurement stations. This anomaly provides information of horizontal density contrast between all the bodies below the survey area. The regional anomaly map (Fig. 9.5) aims to represent the influence of all the bodies below the sedimentary infill and was calculated from data located on the metamorphic basement. This regional anomaly is in agreement with the trend in the 1:1,000,000 Bouguer Anomaly Map (IGN, 1976). The residual anomaly map (Fig. 9.6) was created by differentiating the Bouguer and regional anomalies. Finally, the residual anomaly is related to the density contrast between the sedimentary infill and the metamorphic bedrock.

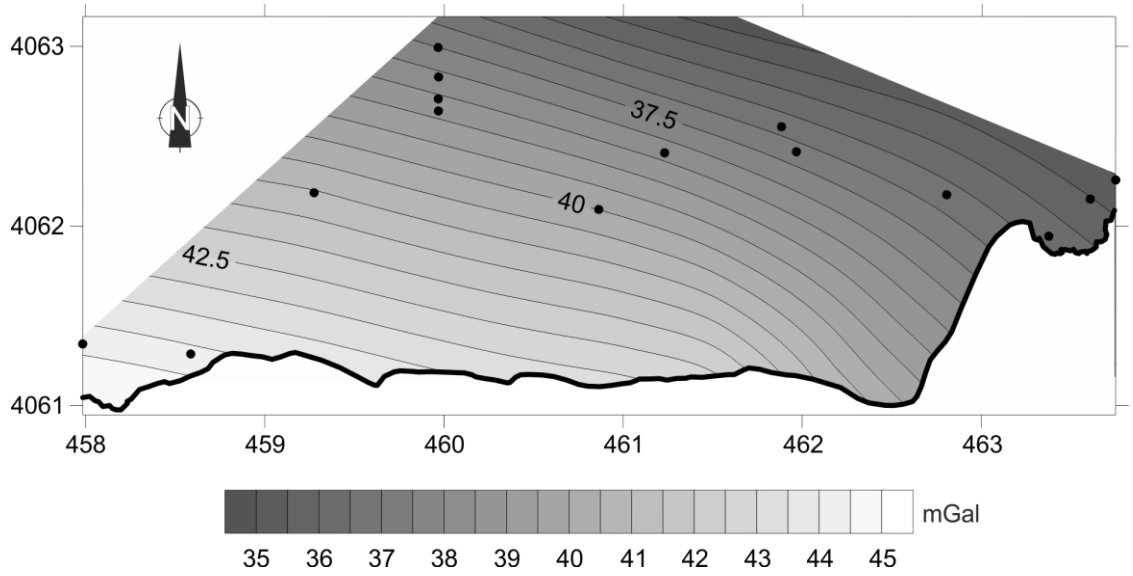

Fig. 9.5 Regional Anomaly map of the study area. Black dots represent gravity stations where the bedrock crops out. UTM coordinates are in km.

We used Gravmag 1.7 software (Pedley et al., 1993) to model the residual anomalies in 2D models and to obtain the sedimentary infill geometry. This software gives the gravity anomaly response along a profile due to one or several bodies characterized by their geometry and density. We took an average density of 2.67 g cm−3 for the metamorphic basement (Robinson and Çoruh, 1988; Telford et al., 1990). The sedimentary infill density was constrained previously as 1.95 g cm−3 in the Motril aquifer (Duque et al., 2008), supported by gravity data and boreholes reaching the basement, which has the same sediments as the Carchuna-Calahonda coastal area. Given the density of the bodies responsible of the residual anomaly, we modeled the contact geometry changing the bodies shape and fitting the anomaly calculated by the model to the observed residual anomaly.

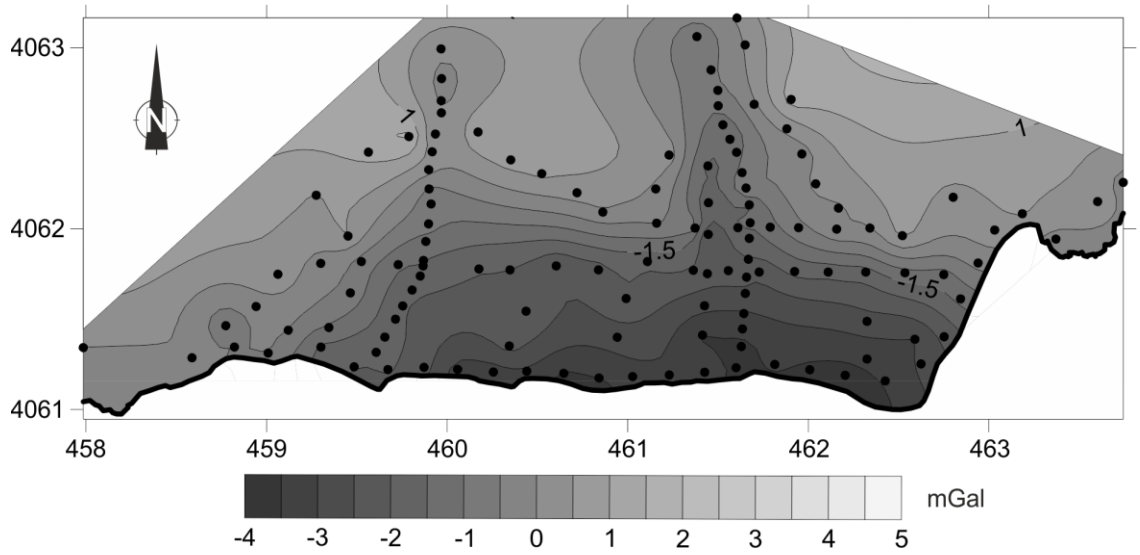

Fig. 9.6 Residual anomaly map of the study area. Black dots represent all gravity stations. UTM coordinates are in km.

9.3.2 Offshore data

In the submerged area, a 5×5 m resolution grid was obtained from available multibeam bathymetric data. These data were measured in 2010 using an Elac Seabeam 1185 system, completed with data collected with a single-beam 24/200 kHz Odom Echotrac system (Fig. 9.3). The surface positional data were acquired with Trimble Ag-132 differential global positioning systems. The data were corrected for heading, depth, pitch, heave, and roll with a redundant Meridian TSS/MAHRS system and with the Motril Port tidal gauge records.

Seismic profiles provide information for the study zone and surrounding areas. The seismic data were collected using two different systems. The first was a 1000-4500 J Sparker source with a shooting rate of 1–2 s and a recording length of 1 s. The seismic profiles were post-processed according to a standard routine, including gain and bandpass filtering (30–500 Hz), However the ghost reflection at the seafloor in the Sparker data appears to overprint the upper ~20 m of the record, so it is difficult to interpret the upper subsurface of this data set. The second system used was a 3.5-kHz sub-bottom profiler. The seismic profiles in the study area trend NNE–SSW and ENE–WSW, both of which are oblique to the local coastline. The lateral spacing between the seismic profiles is 2 km.

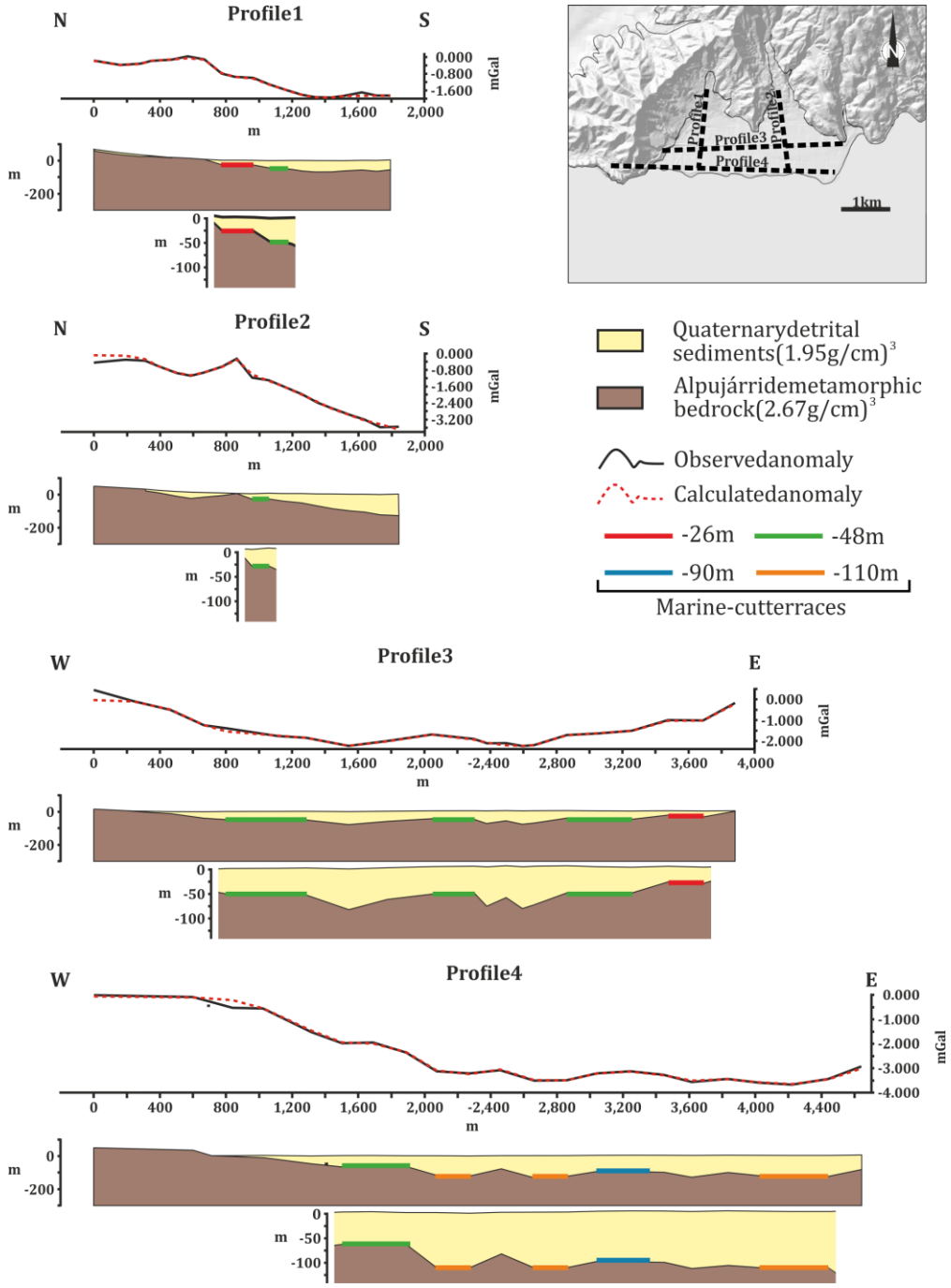

Fig. 9.7 Gravity anomaly profiles, models and their location in the study area. Models are plotted with equal horizontal and vertical scales. Zoomed sections displayed below each model show a vertical scale multiplied by 3 to clearly show the terraces depth. Zero level corresponds to the medium sea-level in Alicante (Spain).

9.4 Results

9.4.1 Onshore gravity study

The regional anomaly map shows an increase of the gravity anomaly southwestwards, from 35.5 to 44 mGal, consequence of the crustal thinning toward the Alboran Sea. The residual anomaly moreover indicates sediment infill thickening towards the sea and two main N–S anomaly minima along the ravines, reaching −3.5 mGal (Fig. 9.6).

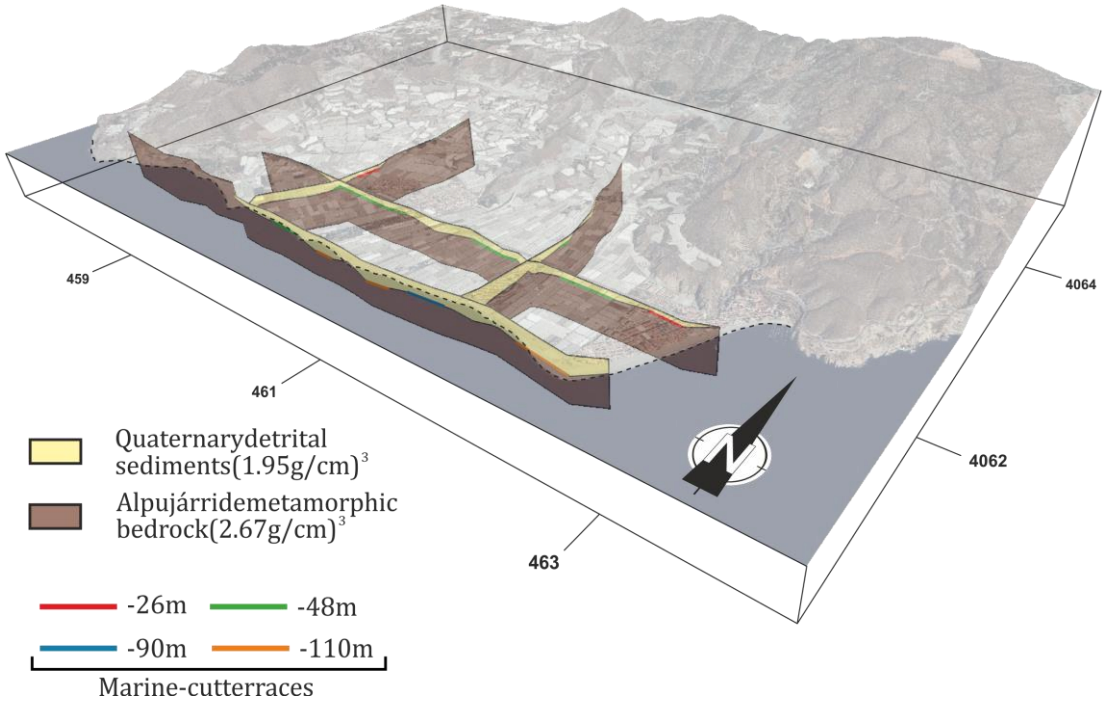

Fig. 9.8 Fence diagram showing the position of the 2D gravity models. UTM coordinates are in km.

Profiles residual anomaly decreasing southwards is the response to a general increase in the thickness of sedimentary infill in the same direction, towards the sea, reaching more than 125 m in the southern part of profile 2 (Fig. 9.7). Buried basement highs transected by valley-shaped features appear in the four profiles, most of them having a flat top, which corresponds with constant residual anomaly values in the profiles and map. In profiles 1 and 2 these surfaces appear around 26 and 48 m below sea-level depth, at 846–1062 m and 664–844 m from

the coastline respectively. Profiles 3 and 4 show flat surfaces at 26, 48, 90 and 110 m depth (Fig. 9.8).

9.4.2 Submarine geomorphology: scarps and sediment bodies

In this study we focus on the submarine morphological features that occur seaward of the Carchuna IPW. It is laterally constrained by two shelf indenting canyons (Carchuna and Calahonda canyons) and southwards ends in the shelf break. Shelf width is higher than 3.5 km in between the two canyons, and lateral shelf extension between the canyons is about 2.5 km.

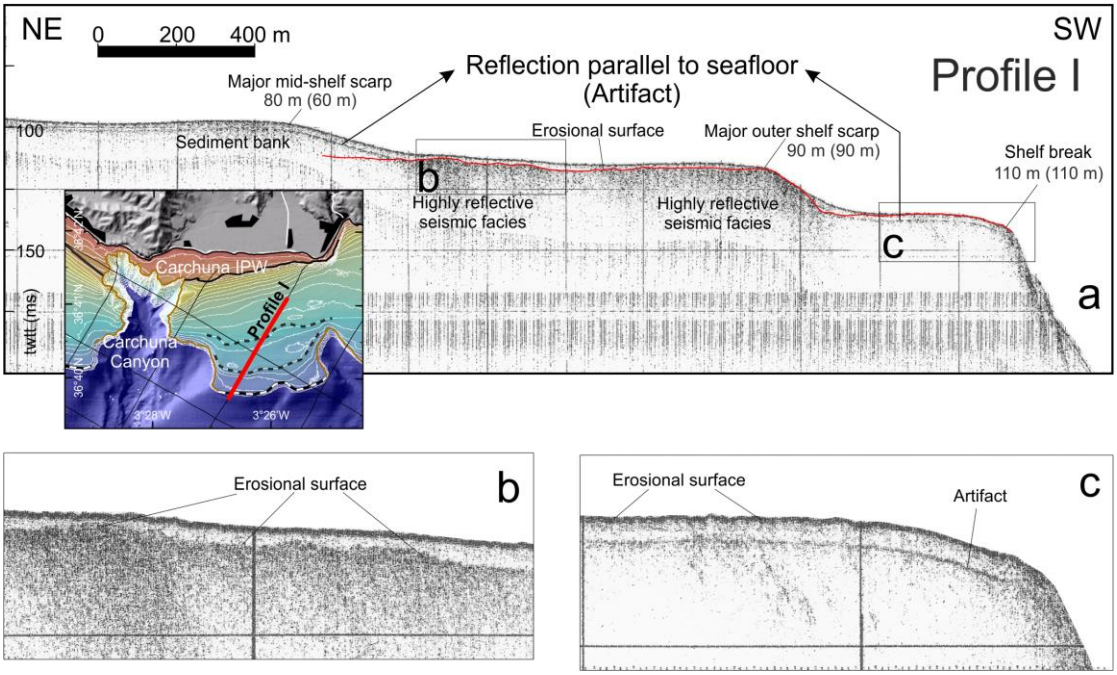

Fig. 9.9 Profile I with sub-bottom profiler (a), zoom boxes showing the erosional surface recognized as the top of the highly reflective seismic facies (b) and an artifact recognized as a reflector parallel to the surface (c), and its location in the study area.

Between the Carchuna IPW and the shelf break, the isobaths trend WSW–ENE and two major breaks of slopes defining two submarine scarps are evident, as well as a minor break of slope located close to the shelf break. The major mid-shelf scarp occurs along the −80 m isobath, except in a small landward indentation. Hence it trends WSW–ENE and extends laterally more than 3 km.

To the west, it merges with the outer shelf slope increase caused by the Carchuna Canyon. To the east, it continues north of the Calahonda Canyon (Figs. 9.9 and 9.10). Despite the low penetration of the sub-bottom profiler (Fig. 9.9), probably due to the coarse size of the detrital sediments, seismic data reveal the 80 m scarp to be the surficial expression of a semitransparent sediment bank that extends over a highly reflective erosional surface located at about 90 m water depth (Fig. 9.9). The sediment bank does not show evidence of internal progradations. Seismic data indicate that the sediment body generating this mid-shelf slope break may be partly buried by a more recent sediment wedge that is strongly eroded by the Carchuna Canyon (Fig. 9.11). Lateral correlations indicate that this most proximal wedge corresponds to the Carchuna IPW, which has a net progradational configuration in the vicinity of the canyon (Fig. 9.11a).

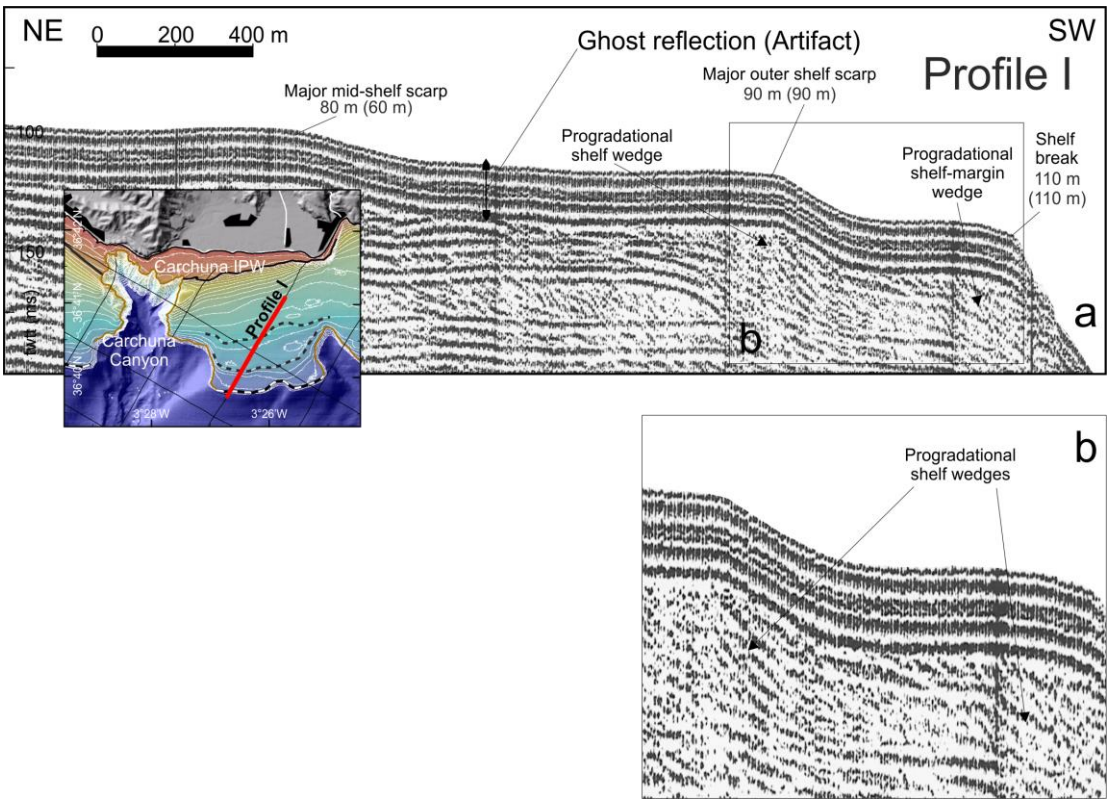

Fig. 9.10 Sparker profile I (a), zoom box showing the progradational shelf wedges (b) and their location in the study area.

The major outer shelf scarp occurs along the −90 m isobath, exhibiting a rather lobate plan-view pattern, where the lateral boundaries are strongly controlled by

the outline of the canyon heads. Its lateral extension is larger than 3 km. Overall, this major outer shelf scarp generates a water depth difference greater than 10 m. The seismic 3.5 kHz data reveals the occurrence of a set of highly reflective seismic facies below the above mentioned erosional surface, terminated seaward by the −90 m scarp. The Sparker seismic profile evidences that the seismic facies below the −90 m scarp are strongly progradational, and the sediment thickness of the progradational body is substantial (i.e., several tens of meters) (Figs. 9.10 and 9.11) suggesting that the scarp probably represents the progradational front of a shelf sediment wedge.

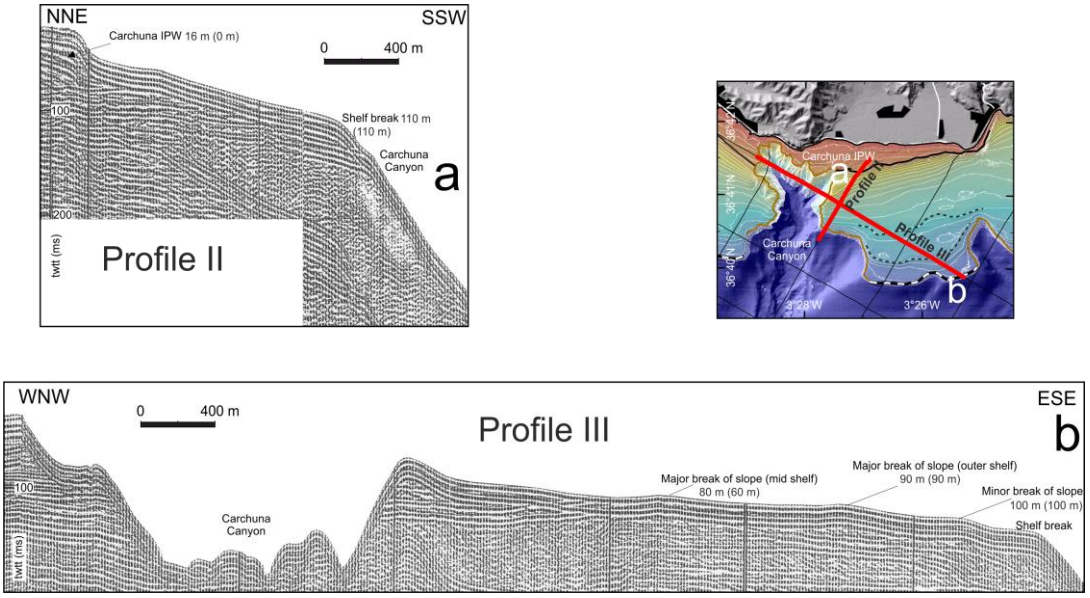

Fig. 9.11 Sparker profiles II (a) and III (b) and their location in the study area.

A small scarp is identified between the major −90 m scarp and the shelf break, close to the Calahonda Canyon head. This scarp occurs at depths of more than 100 m, extending laterally for nearly 700 m with a main SW–NE trend (Fig. 9.11b). Seismic data seem to indicate that progradational reflections occur below this minor scarp (Fig. 9.11b).

The shelf break is located at an approximate water depth of 110 m. In seismic profiles, it marks an abrupt change between a relatively flat outer shelf (seaward of the major outer shelf scarp) and a steep upper slope that exhibits some

irregular morphologies. The Sparker profile reveals that the sub-surface below the shelf break contains steeply dipping progradational reflections characteristic of a shelf-margin wedge (Figs. 9.10 and 9.11b).

In summary, in the submerged area, different slope breaks can be clearly observed at water depths around 80 and 90 m, and there is a shelf break at 110 m depth (Fig. 9.3). In addition, the IPW produced a break 5.1oughly constant or ascends slightly up to the next slope break, so they clearly separate different marine-build terraces.

9.5 Discussion

9.5.1 Development of marine terraces

The integration of field and marine geophysical data permits a comprehensive analysis of the marine terraces, including marine-cut and marine-built terraces. Although previous geodetic studies based on high precision leveling indicated quick subsidence in the study area (Gimenez et al., 2000), there is no geomorphically accurate studies in this region that clearly determine the evidence of tectonic uplifting or subsidence. Our data reveal a roughly stable littoral, meaning the different heights of the marine terraces are mainly due to sea-level changes operating during the last 150 ka, as suggested by other studies (Sanz de Galdeano, 2006, and references therein).

In this work we distinguish marine-cut terraces and marine-built terraces. Among the last ones, it is important to divide the ones formed in a generally transgressive period from those formed in a generally regressive period. Marine-cut terraces may be perfectly distinguished since they are formed as a result of wave erosion in hard rocks. We observe these terraces with gravity data because of the density contrast between the bedrock and the sedimentary infill. After the formation of marine-cut terraces, detrital deposits buried them and preserved them from erosion. This observation suggests that the cut terraces in this area were generally formed during transgressive periods when sea-level was rising, together with constant sediment supply that allowed the burial of this

geomorphic features before they were eroded. The 90 m depth terrace better fits a stable period during the regression, with a well-developed flat surface, which has been preserved up to later transgressive periods.

Marine-built terraces, in contrast, are the result of deposition of a sedimentary bank. They may be formed in periods of steady sea-level either in regressive or transgressive contexts. We identified the marine-built terraces formed in either regressive or transgressive contexts by their stratigraphic relation with the erosional surface observed in the sub-bottom profile. The main surface where formed during the last Glacial Maximum and it appears cutting the marine-built terraces at 90 and 100 m water depth, reaching the shelf edge at 110 m depth. Thus, the mentioned terraces precede the erosional surface formation and therefore, they belong to steady sea-level period in a regressive context. However, marine-built terraces formed at 80 and 20 m water depth are deposited above the erosional surface, so they belong to the last sea-level rise and where formed in a transgressive context. With these criteria we were able to distinguish marine-cut from marine-built terraces and determine those marine-built terraces formed either in a transgressive or regressive context.

9.5.2 Onshore buried marine-cut terraces

In onshore areas, gravity research is a very suitable method for determining the geometry of sedimentary infill, given the high-density contrast between bedrock and sediments. Although the best procedure would be to combine gravity data and observations of boreholes reaching the basement, the available boreholes do not completely cross-cut the sedimentary infill. However, a recent gravity study in the nearby Motril coastal area (Duque et al., 2008), with the same geological setting, allowed us to precisely appraise the average densities for the basement (2.67 g cm−3) and the detrital sediments (1.95 g cm−3). Profiles 1 and 2 (Figs. 9.7 and 9.8), roughly coincide with the present-day ravines. Erosion in the bedrock attributed to former water courses is evidenced in profiles 3 and 4 orthogonal to the ravines that show V-shaped cross-sections corresponding to sedimentary

filled valleys. This observation suggests that water course base level, related to the ancient sea-level, was lower than the current one; accordingly, its evolution should be more accurately constrained by the study of marine-cut terraces.

Gravity models clearly show the presence of flat surfaces located at 26, 48, 90 and 110 m water depth indicating bedrock erosion (Figs. 9.7 and 9.8 and Table 9.1). Since these planar forms appear in a rocky coast and accordingly with the previous mentioned criteria, we interpret them as basement marine-cut terraces that were buried by subsequent sedimentary bodies. Some of these terraces are also recognized in the gravity study of the Motril area (26 m depth in profiles 3 and 4; 48 m depth in profiles 4 and 5; 90 m depth in profiles 2, 4 and 7 of Duque et al., 2008) that was developed only for hydrogeological purposes. These results support a broad extension along the coast of the studied features.

9.5.3 Offshore marine terraces

A set of marine terraces was identified from the marine geophysical data comprising multibeam bathymetric data, sub-bottom profiler and Sparker seismic data (Figs. 9.9, 9.10 and 9.11). In contrast to the buried onshore terraces, most of the offshore marine terraces seem to be depositional features (Table 9.2). The reflectors geometry in the sedimentary infill below most of the marine-built terraces corresponds to progradational shelf wedges characterized by cross bedding. This is evidenced by seawards dipping reflectors observed in sparker profiles (Figs. 9.10 and 9.11).

We propose an evolutionary scheme for terrace development in the study area taking into account the identification of an erosional surface that separates the two major terraces identified (i.e., −80 and −90 m terraces). Under this scheme, the −90 m terrace would be the oldest offshore feature formed in a regressive context. The identification of a forestepping pattern of progradational wedges in the outer shelf supports our interpretation; in this sense, the −90 m terrace is interpreted as a scarp marking the seaward edge of an offlapping forced-regressive wedge, and therefore should be regarded as a depositional terrace. Similar terrace-built features developed within regressive contexts have been

observed in the Mid-Atlantic Bight (Goff et al., 2013) or the Brazilian Shelf (Reis et al., 2013). The successive development of terrace-built features seaward, including the minor outer shelf terrace at about 100 m water depth and the shelf break at about 110 m water depth, would have occurred within a regressive context during falling sea-level or lowstand conditions, taking into account the stacking pattern of outer shelf wedges. The correlation between water depths of depositional terraces and the Late Quaternary sea-level curves implies that the -90 m terrace could be related with the Marine Isotopic Stage (MIS) 4 (65 ka), whereas the shelf break would be linked to MIS 2 (20 ka). Therefore, the set of depositional terraces documented on the outer shelf of the study area would record an overall sea-level change between MISs 4 and 2 (e.g., Rohling et al., 2009; Siddall et al., 2010; Grant et al., 2012).

The −80 m marine terrace should also be regarded as a marine-built terrace, as it is the surface expression of a sediment bank. However, its stratigraphic position, overlying an erosional surface and capped by the regressive facies of the most recent Carchuna IPW, would be compatible with a transgressive context. Therefore, we postulate that the −80 m depositional terrace is a postglacial feature. In attempting to correlate this depositional terrace with the sea-level record, we propose that this sedimentary body could be regarded as an older analogue of the Carchuna IPW. The generation of the IPW is related to submarine deposition, with the offlap break located at 20 m water depth with regard to the present-day sea-level (Ortega-Sánchez et al., 2014). Assuming a similar genesis for the formation of the −80 m depositional terrace, we infer a sea-level position at approximately 60 m water depth during the formation of the depositional body. In several Mediterranean settings, the formation of depositional bodies at similar water depths has been related with the Younger Dryas event (Berné et al., 2007; Schattner et al., 2010). The correlation of water depths with postglacial sea-level curves would be in agreement with those interpretations. Indeed, a deceleration in the rate of sea-level rise linked to the Younger Dryas event

apparently occurred when sea-level was 60–65 m below the present-day level (e.g., Bard et al., 2010; Stanford et al., 2011).

9.5.4 Age of marine terraces and onshore-offshore relation

The sea-level evolution (Fig. 9.12) determines the development of marine terraces. Marine-built terraces that formed in regressive periods and marine-cut terraces in either transgressive or regressive periods indicate a paleo sea-level position at the same depth. However, we surmise that marine-built terraces formed during transgressive periods indicate a 20 m shallower paleo sea-level. This is because the tops of the most recent sedimentary bodies off the coasts of Mediterranean Iberia, assumed to have been deposited during the Holocene highstand, appear to be levelled by the base of storm waves (Hernández-Molina et al., 2000; Fernández-Salas et al., 2009). In the study area, the top surface of the most recent IPW occurs at approximately 20 m water depth (Ortega-Sánchez et al., 2014). Therefore, we infer that a similar water depth correction should be made when estimating paleo sea-levels from older marine-built terraces.

We observe that the 90 m depth marine-cut terrace detected with gravity data is found offshore at the same depth in the multibeam bathymetry, sub-bottom profiler and Sparker seismic data (Figs. 9.7 to 9.11). This allows us to relate marine terraces detected offshore and onshore and present a relative timing of events (Fig. 9.13).

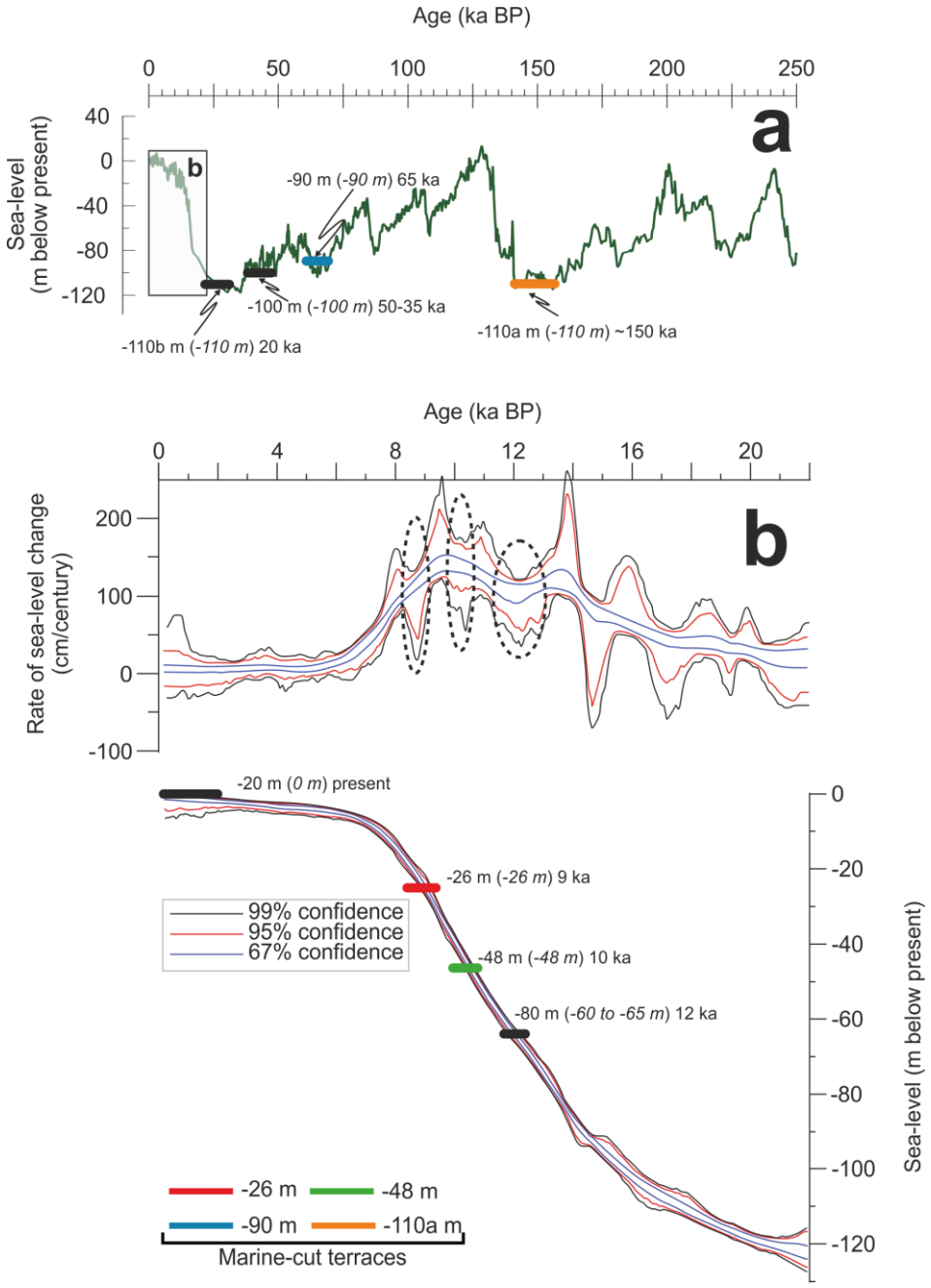

Fig. 9.12 Sea-level curves and position of the studied terraces in them. Black and colored markers show the sea-level depth when the studied terraces were formed. a) Sea-level change curve for the last 250 ka modified from Rohling et al. (2009). b) Detailed sea-level curve for the last 22 ka modified from Stanford et al. (2011). Horizontal lines mark the age of the described marine terraces. Dashed elipses indicate sea-level change minima coinciding with the described marine terraces. Arrows indicate the depth of the different marine terraces, their related sea-level in brackets and their attributed ages.

An absolute age can be assigned to all the terraces identified (Figs. 9.12 and 9.13). A basement marine-cut terrace at 110 m depth (110a) is the oldest and was formed at approximately 150 ka (Fig. 9.12). This terrace is only detected by gravity data (Figs. 9.7 and 9.8). The next recognizable terrace is the one located at 90 m depth and detected buried onshore (Figs. 9.7 and 9.8) as well as offshore (Figs. 9.9 to 9.11). This terrace formed at 65 ka during a regressive period (Fig. 9.12). Later on, in the next regressive period, the marine terrace at 100 m depth was formed at 50–35 ka. It can be identified offshore (Fig. 9.11), but there are no evidences of this terrace in the bedrock since it is not detected by gravity data. The regressive period finished with the formation of the shelf break at 110 m depth (110b) at about 20 ka (Fig. 9.12). The following terrace was formed under a transgressive trend at 80 m water depth, when the sea-level was 60 m lower than at present. This terrace does not have expression as a marine-cut terrace in the basement, and is not detected by gravity data. This terrace would have formed at about 12 ka. Gravity data point to new marine-cut terraces appearing as flat surfaces in the bedrock at 48 and 26 m (Figs. 9.7 and 9.8) that formed after the one at 80 m depth. The age attributed to these marine-cut terraces is 10 and 9 ka, respectively, and coincides with low rates of sea-level change (Fig. 9.12). These terraces remained unknown, as did the one at 110 m depth (110a), until gravity data were acquired. The marine-terraces evolution model proposed in this study provides a reliable explanation of the tectono-eustatic history in this sector of Betic Coast since it solves the location of the newly founded buried marine-cut terraces without invoking uplift or subsidence. It is also in agreement with geomorphic studies pointing to a marine terraces position dependent in sea-level changes rather than tectonics since the Pliocene (Sanz de Galdeano 2006; El Kadiri et al., 2010). The data presented here shed new light on the recent tectono-eustatic relations between the Western Mediterranean and the Betic Cordillera coast. In addition, we arrive at new relations between the erosional geomorphic features of marine-cut terraces with depositional marine terraces at the same depth. Moreover, buried marine-cut terraces are described inland, highlighting their importance for tectono-eustatic studies.

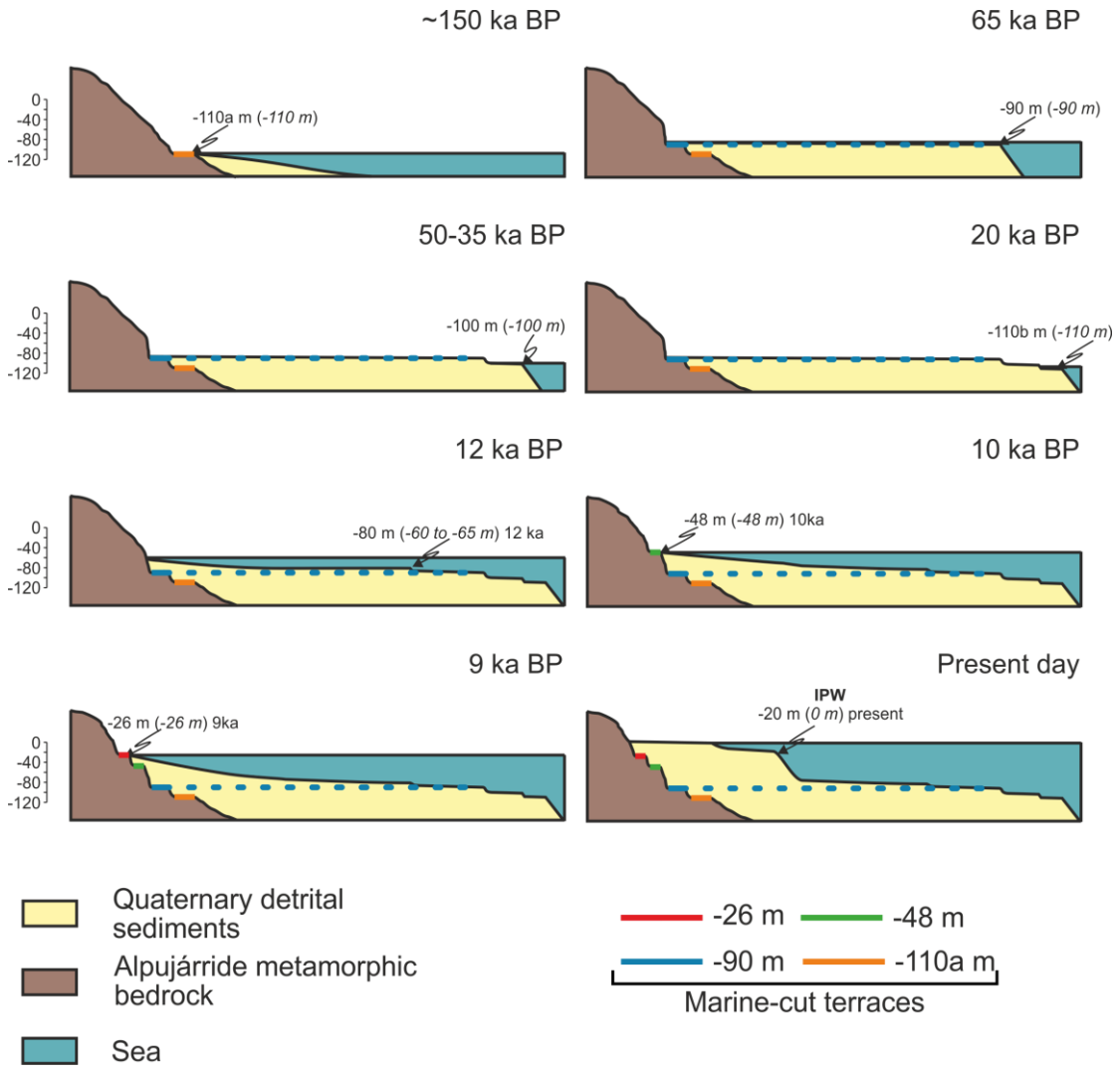

Fig. 9.13 Evolution model proposed for the formation of different marine terraces in the study area. Arrows show the depth of the different marine terraces, their related sea-level (in brackets) and their attributed age. Dashed colored lines show the relation between marine-cut and marine-built terraces.

9.6 Conclusions

Four buried marine-cut terraces at 26, 48, 90 and 110 m below the current sea-level were detected using gravity data. They are integrated with depositional marine terraces offshore at 20, 80, 90 and 100; and with the shelf break at 110 m depths. The terrace located at 90 m water depth, which shows erosional features, is the only one identified both onshore and offshore. These data lead us to propose ages for the different marine terraces in view of different sea-level curves

(Table 9.1 and Fig. 9.13). At approximately 150 ka the marine-cut terrace at 110 m depth (110a) was formed. After that, at 65 ka, the marine terrace at 90 m depth was formed. The marine-built terrace at 100 m depth and the shelf break at 110 m depth (110b) were formed at 50–35 and 20 ka, respectively. Terraces at 80, 48, 26 and 16 m depth formed after 20–12 ka during short stable periods. All these data suggest a tectonically stable coastal condition.

Gravity studies are a quick and useful means of finding and describing marine-cut terraces and other structural surfaces in the bedrock that may be hidden by sedimentary bodies inland. Consequently, they stand as a useful tool to support studies on the recent geological history of a region by revealing key aspects of the geomorphology that remain buried in sediments.

Acknowledgements

We acknowledge the comments from two anonymous reviewers and the editor Prof. Takashi Oguchi, which improved the quality of this paper. The field assistance of Mr. Guillermo is recognized. This research was funded by the Spanish Government through projects CGL2010-21048, P09-RNM-5388 and the RNM148 and research groups of the Junta de Andalucía.

CHAPTER 10

Irregular mountain front development in a fold-and-thrust belt: (Central Betic Cordillera, S Spain)

Manuel Martínez-Martos[a,b]*, Jesús Galindo-Zaldivar[a,b], Ana Ruiz-Constán[c], Antonio Pedrera[c], Sergio Martos-Rosillo[c], Antonio González-Ramón[c]

Under preparation to:

Terra Nova, 2017

[a] Dpto. de Geodinámica, Universidad de Granada. 18071 Granada, Spain.

[b] Instituto Andaluz de Ciencias de la Tierra, CSIC-Universidad de Granada, Avenida de las Palmeras, nº 4, 18100 Armilla, Spain.

[c] Instituto Geológico y Minero de España (IGME), Calle Ríos Rosas, 23, 28003, Madrid, Spain.

ABSTRACT

Mountain fronts generally develop straight and their sinuosity is considered to indicate their relief relative age. In the Betic Cordillera frontal part, two mountain front geometries can be distinguished: the NNE-SSW Sierra de Cazorla straight mountain front and the highly irregular mountain front in the Jódar area, roughly E-W. Both sections are separated by the dextral Tíscar fault. This irregular shape is highly controlled by the presence of transfer faults probably consequence of the heterogeneous fold and thrust slip-rate along strike due to the uneven distribution of the tectonic mélange. This setting facilitates the development of the Jódar Sierra tectonic arc and avoids the displacement of the thrust sheets in the Albánchez Depression, both separated by the Bedmar Fault. In addition, extension orthogonal to shortening, highly increase the mountain front sinuosity. Both deformational mechanisms be taken into account when comparing the tectonic activity in mountain fronts by sinuosity index.

Running title: Irregular Central Betic Cordillera mountain front

10.1 Introduction

Active ranges are often characterized by straight mountain fronts since their relief is generally controlled by the elongated folds-and-thrust belts propagation (Bull and McFadden, 1977; Bull, 1978). The sinuosity index has been stablished as a parameter widely used to determine the tectonic activity in mountain fronts due to its increase by erosional processes (Keller and Pinter, 1996). However, the contribution of other aspects as the rheological irregularities at the deformed front could lead to a much more complex setting, as occur during the development of narrow arched structures (Callot et al., 2012).

The Betic Cordillera (Fig. 10.1), situated in southern Iberian Peninsula, belongs to the westernmost part of the Alpine Mediterranean belt. Its relief is consequence of the Africa-Eurasia convergence, which formed a collisional orogen since the Early Miocene (Platt and Vissers, 1989). The mountain front bounding the Guadalquivir foreland basin and the Betic Cordillera External Zone fold-and-thrust belt (Fig. 10.1), has two different tectonic deformation patterns. Eastwards, the NNE-SSW Cazorla Prebetic front is very regular, straight and highly continuous. However, in the Betic Cordillera central and western part, the ENE-WSW front is highly irregular and includes discontinuous Prebetic and Subbetic outcrops. These two sectors are separated by the NW-SE dextral Tíscar Fault (Sanz de Galdeano et al., 2006).

The aim of this research is to unravel the mechanisms involved in the development of irregular mountain fronts, considering the sinuous central Betic Cordillera front as a field example (Fig. 10.2). Field tectonic observations are integrated with gravity data to constrain the deep structure of the Jódar area.

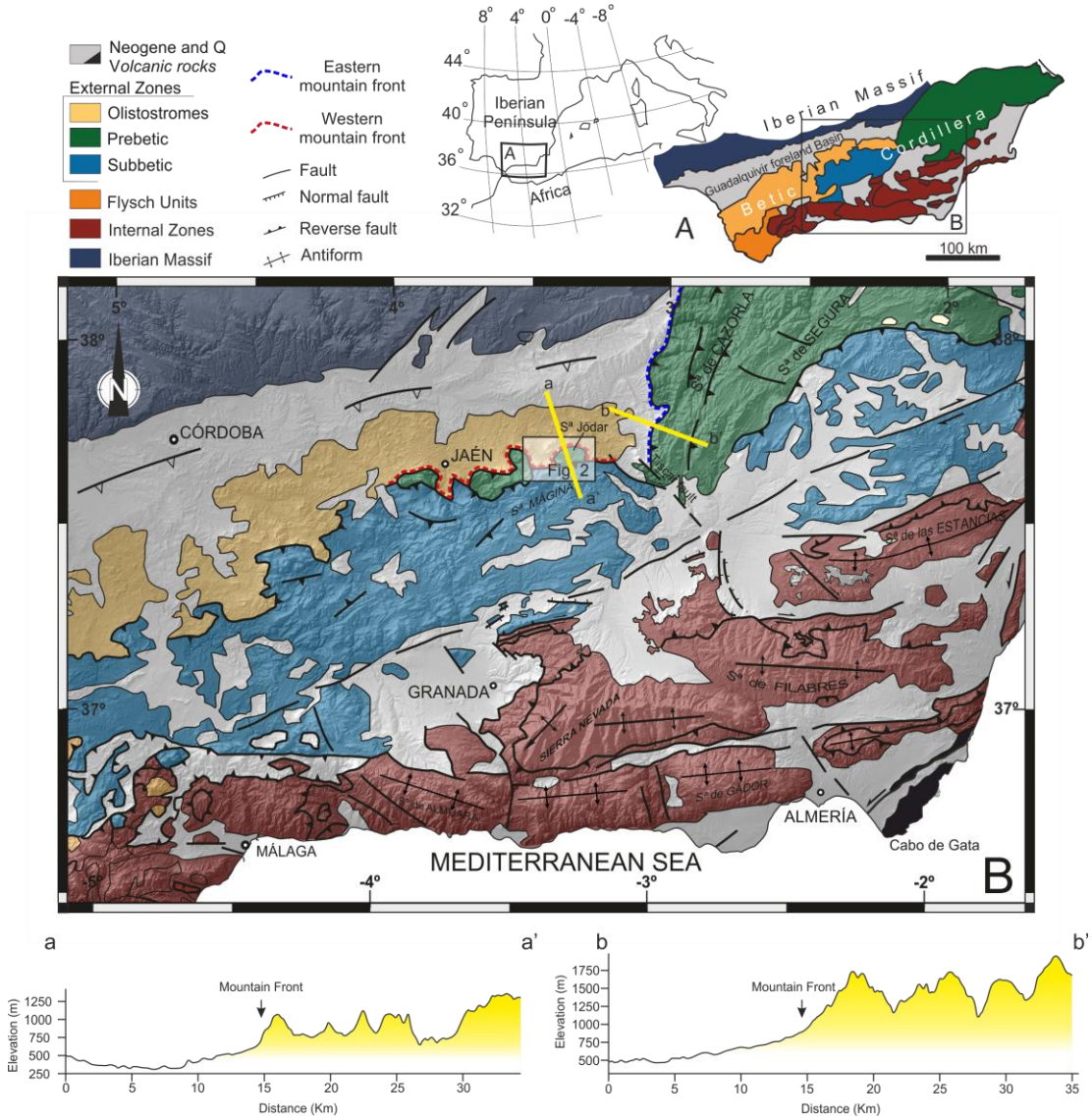

Fig. 10.1 Betic Cordillera geological sketch showing the mountain fronts eastwards and westwards the Tíscar Fault and a topographic profile of each one.

10.2 Geological setting

The Betic Cordillera (Fig. 10.1) is divided into the Internal and the External Zones, together with the Flysch units and the Neogene basins. The Gibraltar Arc is consequence of the Internal Zones westwards displacement (Andrieux et al., 1971) since the Late Oligocene (Sanz de Galdeano, 1990). In the central Betics, the collision with the External Zones occurred during Burdigalian (Hermes, 1985)

producing the thrusting of the Subbetic onto the Prebetic (Foucault, 1971; López-Garrido, 1971; Frizon de Lamotte et al., 1991).

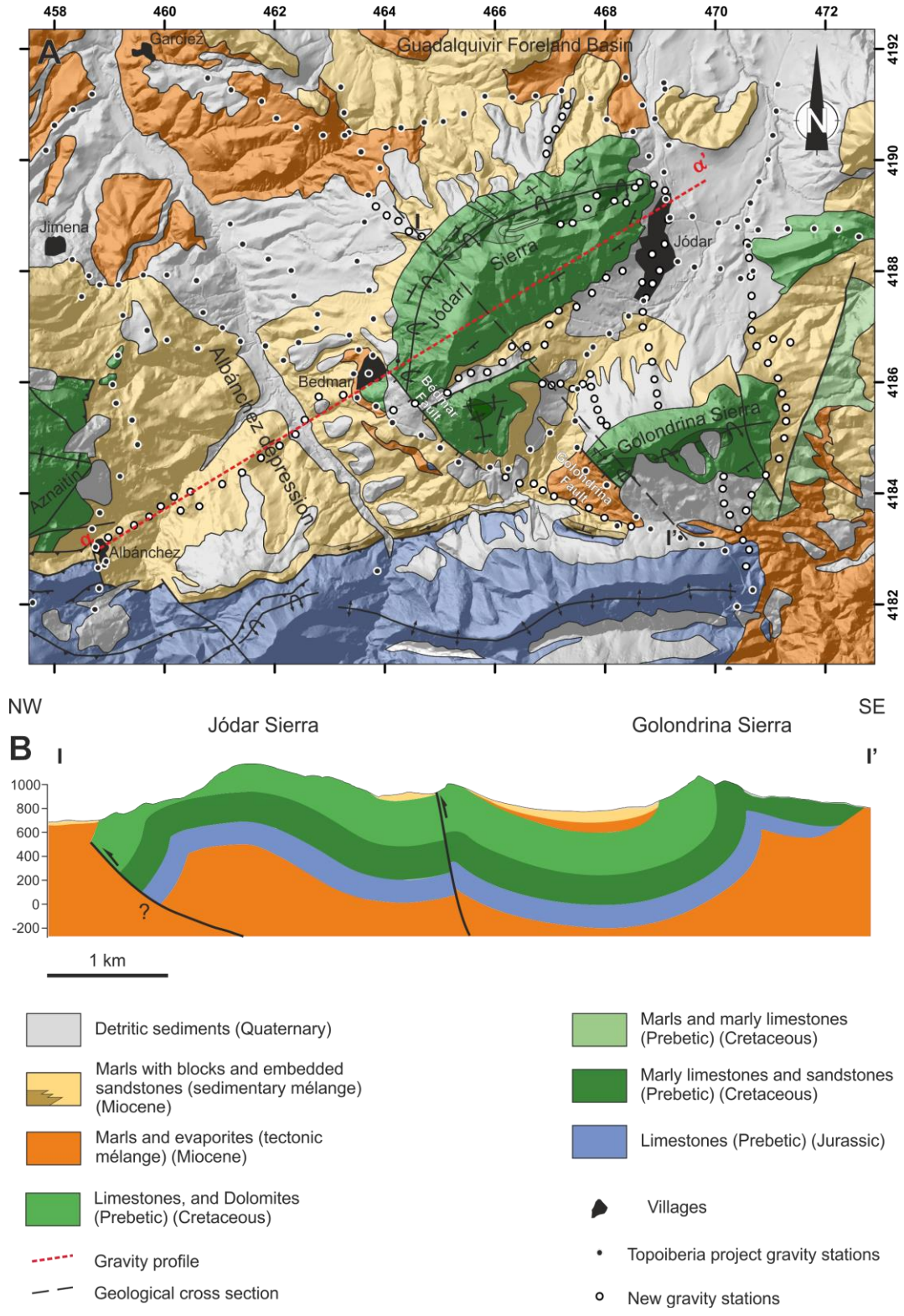

Fig. 10.2 Study area geological sketch and gravity survey stations (A). Black dashed line indicates the geological cross-section location showed in (B).

The External Zones –Subbetic and Prebetic– constitute a fold-and-thrust belt mainly formed by Mesozoic to Tertiary carbonate series on the South-Iberian palaeomargin. The Subbetic is a deep platform with pelagic domains while the Prebetic has shallower marine and continental facies (García-Hernández et al., 1980). In addition, undeformed Prebetic sediments known as the Tabular Cover are located on top of the South Iberian margin (López-Garrido, 1971). Olistostromic units were emplaced in its western and central frontal part (Pérez-López and Sanz de Galdeano, 1994). The mountain front of the central Betic Cordillera is well delineated at a regional scale, defined by discontinuous hills mainly formed by Jurassic and Cretaceous limestones that constitute the boundary with the Neogene Guadalquivir foreland basin.

10.3 Gravity prospecting

Gravity research helps to unravel the deep structure since it highlights the horizontal density change in subsurface geological bodies. A total of 138 pre-existing gravity measurements compiled by the Topoiberia project (Ayala, 2013) were combined with 116 new gravity data acquired with a Scintex Autograv CG-5 of 1 μGal accuracy. Gravity measurements where referred to the Granada absolute gravity station (IGN, www.ign.es) and a standard 2.67 g/cm3 density was used to calculate the Bouguer and Terrain corrections. Kane (1962) and Nagy (1966) methods were combined to derive the Terrain correction up to 160 km by means of the 5 m accuracy DEM provided by the IGN (www.ign.es). The complete Bouguer anomaly map was determined taking into account all the gravity measurements. GravMag v.1.7 software (Pedley et al., 1993) was used to obtain a 2D forward model. Densities were considered according to the standard values for the main lithologies (Telford et al., 1990).

10.4 Central Betic mountain front structure

The central Betic Cordillera mountain front is highly irregular, with a 2.52 sinuosity index (Fig. 10.1). The Jódar and the Golondrina sierras are cut to their south-western parts by NW-SE faults (García-Tortosa, et al., 2008; Sanz de Galdeano et al., 2013) along the boundary with the Albánchez Depression,

followed by the Aznaitín High (Figs. 10.2 and 10.3). However, eastwards it is separated by the Tíscar fault from the Cazorla straight mountain front with a sinuosity index of 1.37 (Fig. 10.1).

10.4.1 Folds and faults shaping the mountain front

The Jódar and Golondrina sierras are NW vergent antiforms affecting Prebetic units (Fig. 10.2). The largest one is the Jódar Sierra, which has a box-fold geometry in the central section, and a sub-vertical northern limb. The most striking feature is the high curvature of the fold hinge line, advanced towards the Guadalquivir foreland basin suggesting a NW-wards tectonic transport. The southern long limb is affected by a secondary fold with a high angle reverse fault. Southwards, the Golondrina antiform is more closed and has a straighter hinge line.

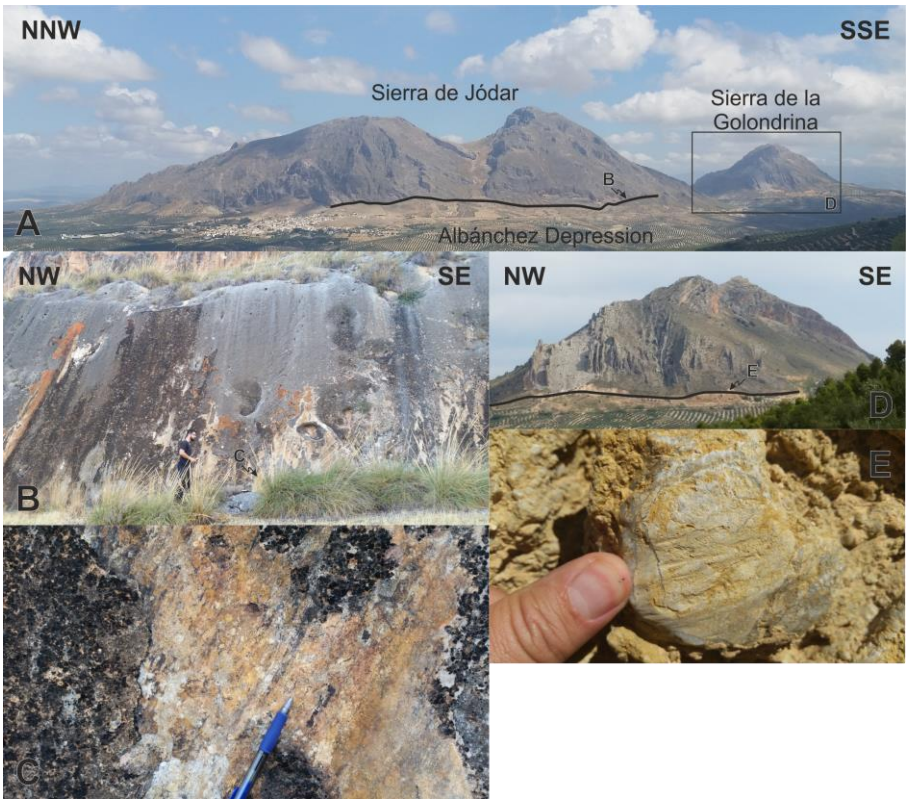

Fig. 10.3 Field view of (A) the Jódar and Golondrina sierras and the Albánchez Depression separated by the Bedmar Fault, (B) the Bedmar Fault escarpment and (C) the Bedmar Fault striae, (D) the Golondrina Fault, and (E) the Golondrina Fault striae.

The Bedmar fault (Fig. 10.3A) has a length of roughly 2 km and a south-westward dip comprised between 75° and 80°. The fault scarp reaches up to 5 m (Fig. 10.3B). The drag of the Jódar antiform in the Prebetic bedding supports a main sinistral kinematics. However, the detailed geometry of the fault surface and its striae suggest at least a more recent normal-dextral component (Fig. 10.3C). The Golondrina fault (Fig. 10.3D) is 700 m long and also dips south-westwards. It shows a first set of sinistral-normal striae (Fig. 10.3E) and a younger set with a normal component, similar to the latest striae set in the Bedmar fault.

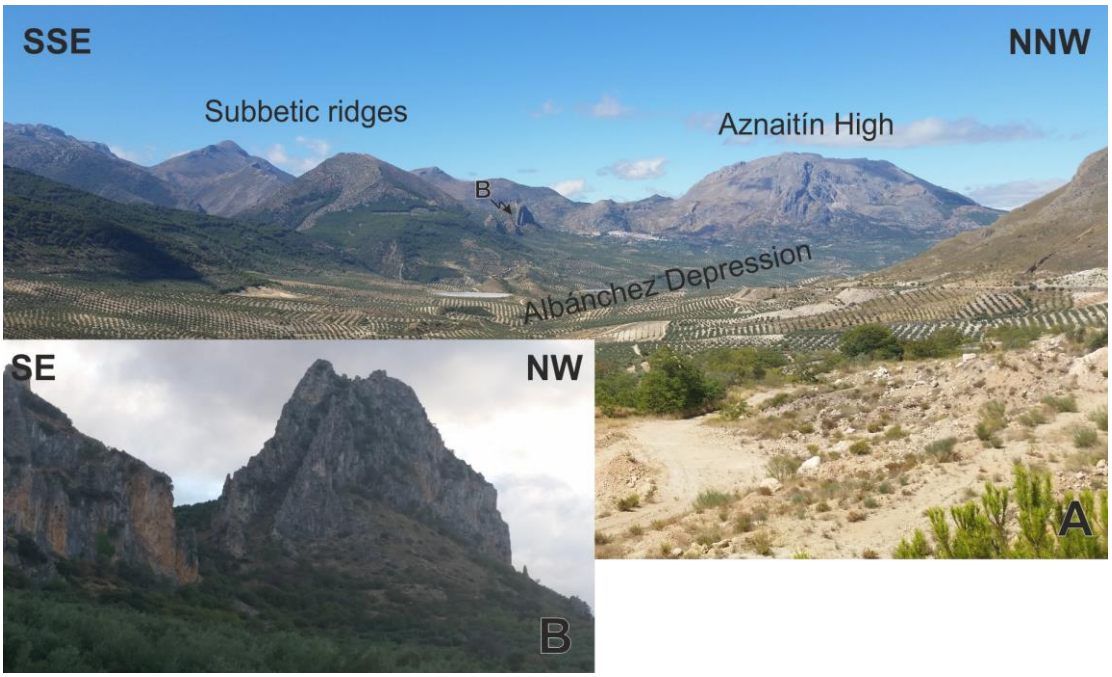

Fig. 10.4 Field view of the (A) the Subbetic ridges and the Aznaitín High with the Albánchez Depression in the foreground. (B) Detail of the sub-vertical Miocene sandstones southwards the Albánchez Depression.

South-westwards the Bedmar fault a chaotically deformed tectonic mélange is composed by evaporite-rich Triassic clays and marls embedding blocks of Subbetic limestones, partly covered by Miocene marls. Sub-vertical Miocene sandstones crop-out in the southern part, near the Subbetic front (Fig. 10.4). Westwards, these sediments lie uncomformably on the Aznaitín High. All the Prebetic structures are south-bounded by the Subbetic front, a continuous fold-and-trust belt.

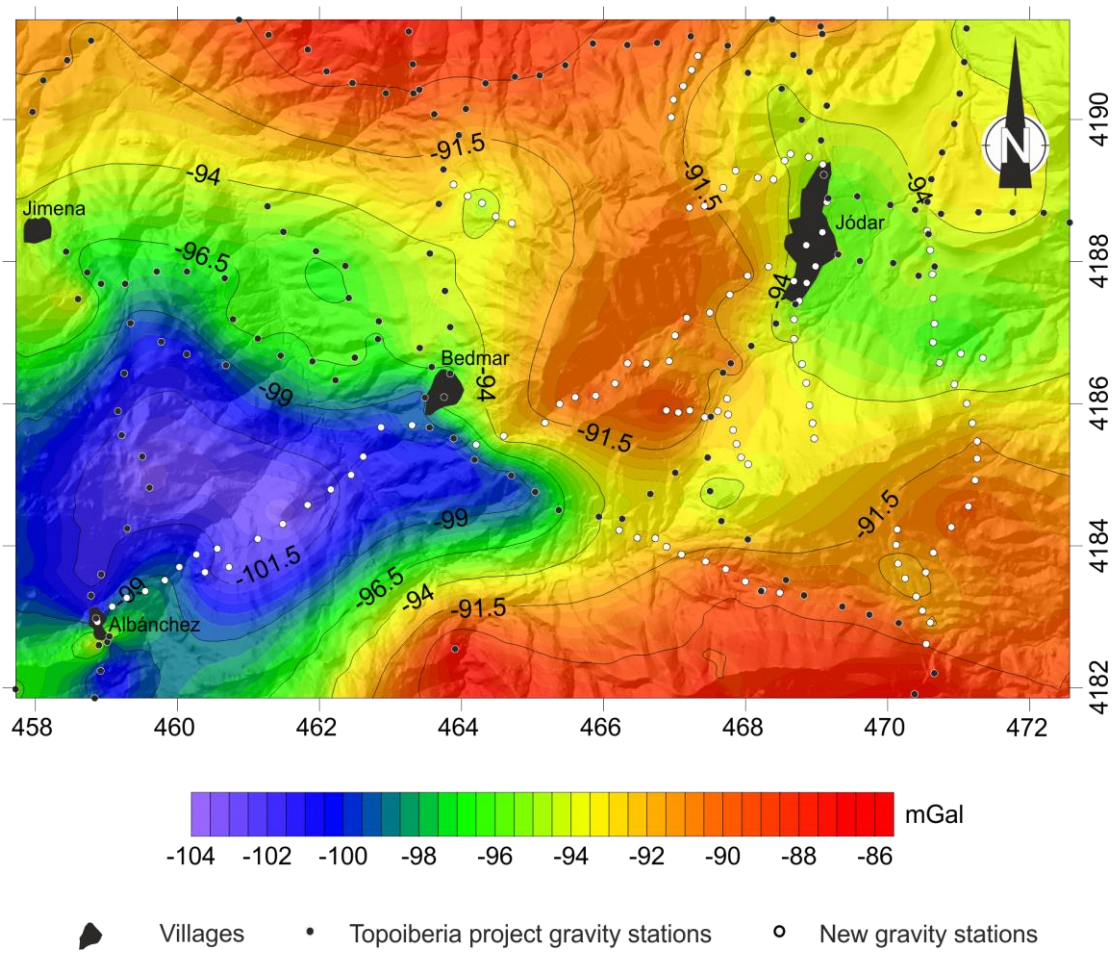

Fig. 10.5 Study area Bouguer anomaly map and gravity stations.

10.4.2 Prebetic units continuity

A gravity research has been developed in order to determine the deep Prebetic continuity between the main sierras. The complete Bouguer anomaly map show values from -104 to -82.3 mGal (Fig. 10.5). The highest anomaly values are located northwards in the Guadalquivir Basin, the Golondrina and Jódar sierras and southwards in the Subbetic. The lowest anomaly values are gathered in the Miocene tectonic mélange covered by Miocene sandstones and marls in the Albánchez Depression. To unravel the basement deep geometry and the continuity of the Prebetic units between the Jódar Sierra and the Aznaitín High, a 2D NE-SW gravity model was carried out orthogonal to the Bedmar fault (Fig. 10.2). Residual anomaly related to the uppermost crustal bodies was estimated subtracting a constant value of 89 mGal to the Bouguer anomaly. The 2D gravity

model includes the main geological bodies (Fig. 10.6): Miocene marls from the sedimentary mélange (2.35 g/cm3), Miocene evaporite-rich sediments from the tectonic mélange (2.20 g/cm3), Prebetic and Subbetic limestones (2.62 g/cm3) and the Tabular Cover and South Iberian margin basement (2.67 g/cm3). This model reveals that the Iberian Massif and the Tabular Cover top is irregular. Above, a low-density evaporite-rich tectonic mélange embedded Jódar sierra thrust sheet. The Prebetic units of the Jódar Sierra are limited westward by the Bedmar fault. The Aznaitín High Prebetic extends below the western Albánchez Depression. This geometry supports a high lateral discontinuity of the Prebetic thrust sheet in this mountain front sector.

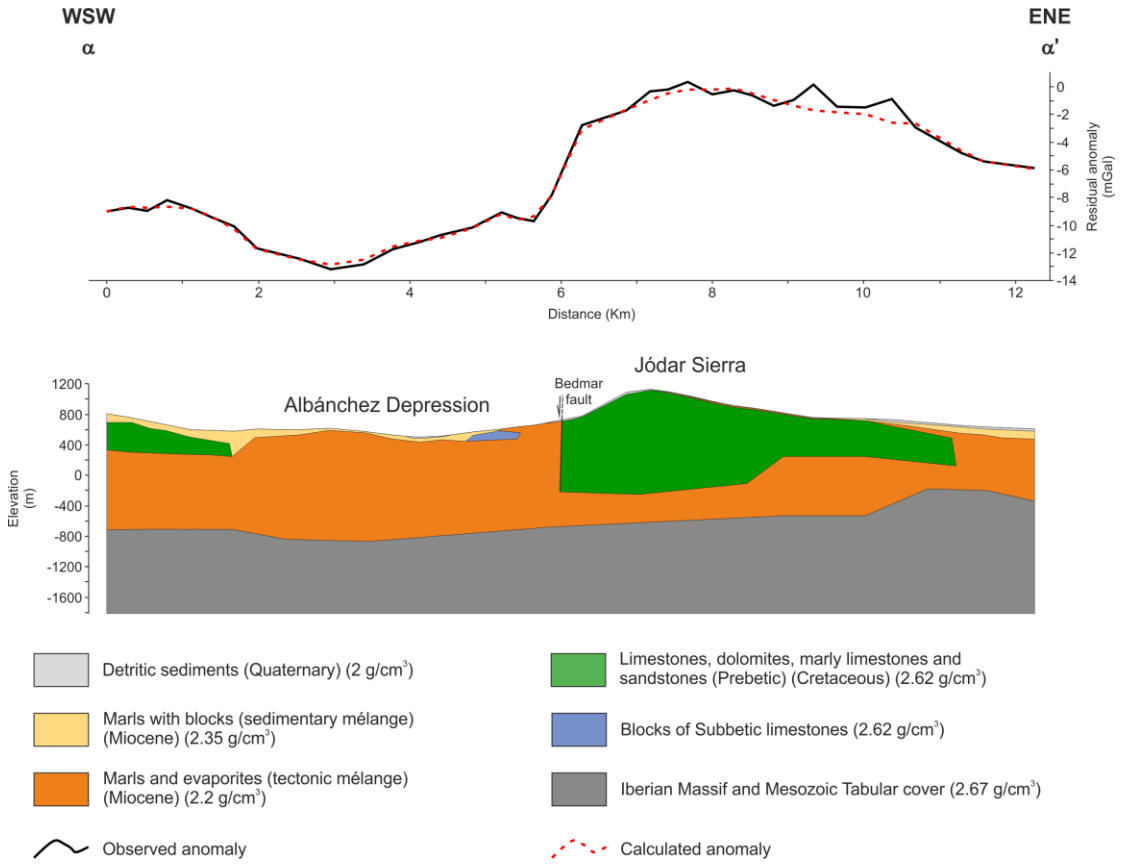

Fig. 10.6 Gravity residual anomaly profile (top) and gravity associated model (bottom).

10.5 Discussion

The mountain front in Sierra de Cazorla present a sinuosity index of 1.37. However, westward the Tíscar fault, where the Jódar area is located, the sinuosity

index reaches a value of 2.52 due to the different development mechanisms. The Jódar and Golondrina sierras Prebetic mountain front has been affected by north-westwards tectonic transport similar to the Prebetic outcrops eastwards the Tíscar fault. However, while the Prebetic arc of Sierra de Cazorla remains NE-SW oriented, westwards the Tíscar Fault it becomes a roughly E-W oriented mountain front (Fig. 10.1).

The faults bounding the south-western part of Jódar and Golondrina sierras, have two deformational phases: a NW-SE Miocene compression –probably simultaneous to an orthogonal extension– and a late dominant NE-SW extension until present (García-Tortosa et al., 2008). This extensional episode was responsible of the NW-SE faults bounding the SW part of the Prebetic outcrops. However, the total fault slip had to be huge in order to explain the lack of Prebetic outcrops in the hanging wall, so the NW-SE faults have been proposed to even cut the basement constituted by the foreland (García-Tortosa et al., 2008). In any case, new gravity data reveal that the Prebetic units are not present in the hanging wall of the Bedmar fault, where the tectonic mélange and the Miocene sedimentary deposits are located, possibly due to its early sinistral slip that displaced the Prebetic towards the NW. Gravity models also reveal that the mountain front deformation in depth is conditioned by the presence of an evaporite-rich tectonic mélange with variable thickness. Irregularities in the basement relief could also affect the propagation front, allowing some parts to displace and holding back others, as has also been evidenced by analogue modelling (Callot et al., 2012). This fact clearly affects the structural deformation pattern increasing the mountain front former irregularity.

In this setting some Prebetic massifs that remained back were thrust by the Subbetic, giving a discontinuous Prebetic front in the area. The Bedmar fault is a main fracture probably reactivated in different settings. At first it might acted as a sinistral-normal fault to accommodate the Prebetic rupture in the southwestern boundary of the curved Jódar antiform. The Golondrina Fault was also sinistral, with a tip line southwards the Jódar antiform that accommodated the NW-SE

shortening. Thereafter, the north-westward Subbetic front advance probably conditioned the Miocene tectonic mélange to occupy the space left in between the Jódar Sierra and the Aznaitín High. The Subbetic front seems to be the responsible for the deformation of the Miocene sandstones that are now sub-vertical. In this setting the Bedmar fault acted as dextral-normal. In a latest stage, the Jódar antiform finished its shortening and the NE-SW External zones extension prevailed determining that the Bedmar fault acted mainly as a pure normal fault. In all these deformation stages, an approximately E-W extension orthogonal to the emplacement of the Subbetic could take place contributing to increase the discontinuity of the Prebetic and Subbetic outcrops and subsecuently, increasing as well the mountain front sinuosity (Fig. 10.7). The well preserved scarp of the Bedmar fault may suggest it is active at present time (García-Tortosa et al., 2008; Sanz de Galdeano et al., 2013).

Prebetic including Cazorla Sierra and Jódar area, was in a first stage displaced north-westwards towards the foreland. Before the Late Tortonian, this displacement slowed in the easternmost part of the cordillera, freezing the Prebetic front as a continuous fold-and-thrust belt. However, in the central and western part, the displacement continued by the development of the Gibraltar Arc. This differential tectonic displacement in the Prebetic front resulted in the dextral Tíscar fault and the development of a highly sinuous and more chaotic mountain front west of this fault. In any case, there is not a general agreement on the ages of these events (Bustillo and García, 1997; Martín et al., 2009; Azañón et al., 2012; Roldán et al., 2012, 2013; Rodríguez-Fernández et al., 2013; Morales et al., 2015).

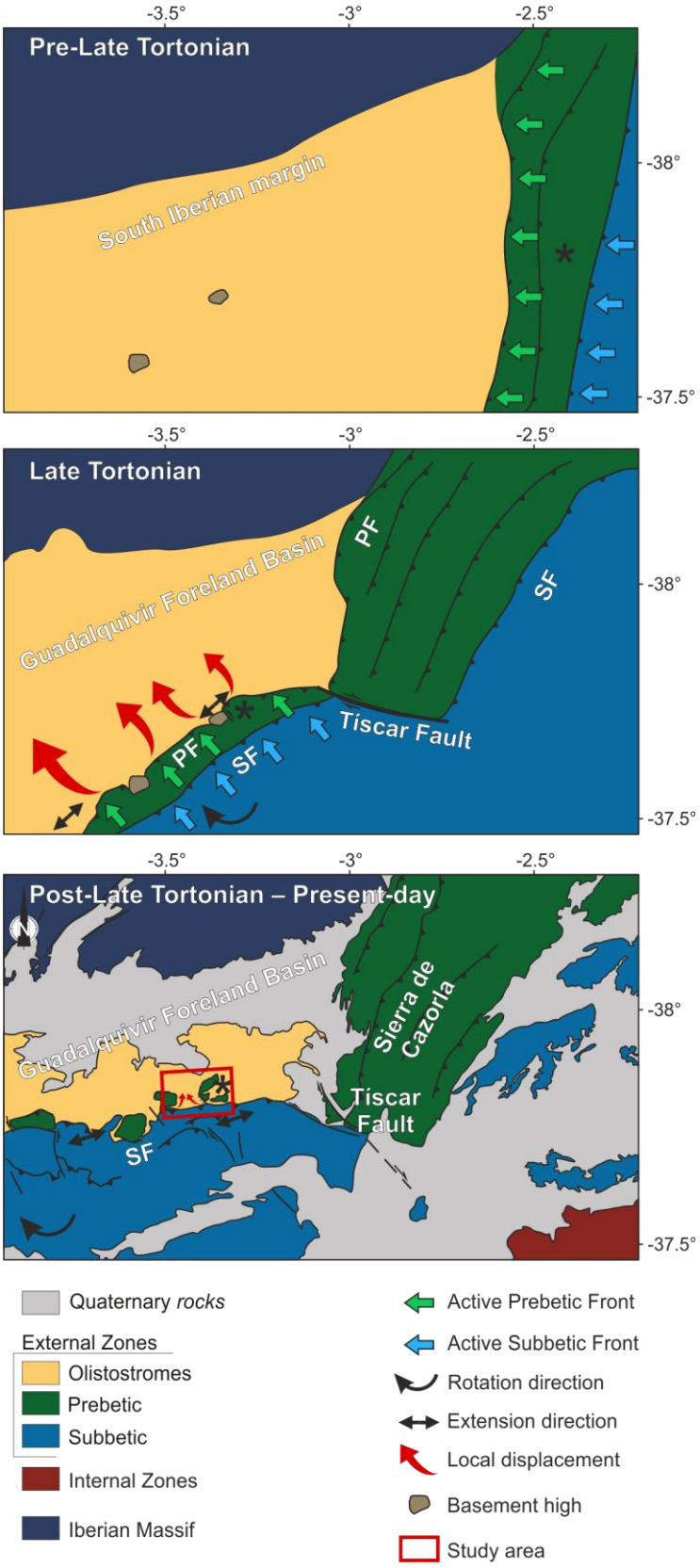

Fig. 10.7 Pre-Tortonian to Present-day evolution model proposed for the Prebetic mountain front. PF (Prebetic Front) and SF (Subbetic Front) indicate the front position in each stage. Asterisk indicates a tentative position of the Jódar and Golondrina Sierras in different deformation stages.

Although active mountain fronts generally have straight shape due to the tectonic control of the relief rather than erosional factors (Keller and Pinter, 1996),

other factors as presence of easily deformable rocks in the basal detachment level of the mountain front, or the existence of irregularities in the thrust units may affect not only the sinuosity of the mountain front but also its orientation. The central Betic Cordillera External Zones present a very good example of this kind of tectonic deformation and highlight the importance of these factors since they can completely change the deformation pattern of a single mountain front in just few kilometres.

10.6 Conclusions

The roughly E-W oriented Betic mountain front in Jódar area has an irregular shape. It is formed by discontinuous highly arched antiformal Prebetic massifs cross-cut by NW-SE faults. Its development is probably consequence of the existence of irregularities in the basal easily deformable tectonic mélange, formed mainly by Triassic evaporites and marls that constitute the detachment of the External Zones above the Iberian massif basement. The highly arched Jódar Sierra and Golondrina sierra were formed by north-westward Late-Tortonian tectonic transport as northwards vergent antiforms separated by a synform probably developed on an easily deformable corridor bounded south-westward by the Bedmar and the Golondrina faults. Gravity data supports the Prebetic units discontinuity south-westwards of these sinistral transfer faults. Later, after the Late Tortonian until Present-day, the thrust of the Subbetic determined a north-westards expulsion of the tectonic mélange and the olistostroms towards the Albánchez depression between the Jódar and Aznaitín Prebetic Massifs and the Bedmar fault become dextral. Finally the late NE-SW extension prevails in the mountain front and late normal activity affects the Bedmar and Golondrina faults.

The westward development of the Gibraltar Arc determined a former straight NNE-SSW Prebetic mountain front that remained in Cazorla Sierra, eastwards of the Tíscar Fault. More intense and recent westward displacements together with the presence of the heterogeneous crustal structure determines the development of the irregular discontinuous mountain front in the central Betic Cordillera.

These factors should be considered when comparing mountain fronts activity by sinuosity geomorphic indexes.

Acknowledgements

We acknowledge the comments provided by of Dr. Francisco Javier Roldán-García, which highly improved this research. This research was funded by the RNM148 and research group of the Junta de Andalucía and project CGL2016-80687-R.

Part III

CHAPTER 11

General discussion

The new data presented in previous chapters increase the knowledge of the geodynamic evolution in the Betic Cordillera central-eastern part. These new enquires contribute to the existent discussion about the different tectonic evolution models proposed for the Gibraltar Arc. This chapter first presents the new general geological and geophysical data contributions with both thematic and regional results. Based on these outcomes, it is proposed a model for the recent and active geodynamic evolution of the Betic Cordillera central-eastern part. The last section provides a discussion on the new insights to shed light to the controversial regional geodynamic models for the Gibraltar Arc development.

11.1 New contributions improving the understanding of methods for active tectonic studies

The geomorphic observations are essential to reveal the activity of tectonic structures. For the first time onshore buried marine-cut terraces have been detected by means of gravity data. This allowed to correlate buried marine-cut terraces with offshore marine-built terraces to shed light on the mechanisms responsible for relative sea-level changes in the Alborán Sea in the last years as a reference for vertical relief motion. Moreover, sinuosity index of mountain fronts is generally considered as an evidence of its tectonic activity. This research contributes to the discussion about the factors affecting the sinuosity of a mountain front during its formation with an example in the Betic Cordillera External Zone front, where the presence of heterogeneous soft layers and extension orthogonal to the mountain front largely increases its sinuosity.

11.2 New insights in the knowledge of the Betic Cordillera structure from geodetic, geophysical and geological data

The central-eastern Betic Cordillera intramontane basins have been previously studied from a tectonic and stratigraphic point of view (Kleverlaan, 1987, 1989; Sanz de Galdeano and Alfaro, 2004; Weijermars et al., 2007; Sanz de Galdeano et al., 2010). However, in the Sierra Nevada southern part, where the basin development is controlled by the interaction of faults and folds, there were no constraints on the deep structure up to date. In this region, the Alhabia basin has an exceptional location amongst Sierra Nevada, Sierra de Gádor, Sierra de Los Filabres and Sierra Alhamilla. The new acquired geophysical data helps to unravel the deep structure of this basin and to infer its sedimentary infill geometry. The depocentre distribution inferred from gravity data reveals the influence of large scale E-W folds and different NW-SE and E-W fault sets interaction in the Alhabia basin, which is the result of the superposition of other three intramontane basins (the Alpujarran Corridor, the Tabernas basin and the Gádor-Almería basin). The main depocentre is consequence of the Alpujarran faulted synform interaction with the NW-SE normal faults separating Sierra de Gádor and Sierra Alhamilla. Then, the basin develops in a setting with N-S to NW-SE compression and NE-SW extension since the Late Miocene, which support a regional ENE-WSW extensional regime in the southern part of the Internal Zone.

CGPS data processed from the Topo-Iberia project in a regional network also combined with geological field observations have helped to shed light into the recent and active structure evolution of the central-eastern Betic Cordillera by determining the rate of tectonic deformation. These results point to the very low activity of the large E-W oriented folds in the Betic Cordillera Internal Zone. The activity of large fault zones surrounding the main antiformal metamorphic massifs accommodates the present day westwards and south-westwards transport of the Internal Zone southern part.

The main active faults recognized in Sierra Nevada are located in the southeastern (Laujar Fault) and western part (Padul Fault) showing in both cases a recentmost normal regime, although with different extensional trends. The E-W southwards dipping Laujar Fault Zone has allowed to characterise the development of an extensional structure parallel to E-W compressional folds. This fault evidence local N-S extension in a regional N-S compressive setting. The Padul Fault GPS networks have constrained the present displacements, accommodating the ENE-WSW extension south-westward Sierra Nevada. This main structure accommodates most of the ENE-WSW extension of the central Betic Cordilleras and hence it has a very high horizontal rates (~0.5 mm/yr in N66°E). However, the Padul Fault area is characterized by a low seismicity compared to the region, so a creep movement may be invoked to explain its activity with a lack of large magnitude events.

The mentioned horizontal tectonic rates are however not accompanied by a consequent tectonic elevation or subsidence in the central part of the Cordillera as seen in the study carried in the central part of the northern Alborán Coast, at least during the last hundreds of thousands of years. The combination of gravity data with seismic reflection profiles and multibeam bathymetry data allowed to correlate buried marine-cut terraces onshore with marine terraces offshore. Comparing the obtained results with previous sea-level studies (Rohling et al., 2009; Stanford et al., 2011) reveal that the marine terraces position is affected by eustatism rather than tectonics. This circumstance might be due to the balance of extension and shortening in this part of the Cordillera.

In the Betic Cordillera External Zone, geological field observations together with gravity data have unravelled the processes related to the mountain front development that determine its sinuosity. The study has been focused in the Jódar-Bédmar area, characterized by a high discontinuity amongst different Prebetic outcrops in the mountain front that constitute the boundary with the Guadalquivir Foreland Basin. These results reveal a different tectonic deformation pattern in each sector of the External Zone. Whilst the Cazorla Arc

remained as a typical straight and continuous fold and thrust belt, the External Zone westwards the Tíscar fault present discontinuous outcrops linked to a more chaotic deformation due to the irregular distribution of easily deformable rocks that acted as a detachment level.

11.3 Late Miocene to Present tectonic evolution model for the central-eastern Betic Cordillera

The integration of the two study areas results in the Internal and External zones improves the knowledge on the development of the Gibraltar Arc in a period essential for the growth of the present-day relief (Fig. 11.1). In a first stage the Betic Cordillera front advanced toward the west and was initially N-S oriented. During the Middle Miocene (Fig. 11.1 a and b), the metamorphic basement in the Internal Zone suffered a dismantling causing low-angle normal faults (Johnson et al., 1997) with a top-to-the-west displacement that propagated towards the External Zone and the Flysch units and produced an E-W compression together with the development of thrust structures (Balanyá and García-Dueñas, 1987; Crespo-Blanc and Campos, 2001; Luján et al., 2003; Platt et al., 2003).

This setting changed in the Late-Tortonian (Fig. 11.1c), when the development of large E-W folds begun in the Internal Zone due to the N-S Africa-Eurasia convergence (Dewey et al., 1989; DeMets et al., 1994), probably with the simultaneous development of E-W dextral transfer faults that favoured the westwards displacement of Internal Zone (Sanz de Galdeano, 1996a). It was in this time when the main Internal Zone ranges and the intramontane basins among them begun to develop (Weijermars et al., 1985; Galindo-Zaldívar et al., 2003; Sanz de Galdeano and Alfaro, 2004). Approximately in the Late Tortonian, the Cazorla Prebetic front stopped its westwards advance. However, the External Zone westwards the Tíscar Fault continued moving toward the W and NW simultaneously to the westwards displacement of the Internal Zone during the development of the Gibraltar Arc (González-Castillo et al., 2015b).

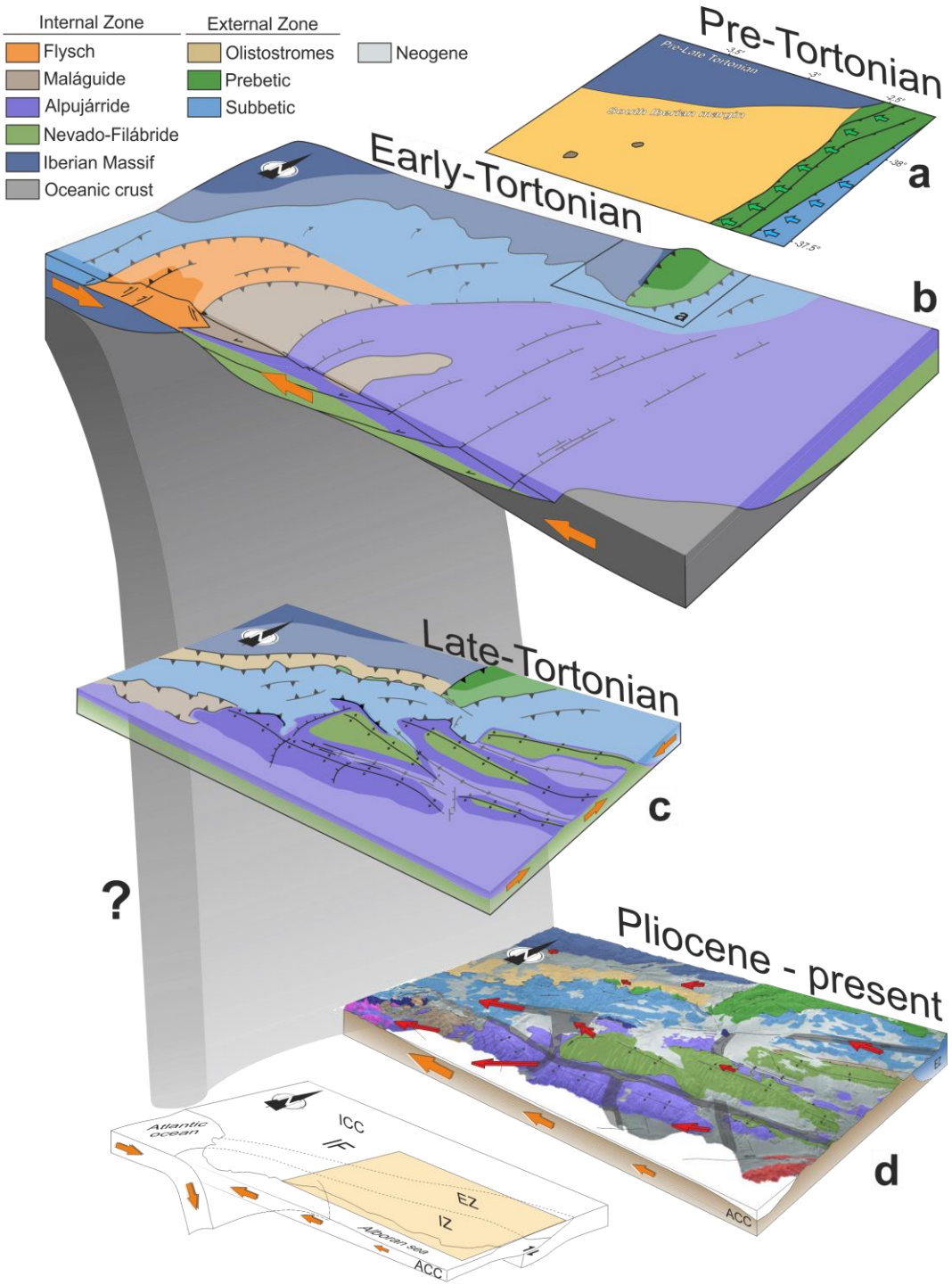

Fig. 11.1 Central-eastern Betic Cordillera Evolution model since Pre-Tortonian times. a) Indicates the initial stage in Fig. 10.7 with the N-S oriented Prebetic Front, b) Shows the Early-Tortonian top-to-the-west displacement and, c) illustrates the Late-Tortonian N-S compression and the E-W large folds development. Finally, c) shows the Pliocene to present-day general westward motion. Red arrows indicate the resent-day displacement rates from CGPS data.

Finally, during the Pliocene (Fig. 11.1d), a counter-clockwise rotation in the Africa-Eurasia convergence (Calais et al., 2003) leaded to a much smaller N-S compression component. As a consequence, uplifting of Sierra Nevada and Sierra de Filabres probably stopped, with the decrease of activity of E-W oriented folds, although scarce NW-SE shortening remained in the Sierra Nevada westernmost part. It is remarkable that this is the region that reaches the highest altitudes. Moreover the area southern and western of Sierra Nevada started a south-westward displacement. In this setting, when E-W to NE-SW extension prevail on NW-SE compression due to the development of the Gibraltar Arc, the thrusting of the External Zone over the Guadalquivir foreland basin stopped its progression in the Betic Cordillera central part, prevailing the ESE-WNW extension in them. However, in the southernmost boundary of the Betic Cordillera Internal Zone where the crust is thinner, the growing of E-W folds in present times is still stable (Marín-Lechado et al., 2005, 2010; Pedrera et al., 2015).

Nevertheless, at present day, whilst the frontal part of the Cordillera has become practically inactive, an extensional setting dominates the Internal Zone. A main ENE-WSW extension occur in the western Sierra Nevada accommodated by the Padul fault zone that constitute one of the main discontinuities of the Betic Cordillera separating the high relieves of Sierra Nevada and the low Granada Basin. South of Sierra Nevada, the Laujar Fault also evidence local N-S extension due to the actual dismantling of the highest Cordillera relief.

The results obtained in the central-eastern Betic Cordillera indicate a general westward motion in the region with a southward component in the Sierra Nevada southern part. The westward motion is attributed to the oblique dextral Africa-Eurasia convergence, whilst the south-westwards component in the southern part of the central-eastern Betic Cordillera may be related to the dismantling of a thickened crust. In this setting, tectonic evolution models suggesting lithospheric delamination (García-Dueñas et al., 1992; Seber et al., 1996; Calvert et al., 2000; Mancilla et al., 2013) should produce a radial extension

in order to compensate the root loss that cannot be assessed with the results here exposed. Models invoking only a subducting slab (Araña and Vegas, 1974; De Jong, 1991, 1993; Wortel and Spakman, 1992; Zeck et al., 1992) may explain the westward component observed in this research, however a simple subduction would imply compression from the back-arc to the fore-arc. New geophysical, geological and geodetical data however, show a present day E-W to NE-SW and locally N-S extensional component in the central-eastern transect of the Betic Cordillera, which is not compatible with a simple subduction model. Finally, the results obtained in this research are only compatible with a subduction model involving a slab active roll-back (Blanco and Spakman, 1993; Morley, 1993; Royden, 1993; Lonergan and White, 1997; Hoernle et al., 1999; Wortel and Spakman, 2000; Gutscher et al., 2002; Gill et al., 2004; Spakman and Wortel, 2004; Thiebot and Gutscher, 2006; Brun and Faccena, 2008; Pedrera et al., 2011; Ruiz-Constán et al., 2011, 2012). This geodynamic model is in agreement with the Rif's roll-back slab proposed by Pérouse et al. (2010) although with a symmetric arrangement. In summary, these results support better the presence of an eastwards- southeastwards subduction with related delamination associated with the westwards propagation of the Gibraltar Arc.

CHAPTER 12

Conclusions

The central-eastern Betic Cordillera has undergone probably since Middle Miocene a top-to-the W translation of tectonics units related to extensional deformations in the Internal Zone and shortening in the External Zone, which developed the N-S to NNE-SSW Sierra de Cazorla front. Since the Late Miocene, the westwards displacements continue in the southern part of the Betic orogen and determines the development in the External Zone of a sinuous mountain front affected by E-W extension. In this time, the Internal Zone are deformed by the simultaneous E-W to NE-SW extension and orthogonal N-S to NW-SE compression.

The interaction of Neogene-Quaternary intramontane basins in the central-eastern Betic Cordillera Internal Zone is related to the activity of large faults and folds that reveals since Tortonian times the counter-clockwise rotation of N-S to NW-SE shortening. While in the Internal Zone shortening is accommodated by large E-W to NE-SW folds, extension produced normal NW-SE faults, being the Padul fault zone the most relevant in the south-western border of Sierra Nevada. This fault has a high activity although with little associated seismicity suggesting a creeping behaviour. Moreover, change in the plate convergence trend produced the dismantling of the unstable thickened crust of Betic Cordillera, and the activity of E-W normal faults in the central Alpujarran Corridor, being the most relevant the Laujar Fault Zone, south of Sierra Nevada. This fault is coeval to N-S compression in southern regions of thinner crust. The coeval shortening and orthogonal extension probably determined a rough equilibrium evidenced by very low vertical tectonic deformations in the last hundreds of thousands of years as supported by the analysis of recent marine terraces of the Alborán Sea northern coast.

The combination of new geological, geophysical and geodetical data acquired in the Central-Eastern Betic Cordillera and presented in this research support a geodynamic model based on a subduction with an associated slab roll-back as the most suitable tectonic model for the Gibraltar Arc recent and active evolution.

CHAPTER 13

Conclusiones

La Cordillera Bética Centro-oriental ha sido sometida desde el Mioceno medio a un desplazamiento de techo hacia el Oeste en las unidades tectónicas relacionadas con deformaciones extensionales en la Zona Interna y con acortamiento en la Zona Externa, las cuales desarollaron el frente de la Sierra de Cazorla con una orientación NNE-SSO. Desde el Mioceno tardío, los desplazamientos hacia el Oeste continuaron en la parte meridional del orógeno Bético y determinaron el desarrollo de un frente montañoso sinuoso en la Zona Externa afectado por extensión E-O. En ese momento, la Zona Interna se deformaba por una extensión simultánea de E-O a NE-SO con una compresión ortogonal asociada.

La interacción de cuencas intramontañosas neógeno-cuaternarias en la Zona Central de la Cordillera Bética centro-oriental está relacionada con la actividad de grandes fallas y pliegues que muestran la rotación antihoraria del acortamiento desde el Tortoniense de N-S a NO-SE. Mientras que en la Zona Interna el acortamiento se acomoda por grandes pliegues E-O y NE-SO, la extensión ha producido fallas normales NO-SE, siendo la Zona de Falla de Padul la más relevante en el límite suroeste de Sierra Nevada. Esta falla presenta gran actividad con poca sismicidad, lo que sugiere una actividad por reptación. Además, los cambios en la tendencia de la convergencia de placas han producido el desmantelamiento de la corteza engrosada inestable de la Cordillera Bética y la actividad de fallas normales E-O en el sector central del Corredor de la Alpujarra, siendo la Zona de Falla de Laujar más relevante, al Sur de Sierra Nevada.

Esta falla es simultánea a la compresión NO-SE en las regiones al Sur de Sierra Nevada, donde la corteza es más delgada. La coexistencia de acortamiento y extensión en la región determina probablemente un equilibrio relativo

evidenciado por muy bajas deformaciones tectónicas en la vertical en los últimos cientos de miles de años, como se concluye en el análisis de terrazas marinas en la costa norte del Mar de Alborán.

La combinación de nuevos datos geológicos, geofísicos y geodésicos adquiridos en la zona centro-oriental de la Cordillera Bética y presentados en este trabajo de investigación, apoya una subducción con un roll-back asociado como el modelo geodinámico más apto para el Arco de Gibraltar.

References

ABEM, 2006. Instruction Manual Terrameter SAS 4000/SAS 1000. ABEM InstrumentAB, Sundbyberg, Sweden, 136 pp.

Aldaya, F., 1981. Mapa Geológico y memoria explicativa de la hoja 1056 (Albuñol) del Mapa Geológico de España. IGME, Madrid.

Aldaya, F., García-Dueñas, V., Navarro-Vilá, F., 1979. Los Mantos Alpujárrides del tercio central de las Cordilleras Béticas. Ensayo de la correlación tectónica de los Alpujárrides. Acta geológica hispánica. 14(1), 154-166.

Aldaya, F., Campos, J., García-Dueñas, V., González-Lodeiro, F., Orozco, M., 1984. El contacto Alpujárrides/Nevado-Filábrides en la vertiente meridional de Sierra Nevada. Implicaciones tectónicas. In: El borde mediterráneo español: evolución del orógeno bético y geodinámica de las depresiones neógenas. Departamento de Investigaciones Geológicas, CSIC and Universidad de Granada, Granada, ISBN 00-05776-7. pp. 18-20.

Aldaya, F., Alvarez, F., Galindo Zaldívar, J., González Lodeiro, F., Jabaloy, A., Navarro Vilá, F., 1991. The Malaguide-Alpujarride contact (Betic Cordilleras, Spain): a brittle extensional detachment. C. R. Acad. Sci. Paris. 313, Série II (101), 1447-1453.

Alfaro, P., Galindo-Zaldivar, J., Jabaloy, A., López-Garrido, A.C., Sanz de Galdeano, C., 2001. Evidence for the activity and paleoseismicity of the Padul fault (Betic Cordillera, Southern Spain). Acta Geologica Hispanica. 36(3-4), 283-295.

Alfaro, P., Delgado, J., Sanz de Galdeano, C., Galindo Zaldívar, J., García Tortosa, F.J., López-Garrido, A.C., López-Casado, C., Marín, C., Gil, A.J., Borque, M.J., 2008. The Baza Fault: a major active extensional fault in the central Betic Cordillera (south Spain). International Journal of Sciences. 97(6), 1353-1365.

Alvarez-Marrón, J., Hetzel, R., Niedermann, S., Menéndez, R., Marquínez, J., 2008. Origin, structure and exposure history of a wave-cut platform more than 1 Ma in age at the coast of northern Spain: A multiple cosmogenic nuclide approach. Geomorphology. 93(3), 316-334.

Amundson, R., Wang, Y., Chadwick, O., Trumbore, S., McFadden, L., McDonald, E., Wells, M., DeNiro, M., 1994. Factors and processes governing the 14 C content of carbonate in desert soils. Earth Planet. Sci. Lett. 125(1), 385-405.

Anderson, E.M., 1951. The Dynamics of Faulting and Dyke Formation. Olyver and Boyd, London, 206 pp.

Andeweg, B., Cloetingh, S., 2001. Evidence for an active sinistral shear zone in the western Alboran region. Terra Nova. 13(1), 44-50.

Andrieux, J., Fontbote, J.M., Mattauer, M., 1971. Sur un modèle explicatif de l'Arc de Gibraltar. Earth Planet. Sci. Lett. 12(2), 191-198.

Araña, V., Vegas R., 1974. Plate tectonics and volcanism in the strait of Gibraltar. Tectonophysics. 24, 197-212.

Ardizone J., Mezcua J., Socias, I., 1989. Mapa aeromagnético de Espanña Peninsular. Instituto Geográfico Nacional, Madrid, Spain.

Argus, D.F., Gordon, R.G., DeMets, C., Stein, S., 1989. Closure of the Africa-Eurasia-North America plate motion circuit and tectonics of the Gloria fault. J. Geophys. Res.: Solid Earth (1978–2012). 94(B5), 5585-5602.

Augier, R., Agard, P., Monié, P., Jolivet, L., Robin, C., Booth-Rea, G., 2005a. Exhumation, doming and slab retreat in the Betic Cordillera (SE Spain): in situ40Ar/39Ar ages and P–T–d–t paths for the Nevado-Filabride complex. J. Metamorph. Geol. 23(5), 357-381.

Augier, R., Jolivet, L., Robin, C., 2005b. Late Orogenic doming in the eastern Betic Cordilleras: Final exhumation of the Nevado-Filabride complex and its relation to basin genesis. Tectonics. 24(4).

Ayala, C., 2013. A new compilation of gravity data over the Iberian Peninsula and surrounding areas. Internal Report Topoiberia project (Consolider-Ingenio). IGME.

Ayala, C., Bohoyo, F., Maestro, A., Reguera, M.I., Torne, M., Rubio, F., Fernàndez, M., García-Lobón, J.L., 2016. Updated Bouguer anomalies of the Iberian Peninsula: a new perspective to interpret the regional geology. Journal of Maps. 1-4.

Azañón, J.M., Galindo-Zaldivar, J., García-Dueñas, V., Jabaloy, A., 2002. Alpine tectonics II: Betic Cordillera and Balearic Islands. In: Gibbons, W., Moreno, T. (Eds.), The geology of Spain. London, pp. 401-416.

Azañón, J.M., Tuccimei, P., Azor, A., Sánchez-Almazo, I.M., Alonso-Zarza, A. M., Soligo, M., Pérez-Peña, J.V., 2006. Calcrete features and age estimates from U/Th dating: implications for the analysis of Quaternary erosion rates in the northern limb of the Sierra Nevada range (Betic Cordillera, southeast Spain). Geol. Soc. Am. Bull. Special Papers. 416, 223-239.

Azañón, J.M., Roldán, F.J., Rodríguez Fernández, J., 2012. Fallas y despegues extensionales en el Subbético Central: implicaciones en la evolución Neógena de las Zonas Externas de La Cordillera Bética. Geogaceta. (52), 107-110.

Bahr, K., 1988. Interpretation of the magnetotelluric impedance tensor: regional induction and local telluric distortion. J. Geophys. 62, 119-127.

Bahr, K., 1991. Geological noise in magnetotelluric data: a classification of distortion types. Phys. Earth Planet. Inter. 66(1-2), 24-38.

Balanyá, J.C., García-Dueñas, V., 1987. Les directions structurales dans le Domaine d'Alborán de part et d'autre du Détroit de Gibraltar. C.R. Acad. Sci. Paris. 304, 929-932.

Balanyá, J.C., García-Dueñas, V., Azañón, J.M., and Sánchez-Gómez, M., 1997. Alternating contractional and extensional events in the Alpujarride nappes of the Alboran Domain (Betics, Gibraltar Arc). Tectonics. 16, 226-238.

Balesdent, J., Guillet, B., 1982. Les datations par le 14C des matieres organiques des sols. Contribution al'etude de l'humification et du renouvellement des substances humiques. Sciences du Sol. Bulletin AFES. 2, 93-112.

Banda, E., Ansorge, J., 1980. Crustal structure under the central and eastern part of the Betic Cordillera. Geophys. J. Roy. Astr. Soc. 63, 515-532.

Banda, E., Gallart, J., García-Dueñas, V., Dañobeitia, J., Makris, J., 1993. Lateral variation of the crust in the Iberian Peninsula: new evidence from the Betic Cordillera. Tectonophysics. 221(1), 53-66.

Bárcenas, P., Lobo, F.J., Macías, J., Fernández-Salas, L.M., del Río, V.D., 2011. Spatial variability of surficial sediments on the northern shelf of the Alboran Sea: the effects of hydrodynamic forcing and supply of sediment by rivers. Journal of Iberian Geology. 37(2), 195-214.

Bard, E., Hamelin, B., Delanghe-Sabatier, D., 2010. Deglacial meltwater pulse 1B and Younger Dryas sea levels revisited with boreholes at Tahiti. Science. 327(5970), 1235-1237.

Berne, S., Jouet, G., Bassetti, M.A., Dennielou, B., Taviani, M., 2007. Late Glacial to Preboreal sea-level rise recorded by the Rhône deltaic system (NW Mediterranean). Mar. Geol. 245(1), 65-88.

Berryman, K., 1993. Age, height, and deformation of Holocene marine terraces at Mahia Peninsula, Hikurangi subduction margin, New Zealand. Tectonics. 12(6), 1347-1364.

Bertiger, W., Desai, S., Dorsey, Haines, B., Harvey, N., Moore, A., Owen, S., Weiss, J.P., 2010. Single receiver phase ambiguity resolution with GPS data. J. Geodyn. 84, 327-337.

Bianco, G., Devoti, R., Luceri, V., 2003. Combination of loosely constrained solutions, in: Proceedings of the IERS Workshop on Combination Research and Global Geophysical Fluids. Richter, B. Schwegmann, W., Dick, W.R. pp. 107–109.

Bird, E., 2010. Spain. In: C.F. Eric, M. Bird (Eds.), Encyclopedia of the World's Coastal Landforms. Springer Netherlands.

Blanco, M.J., Spakman, W., 1993. The P-wave velocity structure of the mantle below the Iberian Peninsula: evidence for subducted lithosphere below southern Spain. Tectonophysics. 221(1), 13-34.

Blumenthal, M., 1927. Versuch einer tektonischen Gliederung der Betischen Kordilleren von Central und Sùdwest Andalusien. Eclogae Geol. Helv. 20, 487- 592.

Bokelmann, G., Maufroy, E., Buontempo, L., Morales, J., Barruol, G., 2011. Testing oceanic subduction and convective removal models for the Gibraltar arc: seismological constraints from dispersion and anisotropy. Tectonophysics. 502, 28-37.

Bonini, W.E., Loomis, T.P., Robertson, J.D., 1973. Gravity anomalies, ultramafic intrusions, and the tectonics of the region around the Strait of Gibraltar. J. Geophys. Res. 78, 1372-1382.

Booth-Rea, G., Azañón, J.M., García-Dueñas, V., Augier, R., 2003. Uppermost Tortonian to Quaternary depocentre migration related with segmentation of the strike-slip Palomares Fault Zone, Vera basin, SE Spain. C. R. Geosci. 335, 751 761.

Botella, M., Martínez, C., Cárdenas, F.J., Cañabate, M.J., 1986. Industria musteriense y achelense de Cueva Horá (Darro, Granada), in: Junta de Andalucía (Ed), 721 Book in Honour of Luis Siret. 79-95.

Bourgois, J., 1978. La transversale de Ronda (Cordillères bétiques, Espagne). Donnés géologiques pour un modéle d'évolution de l'arc de Gibraltar. Tesis Doctoral, Universidad de Besançon, Besançon, 445 pp.

Boutton, T.W., 1996. Stable carbon isotope ratios of soil organic matter and their use as indicators of vegetation and climate change. In: Boutton, T.W., Yamasaki, S.I. (Eds.), Mass Spectrometry of Soils. Marcel Dekker, New York, pp. 47–82.

Bradley, W.C., Griggs, G.B., 1976. Form, genesis, and deformation of central California wave-cut platforms. Geol. Soc. Am. Bull. 87(3), 433-449.

Braga, J.C., Martin, J.M., Quesada, C., 2003. Patterns and average rates of late Neogene-Recent uplift of the Betic Cordillera, SE Spain. Geomorphology. 50(1), 3-26.

Brun, J.P., Faccenna, C., 2008. Exhumation of high-pressure rocks driven by slab rollback. Earth and Planet. Sci. Lett. 272, 1-7.

Buforn, E., Udias, A., Madariaga, R., 1991. Intermediate and deep earthquakes in Spain. Pure Appl. Geophys. 136, 375-393.

Buforn, E., Sanz de Galdeano, C., Udias, A., 1995. Seismotectonics of the lbero-Maghrebian region. Tectonophysics. 248, 247-261.

Buforn, E., Bezzeghoud, M., Udias, A., Pro, C., 2004. Seismic sources on the Iberia-African plate boundary and their tectonic implications. Pure Appl. Geophys. 161(3), 623-646.

Bull, W.B., 1978. Final technical report south front of the San Gabriel Mountains, Geosciences Department, University of Arizona, California.

Bull, W.B., McFadden, L.D., 1977. Tectonic geomorphology north and south of the Garlock fault, California. In Geomorphology in arid regions. Proceedings of the eighth annual geomorphology symposium. State University of New York, Binghamton (pp. 115-138).

Burg, J.P., Podladchikov, Y., 1999. Lithospheric scale folding: numerical modelling and application to the Himalayan syntaxes. Int. J. Earth Sci. 88, 190-200.

Bustillo, M.A., García, M.J.L., 1997. Age, distribution and composition of Miocene diatom bearing sediments in the Guadalquivir Basin, Spain. Geobios. 30(3), 335-350.

Cagniard, L., 1953. Basic theory of the magneto-telluric method of geophysical prospecting. Geophysics. 18, 605-635.

Calais, E., DeMets, C., Nocquet, J. M., 2003. Evidence for a post-3.16-Ma change in Nubia–Eurasia–North America plate motions?. Earth Planet. Sci. Lett. 216(1), 81-92.

Callot, J.P., Trocmé, V., Letouzey, J., Albouy, E., Jahani, S., Sherkati, S., 2012. Pre-existing salt structures and the folding of the Zagros Mountains. Geol. Soc. London, Spec. Publ. 363(1), 545-561.

Calvache, M.L., Viseras, C., Fernández, J., 1997. Controls on fan development-evidence from fan morphometry and sedimentology; Sierra Nevada, SE Spain. Geomorphology. 21, 69-84.

Calvert, A., Sandvol, E., Seber, D., Barazangi, M., Roecker, S., Mourabit, T., Vidal, F., Alguacil, G., Jabour, N., 2000. Geodynamic evolution of the lithosphere and upper mantle beneath the Alboran region of the western Mediterranean: Constraints from travel time tomography. J. Geophys. Res.: Solid Earth (1978-2012). 105(B5), 10871-10898.

Carbonell, R., Sallarés, V., Pous, J., Dañobeitia, J., Queralt, P., Ledo, J., García-Dueñas, V., 1998. A multidisciplinary geophysical study in the Betic chain (southern Iberia Peninsula). Tectonophysics. 288, 137-152.

Carmignani, L., Conti, P., Cornamusini, G., Meccheri, M., 2004. The internal Northern Apennines, the northern Tyrrhenian Sea and the Sardinia-Corsica block. Geology of Italy. Special Volume, Italian Geological Society. IGC 32, 59-77.

Carminati, E., Lustrino M., Doglioni, C., 2012. Geodynamic evolution of the central and western Mediterranean: Tectonics vs. igneous petrology constraints. Tectonophysics. 579, 173–192.

Casas, A., Carbo, A., 1990. Deep structure of the Betic Cordillera derived from the interpretation of a complete Bouguer anomaly map. J. Geodyn. 12(2), 137-147.

Cello, G., Nur, A., 1988. Emplacement of foreland thrust systems. Tectonics. 7(2), 261-271.

Chalouan, A., Michard, A., 1990. The Ghomarides nappes, Rif coastal range, Morocco: a variscan chip in the Alpine belt. Tectonics. 9, 1565-1583.

Chalouan, A., Michard, A., 2004. The Alpine Rif Belt (Morocco): a case of mountain building in a subduction-subduction-transform fault triple junction. Pure Appl. Geophys. 161, 489-519.

Chapple, W.M., 1978. Mechanics of thin-skinned fold-and-thrust belts. Geol. Soc. Am. Bull. 89, 1189-1198.

Chiocci, F.L., Orlando, L., 1996. Lowstand terraces on Tyrrhenian Sea steep continental slopes. Mar. Geol. 134(1), 127-143.

Choi, S.J., Merritts, D.J., Ota, Y., 2008. Elevations and ages of marine terraces and late Quaternary rock uplift in southeastern Korea. J. Geophys. Res. Solid Earth. 113(B10), 1978-2012.

Cloetingh, S., Nieuwland, F., 1984. On the mechanics of lithospheric stretching and doming: a finite element analysis. Neth. J. Geosci 63, 315-322.

Collina-Girard, J., 1999. Observation en plongée de replats d'érosion eustatique à l'île d'Elbe (Italie) et à Marie-Galante (Antilles): une séquence bathymétrique mondiale? C. R. Acad. Sci., Ser. IIA: Earth Planet. Sci. 328(12), 823-829.

Collina-Girard, J., 2002. Underwater mapping of Late Quaternary submerged shorelines in the Western Mediterranean Sea and the Caribbean Sea. Quat. Int. 92(1), 63-72.

Colomina, I., Fleta, J., Giménez, J., Goula, X., Masana, E., Ortiz, M.A., Santanach, P., Soro, M., Suriñach, E., Talaya, J., Térmens, A. 1998. The CuaTeNeo GPS network to quantify horizontal movements in the Southeastern part of the Iberian Peninsula. 1ª Asamblea Hispano-Portuguesa de Geodesia y Geofísica, 9ª Asamblea Nacional de Geodesia y Geofísica, Aguadulce, Almería: 199-204.

Coney, P.J., Harms, T.A., 1984. Cordilleran metamorphic core complexes: Cenozoic extensional relics of Mesozoic compression. Geology. 12(9), 550-554.

Crespo-Blanc, A., Campos, J., 2001. Structure and kinematics of the South Iberian paleomargin and its relationship with the Flysch Trough units: extensional tectonics within the Gibraltar Arc fold-and- thrust belt (western Betics). J. Struct. Geol. 23, 1615-1630.

Dahlin, T., Zhou, B., 2006. Multiple-gradient array measurements for multichannel 2D resistivity imaging. Near Surf. Geophys. 4(2), 113-123.

Dañobeitia, J.J., Sallarés, V., Gallart, J., 1998. Local earthquakes seismic tomography in the Betic Cordillera (southern Spain). Earth Planet. Sci. Lett. 160, 225-239.

Davis, D., Suppe, J., Dahlen, F.A., 1983. Mechanics of fold and thrust belts and accretionary wedges. J. Geophys. Res. 88, 1153-1172.

De Jong, K., 1991. Tectono-metamorphic studies and radiometric dating in the Betic Cordilleras (SE Spain) - with implications for the dynamics of extension and compression in the Western Mediterranean area. Tesis Doctoral, Universidad Libre de Amsterdam, Amsterdam, 204 pp.

De Jong, K., 1993. The Tectono-Metamorphic and Chronological Development of the Betic Zone (Se Spain) with Implications for the Geodynamic Evolution of the Western Mediterranean Area. Proc. Kon. Ned. Akad. Wet. 96, 295-333.

De Lamotte, D.F., Andrieux, J., Guézou, J.C., 1991. Cinematique des chevauchements neogenes dans l'Arc betico-rifain; discussion sur les modeles geodynamiques. Bull. Soc. Geol. Fr. 162(4), 611-626.

De Lamotte, D.F., Guezou, J.C., Averbuch, O., 1995. Distinguishing lateral folds in thrust-systems; examples from Corbières (SW France) and Betic Cordilleras (SE Spain). J. Struct. Geol. 17(2), 233-244.

Delgado, J., Alfaro, P., Galindo-Zaldívar, J., Jabaloy, A., López-Garrido, A.C., Sanz de Galdeano, C., 2002. Structure of the Padul-Nigüelas basin (S Spain) from H/V spectral ratios of ambient noise: Analysis of the applicability of the method to study coarse sediments. Pure Appl. Geophys. 159, 2733-2749.

DeMets, C., Gordon, R.G., Argus, D., Stein, S., 1990. Current plate motions. Geophys. J. Int. 101(2), 425-478.

DeMets, C., Gordon, R.G., Argus, D.F., Stein, S., 1994. Effect of recent revisions to the geomagnetic reversal time scale on estimates of current plate motions. Geophys. Res. Lett. 21(20), 2191-2194.

Devoti, R., Riguzzi, F., Cuffaro, M., Doglioni, C., 2008. New GPS constraints on the kinematics of the Apennines subduction. Earth Planet. Sci. Lett. 273(1), 163-174.

Devoti, R., Esposito, A., Pietrantonio, G., Pisani, A.R., Riguzzi, F., 2011. Evidence of large scale deformation patterns from GPS data in the Italian subduction boundary. Earth Planet. Sci. Lett. 311(3), 230-241.

Dewey, J. F., 1988. Extensional collapse of orogens. Tectonics. 7(6), 1123-1139.

Dewey, J.F., Helman, M.L., Knott, S.D., Turco, E., Hutton, D.H.W., 1989. Kinematics of the western Mediterranean. Spec. Publ. Geol. Soc. London. 45(1), 265-283.

Diaz, J., Gallart, J., Villaseñor, A., Mancilla, F., Pazos, A., Córdoba, D., Pulgar, J.A., Ibarra, P., Harnafi, M., 2010. Mantle dynamics beneath the Gibraltar Arc (western Mediterranean) from shear-wave splitting measurements on a dense seismic array. Geophys. Res. Lett. 37, L18304.

Dixon, T.H., 1991. An introduction to the Global Positioning System and some geological applications. Rev. Geophys. 29(2), 249-276.

Do Couto, D., Gumiaux, C., Augier, R., Lebret, N., Folcher, N., Jouannic, G., Jolivet, L., Suc, J.P., Gorini, C., 2014. Tectonic inversion of an asymmetric graben: insights from a combined field and gravity survey in the Sorbas basin. Tectonics. 33, 1360-1385.

Docherty, C., Banda, E., 1995. Evidence for the eastward migration of the Alboran Sea based on regional subsidence analysis: a case for basin formation by delamination of the subcrustal lithosphere? Tectonics. 14(4), 804-818.

Domingo-García, M., Fernández-Rubio, R., López, J.D., González, C., 1983. Aportación al conocimiento de la Neotectónica de la Depresión de Padul (Granada). Tecniterrae. 53, 6-16.

Duggen, S., Hoernle, K., van den Bogaard, P., Rupke, L., Phipps Morgan, J., 2003. Deep roots of the Messinian salinity crisis. Nature. 422, 602-606.

Duggen, S., Hoernle, K., Van den Bogaard, P., Garbe-Schonberg, D., 2005. Post-collisional transition from subduction- to intraplate-type magmatism in the westernmost Mediterranean: Evidence for continental-edge delamination of subcontinental lithosphere. J. Petrol. 46(6), 1155-1201.

Duggen, S., Hoernle, K., Klügel, A., Geldmacher, J., Thirlwall, M., Hauff, F., Lowry, D., Oates, N., 2008. Geochemical zonation of the Miocene Alborán Basin volcanism (westernmost Mediterranean): geodynamic implications. Contrib. Mineral. Petrol. 156, 577-593.

Duque, C., Calvache, M.L., Pedrera, A., Martín-Rosales, W., López-Chicano, M., 2008. Combined time domain electromagnetic soundings and gravimetry to determine marine intrusion in a detrital coastal aquifer (Southern Spain). J. Hydrol. 349(3), 536-547.

Durand-Delga, M., Rossi, P., Olivier, P., Puglisi, D., 2000. Situation structurale et nature ophiolitique de roches basiques jurassiques associées aux flyschs maghrébins du Rif (Maroc) et de Sicile (Italie). C.R. Acad. Sci., Ser. IIa: Earth Planet. Sci. 331, 29-38.

Echeverria, A., Khazaradze, G., Asensio, E., Gárate, J., Dávila, J.M., Suriñach, E., 2013. Crustal deformation in eastern Betics from CuaTeNeo GPS network. Tectonophysics. 608, 600-612.

Egeler, C. G., 1963. On the tectonics of the eastern Betic Cordilleras (SE Spain), Geol. Rundsch. 52, 260-269.

Egeler, C.G., Simon, O.J., 1969. Sur la Tectonique de la Zone Bétique: (Cordillères Bétiques, Espagne). Verh. K. Ned. Akad. Wet. 25, 1-90.

El Kadiri, K., Sanz de Galdeano, C., Pedrera, A., Chalouan, A., Galindo-Zaldívar, J., Julià, R., Akil, M., Rachid, H., Ahmamou, M., 2010. Eustatic and tectonic controls on Quaternary Ras Leona marine terraces (Strait of Gibraltar, northern Morocco). Quat. Res. 74(2), 277-288.

Estey, L.H., Meertens, C.M., 1999. TEQC: the multi-purpose toolkit for GPS/GLONASS data. GPS solutions. 3(1), 42-49.

Fadil, A., Vernant, P., McClusky, S., Reilinger, R., Gomez, F., Ben Sari, D., Mourabit, T., Feigl, K., Barazangi, M., 2006. Active tectonics of the western Mediterranean: Geodetic evidence for rollback of a delaminated subcontinental lithospheric slab beneath the Rif Mountains, Morocco. Geology. 34(7), 529-532.

Fallot, P., 1948. Les Cordillères Bétiques. Estudios Geol. 6, 259-279.

Fernandes, R.M.S., Miranda, J.M., Meijninger, B.M.L., Bos, M.S., Noomen, R., Bastos, L., Ambrosius, B.A.C., Riva, R.E.M., 2007. Surface velocity field of the Ibero-Maghrebian segment of the Eurasia-Nubia plate boundary. Geophys. J. Int. 169(1), 315-324.

Fernández-Ibáñez, F., Soto, J., 2008. Crustal rheology and seismicity in the Gibraltar Arc (western Mediterranean). Tectonics. 27(2).

Fernández-Salas, L.M., Dabrio, C.J., Goy, J.L., Del Río, V.D., Zazo, C., Lobo, F.J., Sanz, J.L., Lario, J., 2009. Land–sea correlation between Late Holocene coastal and infralittoral deposits in the SE Iberian Peninsula (Western Mediterranean). Geomorphology. 104(1), 4-11.

Foucault, A., 1971. Etude géologique des environs des sources du Guadalquivir, provinces de Jaén et de Grenade, Espagne méridionale. Unpubl. doctoral disertation, Université Pierre et Marie Curie-Paris V, Paris, 633 pp.

Fullea, J., Fernàndez, M., Zeyen, H., Vergés, J., 2007. A rapid method to map the crustal and lithospheric thickness using elevation, geoid anomaly and thermal analysis. Application to the Gibraltar Arc System, Atlas Mountains and adjacent zones. Tectonophysics. 430, 97-117.

Fullea, J., Fernàndez, M., Afonso, J.C., Vergés, J., Zeyen, H., 2010. The structure and evolution of the lithosphere–asthenosphere boundary beneath the Atlantic–Mediterranean Transition Region. Lithos. 120, 74-95.

Galindo Zaldívar, J., 1986. Etapas de fallamiento neógenas en la mitad occidental de la depresión de Ugijar (Cordilleras Béticas). Estudios Geológicos. 42(1), 1-10.

Galindo-Zaldívar, J., González-Lodeiro, F., 1990. Diaclasas de tensión regionales en el Complejo Nevado-Filábride y su relación con el contacto Alpujárride/Nevado-Filábride (Sierra Nevada, Cordilleras Béticas). Geogaceta. 7, 9-11.

Galindo-Zaldivar, J., Gonzalez-Lodeiro, F., Jabaloy, A., 1989. Progressive extensional shear structures in a detachment contact in the western Sierra Nevada, (Betic Cordilleras, Spain). Geodinamica Acta. 3(1), 73-85.

Galindo-Zaldivar, J., González-Lodeiro, F., Jabaloy, A., 1993. Stress and palaeostress in the Betic-Rif cordilleras (Miocene to the present). Tectonophysics. 227, 105-126.

Galindo-Zaldívar, J., Jabaloy, A., González Lodeiro, F., 1996. Reactivation of the Mecina detachment in the western sector of Sierra-Nevada (Betic-Cordilleras, SE Spain). C. R. Acad. Sci. Paris 323, 615-622

Galindo-Zaldívar, J., Jabaloy, A., González-Lodeiro, F., Aldaya, F., 1997. Crustal structure of the central sector of the Betic Cordillera (SE Spain). Tectonics. 16(1), 18-37.

Galindo-Zaldivar, J., Gonzalez-Lodeiro, F., Jabaloy, A., Maldonado, A., Schreider, A.A., 1998. Models of magnetic and Bouguer gravity anomalies for the deep structure of the central Alboran Sea basin. Geo-Mar. Lett. 18, 10-18.

Galindo-Zaldívar, J., Jabaloy, A., Serrano, I., Morales, J., González-Lodeiro, F., Torcal, F., 1999. Recent and present-day stresses in the Granada Basin (Betic Cordilleras): Example of a late Miocene-present-day extensional basin in a convergent plate boundary. Tectonics. 18(4), 686-702.

Galindo-Zaldivar, J., Gil, A.J., Borque, M.J., Gonzalez-Lodeiro, F., Jabaloy, A., Marin-Lechado, C., Ruano, P., Sanz de Galdeano, C., 2003. Active faulting in the internal zones of the central Betic Cordilleras (SE, Spain). J. Geodyn. 36(1), 239-250.

Galindo-Zaldívar, J., Bohoyo, F., Maldonado, A., Schneider, A., Surinach, E., Vázquez, J.T., 2006. Propagating rift during the opening of a small oceanic basin: the Protector Basin (Scotia Arc, Antartica). Earth Planet. Sci. Lett. 241(3), 398-412.

Galindo-Zaldívar, J., Borque, M.J., Pedrera, A., Marín-Lechado, C., Gil, A.J., López-Garrido, A.C., 2013. Deformation behaviour of the low-rate active Balanegra Fault Zone from high-precision levelling (Betic Cordillera, SE Spain). J. Geodyn. 71, 43-51.

Galindo-Zaldivar, J., Gil, A.J., Sanz de Galdeano, C., Lacy, M.C., García-Armenteros, J.A., Ruano, P., Ruiz, A.M., Martinez-Martos, M., Alfaro, P., 2015. Active shallow extension in central and eastern Betic Cordillera from CGPS data. Tectonophysics. 663, 290-301.

Garate, J., Martin-Davila, J., Khazaradze, G., Echeverria, A., Asensio, E., Gil, A.J., de Lacy, M.C., Armenteros, J.A., Ruiz, A.M., Gallastegui, J., Alvarez-Lobato, F., Ayala, C., Rodríguez-Caderot, G., Galindo-Zaldívar, J., Rimi, A., Harnafi, M., 2015. Topo-Iberia project: CGPS crustal velocity field in the Iberian Peninsula and Morocco. GPS Solutions. 19. 287-295.

Garcia, A.F., Zhu, Z., Ku, T.L., Sanz de Galdeano, C., Chadwick, O.A., Montero, J.C., 2003. Tectonically driven landscape development within the eastern Alpujarran Corridor, Betic cordillera, SE Spain (Almeria). Geomorphology. 50(1), 83-110.

Garcia-Castellanos, D., Villaseñor, A., 2011. Messinian salinity crisis regulated by competing tectonics and erosion at the Gibraltar arc. Nature. 480, 359-363.

García-Dueñas, V., Balanyá, J., 1986. Estructura y naturaleza del Arco de Gibraltar. Maleo-Bol. Inf. Soc. Geol. Portugal, 2, 23.

García-Dueñas, V., Martínez-Martínez, J.M., Orozco, M., Soto, J., 1988. Plisnappes, cisillements syn- à post-métamorphiques et cisaillements ductilesfragiles en distension dans les Nevado-Filabrides (Cordillères bétiques, Espagne). C. R. Acad. Sci. Paris. 307, 1389-1395.

García-Dueñas, V., Balanyá, J., Martínez-Martínez, J., 1992. Miocene extensional detachments in the outcropping basement of the Northern Alboran Basin (Betics) and their tectonic implications. Geo-Mar. Lett. 12(2-3), 88-95.

García-Dueñas, V., Banda, E., Torné, M., Córdoba, D., ESCI-Béticas Working Group., 1994. A deep seismic reflection survey across the Betic Chain (southern Spain): First results. Tectonophysics. 232, 77-89.

García-Hernández, M., López-Garrido, A.C., Rivas, P., Sanz de Galdeano, C., Vera, J.A., 1980. Mesozoic palaeogeographic evolution of the external zones of the Betic Cordillera. Neth. J. Geosci. 59, 155-168.

García-Tortosa, F.J., Sanz de Galdeano, C., 2007. Evidencias geomorfológicas de actividad tectónica cuaternaria en el frente montañoso del borde sur de Sierra Nevada: la falla normal de Laujar de Andarax. Cuaternario y geomorfología. Revista de la Sociedad Española de Geomorfología y Asociación Española para el Estudio del Cuaternario. 21(3), 101-112.

García-Tortosa, F.J., Sanz de Galdeano, C., Sánchez-Gómez, M., Alfaro-García, P., 2008. Tectónica reciente en el frente de Cabalgamiento Bético. Las deformaciones de Jimena y Bedmar (Jaén). Geogaceta. (44), 59-62.

Geyh, M.A., Eitel, B., 1998. Radiometric dating of young and old calcrete. Radiocarbon. 40(2), 795-802.

Giaconia, F., Booth-Rea, G., Martínez-Martínez, J.M., Azañón, J.M., Pérez-Peña, J.V., Pérez-Romero, J., Villegas, I., 2012. Geomorphic evidence of active tectonics in the Sierra Alhamilla (eastern Betics, SE Spain). Geomorphology. 145, 90-106.

Gianniou M., Stavropoulou., I., 2016. Estimation of tectonic velocities using GPS Precise Point Positioning: The case of Hellenic RTK network HEPOS. EUREF 2016 Symposium

Gil, A.J., Rodríguez-Caderot, G., Lacy, M., Ruiz, A.M., Sanz de Galdeano, C., Alfaro, P., 2002. Establishment of a non-permanent GPS network to monitor the recent NE-SW deformation in the Granada Basin (Betic Cordillera, Southern Spain). Stud. Geophys. Geod. 46(3), 395-410.

Gill, R.C.O., El Aparicio, A., El Azzouzi, M., Hernandez, J., Thirlwall, M.F., Bourgois, J., Marriner, G.F., 2004. Depleted arc volcanism in the Alborán Sea and shoshonitic volcanism in Morocco: geochemical and isotopic constraints on Neogene tectonic processes. Lithos. 78, 363-388.

Giménez, J., Suriñach, E., Goula, X., 2000. Quantification of vertical movements in the eastern Betics (Spain) by comparing levelling data. Tectonophysics. 317(3), 237-258.

Goff, J.A., Austin, J.A., Fulthorpe, C.S., 2013. Reinterpretation of the Franklin "Shore" in the Mid-Atlantic bight as a paleo-shelf edge. Cont. Shelf Res. 60, 64-69.

González-Castillo, L., 2015, Crustal structure and active deformation in the westernmost Betic Cordillera and its Foreland, Tesis doctoral. Universidad de Granada. 190 pp.

González-Castillo, L., Galindo-Zaldívar, J., Ruiz-Constán, A., Pedrera, A., 2014. Magnetic evidence of a crustal fault affecting a linear laccolith: The Guadiana Fault and the Monchique Alkaline Complex (SW Iberian Peninsula). J. Geodyn. 77, 149-157.

Gonzalez-Castillo, L., Galindo-Zaldivar, J., de Lacy, M.C., Borque, M.J., Martinez-Moreno, F.J., García-Armenteros, J.A., Gil, A.J., 2015a. Active rollback in the Gibraltar Arc: Evidences from CGPS data in the western Betic Cordillera. Tectonophysics. 663, 310-321.

González-Castillo, L., Galindo-Zaldívar, J., Junge, A., Martínez-Moreno, F.J., Löwer, A., Sanz de Galdeano, C., Pedrera, A., López-Garrido, A.C., Ruiz-Constán, A., Ruano, P., Martínez-Martos, M., 2015b. Evidence of a large deep conductive body within the basement of the Guadalquivir foreland Basin (Betic Cordillera, S-Spain) from tipper vector modelling: Tectonic implications. Tectonophysics, 663, 354-363.

Grant, K.M., Rohling, E.J., Bar-Matthews, M., Ayalon, A., Medina-Elizalde, M., Ramsey, C.B., Satow, C., Roberts, A.P., 2012. Rapid coupling between ice volume and polar temperature over the past 150,000 years. Nature. 491(7426), 744-747.

Gregorius, T., 1996. GIPSY OASIS II: How it works. University of Newcastle upon Tyne.

Groupe de Recherche Néotectonique de l'Arc de Gibraltar, 1977. L'histoire tectonique récente (Tortonien à Quaternaire) de l'Arc de Gibraltar et des bordures de la mer d'Alboran. Bull. Soc. Geol. Fr. 19(3), 575-614.

Gueguen E., Doglioni C., Fernandez M., 1997. Lithospheric boudinage in the Western Mediterranean back-arc basins. Terra Nova. 9, 184-187.

Gueguen, E., Doglioni, C., Fernandez, M., 1998. On the post-25 Ma geodynamic evolution of the western Mediterranean. Tectonophysics. 298, 259-269.

Guest, B., Horton, B.K., Axen, G.J., Hassanzadeh, J., McIntosh, W.C., 2007. Middle to late Cenozoic basin evolution in the western Alborz Mountains: Implications for the onset of collisional deformation in northern Iran. Tectonics. 26(6).

Guezou J.C., De Lamotte D.F., Coulon M. y Morel J.C. 1991. Structure and kinematics of the Prebetic nappe complex (southern Spain): definition of a "Betic Floor Thrust" and implications in the Betic-Rif orocline. Annales Tectonicae. 1(5), 32-48.

Gurer, A., Gürer, Ö.F., Pinçe, A., Ilkisik, O.M., 2001. Conductivity structure along the Gediz graben, west Anatolia, Turkey: tectonic implications. Int. Geol. Rev. 43, 1129-1144.

Gurria, E., Mezcua, J., 2000. Seismic tomography of the crust and lithospheric mantle in the Betic Cordillera and Alboran Sea. Tectonophysics. 329, 99-119.

Gutscher, M.A., Malod, J., Rehault, J.P., Contrucci, I., Klingelhoefer, F., Mendes-Victor, L., Spakman, W., 2002. Evidence for active subduction beneath Gibraltar. Geology. 30(12), 1071-1074.

Hager, B.H., King, R.W., Murray, M.H., 1991. Measurement of crustal deformation using the Global Positioning System. Annu. Rev. Earth Planet. Sci. 19, 351-382.

Hatzfeld, D., 1976. Etude sismologique et gravimetrique de la estructure profonde de la mer d´Alborán: Mise n évidence d´un manteau anormal. C. R. Acad. Sci. Paris. 283, 1021-1024

Hermann, J., Rubatto, D., Korsakov, A., Shatsky, V. S., 2001. Multiple zircon growth during fast exhumation of diamondiferous, deeply subducted continental crust (Kokchetav Massif, Kazakhstan). Contrib. Mineral. Petrol. 141(1), 66-82.

Hermes, J.J., 1985. Algunos aspectos de la estructura de la Zona Subbética (Cordilleras Béticas. España meridional). Estudios Geológicos. 41(3-4), 157-176.

Hernández-Molina, F.J., Gracia, F.J., Somoza, L., Rey, J., 1996. Distribución batimétrica de las terrazas submarinas en la plataforma continental de Málaga Gibraltar. Implicaciones eustáticas durante el Cuaternario terminal. Geogaceta. 20(2), 416-419.

Hernández-Molina, F.J., Fernández-Salas, L.M., Lobo, F., Somoza, L., Díaz-del-Río, V., Dias, J.A., 2000. The infralittoral prograding wedge: a new large-scale progradational sedimentary body in shallow marine environments. Geo-Mar. Lett. 20(2), 109-117.

Hinsbergen, D.J., Meulenkamp, J.E., 2006. Neogene supradetachment basin development on Crete (Greece) during exhumation of the South Aegean core complex. Basin Res. 18(1), 103-124.

Hodges, K., Bowring, S., Davidek, K., Hawkins, D., Krol, M., 1998. Evidence for rapid displacement on Himalayan normal faults and the importance of tectonic denudation in the evolution of mountain ranges. Geology. 26, 483-486.

Hoernle, K., Van den Bogaard, P., Duggen, S., Mocek, B. and Garbe Schönberg, D., 1999. Evidence for Miocene subduction beneath the Alborán Sea: 40Ar/39Ar dating and geochemistry of volcanic rocks from Holes 977A and 978A. En: Proc. ODP. Sci. Results. (Zahn, R., Comas, M. C. y Klaus, A., Eds.). College Station, TX (Ocean Drilling Program). 161, 357-373.

Houseman, G.A., McKenzie, D.P., Molnar, P., 1981. Convective instability of a thickened boundary layer and its relevance for the thermal evolution of the continental crust. J. Geophys. Res. 86, 6115-6132.

Hreinsdóttir, S., Freymueller, J.T., Bürgmann, R., Mitchell, J., 2006. Coseismic deformation of the 2002 Denali fault earthquake: insights from GPS measurements. J. Geoph. Res. 111, B3.

IAGA, Working group V-MOD, 2010. International geomagnetic reference field: the eleventh generation. Geophys. J. Int. 183, 1216-1230.

Instituto Geológico y Minero de España, IGME. http://info.igme.es/qafi.

Iribarren, L., Vergés, J., Camurri, F., Fullea, J., Fernandez, M., 2007. The structure of the Atlantic–Mediterranean transition zone from the Alboran Sea to the Horseshoe Abyssal Plain (Iberia–Africa plate boundary). Mar. Geol. 243, 97-119.

Jabaloy, A., Galindo-Zaldívar, J., González-Lodeiro, F., 1992. The Mecina Extensional System: its relation with the post-Aquitanian piggy-back basins and the paleostresses evolution (Betic Cordilleras, Spain). Geo-Mar. Lett. 12(2-3), 96-103.

Jabaloy, A., Galindo-Zaldivar, J., González-Lodeiro, F., 1993. The Alpujárride-Nevado-Fibábride extensional shear zone, Betic Cordillera, SE Spain. J. Struct. Geol. 15, 555-569.

Jabaloy-Sánchez, A., Gómez-Pugnaire, M.T., Padrón-Navarta, J.A., Sánchez-Vizcaíno, V. L., Garrido, C.J., 2015. Subduction-and exhumation-related structures preserved in metaserpentinites and associated metasediments from the Nevado–Filábride Complex (Betic Cordillera, SE Spain). Tectonophysics. 644, 40-57.

Jacobs, J., Thomas, R.J., 2004. Himalayan-type indenter-escape tectonics model for the southern part of the late Neoproterozoic–early Paleozoic East African–Antarctic orogen. Geology. 32, 721-724.

Johnson, C., Harbury, N., Hurford A.J., 1997, The role of extension in the Miocene denudation of the Nevado-Filábride Complex, Betic Cordillera (SE Spain), Tectonics. 16, 189-204.

Jolivet, L., Goffé, B., Monié, P., Truffert-Luxey, C., Patriat, M., Bonneau, M., 1996. Miocene detachment in Crete and exhumation P-T-t paths of high-pressure metamorphic rocks. Tectonics. 15(6), 1129-1153.

Julivert, M., Fontboté, J. M., Ribeiro, A., Conde, L., 1974. Mapa tectónico de la península Ibérica y Baleares. E. 1:1.000.000. Memoria Explicativa. IGME, Madrid. 113 págs.

Kane, M.F., 1962. A comprehensive system of terrain corrections using a digital computer. Geophysics. 27, 455-462.

Keller, E.A., Pinter, N., 1996. Active tectonics (Vol. 1338). Upper Seddle River, NJ, USA: Prentice Hall.

Kelsey, H.M., 1990. Late Quaternary deformation of marine terraces on the Cascadia subduction zone near Cape Blanco, Oregon. Tectonics. 9(5), 983-1014.

Kleverlaan, K., 1987. Gordo megabed: a possible seismite in a Tortonian submarine fan, Tabernas basin, Province Almeria, southeast Spain. Sediment. Geol. 51, 165-180.

Kleverlaan, K., 1989. Three distinctive feeder-lobe systems within one time slice of the Tortonian Tabernas fan, SE Spain. Sedimentology. 36(1), 25-45.

Kouba, J., 2005. A possible detection of the 26 December 2004 great Sumatra-Andaman Islands earthquake with solution products of the international GNSS service. Stud. Geophys. Geod. 49, 463-483.

Koulali, A., Ouazar, D., Tahayt, A., King, R.W., Vernant, P., Reilinger, R.E., McClusky, S., Mourabit, T., Davila, J.M., Amraoui, N., 2011. New GPS constraints on active deformation along the Africa–Iberia plate boundary. Earth Planet. Sci. Lett. 308(1), 211-217.

Lagares, F., 2008. Relevés de profils bathymétriques en Croatie du Nord: indices de pauses holocènes du niveau marin. C. R. Geosci. 340(1), 49-56.

Lario, J., Zazo, C., Somoza, L., Goy, J.L., Hoyos, M., Silva, P.G., Hernández-Molina, F.J., 1993. Los episodios marinos cuaternarios de la costa de Málaga (España). Rev. Soc. Geol. España. 6(3-4), 41-46.

Lario, J., Zazo, C., Goy, J.L., 1999. Fases de progradación y evolución morfosedimentaria de la flecha litoral de Calahonda (Granada) durante el Holoceno. Estudios Geológicos, 55(5-6), 247-250.

Larson, K.M., Lowry, A.R., Kostoglodov, V., Hutton, W., Sánchez O., Hudnut, K., Suárez, G., 2004. Crustal deformation measurements in Guerrero, Mexico. J. Geoph. Res. 109, 1-19.

Leblanc, D., Olivier, P., 1984. Role of strike-slip faults in the Betic-Rifian orogeny. Tectonophysics. 101, 345-355.

Lhénaff, R., 1965. Néotectonique quaternaire sur le bord occidental de la Sierra Nevada (province de Grenade, Espagne). Revue de Géographie Physique et de Géologie Dynamique. 2 (VII/3), 205-207.

Li, Q., Ruano, P., Pedrera Parias, A., Galindo Zaldívar, J., 2012. Estructura de la cuenca sedimentaria de Tabernas-Sorbas mediante prospección gravimétrica y magnética (Zonas Internas, Cordillera Bética Oriental). Geogaceta. 52, 117-120.

Loke, M.H., 2014. Tutorial: 2-D and 3-D Electrical Imaging Surveys. Geotomo Software Company.

Lonergan, L., Platt, J., 1995. The Malaguide-Alpujarride boundary: a major extensional contact in the Intenal Zone of the eastern Betic Cordillera, SE Spain. J. Struct. Geol. 17, 1665-1671.

Lonergan, L., White, N., 1997. Origin of the Betic-Rif mountain belt. Tectonics. 16(3), 504-522.

Loomis, T.P., 1975. Tertiary mantle diapirism, orogeny and plate tectonics east of the Strait of Gibraltar. Am. J. Sci. 275, 1-33.

López Sánchez-Vizcaíno, V., Rubatto, D., Gómez-Pugnaire, M. T., Trommsdorff, V., Müntener, O., 2001. Middle Miocene high-pressure metamorphism and fast exhumation of the Nevado-Filábride Complex, SE Spain. Terra Nova. 13(5), 327-332.

López-Garrido, A.C., 1971. Geología de la Zona Prebética, al NE de la Provincia de Jaén. Unpubl. doctoral disertation, Universidad de Granada, Granada, 317 pp.

Luján, M., Storti, F., Balanyá, J. C., Crespo-Blanc, A., F. Rossetti, 2003. Role of decollement material with different rheological properties in the structure of the Aljibe thrust imbricate (Flysch Trough, Gibraltar Arc): an analogue modelling approach. J. Struc. Geol. 25, 867-881.

Lyard, F., Lefevre, F., Letellier, T., Francis, O., 2006. Modelling the global ocean tides: modern insights from FES2004. Ocean Dyn. 56, 394-415.

Mancilla, FdL., Stich, D., Berrocoso, M., Martín, R., Morales, J., Fernandez-Ros, A., Páez, R., Pérez-Peña, A., 2013. Delamination in the Betic Range: Deep structure, seismicity, and GPS motion. Geology. 41, 307-310.

Marín-Lechado, C., Galindo-Zaldivar, J., Rodriguez-Fernandez, L.R., Serrano, I., Pedrera, A., 2005. Active faults, seismicity and stresses in an internal boundary of a tectonic arc (Campo de Dalias and Nijar, southeastern Betic Cordilleras, Spain). Tectonophysics. 396(1), 81-96.

Marín-Lechado, C., Galindo-Zaldivar, J., Rodríguez-Fernández, L.R., Pedrera A., 2006. Mountain front development by folding and crustal thickening in the Internal Zone of the Betic Cordillera-Alboran Sea Boundary. Pure Appl. Geophys. 164, 1-21.

Marín-Lechado, C., Galindo-Zaldívar, J., Rodríguez-Fernández, L.R., Pedrera, A., 2007. Mountain front development by folding and crustal thickening in the Internal Zone of the Betic Cordillera-Alboran Sea boundary. Pure Appl. Geophys. 164(1), 1-21.

Marin-Lechado, C., Galindo-Zaldívar, J., Gil, A.J., Borque, M.J., De Lacy, M.C., Pedrera, A., López-Garrido, A.C., Alfaro, P., García-Tortosa, F., Ramos, M.I., Rodríguez-Calderot, G., Rodríguez-Fernández, J., Ruiz-Constán, A., Sanz de Galdeano, C., 2010. Leveling profiles and a GPS network to monitor the active folding deformation in the Campo de Dalías (Betic Cordillera, Southeastern Spain). Sensors. 10(4), 3504-3518.

Mart, Y., Belknap, D.F., 1991. Origin of late Pleistocene submerged marine terraces on the outer continental shelf, northern Israel. Geo-Mar. Lett. 11(2), 66-70.

Martí. A., 2006. A magnetotelluric investigation of geoelectrica dimensionality and study of the Central Betic crustral structure. Ph. D. Thesis. University of Barcelona. 307 pp.

Martí, A., Queralt, P., Roca, E., Ledo, J., Galindo-Zaldívar, J., 2009. Geodynamic implications for the formation of the Betic-Rif orogen from magnetotelluric studies. J. Geophys. Res. Solid Earth (1978–2012) 114 (B1).

Martín, J., Braga, J.C., 1994. Messinian events in the Sorbas Basin in southeastern Spain and their implications in the recent history of the Mediterranean. Sediment. Geol. 90, 257-268.

Martín, J.M., Braga, J.C., Aguirre, J., Puga-Bernabéu, A., 2009. History and evolution of the North-Betic Strait (Prebetic Zone, Betic Cordillera): a narrow, early Tortonian, tidal-dominated, Atlantic–Mediterranean marine passage. Sediment. Geol. 216(3), 80-90.

Martín-Algarra, A., Mazzoli, S., Perrone, V., Rodríguez-Cañero, R., Navas-Parejo, P., 2009. Variscan tectonics in the Malaguide Complex (Betic Cordillera, southern Spain): stratigraphic and structural Alpine versus pre-Alpine constraints from the Ardales area (Province of Malaga). I. Stratigraphy. The Journal of geology. 117, 241-262.

Martínez-Díaz, J.J., 2000. Actividad neotectónica en el sureste de Almería y su incidencia en la morfotectónica de la zona (Cordilleras Béticas). Rev. Soc. Geol. España. 13(3-4), 417-429.

Martínez-Díaz, J.J., Hernández-Enrile, J., 2004. Neotectonics and morphotectonics of the southern Almería region (Betic Cordillera-Spain) kinematic implications. Int. J. Earth Sci. 93, 189-206.

Martínez-Martínez, J.M., 2006. Lateral interaction between metamorphic core complexes and less-extended, tilt-block domains: the Alpujarras strike-slip transfer fault zone (Betics, SE Spain). J. Struct. Geol. 28(4), 602-620.

Martínez-Martínez, J.M., Azañón, J.M., 1997. Mode of extensional tectonics in the southeastern Betics (SE Spain). Implications for the tectonic evolution of the peri-Alborán orogenic system. Tectonics. 16, 205-225.

Martínez-Martínez, J.M., Soto, J.I., Balanyá, J.C., 1997. Large scale structures in the Nevado-Filabride Complex and crustal seismic fabrics of the deep seismic reflection profile ESCIBéticas 2. Rev .Soc. Geol. Esp. 8, 477-489.

Martínez-Martínez, J.M., Soto, J.I., Balanyá, J.C., 2004. Elongated domes in extended orogens: A mode of mountain uplift in the Betics (southeast Spain). Geol. Soc. Am. Spec. Paper. 380, 243-265.

Martínez-Martínez, J.M., Booth-Rea, G., Azañón, J.M., Torcal, F., 2006. Active transfer fault zone linking a segmented extensional system (Betics, southern Spain): Insight into heterogeneous extension driven by edge delamination. Tectonophysics. 422(1), 159-173.

Martínez-Moreno, F.J., Pedrera, A., Ruano, P., Galindo-Zaldívar, J., Martos-Rosillo, S., González-Castillo, L., Sánchez-Úbeda, J.P., Marín-Lechado, C., 2013. Combined microgravity, electrical resistivity tomography and induced polarization to detect deeply buried caves: Algaidilla cave (Southern Spain). Eng. Geol. 162, 67-78.

Martínez-Moreno, F.J., Galindo-Zaldívar, J., Pedrera, A., Teixidó, T., Peña, J.A. González-Castillo, L., 2015. Regional and residual anomaly separation in microgravity maps for cave detection: The case study of Gruta de las Maravillas (SW Spain). J. Appl. Geophys. 114, 1-11.

Martínez-Moreno, F.J., Galindo-Zaldívar, J., González-Castillo, L., Azañón, J.M., 2016. Collapse susceptibility map in abandoned mining areas by microgravity survey: A case study in Candado hill (Málaga, southern Spain). J. Appl. Geophys. 130, 101-109.

Martín-Penela, A., 1988. Los grandes mamíferos del yacimiento Achelense de la Solana del Zamborino, Fonelas (Granada, España). Antropología y Paleoecología humana. 5, 29-187.

Masana, E., Martinez-Diaz, J.J., Santanach, P., Hernandez-Enrile, J.L., 2004. The Alhama de Murcia Fault (SE Spain), a seismogenic fault in a diffuse plate boundary. Seis-motectonic implications for the Iberomagrebian region. J. Geophys. Res. 109, B01301.

Masselink, G., Hughes, M., 2003. Introduction to coastal processes and geomorphology. 368p. Hodder Education Publishers, London, UK.

Mazzoli, S., Helman, M.L., 1994. Neogene patterns of relative plate motion for Africa-Europe: some implications for recent central Mediterranean tectonics. Neth. J. Geosci. 83, 464-468.

McDermott, J.A., Hodges, K.V., Whipple, K.X., Van Soest, M.C., Hurtado Jr, J.M., 2015. Evidence for Pleistocene low-angle normal faulting in the Annapurna-Dhaulagiri Region, Nepal. The Journal of Geology 123, 133-151.

Meijninger, B.M.L., 2006. Late-orogenic extension and strike-slip deformation in the Neogene of southeastern Spain. PhD Thesis, Universiteit Utrecht. Geologica Ultraiectina. 269, 179 pp.

Merritts, D., Bull, W.B., 1989. Interpreting Quaternary uplift rates at the Mendocino triple junction, northern California, from uplifted marine terraces. Geology. 17(11), 1020-1024.

Monie, P., Galindo-Zaldivar, J., González-Lodeiro, F., Goffe, B., Jabaloy, A., 1991. Ar-40/Ar-39 geochronology of alpine tectonism in the Betic Cordilleras (Southern Spain). Journal of the Geological Society 148, 289-297.

Monié, P., Torres-Roldan, R.L., García-Casco, A., 1994. Cooling and exhumation of the Western Betic Cordilleras, 40Ar/39Ar thermochronological constraints on a collapsed terrane. Tectonophysics. 238, 353-379.

Mora, M., 1993. Tectonic and sedimentary analysis of the Huércal-Overa region, SE Spain, Betic Cordillera, PhD Thesis, Oxford Univ., Oxford, England, p. 300.

Morales, J., Serrano, I., Vidal, F., Torcal, F., 1997. The depth of the earthquake activity in the Central Betics (Southern Spain). Geophys. Res. Lett. 24(24), 3289-3292.

Morales, J., Serrano, I., Jabaloy, A., Galindo-Zaldivar, J., Zhao, D., Torcal, F., Vidal, F., Gonzalez-Lodeiro, F., 1999. Active continental subduction beneath the Betic Cordillera and the Alboran Sea. Geology. 27(8), 735-738.

Morales, J., Azañón, J.M., Stich, D., Roldán, F.J., Pérez-Peña, J.V., Martín, R., Cantavella, J.V., Martín, J.B., Mancilla, FdL., González-Ramón, A., 2015. The 2012–2013 earthquake swarm in the Eastern Guadalquivir basin (South Spain): A case of heterogeneous faulting due to oroclinal bending. Gondwana Res. 28(4), 1566-1578.

Morley, C.K., 1993. Discussion of Origins of Hinterland Basins to the RIF-Betic Cordillera and Carpathians. Tectonophysics. 226, 359-376.

Muhs, D.R., Kelsey, H.M., Miller, G.H., Kennedy, G.L., Whelan, J.F., McInelly, G.W., 1990. Age estimates and uplift rates for late pleistocene marine terraces' Southern Oregon portion of the Cascadia forearc. J. Geophys. Res. 95, 6685-6698.

Müller, P.D., Roest, W.R., 1992. Fracture Zones in the North Atlantic from Combined Geosat and Seasat Data. J. Geophys. Res. 97, 3337-3350.

Nagy, D., 1966. The gravitational attraction of a right rectangular prism. Geophysics. 31, 362-371.

National Geographical Service of Spain, IGN. http://centrodedescargas.cnig.es/CentroDescargas/index.jsp.

National Geographical Service of Spain, IGN. www.ign.es/ign/none/gravimetriaResena.do?indice=6.

National Geographical Service of Spain, IGN., 1976. Mapa de anomalías de Bouguer. Escala 1:500000. IGN, Madrid.

Nocquet, J.M., 2012. Present-day kinematics of the Mediterranean: A comprehensive overview of GPS results. Tectonophysics. 579, 220-242.

Oldenburg, D. W., & Li, Y., 1999. Estimating depth of investigation in DC resistivity and IP surveys. Geophysics. 64(2), 403-416.

Ortega-Sánchez, M., Lobo, F.J., López-Ruiz, A., Losada, M.A., Fernández-Salas, L.M., 2014. The influence of shelf-indenting canyons and infralittoral prograding wedges on coastal morphology: The Carchuna system in Southern Spain. Mar. Geol. 347, 107-122.

Parker, R.L., Booker, J.R., 1996. Optimal one-dimensional inversion and bounding of magnetotelluric apparent resistivity and phase measurements. Phys. Earth Planet. Inter. 98(3), 269-282.

Passaro, S., Milano, G., Sprovieri, M., Ruggieri, S., Marsella, E., 2011. Quaternary still-stand landforms and relations with flank instability events of the Palinuro Bank (southeastern Tyrrhenian Sea). Quat. Int. 232(1), 228-237.

Pedley, R.C., Busby, J.P., Dabek, Z.K., 1993. GRAVMAG user manual–interactive 2.5 D gravity and magnetic modelling. British Geological Survey, Technical Report WK/93/26/R. 73.

Pedrera, A., Marín-Lechado, C., Galindo-Zaldivar, J., Rodríguez-Fernández, L.R., Ruiz-Constán, A., 2006. Fault and fold interaction during the development of the Neogene-Quaternary Almería-Níjar basin (SE Betic Cordilleras). Geological Society, London, Special Publications. 262, 217-230.

Pedrera, A., Galindo-Zaldívar, J., Sanz de Galdeano, C., López-Garrido, A.C., 2007. Fold and fault interactions during the development of an elongated narrow basin: The Almanzora Neogene-Quaternary Corridor (SE Betic Cordillera, Spain). Tectonics. 26.

Pedrera, A., Galindo-Zaldívar, J., Ruiz-Constán, A., Duque, C., Marín-Lechado, C., Serrano, I., 2009a. Recent large fold nucleation in the upper crust: Insight from gravity, magnetic, magnetotelluric and seismicity data (Sierra de Los Filabres–Sierra de Las Estancias, Internal Zones, Betic Cordillera). Tectonophysics. 463, 145-160.

Pedrera, A., Pérez-Peña, J.V., Galindo-Zaldívar, J., Azañón, J.M., Azor, A., 2009b. Testing the sensitivity of geomorphic indices in areas of low-rate active folding (eastern Betic Cordillera, Spain). Geomorphology. 105(3), 218-231.

Pedrera, A., Ruiz-Constán, A., Galindo-Zaldívar, J., Chalouan, A., Sanz de Galdeano, C., Marín-Lechado, C., Ruano, P., Benmakhlouf, M., Akil, M., López-Garrido, A.C., Chabli, A., Ahmamou, M., González-Castillo, L., 2011. Is there an active subduction beneath the Gibraltar orogenic arc? Constraints from Pliocene to present-day stress field. J. Geodyn. 52(2), 83-96.

Pedrera, A., Galindo-Zaldivar, J., Marin-Lechado, C., Garcia-Tortosa, F.J., Ruano, P., Lopez-Garrido, A.C., Azañon, J.M., Pelaez, J.A., Giaconia, F., 2012. Recent and active faults and folds in the central-eastern Internal Zones of the Betic Cordillera. Journal of Iberian Geology 38, 191-208.

Pedrera, A., Ruiz-Constán, A., Marín-Lechado, C., Galindo-Zaldívar, J., González, A., Peláez, J.A., 2013. Seismic transpressive basement faults and monocline development in a foreland basin (Eastern Guadalquivir, SE Spain). Tectonics. 32(6), 1571-1586.

Pedrera, A., Marín-Lechado, C., Galindo-Zaldívar, J., Lobo, F.J., 2015. Smooth folds favoring gypsum precipitation in the Messinian Poniente marginal basin (Western Mediterranean). Tectonophysics. 663, 48-61.

Perconig, E., 1962. Sur la constitution géologique de l'Andalousie occidentale en particulier du bassin du Guadalquivir (Espagne méridionale). Mémoires hors-Série de la Société Géologique de France. pp. 145-161.

Pérez-López, A., Sanz de Galdeano, C., 1994. Tectónica de los materiales triásicos en el sector central de la Zona Subbética (Cordillera Bética). Rev. Soc. Geol. España. 7(1-2), 141-153.

Pérez-Peña, A., Martín-Davila, J., Gárate, J., Berrocoso, M., Buforn, E., 2010a. Velocity field and tectonic strain in Southern Spain and surrounding areas derived from GPS episodic measurements. J. Geodyn. 49(3), 232-240.

Pérez-Peña, J.V., Azor, A., Azañón, J.M., Keller, E.A., 2010b. Active tectonics in the Sierra Nevada (Betic Cordillera, SE Spain): insights from geomorphic indexes and drainage pattern analysis. Geomorphology. 119, 74-87.

Pérouse, E., Vernant, P., Chéry, J., Reilinger, R., McClusky, S., 2010. Active surface deformation and sub-lithospheric processes in the western Mediterranean constrained by numerical models. Geology. 38, 823-826.

Peyre, Y., 1974. Géologie d'Antequera et de sa Région (Cordilleres détiques-Espagne). Ph.D. Thesis, Inst. Agr. Of Paris, 250 pp.

Pirazzoli, P.A., 2005. Marine terraces. In: M. Schwartz (Ed.), Encyclopedia of Coastal Science. Springer Nederlands.

Pirazzoli, P.A., Stiros, S.C., Fontugne, M., Arnold, M., 2004. Holocene and Quaternary uplift in the central part of the southern coast of the Corinth Gulf (Greece). Mar. Geol. 212(1), 35-44.

Platt, J.P., 1986. Dynamics of orogenic wedges and the uplift of high-pressure metamorphic rocks. Geol. Soc. Am. Bull. 97(9), 1037-1053.

Platt, J.P., Vissers, R.L.M., 1989. Extensional collapse of thickened continental lithosphere: A working hypothesis for the Alboran Sea and Gibraltar arc. Geology, 17(6), 540-543.

Platt, J.P, Allerton, S., Kirker, A., Mandeville, C., Mayfield, A., Platzman, E., Rimi, A., 2003. The ultimate arc: Differential displacement, oroclinal bending, and vertical axis rotation in the External Betic-Rif arc. Tectonics. 22.

Platt, J.P., Kelley, S.P., Carter, A., Orozco, M., 2005. Timing of tectonic events in the Alpujárride Complex, Betic Cordillera, southern Spain. Journal of the Geological Society, London. 162, 2005, pp. 1-12.

Platt, J.P., Anczkiewicz, R., Soto, J.I., Kelley, S. P., Thirlwall, M., 2006. Early Miocene continental subduction and rapid exhumation in the western Mediterranean. Geology. 34, 11981-984.

Polyak, B.G., Fernández ,M., Khutorskoy, M.D., Soto, J.I., Basov, I.A., Comas, M.C., Khain, V.E., Alonso, B., Agapova, G.V., Mazurova, I.S., Negredo, A., Tochitsky, V.O., de la Linde, J., Bogdanov, N.A., Banda, E., 1996. Heat flow in the Alboran Sea, western Mediterranean. Tectonophysics. 263, 191-218.

Potts, A.J., Midgley, J.J., Harris, C., 2009. Stable isotope and 14 C study of biogenic calcrete in a termite mound, Western Cape, South Africa, and its palaeoenvironmental significance. Quat. Res. 72(2), 258-264.

Poujol, A., Ritz, J.F., Tahayt, A., Vernant, P., Condomines, M., Blard, P.H., Billant, J., Vacher, L., Tibari, B., Hni, L., Idrissi, A.K., 2014. Active tectonics of the Northern Rif (Morocco) from geomorphic and geochronological data. J. Geodyn. 77, 70-88.

Pous, J., Queralt, P., Leo, J., Roca, E., 1999. A high electrical conductive zone at lower crustal depth beneath the Betic Chain (Spain). Earth Planet. Sci. Lett. 167, 35-45.

Rayan, A., Fernandes, R.M.S., Khalil, H.A., Mahmoud, S., Miranda, J.M., Tealab, A., 2010. Evaluation of the crustal deformations in the northern region of Lake Nasser (Egypt) derived from 8 years of GPS campaign observations. J. Geodyn. 49, 210-215.

Real Instituto y Observatorio de la Armada (Spain). http://www.intermagnet.org/data-donnee/dataplot-eng.php?type=hdz.

Reicherter, K.R., Jabaloy, A., Galindo-Zaldívar, J., Ruano, P., 1999. Active faults in the Granada Depression and Zafarraya areas (Betic Cordilleras). Geogaceta. 27, 193-196.

Reicherter, K.R, Jabaloy, A., Galindo-Zaldívar, J., Ruano, P., Becker-Heidmann, P., Morales, J., Reiss, S., González-Lodeiro, F., 2003. Repeated palaeoseismic activity of the Ventas de Zafarraya Fault (S Spain) and its relation with the 1884 Andalusian earthquake. Int. J. Earth Sci. 92(6), 912-922.

Reis, A.T., Maia, R.M.C., Silva, C.G., Rabineau, M., Guerra, J.V., Gorini, C., Ayres, A., Arantes-Oliveira, R., Benabdellouahed, M., Simões, I., Tardin, R., 2013. Origin of step-like and lobate seafloor features along the continental shelf off Rio de Janeiro State, Santos basin-Brazil. Geomorphology. 203, 25-45.

Reynolds, S.J., Spencer, J.E., 1985. Evidence for large-scale transport on the Bullard detachment fault, west-central Arizona. Geology. 13(5), 353-356.

Ring, U., Brachert, T., Fassoulas, C., 2001. Middle Miocene graben development in Crete and its possible relation to large-scale detachment faults in the southern Aegean. Terra Nova. 13(4), 297-304.

Robinson, E.S., Çoruh, C., 1988. Basic Exploration Geophysics. Wiley, New York.

Rodríguez-Fernández, J., Sanz de Galdeano, C., 2006. Late orogenic intramontane basin development: the Granada basin, Betics (southern Spain). Basin Res. 18(1), 85-102.

Rodríguez Fernández, J., Sanz de Galdeano, C., Serrano, F., 1990. Le couloir des Alpujarras. In: Montenat, C. (Ed.), Les bassins Néogènes du Domaine Bétique Oriental (Espagne), Doc. Trav. IGAL 12-13, Paris, pp. 87-100.

Rodríguez-Fernández, J., Roldán, F.J., Azañón, J.M., García-Cortés, A., 2013. El colapso gravitacional del frente orogénico alpino en el Dominio Subbético durante el Mioceno medio-superior: El Complejo Extensional Subbético. Bol. Geol. Min. de España, 124, 477-504.

Rohling, E.J., Grant, K., Bolshaw, M., Roberts, A.P., Siddall, M., Hemleben, C., Kucera, M., 2009. Antarctic temperature and global sea level closely coupled over the past five glacial cycles. Nat. Geosci. 2(7), 500.

Roldán-García, F.J., 1994. Evolución neógena de la cuenca del Guadalquivir. Ph.D. Thesis, Univ. Granada, 260 pp.

Roldán-García, F.J., Rodríguez Fernández, J., Azañón, J.M., 2012. La Unidad Olistostrómica, una formación clave para entender la historia neógena de las Zonas Externas de la Cordillera Bética. Geogaceta. 52, 103-106.

Roldán-García, F.J., Azañón, J.M., Rodríguez Fernández, J., Mateos, R.M., 2013. Fallas ciegas de carácter transtensivo en la Cuenca del Guadalquivir: posible origen del enjambre sísmico de Torreperogil (Octubre 2012-Enero 2013). Geogaceta. (54), 83-86.

Rosell, O., Martí, A., Marcuello, A., Ledo, J., Queralt, P., Roca, E., Campanyà, J., 2011. Deep electrical resistivity structure of the northern Gibraltar Arc (western Mediterranean): evidence of lithospheric slab break-off. Terra Nova. 23, 179-186.

Rosenbaum, G., Lister, G.S., 2004. Formation of arcuate orogenic belts in the western Mediterranean region. Geol. Soc. Am. Special Papers. 383, 41-56.

Rosenbaum, G., Lister, G.S., Duboz, C., 2002. Relative motions of Africa, Iberia and Europe during Alpine orogeny. Tectonophysics. 359(1), 117-129.

Rostami, K., Peltier, W.R., Mangini, A., 2000. Quaternary marine terraces, sea-level changes and uplift history of Patagonia, Argentina: comparisons with predictions of the ICE-4G (VM2) model of the global process of glacial isostatic adjustment. Quat. Sci. Rev. 19(14), 1495-1525.

Rovere, A., Vacchi, M., Firpo, M., Carobene, L., 2011. Underwater geomorphology of the rocky coastal tracts between Finale Ligure and Vado Ligure (western Liguria, NW Mediterranean Sea). Quat. Int. 232(1), 187-200.

Royden, L.H., 1993. Evolution of retreating subduction boundaries formed during continental collision. Tectonics. 12(3), 629-638.

Ruano, P., 2003, Estructuras tectónicas recientes en la transversal central de las Cordilleras Béticas, Tesis doctoral. Universidad de Granada. 446 pp.

Ruano, P., Galindo-Zaldívar, J., Jabaloy, A., 2004. Recent Tectonic Structures in a Transect of the Central Betic Cordillera. Pure Appl. Geophys. 161, 541-563.

Ruegg, G.J.H., 1964. Geologische onderzoekingen in het bekken van Sorbas, S Spanje. Amsterdam Geological Institut, University of Amsterdam.

Ruiz, A.M., Ferhat, G., Alfaro, P., Sanz de Galdeano, C., Lacy, M.C., Rodrıguez-Caderot, G., Gil, A.J., 2003. Geodetic measurements of crustal deformation on NW–SE faults of the Betic Cordillera, southern Spain, 1999–2001. J. Geodyn. 35(3), 259-272.

Ruiz-Constán, A., Galindo-Zaldivar, J., Pedrera, A., Arzate, J.A., Pous, J., Anahnah, F., Heise, W., Santos, F.A.M., Marín-Lechado, C., 2010. Deep deformation pattern from electrical anisotropy in an arched orogen (Betic Cordillera, western Mediterranean). Geology. 38, 731-734.

Ruiz-Constán, A., Galindo-Zaldívar, J., Pedrera, A., Célérier, B., Marín-Lechado, C., 2011. Stress distribution at the transition from subduction to continental collision (northwestern and central Betic Cordillera). Geochem. Geophys. Geosyst. 12(12), Q12002.

Ruiz-Constán, A., Pedrera, A., Galindo-Zaldivar, J., Pous, J., Arzate, J., Roldán-García, F.J., Marín-Lechado, J., Anahnah, F., 2012. Constraints on the frontal crustal structure of a continental collision from an integrated geophysical research: The central-western Betic Cordillera (SW Spain). Geochem. Geophys. Geosyst. 13.

Ruiz-Constán, A., Galindo Zaldívar, J., Andrés Martínez, M., Martínez Martos, M., Pedrera Parias, A., 2013. Estructura de la Cuenca de Ugíjar a partir de datos gravimétricos y magnéticos (Zonas Internas, Cordillera Bética Central). Geogaceta. 54, 95-98.

Sánchez Alzola, A., Borque Arancón, M.J., Martín Rojas, I., García Tortosa, F.J., Alfaro García, P., Estévez Rubio, A., Molina Palacios, S., Rodríguez-Caderot, G., Lacy, M.C., García-Armenteros, J.A., 2014b. Tasas de deformación GPS en la cuenca del Bajo Segura (Cordillera Bética oriental). Geogaceta. 56, 3-6.

Sánchez-Alzola, A., Sánchez, C., Giménez, J., Alfaro, P., Gelabert, B., Borque, M.J., Gil, A.J., 2014a. Crustal velocity and strain rate fields in the Balearic Islands based on continuous GPS time series from the XGAIB network (2010–2013). J. Geodyn. 82, 78-86.

Sanli, D.U., Coban, K., Akarsu, V., Arslan, E., 2012. Effect of Span of GPS Campaigns on Estimated Static Positioning Velocities. Geophysical Research Abstracts. 14, 2012 EGU General Assembly

Santanach, P., Sanz de Galdeano, C., Bousquet, J., 1980. Neotectónica de las regiones mediterráneas de España (Cataluña y Cordilleras Béticas). Bol. Geol. Min. 91, 417-440.

Sanz de Galdeano, C., 1983. Los accidentes y fracturas principales de las Cordilleras Béticas. Estudios geológicos. 39, 157-165.

Sanz de Galdeano, C., 1986. Las fallas de desgarre del borde Sur de la cuenca de Sorbas-Tabernas (Norte de Sierra Alhamilla, Almería, Cordilleras Béticas). Bol. Geol. Min. 100, 73-85.

Sanz de Galdeano, C., 1989. Las fallas de desgarre del borde Sur de la cuenca de Sorbas-Tabernas (norte de Sierra Alhamilla, Almería, Cordilleras Béticas). Bol. Geol. Min. 100(1), 73-85.

Sanz de Galdeano, C., 1990. Geologic evolution of the Betic Cordilleras in the Western Mediterranean, Miocene to the present. Tectonophysics. 172(1-2), 107-119.

Sanz de Galdeano, C., 1996a. The E-W segments of the contact between the external and internal zones of the Betic and Rif cordilleras and the E-W corridors of the internal zone (a combined explanation). Estudios Geologicos. 52(3-4), 123-136.

Sanz de Galdeano, C., 1996b. Neotectónica y Tectónica Activa en el sector de Padul-Dúrcal (Borde SW de Sierra Nevada, España). 1 Conf. Int. Sierra Nevada, Granada, 219–231.

Sanz de Galdeano, C., 2006. Formas de erosión marinas en el sector comprendido entre Maro y Castell de Ferro (costa de Málaga y Granada). Geogaceta. 39, 139-142.

Sanz de Galdeano, C., Vera, J.A., 1991. Una propuesta de clasificación de las cuencas neógenas béticas. Acta geológica hispánica. 26, 205-227.

Sanz de Galdeano, C., Vera, J.A., 1992. Stratigraphic record and palaeogeographical context of the Neogene basins in the Betic Cordillera, Spain. Basin. Res. 4, 21-36.

Sanz de Galdeano, C., Alfaro, P., 2004. Tectonic significance of the present relief of the Betic Cordillera. Geomorphology. 63(3), 175-190.

Sanz de Galdeano, C., Rodriguez-Fernandez, J., López-Garrido, A.C., 1985. A strike-slip fault corridor within the Alpujarra Mountains (Betic Cordilleras, Spain). Geol. Rundsch. 74(3), 641-655.

Sanz de Galdeano, C., López-Casado, C., Delgado, J., Peinado, M.A., 1995. Shallow seismicity and active faults in the Betic Cordillera. A preliminary approach to seismic sources associated with specific faults. Tectonophysics. 248(3-4), 293-302.

Sanz de Galdeano, C., Montilla, J.P., Lopez-Casado, C., 2003. Seismic potential of the main active faults in the Granada Basin (southern Spain). Pure Appl. Geophys. 160, 1537-1556.

Sanz de Galdeano, C., Galindo-Zaldívar, J., López-Garrido, A.C., Alfaro, P., Pérez-Valera, F., Pérez-López, A., García-Tortosa, F.J. 2006. La falla de Tíscar: su significado en la terminación sudoeste del arco Prebético. Rev. Soc. Geol. España. 19, 271-280.

Sanz de Galdeano, C., Galindo-Zaldivar, J., Morales, S., López-Chicano, M., Azañón, J.M., Martín-Rosales, W., 2008. Travertinos ligados a fallas: ejemplos del desierto de Tabernas (Almería, Cordillera Bética). Geogaceta. 45, 31-34.

Sanz de Galdeano, C., Shanov, S., Galindo-Zaldívar, J., Radulov, A., Nikolov, G., 2010. A new tectonic discontinuity in the Betic Cordillera deduced from active tectonics and seismicity in the Tabernas Basin. J. Geodyn. 50(2), 57-66.

Sanz de Galdeano, C., García-Tortosa, F.J., Peláez, J. A., Alfaro, P., Azañón, J.M., Galindo-Zaldívar, J., López-Casado, C., López-Garrido, A.C., Rodríguez-Fernández, J., Ruano, P., 2012. Main active faults in the Granada and Guadix-Baza Basins (Betic Cordillera). Journal of Iberian Geology. 38, 209-223.

Sanz de Galdeano, C., García-Tortosa, F.J., Peláez, J.A., 2013. Estructura del Prebético de Jaén (sector de Bedmar). Su relación con el avance del Subbético y con las fallas en el basamento. Rev. Soc. Geol. España. 26(1), 55-68.

Schattner, U., Lazar, M., Tibor, G., Ben-Avraham, Z., Makovsky, Y., 2010. Filling up the shelf—A sedimentary response to the last post-glacial sea rise. Mar. Geol. 278(1), 165-176.

Seber, D., Barazangi, M., Ibenbrahim, A., Demnati, A., 1996. Geophysical evidence for lithospheric delamination beneath the Alboran Sea and Rif-Betic mountains. Nature. 379, 785-790.

Serpelloni, E., Vannucci, G., Pondrelli, S., Argnani, A., Casula, G., Anzidei, M., Baldi, P., Gasperini, P., 2007. Kinematics of the Western Africa-Eurasia plate boundary from focal mechanisms and GPS data. Geophys. J. Int. 169(3), 1180-1200.

Serrano, I., Morales, J., Zhao, D., Torcal, F., Vidal, F., 1998. P-wave tomographic images in the Central Betics-Alboran sea (South Spain) using local earthquakes: Contribution for a continental collision. Geophys. Res. Lett. 25, 4031-4034.

Serrano, I., Hearn, T., Morales, J., Torcal, F., 2005. Seismic anisotropy and velocity structure beneath the southern half of the Iberian Peninsula. Phys. Earth Planet. Inter. 150, 317-330.

Siddall, M., Kaplan, M.R., Schaefer, J.M., Putnam, A., Kelly, M.A., Goehring, B., 2010. Changing influence of Antarctic and Greenlandic temperature records on sea-level over the last glacial cycle. Quat. Sci. Rev. 29(3), 410-423.

Silva, P.G., Goy, J.L., Somoza, L., Zazo, C., Bardaji, T., 1993. Landscape response to strike-slip faulting linked to collisional settings: quaternary tectonics and basin formation in the Eastern Betics, Southeastern Spain. Tectonophysics. 224, 289-303.

Smith, K.D., von Seggern, D., Blewitt, G., Preston, L., Anderson, J.G., Wernicke, B.P., Davis, J.L., 2004. Evidence for deep magma injection beneath lake Tahoe, Nevada-California. Science. 305, 1277-1280.

Soria, J.M., 1998. La Cuenca de Antepaís Norbética en la Cordillera Bética Central (sector del Mencal): evolución tectosedimentaria e historia de la subsidencia. Rev. Soc. Geol. España. 11, 23-31.

Spakman, W., Wortel, R., 2004. A tomographic view on western Mediterranean geodynamics, The TRANSMED atlas. The Mediterranean region from crust to mantle. Springer, pp. 31-52.

Srivastava, S.P., Roest, W.R., Kovacs, L.C., Oakey, G., Levesque, S., Verhoef, J., Macnab, R., 1990. Motion of Iberia since the Late Jurassic: Results from detailed aeromagnetic measurements in the Newfoundland basin. Tecontophysics. 184, 229-260.

Stanford, J.D., Hemingway, R., Rohling, E.J., Challenor, P.G., Medina-Elizalde, M., Lester, A.J., 2011. Sea-level probability for the last deglaciation: A statistical analysis of far-field records. Global Planet. Change. 79(3), 193-203.

Stirling, M., Rhoades, D., Berryman, K., 2002. Comparison of earthquake scaling relations derived from data of the instrumental and preinstrumental era. Bull. Seismol. Soc. Am. 92(2), 812-830.

Stuiver, M., Reimer, P.J., 1993. Extended 14C data base and revised CALIB 3.0 14C age calibration program. Radiocarbon. 35, 215-230.

Stuiver, M., Reimer, P.J., Bard, E., Beck, J.W., Burr, G.S., Hughen, K.A., Kromer, B., McCormac, F.G., Van der Plicht, J., Spurk, M., 1998. INTCAL98 Radiocarbon age calibration 24,000-o cal BP. Radiocarbon. 40, 1041-1083.

Sue, C., Delacou, B., Champagnac, J. D., Allanic, C., Tricart, P., Burkhard, M., 2007. Extensional neotectonics around the bend of the Western/Central Alps: an overview. Int. J. Earth Sci. 96(6), 1101-1129.

Suriñach, E., Udías, A., 1978. Determinación de la raíz de Sierra Nevada-Filabres a partir de medidas de refracción sísmica y gravimetría, Geodinámica de la Cordillera Bética y Mar de Alborán. University of Granada. pp. 25-34.

Suriñach E., Vegas R., 1993. Estructura general de la corteza en una transversal del Mar de Alborán a partir de datos de sísmica de refracción-reflexión de gran ángulo. Interpretación geodinámica. Geogaceta. 14, 126-128.

Tahayt, A., Mourabit, T., Rigo, A., Feigl, K.L., Fadil, A., McClusky, S., Reilinger, R., Serroukh, M., Ouazzani-Touhami, A., Sari, D.B., 2008. Mouvements actuels des blocs tectoniques dans l'arc Bético-Rifain à partir des mesures GPS entre 1999 et 2005. C. R. Geosci. 340, 400-413.

Talma, A.S., Netterberg, F., 1983. Stable isotope abundances in calcretes. Spec. Publ. Geol. Soc. London 11(1), 221-233.

Tapponnier, P., 1977. Evolution tectonique du systeme alpin en Mediterranee; poinconnement et ecrasement rigide-plastique. Bull. Soc. Geol. Fr. S:7 Vol. XIX, 437-460.

Tarı, U., Tüysüz, O., Can Genç, Ş., İmren C, Blackwell, B.A., Lom, N., Tekeşin, Ö., Üsküplü, S., Erel, L., Atiok, S., Beyhan, M., 2013. The geology and morphology of the Antakya Graben between the Amik Triple Junction and the Cyprus Arc. Geodinamica Acta. 26, 27-55.

Telford, W.M., Geldart, L.P., Sheriff, R.E., 1990. Applied geophysics (Vol. 1). Cambridge university press.

Teza, G., Pesci, A., Galgaro, A., 2008. Grid_strain and grid_strain3: Software packages for strain field computation in 2D and 3D environments. Comput. Geosci. 34, 1142-1153.

Thiebot, E., Gutscher, M.A., 2006. The Gibraltar Arc seismogenic zone: Constraints on a shallow east dipping fault plane source for the 1755 Lisbon earthquake provided by seismic data, gravity and thermal modelling. Tectonophysics. 426, 135-166.

Torné, M., Banda, E., 1992. Crustal thinning from the Betic Cordillera to the Alboran Sea. Geo-Mar. Lett. 12(2-3), 76-81.

Torné, M., Fernández, M., Comas, M.C., Soto J.I., 2000. Lithospheric structure beneath the Alboran Basin: Results from 3D gravity modeling and tectonic relevance, J. Geophys. Res. 105, 3209-3228.

Torres Roldán, R., Poli, G., Peccerillo, A., 1986. An Early Miocene arc.tholeiitic magmatic dike event from the Alborán Sea -Evidence for precollisonal subduction and back-arc crustal extension in the westernmost Mediterranean. Neth. J. Geosci. 75, 219-234.

Udias, A., Buforn, E., 1991. Regional stresses along the Eurasia-Africa plate boundary derived from focal mechanisms of large earthquakes. Pure Appl. Geophys. 136, 433-448.

Ulzega, A., Leone, F., Orrù, P., 1986. Geomorphology of Submerged Late Quaternary Shorelines on the South Sardinian Continental-Shelf. J. Coastal Res. 1(1), 73-82.

Van Bemmelen, R.W., 1927. Bijdrage tot de geologie der Betisch Ketens in de provincie Granada. Ph. D. Thesis, Univ. Delft, 176 pp.

Vazquez, M., Jabaloy, A., Barbero, L., Stuart, F.M., 2011. Deciphering tectonic- and erosion-driven exhumation of the Nevado–Filábride Complex (Betic Cordillera, Southern Spain) by low temperature thermochronology. Terra Nova. 23(4), 257-263.

Vegas, R., Vázquez, J.T., Medialdea, T., Suriñach, E., 1997. Seismic and tectonic interpretation of the ESCI-Béticas and ESCI-Alborán deep seismic reflection profiles: structure of the crust and geodynamic implications. Rev. Soc. Geol. España. 8(4), 449-460.

Vera, J.A., 2000. El Terciario de la Cordillera Bética: estado actual de conocimientos. Rev. Soc. Geol. España. 13, 345-373.

Vernant, P., Fadil, A., Mourabit, T., Ouazar, D., Koulali, A., Davila, J.M., Garate, J., McClusky, S., Reilinger, R., 2010. Geodetic constraints on active tectonics of the Western Mediterranean: Implications for the kinematics and dynamics of the Nubia-Eurasia plate boundary zone. J. Geodyn. 49(3), 123-129.

Vissers, R.L.M, Platt, J.P. and Van der Wal, D., 1995. Late orogenic extension of the Betic Cordillera and the Alboran Domain: A lithospheric view. Tectonics, 14, 786-803.

Vozoff, K., 1972. The magnetotelluric method in the exploration of sedimentary basins. Geophysics. 37(1), 98-141.

Vozoff, K., 1991. The magnetotelluric method. In: Nabighian, M.N. (Ed.), Electromagnetic Methods in Applied Geophysics. 2, pp. 641–711.

Weijermars, R., Roep, T.B., Vandeneeckhout, B., Postma, G., Kleverlaan, K., 1985. Uplift history of a Betic fold nappe inferred from Neogene-Quaternary sedimentation and tectonics (in the Sierra Alhamilla and Almeria, Sorbas and Tabernas Basins of the Betic Cordilleras, SE Spain). Neth. J. Geosci. 64, 397-411.

Weijermars, R., Roep, T.B., Eeckhout, B., Postma, G., Kleverlaan, K., 2007. Uplift history of a Betic fold nappe inferred from Neogene-Quaternary sedimentation and tectonics (in the Sierra Alhamilla and Almeria, Sorbas and Tabernas Basins of the Betic Cordilleras, SE Spain). Neth. J. Geosci. (Classic Papers).

Wells, D.L., Coppersmith, K.J., 1994. New empirical relationships among magnitude, rupture length, rupture width, rupture area, and surface displacement. Bull. Seismol. Soc. Am. 84, 974-1002.

Wernicke, B.P., England, P.C., Sonder, L.J., Christiansen, R.L., 1987. Tectonomagmatic evolution of Cenozoic extension in the North American Cordillera. Spec. Publ. Geol. Soc. London. 28(1), 203-221.

Wesnousky, S.G., 1986. Earthquakes, Quaternary faults, and seismic hazard in California. J. Geophys. Res. B: Solid Earth. 91(B12), 12587-12631.

Wessel, P., Smith, W.H.F., Scharroo, J.F.L., Wobbe, F., 1998. Generic Mapping Tools: Improved version released, EOS Trans. AGU. 94, 409-410.

Williams, S.D.P., 2003. The effect of coloured noise on the uncertainties of rates estimated from geodetic time series. J. Geodyn. 76, 483–494.

Working Group for Deep Seismic Sounding in the Alboran Sea 1974-1975 (WGDSSAS-1974-1975), 1978. Crustal seismic profiles in the Alborán Sea preliminary results. Pure Appl. Geophys. 116, 167-180

Wortel, M.J., Spakman, R.W., 1992. Structure and Dynamics of subducted lithosphere in the Mediterranean region. Proc. Kon. Ned. Akad. Wet. 95, 325-347.

Wortel, M.J., Spakman, R.W., 2000. Subduction and Slab detachment in the Mediterranean-Carpathian Region. Science. 290, 1910-1917.

Yijian, C., Jinfen, L., Head, J., Arakel, A.V., Jacobson, G., 1988. 14C and ESR dating of calcrete and gypcrete cores from the Amadeus Basin, Northern Territory, Australia. Quat. Sci. Rev. 7(3-4), 447-453.

Yilmaz, M., Gelisli, K., 2003. Stratigraphic–structural interpretation and hydrocarbon potential of the Alaşehir Graben, western Turkey. Pet. Geosci. 9, 277-282.

Zagorčev, I.S., 1992. Neotectonics of the central parts of the Balkan Peninsula: basic features and concepts. Geol. Rundsch. 81, 635-654.

Zazo, C., Silva, P.G., Goy, J.L., Hillaire-Marcel, C., Ghaleb, B., Lario, J., Bardaji, T., González, A., 1999. Coastal uplift in continental collision plate boundaries: data from the Last Interglacial marine terraces of the Gibraltar Strait area (south Spain). Tectonophysics. 301(1), 95-109.

Zeck, H.P., 1996. Betic-Rif orogeny: Subduction of Mesozoic Tethys lithosphere under eastward drifting Iberia, slab detachment shortly before 22 Ma, and subsequent uplift and extensional tectonics. Tectonophysics. 254(1), 1-16.

Zeck, H.P., Monié, P., Villa, I.M., Hansen, B.T., 1992. Very high rates of cooling and uplift in the Alpine belt of the Betic Cordilleras, southern Spain. Geology. 20, 79-82.

Zhang, J., Ding, L., Zhong, D., Zhou, Y., 2000. Orogen-parallel extension in Himalaya: Is it the indicator of collapse or the product in process of compressive uplift?. Chin. Sci. Bull. 45(2), 114-120.

Zumberge, J.F., Heflin, M.B., Jefferson, D.C., Watkins, M.M., Webb, F.H., 1997. Precise Point Positioning for the efficient and robust analysis of GPS data from large networks. J. Geophys. Res. 102, 5005-5017.